GEORGIA INSTITUTE OF TECHNOLOGY
OFFICE OF RESEARCH ADMINISTRATION

RESEARCH PROJECT INITIATION

Date: October 11, 1972

Project Title: Catalytic Behavior in Composite Solid Propellant Combustion

Project No: E-16-626

Principal Investigator: Dr. W. C. Strahle

Sponsor: Office of Naval Research

Agreement Period: From 9-2-72 Until 9-1-73

Type Agreement: Task Order No. N00014-67-A-0159-0016

Amount: $25,0004.00

Reports Required: Annual Progress Report; Final Technical Report

Sponsor Contact Person (s):

Technical Matters
Director, Power Programs
Material Sciences Division
Office of Naval Research
800 North Quincy Street
Arlington-, Virginia 22217

Contractual Matters
(Thru ORA)
Mr. R. J. Whitcomb
ONR Resident Representative
Hinman Research Building
Campus

Assigned to: School of Aerospace Engineering

COPIES TO:

Principal Investigator	Library
School Director	Rich Electronic Computer Center
Dean of the College	Photographic Laboratory
Director, Research Administration	Project File
Director, Financial Affairs (2)	
Security-Reports-Property Office	
Patent Coordinator	Other

RA-3 (6-71)

GEORGIA INSTITUTE OF TECHNOLOGY

OFFICE OF CONTRACT ADMINISTRATION

RESEARCH PROJECT TERMINATION

Date: February 10, 1976

Project Title: Catalytic Behavior in Composite Solid Propellant Combustion

Project No: E-16-626

Principal Investigator: Dr. W. C. Strahle

Sponsor: Office of Naval Research

Effective Termination Date: 9/1/74

Clearance of Accounting Charges: 11/1/74

Grant/Contract Closeout Actions Remaining: Final Report of Inventions (JWM)

Assigned to School of Aerospace Engineering

COPIES TO:

Principal Investigator
School Director
Dean of the College
Office of Financial Affairs (2)
Patent and Inventions Coordinator
Research Services/Photo Lab ✓
Library, Technical Reports Section
Office of Computing Services
Terminated Project File No. _____
Other _____

E-16-624

GEORGIA INSTITUTE OF TECHNOLOGY
ATLANTA, GEORGIA 30332

SCHOOL OF
AEROSPACE ENGINEERING

404-894-3000

DANIEL GUGGENHEIM SCHOOL
OF AERONAUTICS

November 28, 1972

Power Program Office
Department of the Navy
Office of Naval Research
Arlington, Virginia 22217

Subject: First Quarterly Report - Task Order No. N00014-67-A-0159-0016

During the first quarter period the cinephotomacrography experiments and data analysis for ferrocene and iron blue catalysts have been completed. This completes the motion picture work with the four catalysts copper chromite, iron (III) oxide, ferrocene, and iron blue. A major finding has been a catalyst which works when placed in the binder alone, in the sandwich configuration; iron blue, below 1000 psia, is the only one of the four to show signs of catalytic activity.

Work on establishing the relevance of sandwich studies to propellant combustion is continuing. A burn rate correlation developed by Thiokol is being used as the guide to propellant behavior. Parameters being investigated are catalyst type, particle size, and pressure.

Efforts on production of an analytical model of sandwich combustion are continuing. The disappointing results achieved during the program when under NAVAIR funding have been thoroughly reviewed. The decision to not attempt a direct numerical integration of the partial differential equations has been made on the basis of computer storage and time limitations. The problem has been reformulated, using a new integral method, and programming is now underway. The adequacy of the technique will be determined during the second quarter of this program.

The conversion of the test rig to a quenched-combustion bomb has begun, and quench testing, together with scanning electron microscopy, will begin in the second quarter.

Very truly yours,

Warren C. Strahle
Principal Investigator

GEORGIA INSTITUTE OF TECHNOLOGY
ATLANTA, GEORGIA 30332

SCHOOL OF
AEROSPACE ENGINEERING

404-894-3000

DANIEL GUGGENHEIM SCHOOL
OF AERONAUTICS

February 28, 1973

Power Program Office
Department of the Navy
Office of Naval Research
Arlington, Virginia 22217

Subject: Second Quarterly Report - Task Order No. N00014-67-A-0159-0016

Quench testing of catalyzed sandwiches was begun during the second quarter. Seven of the planned twenty-eight tests have been completed and the samples viewed under the scanning electron microscope. Predictions concerning the behavior have been borne out, in that there appears a slope discontinuity at the binder-oxidizer interface when catalyst is put into the AP. The binder melt flows, which are so apparent in non-catalyzed situations, virtually disappear in the catalyzed cases.

Work on the analytical model of sandwich deflagration is progressing. The new formulation has yielded asymptotic solutions valid away from the binder, out onto the AP surface. These asymptotic solutions are being used to start a numerical integration of the governing equations toward the binder.

Study of the relevance of sandwich work to real propellant behavior has been completed with respect to ferrocene and iron oxide catalysts. Points of correspondence between sandwich and propellant results exist in regard to the particle size and pressure effects. The real propellant results show, however, that ferrocene is a better catalyst than iron oxide over the pressure range 600-2000 psi. The sandwich results indicate they are equivalent.

The third quarter work will be devoted to analytical modeling and quench testing.

Very truly yours,

Warren C. Strahle
Principal Investigator

tk

June 5, 1973

Power Program Office
Department of the Navy
Office of Naval Research
Arlington, Virginia 22217

Subject: Third Quarterly Report - Task Order No. N00014-67-A-0159-0016

Quench testing of catalyzed sandwiches is now 90% complete. It has been discovered that there is a severe reproducibility problem when catalyst is loaded onto the interface between the binder and oxidizer. Consequently the burn rates reported for this configuration are suspect. The SEM results also show no new phenomena as compared with catalyst-in-AP or catalyst-in-binder results. Therefore, interface loading runs have been suspended.

Quench testing of iron blue in AP has revealed a color change from blue to red at the surface. It has been decided to initiate electron microprobe studies of the surface to determine the chemical change which is taking place. This will also be repeated for ferrocene-in-AP to elucidate any surface processes taking place.

The primary results from the quench testing appear to be that a) the binder melt is removed under catalysis and b) in some cases attack appears to be taking place upon the binder by the catalyst-laden oxidizer gases, because there is an undercutting of the binder.

Analytical modelling of the sandwich configuration is progressing. An analytical solution to the problem has been discovered in a linear limit which is still valid for practical cases. This solution, for the case of dry surfaces and no chemical interaction between the binder and oxidizer, is being explored for its general usefulness. The theory in its current form is a valuable aid in interpretation of experiment. It correctly predicts a) pressure independence of the surface shape and b) a slope discontinuity at the binder-oxidizer interface. The theory also suggests the reason for binder notches appearing with thin binders in the sandwich configuration.

The fourth quarter will be devoted to a) the completion of quench, SEM, and microprobe testing, b) complete data analysis and c) a continuation of the analysis.

Warren C. Strahle,
Principal Investigator

LIBRARY DOES NOT HAVE

Fourth Quarterly Report

GEORGIA INSTITUTE OF TECHNOLOGY
ATLANTA, GEORGIA 30332

SCHOOL OF
AEROSPACE ENGINEERING

404-894-3000

DANIEL GUGGENHEIM SCHOOL
OF AERONAUTICS

November 29, 1973

Power Program Office
Department of the Navy
Office of Naval Research
Arlington, Virginia 22217

Subject: Fifth Quarterly Report - Task Order No. N00014-67-A-0159-0016

During the fifth quarter the tasks covered were a) generation of an Annual Summary Report entitled "Catalytic Behavior in Solid Propellant Combustion," b) conversion of the combustion quench rig back into a cinephotomacrography rig, c) construction of sandwich samples for the exploratory round of synergistic catalytic runs, d) analysis to explain the synergistic effect and e) program replanning in the light of results obtained to date.

The Annual Summary Report contains the results of scanning electron microscopy, cinephotomacrography, electron microprobing and analysis of the sandwich configuration under catalysis. This report has been distributed. Results from this report which have bearing on the replanning of the current program are a) the sandwich configuration attained is insensitive to the binder type and b) there is some indication that catalysts are altering the melt behavior of the binder.

For the above reasons it has been decided to delete from the program runs attempting to change the binder heat of decomposition by introduction of polyacetylene into the HTPB and to increase differential scanning calorimetry of HTPB with catalyst loaded into the binder. The deflagration runs with ferrocene loaded chemically into the R-45 binder will be retained because of the expected novel effects; however, it has been learned from NOL-Indian Head that they are no longer producing the polymer. The instructions for making this catalyst loaded polymer have been obtained from Mr. Robert Cassel and the chemical will be manufactured in our laboratory.

Construction of eleven initial synergistic effect sandwich samples has been completed. These will be tested during the sixth quarter to determine directions for future testing. Conversion of the combustion quench rig to a cinephotomacrography rig has been completed.

Analysis of a simple system - the deflagration of AP - with catalysts is proceeding. While the physical picture is clear with respect to catalysts operating in a synergistic manner, numerically the magnitude of this effect for gas phase catalysis is unknown. This work will be completed during the sixth quarter. Analysis on the effect of melts on the attained sandwich shape is proceeding.

It is anticipated that one or more patents will result from the current program. It is requested that the Principal Investigator be informed of the procedure for initiating the patents.

Sincerely,

Warren C. Strahle
Principal Investigator

WCS:ca

GEORGIA INSTITUTE OF TECHNOLOGY
ATLANTA, GEORGIA 30332

SCHOOL OF
AEROSPACE ENGINEERING

404-894-3000

DANIEL GUGGENHEIM SCHOOL
OF AERONAUTICS

March 11, 1974

Power Program Office
Department of the Navy
Office of Naval Research
Arlington, Virginia 22217

Subject: Sixth Quarterly Report - Task Order No. N00014-67-A-0159-0016

During the sixth quarter the tasks covered were a) analysis of synergistic catalysis effects, b) exploratory experiments on the synergistic effect in sandwich samples, c) initiation of differential scanning calorimetry on catalyst-laden binders and d) sandwich deflagration analysis.

Analysis was completed on the potential of synergistic effects to augment the burn rate of AP. Selecting two different catalytic reactions to augment the gas phase reaction scheme of Guirao-Williams it has definitely been shown that the nonlinearities in the governing equations will allow a synergistic effect. Because this is a rather complex reaction system, however, analysis on a simple model system has begun to better elucidate the basic mechanism.

A patent disclosure was filed with the ONR representative at Georgia Tech disclosing the initial results of exploratory experimentation on synergistic effects with Harshaw Catalyst Cu0202, Fe_2O_3, ferrocene and iron blue. The experimental results have shown synergisms with all combinations of catalysts. The strongest effect so far (at 600 psi) has been with an iron blue-iron oxide mixture. While the synergism with copper chromite-iron oxide was not strong the maximum burn rate was attained with this mixture. This is a sandwich effect: since the catalyst is pressed with the AP and copper chromite strongly augments the pure AP rate while the iron oxide depresses it the copper chromite is driving the result. In a real propellant the catalyst is mixed with the binder and a synergism is expected as both catalysts augment the binder-oxidizer deflagration kinetics.

On the basis of the exploratory runs the combinations of copper chromite-iron oxide and iron blue-iron oxide are being carried along in further sandwich and propellant runs.

Differential scanning calorimetry runs have been made with HTPB and HTPB-catalyst binders. The data are currently being reduced.

Analysis of sandwich deflagration with finite rate chemistry between the binder and oxidizer has been initiated. This will build upon the no-interaction model which was completed under last year's program. It is necessary to determine theoretically the magnitude of chemical rates necessary to drive the burning rate down the interface between the binder and oxidizer, since this is precisely what is happening in the catalyzed sandwich runs.

Uncured propellant (HTPB-AP) has been ordered from Princeton University to be used for synergistic runs with real propellants. The seventh quarter will be devoted to a) sandwich synergism experiments over the 300-2000 psia pressure range, b) construction of the propellant samples, c) completion of the differential scanning calorimetry and d) continuation of synergism and sandwich deflagration analysis.

Sincerely,

Warren C. Strahle
Principal Investigator

WCS:ca

GEORGIA INSTITUTE OF TECHNOLOGY
ATLANTA, GEORGIA 30332

SCHOOL OF
AEROSPACE ENGINEERING

404-894-3000

DANIEL GUGGENHEIM SCHOOL
OF AERONAUTICS

June 4, 1974

Power Program Office
Department of the Navy
Office of Naval Research
Arlington, Virginia 22217

Subject: Seventh Quarterly Report - Task Order No. N00014-67-A-0159-0016

During the seventh quarter the experimental tasks covered were a) the completion of differential scanning caloremetry on catalyst-laden binders, b) the pressure survey of the sandwich synergistic experiments and c) initiation of tests to determine possible synergistic effects in cast composite propellant strands.

The tests to determine the synergistic effects as a function of pressure from 300 to 2000 psia, have been conducted for two combinations of catalysts in the two dimensional sandwiches. These two systems were determined from the earlier exploratory experiments at 600 psia. The Harshaw Catalyst Cu0202 - ferric oxide system exhibited the highest sandwich burn rate, while the ferric oxide-iron blue system demonstrated the largest synergistic effect. Twenty three additional tests have been completed leaving only one base case, 2% Harshaw Catalyst Cu0202 at 300 psia to be conducted. Data reduction will be completed in the next quarter.

It was determined that the uncured propellant (82.7% AP-17.3% HTPB) that was ordered from Princeton University's Solid Propellant Processing Laboratory for the determination of synergistic effects in cast composite propellant could not be conveniently shipped from Princeton, New Jersey to Atlanta, Georgia. It is classified, by analogy, as a class B explosive. Up to 10 pounds of this type of material can be shipped by air cargo freighter, but this service is only available from Kennedy Airport to Atlanta. Transportation of this type of material over all bridges and through tunnels connecting Long Island and New Jersey is prohibited. The truck freight rates for this type of material are based on minimum amounts of 7500 pounds if shipped in the truck or 2500 pounds if shipped in a trailer attached to a truck. This would be a minimum charge of $400 for transporting two pounds of propellant. The order to Princeton University has been cancelled.

The composite propellant will be mixed in our own laboratory. We do not have the capability of maintaining close quality control on a batch to batch basis, therefore all comparison samples will be prepared from a common base batch of uncured composite propellant of the same composition as ordered from Princeton University. Strand molds of .25" x .25" x 1.7" size have been fabricated of teflon. An initial set of cured samples have been prepared for evaluation of this synergistic effect in the cast composite propellants.

The eighth quarter will be devoted to testing the cast composite propellants with catalyst present. Both cinephotomacrography and fuse wire determination of the burning rates will be used. This data reduction for the sandwich synergistic effects will be completed.

In the differential scanning calorimetry of catalyst laden binders, no effect of catalyst has been found on the total heat of decomposition or the kinetics of decomposition for HTPB. Ferrocene and iron blue have been tested. This was in accord with expectations from sandwich work and no further DSC work is planned.

In what was previously thought to be an indeterminate problem, it has been theoretically discovered that the sandwich burning problem is a determinate eigenvalue problem with the burn rate as the eigenvalue. Calculations are being performed to check the previous sandwich analysis to see if any conclusions are altered by this new analytical discovery. The student who has been working on the analysis has decided to terminate his education and future analysis will be more heavily done by the Principal Investigator.

Sincerely,

Warren C. Strahle
Principal Investigator

WCS:cm

LIBRARY DOES NOT HAVE !

Eighth Quarterly Report

GEORGIA INSTITUTE OF TECHNOLOGY
ATLANTA, GEORGIA 30332

SCHOOL OF
AEROSPACE ENGINEERING

404-894-3000

DANIEL GUGGENHEIM SCHOOL
OF AERONAUTICS

December 3, 1974

Power Program Office
Department of the Navy
Office of Naval Research
Arlington, Virginia 22217

Subject: Ninth Quarterly Report - Task Order No. N00014-67-0159-0016

During the ninth quarter the primary tasks accomplished were a) generation of the Second Annual Summary Report, b) replanning of the program in the light of results obtained during the eighth quarter, c) propellant sample preparation and burn rate determination for investigation of synergistic catalytic effects and d) analysis of the sandwich configuration to include binder-oxidizer reactions. In addition, a visit was paid to our facility by Dr. Ralph Roberts; in a fruitful discussion two future avenues of research were explored, to be mentioned later.

As will be recalled, the synergistic effects expected from sandwich testing did not materialize in the propellant testing when 2% catalyst by weight was employed in an HTPB-AP propellant at 600 psia. The catalyst systems used were Harshaw Catalyst CU-0202 - Iron Oxide and Iron Oxide-Iron Blue. Two reasons were suspected for this behavior; a) the catalyst loading may have been too heavy, beyond the saturation point and b) the sandwich tests employed catalyst pressed into the oxidizer whereas the propellant has the catalyst in the binder alone. Exploring the first possibility, samples were prepared using only 1% catalyst by weight. Extreme difficulties then occurred in burn rate determination. Over 20 runs using the fuze wire technique were attempted and various redesigns of the combustion bomb were tried. On each attempt the propellant apparently "disappeared" in the time span of the order of milliseconds. Various inhibitors were also used, but to no avail. Finally, motion pictures were taken and it was indeed found that the propellant was virtually exploding and crumbling. It is believed that during manufacture too exact an AP particle size distribution was being employed, preventing binder wetting and good packing. Samples have now been manufactured using a wider spread of particle sizes while basically retaining a bimodal distribution. Visual inspection of these samples shows that wetting and packing has been markedly improved and testing will resume in the second quarter.

Following the second hypothesis, that the catalyst will only produce the synergistic effect when also loaded into the AP, discussions were had with Dr. Roberts concerning the feasibility of pressing the catalyst into the AP, then breaking it up for incorporation into a propellant. This

approach will be attempted. When it will be tried will depend upon the outcome of the current series of 1% catalyst tests.

Analysis was continued on the case of deflagration behavior near a binder-oxidizer interface in the case where reactions are taking place between the binder and oxidizer. The analysis has two purposes; a) to explain the catalysed sandwich surface shapes and b) to explore the possibility of a propellant deflagration theory on the basis of interface phenomena.

It was also learned from Dr. Roberts that Dr. Ashby of the Department of Chemistry at Georgia Tech has developed two new compounds under an ONR grant that are of interest to solid propellants. One, in particular, a lithium aluminum hydride, appears capable of being tested by us. Discussions have been held with Dr. Ashby and exact procedures for testing of this compound in a propellant configuration will be explored in the future.

Sincerely,

Warren C. Strahle
Principal Investigator

WCS:cm

LIBRARY DOES NOT HAVE:

Tenth Quarterly Report

GEORGIA INSTITUTE OF TECHNOLOGY
ATLANTA, GEORGIA 30332

SCHOOL OF
AEROSPACE ENGINEERING

404-894-3000

DANIEL GUGGENHEIM SCHOOL
OF AERONAUTICS

July 15, 1975

Power Program Office
Department of the Navy
Office of Naval Research
Arlington, Virginia 22217

Attention: Lt. Richard S. Miller

Subject: 11th Quarterly Report - Task Order No. NOOO 14-67-0159-0016

During the 11th quarter the primary tasks accomplished were, a) cast propellant samples with the bimodal AP distribution were prepared to test for possible synergistic effects on sample burn rate using ferrocene as one of the burn rate modifiers, b) the high speed motion picture camera was returned to the factory for retrofitting of an LED timing system, c) tests were completed of Harshaw catalyst Cu0202P loaded into polycrystalline ammonium perchlorate at 2000 psia, d) a procedure was developed for determining the amount of Harshaw catalyst Cu0202P in the ammonium perchlorate and e) the analytical model of sandwich deflagration was completed.

Harshaw catalyst Cu0202P was selected for tests of loading into the oxidizer because of its catalysis of the amonium perchlorate deflagration process. One percent by weight of Cu0202P was mixed with fine ammonium perchlorate (< 37 μm) and pressed into polycrystaline disks. These disks were reground in a motar and pestle and sieved. All particles less than 37 μm in diameter were not used. The percent of all remaining size distribution were retained for determination of the actual catalyst content. The size distribution of the oxidizer and catalyst was 125 μm $<$ 43.7% $<$ 212 μm , 63 μm $<$ 50.8% $<$ 125 μm and 37 μm $<$ 5.5% $<$ 63 μm. Cast composite propellants were prepared using this oxidizer size distribution and a 82.7% / 17.3% ratio of oxidizer to binder. Three propellants were prepared using these ratios, 1) a pure AP - HTPB sample, 2) pure AP - HTPB with 1w% of Harshaw catalyst Cu0202P added to the mixture (binder loaded), and 3) polycrystaline AP and Cu0202P - HTPB. The initial tests at 600 psia were completed during the 10th quarter. The maximum burnrate was obtained for the catalyst added to the binder. The tests at 2000 psi were completed this quarter and the sample with no catalyst present had the maximum burnrate. Close examination of these samples showed that this particle distribution of oxidizer with 17.3% binder yielded propellant packing problems. The pure AP - HTPB sample had voids in the upper half of the sample that appeared to be crumbly. The sample with catalyst loaded in the binder was hard and difficult to cut. A new pure AP-HTPB sample with the same special oxidizer particle size has been prepared and it appears to be uniform and flexible. It has not been tested as yet.

A procedure for determining the amount of Harshaw catalyst Cu0202P in the polycrystalline oxidizer structure was developed. The reason this procedure is needed is that upon regrinding and sieving the initial loading may not correspond to the final loading. Measurements indicated a loading of $1.6 \pm .3\%$ by weight of Cu0202P. The polycrystaline oxidizer and catalyst mixture was placed

in a 60 ml vacuum funnel with a built-in 40 mm diameter ultra fine fritted disk. The ammonium perchlorate was dissolved by repeated washings with distilled water. The washing was continued for three cycles after the liquid showed no perchlorate ions when tested with a methylene blue solution. This deep blue solution turns violet in the presence of the perchlorate ions. A catalyst balance was performed considering the initial amount of catalyst loaded with the oxidizer, the amount retained in the 10% sample and the amount in the oxidizer less than 37 μm. This indicated a possible oxidizer loading of .7 ± .2% by weight of Cu0202P. The difference between these two indicated loadings is unresolved.

Cast propellant samples for further testing of possible synergistic effects on sample burn rate have been prepared. The oxidizer size distribution of 37 μm < 30% < 63 μm and 125 μm < 70% < 212 μm was used. The following samples have been prepared from a common lot of AP - HTPB: 1) no catalyst, 2) 1w% ferrocene, 3) ½w% ferrocene, and ½w% Harshaw catalyst Cu0202P, 4) ½w% ferric oxide, 5) ½w% ferrocene and ½w% iron blue, and 6) ½w% Harshaw catalyst Cu0202P and ½w% iron blue. All of these samples have been examined and show a good uniformity of packing with very little porosity and good flexibility.

All previous cinephotomacrographic observations had been made using Kodak Ektachrome type 7241 daylight film. A shortage of this type film resulted in a delay of testing at the beginning of this quarter. Type 7242 tungsten film has been substituted for current tests.

The Hycam 16 mm high speed motion picture camera was returned to the factory for a retro fit of an LED timing system. This consists of dual light emitting diodes with a built-in timing light generator. These LED's replace the neon lamp system which was not as reliable or did not have as long of a useful life. The mark generated on the film edge is much brighter and narrower than the neon bulb mark. All bearings were cleaned and inspected. All optical surfaces were cleaned. This camera maintenance required six weeks.

The analytical model of sandwich deflagration has been completed. The effects of dilution, in the sense of the Guirao-Williams model of AP-deflagration, have been included but with little effect on the final results. The model has been constructed as a small perturbation deviation from a planar deflagration. It has been found that binders with only a very narrow variation in properties will allow this kind of a solution. Nevertheless the following conclusions may be derived from the model: a) the kinitics of normal binder-oxidizer reactions are too slow to affect the deflagration rate, but, if catalysed sufficiently well, the sandwich will deform so that a more acute angle is made with respect to the binder, as is observed experimentally and b) the AP surface should be nearly horizontal, sufficiently far from the binder, as is experimently observed. Solutions for a wider range of binder properties would require a different solution procedure; consequently, considering the effort that has already been expended and the contract funding level this work will be terminated.

The cast propellant samples for possible synergistic effects on sample burn rate are ready to be tested at 2000 psia. More tests of the special size distribution samples for the determination of the effect of catalyst loading are planned.

July 15, 1975

Power Program Office
Department of the Navy

Lt. Richard S. Miller

11th Quarterly Report - Task Order No. N000 14-67-0159-0016

A new set of samples are planned with all of the reground polycrystaline oxidizer used in the cast solid propellant.

Sincerely.

Warren C. Strahle
Principal Investigator

John C. Handley
Research Engineer

WCS/JCH/jj

LIBRARY DOES NOT HAVE:

Twelth Quarterly Report

E-16,626

GEORGIA INSTITUTE OF TECHNOLOGY
ATLANTA, GEORGIA 30332

SCHOOL OF
AEROSPACE ENGINEERING

404-894-3000

DANIEL GUGGENHEIM SCHOOL
OF AERONAUTICS

December 30, 1975

Power Program Office
Department of the Navy
Office of Naval Research
Ballston Tower # 1
800 North Quincy Street
Arlington, Virginia 22217

Attention: Lt. Richard S. Miller

Subject: 13th Quarterly Report - Task Order N00014-67-0159-0016

During the 13th quarter the primary tasks accomplished were a) preparation and distribution of a yearly report on catalytic effects, b) initiation of a statistical analysis for composite propellant burn rate c) continuation of a review of previous models of composite propellant combustion and d) initiation of experimental procedures to produce ordered structures. It should be noted that the report issued under item a) was designated as a final report on synergistic catalytic effects, anticipating a new contract number and name for the follow-on. Since the old contract was renewed and the name retained, we are in the embarrasing position of working under a misnamed work order. Is it possible that the title can be changed to "Combustion of Nonaluminized Heterogeneous Solid Propellants"?

An initial set-up of the problem of flame propagation through a heterogeneous array of AP and binder has been accomplished. There have been found three important specifications required in order to properly pose the statistical problem. There are a) the combustion law(s) b) the type of heterogeneous matrix and c) a "mixedness" assumption. The first two have been previously recognized and are reasonably obvious. The last has been discovered in attempts to properly specify the statistics. To explain, consider a set of AP spheres of uniform size set in a binder matrix at a loading density very close to the maximum packing density (which would be an ordered array). Considering a finite block of propellant, and a statement of complete randomness in mixing, there is a finite probability that a thick AP void line would appear in the propellant that would extinguish the propellant for any overall loading level of AP at a value less than the maximum loading level. The only way to avoid this is to introduce a "mixedness" assumption which prespecifies the maximum excursion about a preselected ordered lattice point. Within this excursion distance the particle position can be random.

With this in mind the simplest possible model has been set-up. The combustion laws are a) AP self-deflagration by a plane wave followed by b) binder cook-through by the energy in the residual thermal wave followed by c) ignition of the closest AP particle. These laws neglect known melt flows and chemical reactions between binder and oxidizer. Furthermore, this model will fail below the self-deflagration limit of AP and at sufficiently small AP particle size that the propellant is effectively homogeneous. The heterogeneous matrix is one of a unimodal distribution of AP spheres at a packing density very close to the maximum packing density.

Furthermore the initial statistical treatment considers only vertical propagation and allows position deviations from the ordered lattice points in only the vertical direction. The mixedness assumption will allow the maximum deviation from the lattice point to be a free parameter.

At the current time a theory for binder cook through has been completed and the binder surface regression distance as a function of time may be calculated for any set of binder thermodynamic properties and pyrolysis kinetics. A computer program is currently being set up to calculate the regression statistics. Even without the computer results, however, several qualitative results are evident beforehand. These are a) the higher the oxidizer loading the faster the burn rate, b) the burn rate will always be slower than that of pure AP, c) the burning rate exponent will always be less than that of pure AP (for pressure independent binder pyrolysis kinetics) and d) the harder the binder is to pyrolyse the slower will be the burn rate. An inspection of the literature at 1000 psia shows the first three predictions are confirmed at sufficiently large AP particle size (>40 μm). The last conclusion cannot be confirmed due to a lack of binder pyrolysis data.

A review of recent analytical models of steady state burning of heterogeneous propellants was continued. This review, started earlier on institutional funding, includes work by Beckstead et al; Miller; Hermance; and Glick. All of these models devise some scheme of statistical averaging of flame behavior, and use the results to calculate the heat transfer back to the solid. The flame behavior is viewed as nonuniform over the surface, but the heat transfer into the solid assumes a flat surface and homogeneous solid. These analyses will be consolidated into one more general model, and then summarized as special cases in order to provide a concise review of the status of this class of theories.

This analysis differs from the model being developed as per paragraphs 1 - 3 above in that the "Georgia Tech" model seeks to trace the propagation of the combustion surface through the heterogeneous propellant structure.

Preliminary experiments were made on dry-pressing AP samples with fuel threads and with dry fuel powders like starch. Tests were also made on pyrolysis, melting and charring of binder materials in a Hot Stage Microscope.

Sincerely,

E. W. Price, Professor
Co-Principal Investigator

W. C. Strahle, Regents' Professor
Co-Principal Investigator

EWP/WCS/jj

E-16-626

CATALYTIC BEHAVIOR IN SOLID PROPELLANT COMBUSTION

W. C. Strahle
J. C. Handley
N. Kumar

November 1, 1973

Annual Summary Report – Research Sponsored
by
The Office of Naval Research

ONR Contract No. N0014–67–A–0159–0016
Requisition Purchase Request NR 092–543

CATALYTIC BEHAVIOR IN SOLID PROPELLANT COMBUSTION

W. C. Strahle
J. C. Handley
N. Kumar

November 1, 1973

Annual Summary Report - Research Sponsored by
The Office of Naval Research

ONR Contract No. N00014-67-A-0159-0016
Requisition Purchase Request NR 092-543

Approved for Public Release; Distribution Unlimited.

ABSTRACT

This report describes experiments and theoretical analysis concerned with sandwich combustion. The ingredients used in the experiment are compacted polycrystalline ammonium perchlorate as the oxidizer, hydroxyl terminated polybutadiene as the binder and four catalysts: Harshaw catalyst CU-0202, Fe_2O_3, ferrocene, and iron blue. The pressure range studied is 600-2000 psia. The experimental techniques used are cinephotomacrography for sample observation during burning and burn rate determination, scanning electron microscopy for observation of quenched samples, and electron microprobing for an exploratory study of surface composition. A theoretical solution to a simple sandwich deflagration problem is attained. The probable sites of catalytic activity are determined, results are compared with actual propellant experience, and the analysis is used to clarify experimental results.

TABLE OF CONTENTS

		Page
ABSTRACT		ii
CHAPTERS		
I.	Introduction	1
II.	Cinephotomacrography with Iron Blue and Ferrocene	3
III.	Scanning Electron Microscopy with Four Catalysts	13
IV.	Electron Microprobe Exploratory Studies	69
V.	Relevance of Sandwich Results to Composite Propellant Behavior	75
VI.	Sandwich Analysis	80
VII.	Conclusions	111
REFERENCES		114
APPENDIX A		
	Catalysts Located at the Binder-Oxidizer Interface	115

I. INTRODUCTION

Under a previous contract N00123-72-C-242 to the Naval Weapons Center, China Lake, California, a study was initiated of sandwich combustion when catalysts were present in sandwiches. The results are described in Reference (1). The sandwiches used compacted polycrystalline ammonium perchlorate(AP) as the oxidizer, hydroxyl terminated polybutadiene (HTPB) as the binder, and the catalysts Harshaw Catalyst CU-0202 (CC) and Fe_2O_3 (IO). The pressure range studied was 600-3200 psia and catalytic effects were studied when the catalyst was placed in either the AP, the binder, or along the binder-AP interface. The technique used was cinephotomacrography for sample observation during burn and for burn rate determination. This work was an outgrowth of the work of Reference (2), using the same ingredients but CTPB binder.

The results of the previous program indicated that at all pressures CC appeared to primarily catalyze the AP deflagration process with a minor effect upon the oxidizer-binder gas phase reactions, and at pressures below 1000 psia the IO had a primary catalysis effect upon the binder-oxidizer gas phase reactions while inhibiting AP deflagration, but at pressures above 1000 psia the IO catalyses primarily the AP deflagration process but not the oxidizer-binder gas phase reactions. In all cases there appeared no evidence that these two catalysts modified the pyrolysis mechanism of the binder.

It is known, however, that extensive melt flows exist with CTPB and HTPB binders during sandwich deflagration (as well as with other binders).[3,4,5] Cinephotomacrography has insufficient resolution to investigate the interface processes or melt flows in any detail and it was not clear what catalytic effects might be taking place near the interface of the binder and oxidizer.

Consequently, it was desired to use high resolution microscopy on quenched samples to view any differences in surface structure and melt behavior in the presence of catalysis as compared with known results[3,4,5] for uncatalyzed cases. It was furthermore desired to investigate more catalysts than previously used and to compare sandwich results with known propellant results.

Accordingly, the current study is concerned with two additional catalysts - iron blue (IB), a complex ammonium iron hexacyanoferrate, and ferrocene (F), biscyclopentadienyl iron. The burn rate behavior is obtained by cinephotomacrography over the pressure range 600-2000 psia, using AP and HTPB. The range 2000-3200 psia is not studied in this work, because it is excluded from the quenched combustion studies by reason of equipment capability. Furthermore, the AP deflagration process is not understood above 2000 psia (as compared with better knowledge below 2000 psia).[6] Quenched samples with all four catalysts are then investigated by scanning electron microscopy to look at surface structure and melt behavior. Analysis is performed on the sandwich deflagration process to aid in interpretation of the experimental results.

II. CINEPHOTOMACROGRAPHY WITH IRON BLUE AND FERROCENE

The composite, two dimensional sandwich samples for this phase of the investigation were prepared by the method outlined in Reference (1). The binder thickness was controlled by Teflon spacers to a nominal 150 μm. The catalysts used were IB and F and were supplied by the Thiokol Chemical Corporation.

Iron Blue is commercially used as a pigment. It is a complex ammonium iron hexacyanoferrate with the chemical formula, $Fe(NH_4)\ Fe(CN)_6$. It has a cubic crystalline structure. The iron is present as both ferric and ferrous ions in the lattice and they are industinguishable. Ferrocene is an organometallic compound for which the chemical name is biscyclopentadienyl iron, $(C_2H_5)_2Fe$. It is a yellow crystalline solid with relatively high thermal stability for an organometallic compound.

The catalysts used were loaded into either the oxidizer, the binder, or at the binder-oxidizer interface. For dispersal in the oxidizer, 2% by weight of catalyst was added to the AP prior to grinding and pressing. For loading in the binder, the same volumetric loading as occurred in the AP was mixed into the binder prior to curing. For HTPB this was 4.37% by weight. When the catalyst was located at the binder-oxidizer interface, the same amount of catalyst as was added to the ammonium perchlorate, 2% by weight, was mixed with 2% AP and pressed onto the surface of a prepressed AP disc.

The prepared samples were mounted in the pressurized combustion apparatus of Jones[2]. Motion pictures of the burning sample were obtained at a rate of either 1600 or 3200 frames per second, at a latent image

magnification of 2 to 1. A summary film of this phase of the investigation is available on loan from the senior author of the report. Two frames from the motion pictures of ferrocene and iron blue added to the AP are reproduced in Figure II-1.

These motion pictures were used to obtain an accurate value of the sample burning rate. The sandwich vertical burn rate and the burn rate normal to the oxidizer surface, as defined in Reference (1), were obtained for the three types of catalyst addition at four pressures, 600, 1000, 1500 and 2000 psi. Burning rate data were taken only after a steady profile had been achieved and the surface was clearly visible over a substantial portion of the run. For the steady profile the sandwich vertical burn rate is the same regardless of the perpendicular distance from the binder-oxidizer interface. The burn rate normal to the oxidizer surface must be taken at a distance sufficiently far away from the interface for the oxidizer to have a definable, constant slope. These results are summarized in Table II-1.

The burn rates for the case of catalyst added to the oxidizer are shown in Figure II-2. The data indicated by CC and IO were obtained earlier and reported in Reference (1). The catalysts indicated are Harshaw Catalyst Cu0202 (CC) and Fe_2O_3, ferric oxide (iron III oxide - IO). The data of Friedman[7] for CC are also shown in this figure. The burn rates are presented as a ratio to the burn rates of an AP-HTPB sandwich with no catalyst present, presented in Reference (1). The solid curves are the ratio of the sandwich vertical burn rates. The dashed curves are the ratio for the burn rates normal to the oxidizer surface. The dashed curves represent the effect of the catalyst addition to pure ammonium perchlorate

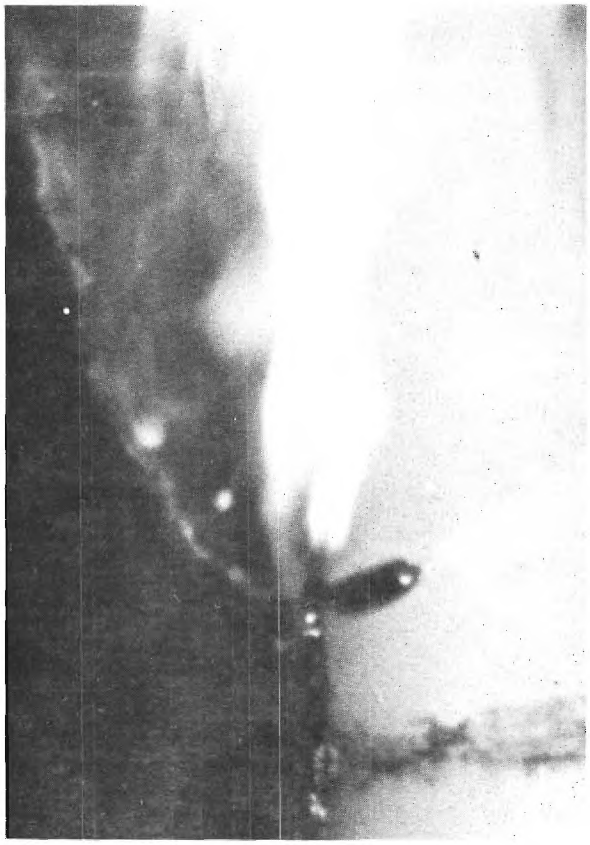

Figure II-1 a. AP and IB-HTPB-AP, 600 psia.

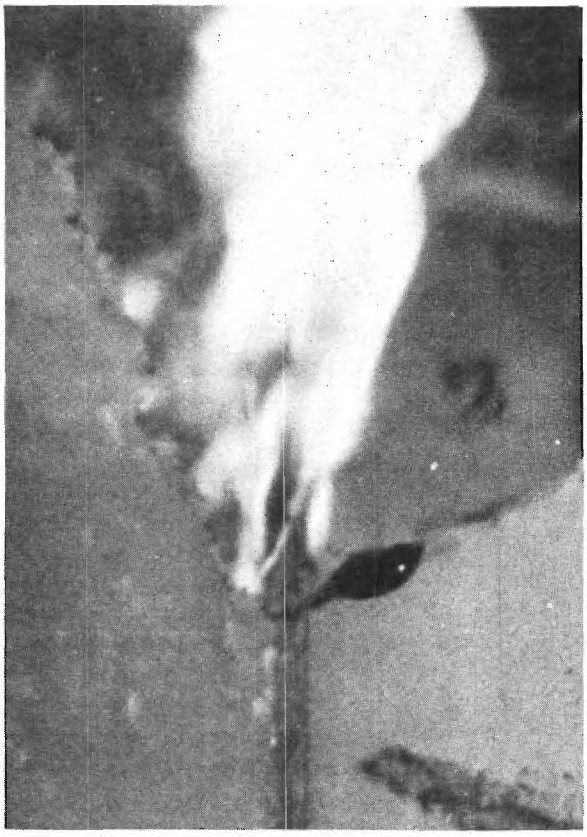

Figure II-1 b. AP and F-HTPB-AP, 1000 psia.

Table II-1

Summary of Results from Cinephotomacrography of Composite Ammonium Perchlorate-HTPB Sandwiches with Catalysts.

Catalyst	Location	Pressure psia	Sandwich Vertical Burn Rate in/sec	Burn Rate Normal to the Oxidizer Surface in/sec
none		600	.237	.237
		1000	.360	.360
		1500	.386	.386
		2000	.351	.339
CuO202	in AP	600	.405	.260
		1000	.612	.501
		1500	1.100	1.035
		2000	1.330	1.250
Ferric Oxide	in AP	600	.255	.137
		1000	.376	.203
		1500	.686	.540
		2000	.740	.695
Ferrocene	in AP	600	.269	.183
		1000	.359	.208
		1500	.450	.278
		2000	.524	.300
Iron Blue	in AP	600	.263	.182
		1000	.375	.246
		1500	.536	.234
		2000	.556	.379
CuO202	in HTPB	600	.262	.246
		1000	.370	.345
		1500	.404	.404
		2000	.386	.386
Ferric Oxide	in HTPB	600	.208	.180
		1000	.337	.335
		1500	.320	.320
		2000	.415	.415

Table II-1 (Continued)

Catalyst	Location	Pressure psia	Sandwich Vertical Burn Rate in/sec	Burn Rate Normal to the Oxidizer Surface in/sec
Ferrocene	in HTPB	600	.293	.290
		1000	.318	.318
		1500	.357	.357
		2000	.383	.378
Iron Blue	in HTPB	600	.367	.367
		1000	.345	.345
		1500	.390	.330
		2000	.333	.322
CuO202	on Interface	600	.323	.248
		1000	.562	.441
		1500	.360	.232
		2000	.543	.230
Ferric Oxide	on Interface	600	.221	.117
		1000	.368	.346
		1500	.645	.273
		2000	.758	.320
Ferrocene	on Interface	600	.342	.246
		1000	.521	.336
		1500	.310	.302
		2000	1.137	.480
Iron Blue	on Interface	600	.300	.197
		1000	.585	.338
		1500	.801	.413
		2000	1.068	.403

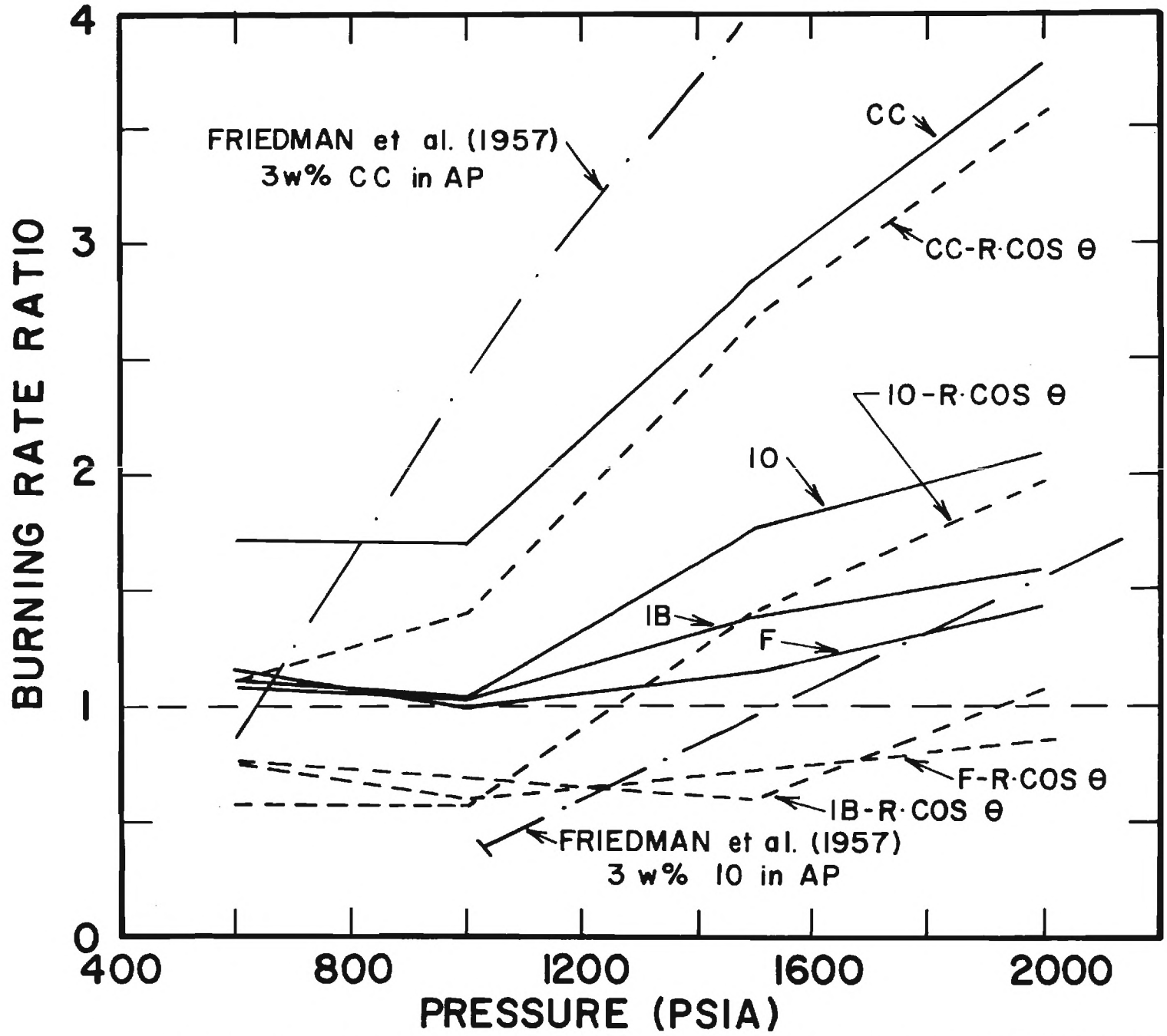

Figure II-2. Ratio of Catalyzed Sandwich Vertical Burn Rate and Burn Rate Normal to the Oxidizer Surface to the Burn Rate of an AP-HTPB Sandwich. Catalyst in AP Alone.

burn rates. Both IB and F retard the burn rate normal to the oxidizer surface for the pressure range investigated. This is in contrast to CC which augments the AP burn rate for the entire pressure range. The IO augments the burn rate for pressures greater than 1200 psi. The separation between the dashed and solid curves is representative of the amount of catalytic activity taking place in the binder-oxidizer reactions. This separation should be directly applicable to real propellant results and will be discussed in Chapter V.

The burn rates for the case of catalyst added to the binder are shown in Figure II-3. Within the accuracy of the experimental techniques there were no detectable angles from the horizontal present in the oxidizer to indicate any alteration of the burn rate normal to the oxidizer surface. Considering the absence of this difference, as was discussed above, this would indicate very little catalytic activity taking place in the vicinity of the binder-oxidizer interface. An exception to the foregoing is seen at 600 psia in the case of F and IB. The scatter of the sandwich vertical burning rate ratios about a ratio of unity in the 1000 to 2000 psi range is indicative of the experimental accuracy, since there is no significant visible effect upon the sandwich deflagration process with catalyst as opposed to an AP-HTPB sandwich. At 600 psia, however, there is a distinct catalytic effect with F and IB.

The burn rate data for the case of catalyst located at the binder-oxidizer interface are shown in Figure II-4. These data were obtained from the motion pictures. After examining scanning electron microscope pictures which are included in Appendix A, it was felt that these interface samples

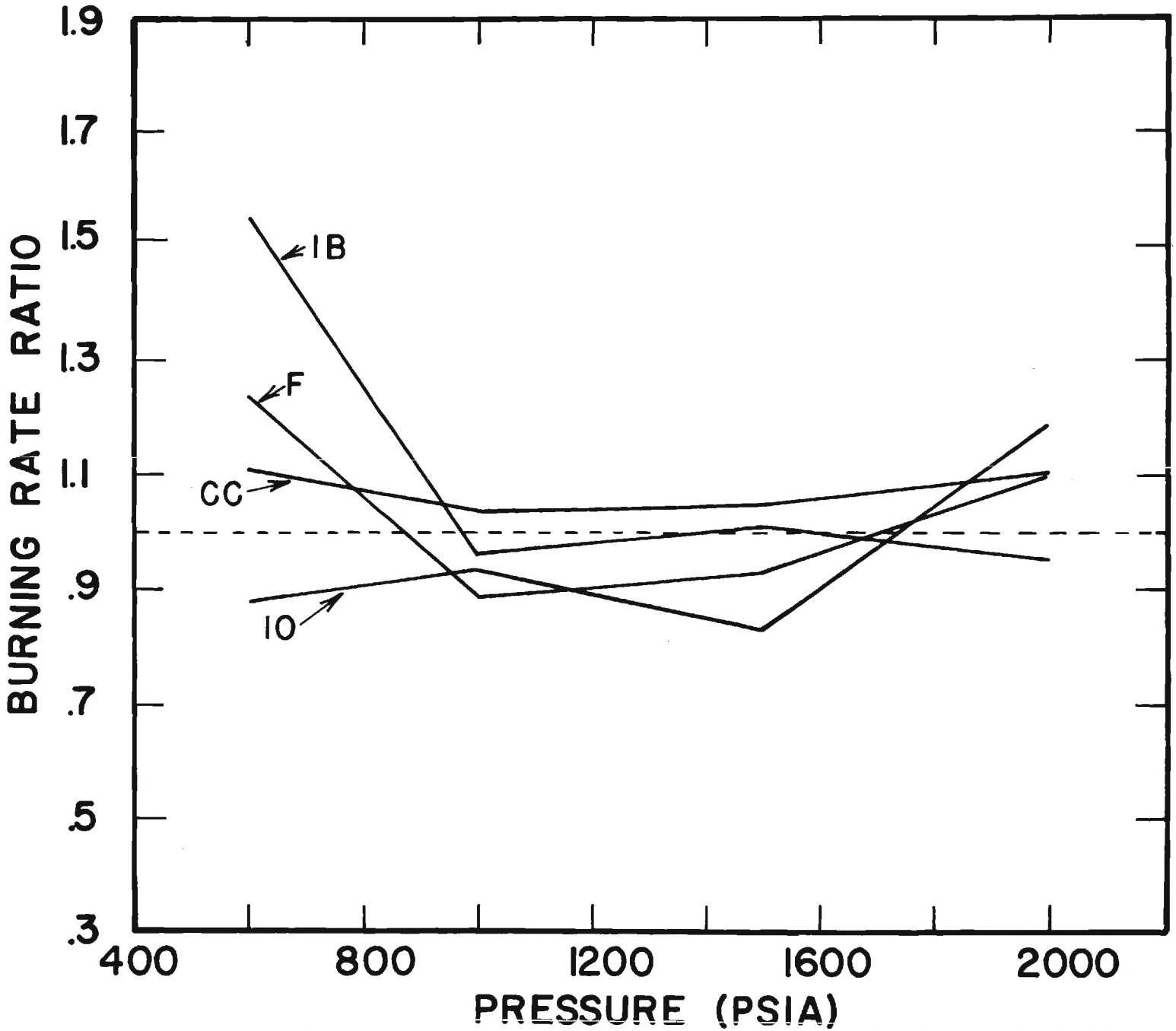

Figure II-3. Ratio of Catalyzed Sandwich Vertical Burn Rate to the Burn Rate of an AP-HTPB Sandwich Catalyst in Binder Alone.

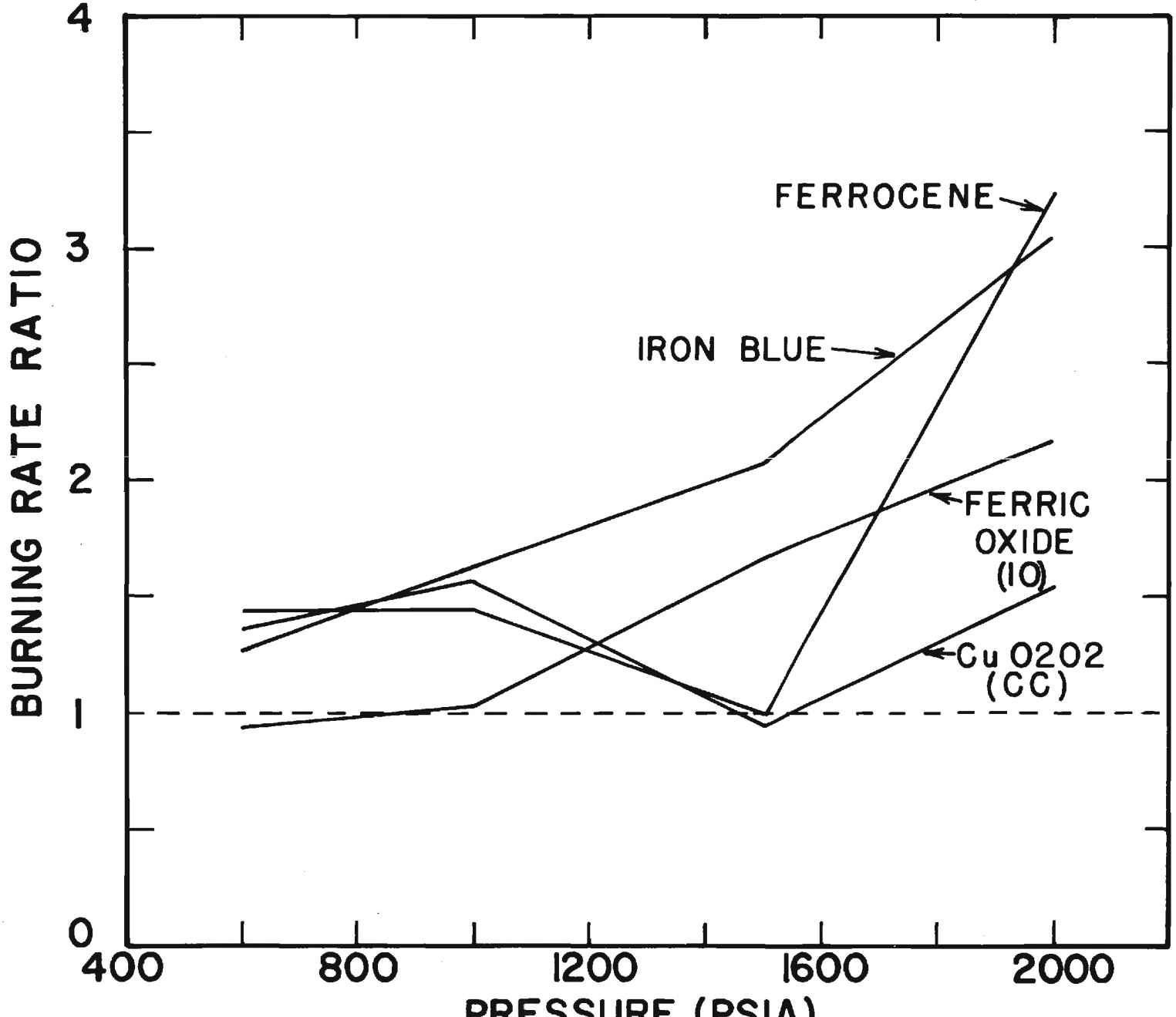

Figure II-4. Ratio of Catalyzed Sandwich Vertical Burn Rate to the Burn Rate of an AP-HTPB Sandwich Catalyst on Binder-Oxidizer Interface.

do not behave uniformly; therefore burn rate data obtained by observing only one edge of the sample may be in considerable error. The data presented in Figure II-4 shows augmentation of burning rates for all catalysts at 2000 psi. Again IO appears to retard the burning for 600 and 1000 psi. Both F and CC show retardation at 1500 psi. This is not in agreement with the observed behavior of quenched samples for these cases. Consequently, the burn rate data for interface samples are suspect and are presented here for interest and completeness only.

Concluding from the motion picture runs, a) there is very little burn rate or visible effect upon placing any of the catalysts in the binder with the exception of IB and F at low pressures, b) CC is the strongest catalyst for the AP deflagration process, c) below 1000 psia all four catalysts show roughly equal effectiveness in augmenting rate processes in the vicinity of the binder-oxidizer interface, d) IB and F show the strongest behavior near the interface above 1000 psia followed by IO and CC and e) IB and F inhibit the AP deflagration process over the entire pressure range studied while IO is an AP inhibitor below 1200 psia.

III. SCANNING ELECTRON MICROSCOPY WITH FOUR CATALYSTS

The samples for this phase of the investigation were prepared in the same manner as those for the cinephotomacrography experiments. In addition to IB and F the catalysts CuO202 (CC) and Ferric Oxide (IO) were loaded in the oxidizer, binder and at the binder-oxidizer interface. Partially burned samples were obtained for scanning electron microscopy by terminating combustion by rapid depressurization using the burst diaphragm method[4]. An electronic timer circuit was used to obtain accurate, reproducible time delays between the ignition of the sample and interruption of burning of the sample. The timer was modified to allow delays of from 22 milliseconds to three seconds. The initial estimates for the time delays were obtained from the cinephotomacrography burn rate data of Chapter II .

The sample observation was carried out in the Physical Science Division of the Engineering Experiment Station of the Georgia Institute of Technology. A Cambridge Stereoscan Scanning Electron Microscope, Mark IIa, was used for all observations in this chapter. Magnifications from x18 to x50,000 were available. A focused electron beam of .01 μm in diameter was used to scan the samples which were placed in the specimen holder under a high vacuum. The high energy beam stimulates the emission of secondary electrons or backscattered electrons, x-rays and, sometimes, light photons from the sample surface. If the sample is electrically non-conducting, it will gradually accumulate an electrical charge and cause an additional scattering of the electron beam. Since the composite propellant samples were non-conducting, they had to be coated with a conducting coating before the surface could be examined with the scanning electron microscope. A combined

coating of carbon and gold-palladium (60-40) was placed on the samples by vacuum deposition. This coating varied from 300 to 400 Å in thickness. It would not be detected unless magnifications in excess of 50,000 were used.

The electrical signal generated by the collected secondary or back-scattered electrons is used to control the brightness of a cathode ray tube which is synchronized to the scan of the electron beam. The photograph of the cathode ray tube is referred to as the electron micrograph. The x-rays emitted by the sample are characteristic of the elements present in the sample and can be collected and analyzed. Both the chemical identity and spatial distribution of the elements in the region of the electron beam can be determined. Iron is always indicated due to the magnet pole pieces. For non-conducting samples the coating materials are also detected. This analysis was used to determine the high iron content of particles visible in the AP-IO samples. The spatial resolution of this measurement is 10^4 times better than the electron microprobe investigation described in Chapter IV, but the number of elements that can be detected is limited and the quantitative results are not as accurate as with the microprobe.

The results of this investigation are presented in a series of 66 micrographs covering the surface details of 21 partially burned samples with catalysts in either the binder or the oxidizer. These samples were partially burned at 600, 1000, 1500 and 2000 psia, in a dry nitrogen atmosphere. A series of 27 micrographs are included in Appendix A covering 7 samples with the catalyst located at the binder-oxidizer interface. These samples were not included in this chapter because of the erratic behavior of these samples. The cinephotomacrography of these samples indicated some

questionable data at 1500 psia. Six attempts were made with F and IB at the interface for 1500 psia to obtain a quenched sample. No satisfactory sample was obtained for this case. Furthermore, even if satisfactory reproducible results could be obtained, there is question in interpretation of the results.

Uncatalyzed Sandwiches

A set of four AP-HTPB sandwiches were included in the study for comparison purposes. These micrographs are shown in Figures III-1 through 13 and the results are summarized in Table III-1. The observations are in accord with those of Boggs and Zurn[5], where experiments are common to both works. The determination of the extent of the binder melt flow is arbitrary. It has been included for comparison with the catalyzed samples. It is a representative value, as is the tabulated binder height. But it is a meaningless observation when trying to generalize results to real propellant behavior. It is known from the cinephotomacrography that there is a substantial binder char layer, which is apparently removed during the quench process. There is a high probability that less viscous binder is also ejected. This would alter the binder height. Nevertheless, the increase of binder height with pressure increase is consistent with the higher AP burn rate at higher pressure. This allows less time for the binder to decompose.

AP-HTPB.

600 psia. Figures 1 and 2 -- The entire oxidizer surface shows evidence of having been covered with a frothy structure. There is a visible binder melt flow out over the oxidizer surface to approximately 140 μm from

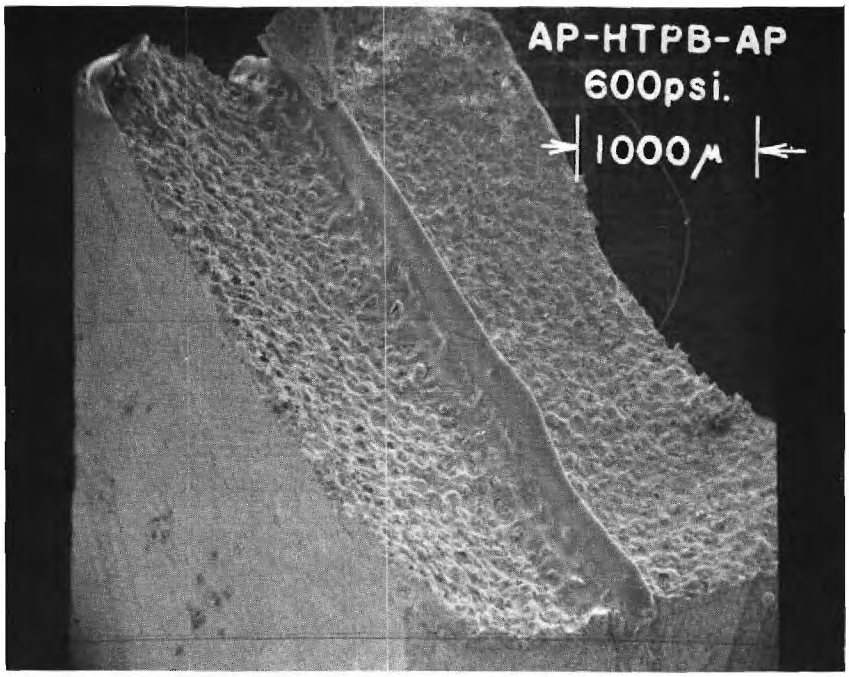

Figure III-1. AP-HTPB-AP 600 psia (x24.3).

Figure III-2. AP-HTPB 600 psia (x121).

Table III-1

Summary of Results from Scanning Electron Microscopy of Uncatalyzed Composite Solid Propellant Sandwiches

Pressure psia	Figure No. III-	Binder Melt Flow μm	Binder Height μm
600	1,2	140	300
1000	3,4,5,6	150	450
1500	7,8,9,10	200	400
2000	11,12,13	350	500

the interface. This flow has retarded the oxidizer regression rate causing the point of maximum regression to be well into the oxidizer layer. The binder height is approximately 300 μm. There is a continuous slope at the binder-oxidizer interface. There is no significant visible edge cooling effect shown by the sample.

1000 psia. Figures III-3 through 6 -- The entire oxidizer surface is covered with ridges and valleys of uniform density. The binder melt flow extends 150 μm over the oxidizer surface. The binder height is 450 μm. There is a continuous slope at the binder oxidizer interface and the point of maximum sandwich regression is at the mid point of the oxidizer layer. Note that in Figure III-6 the cracks in the binder melt flow reveal a porous AP structure. This flow is approximately one μm thick.

1500 psia. Figures III-7 through 10 -- The density of the ridges and valleys has decreased. The distribution of these ridges and valleys is

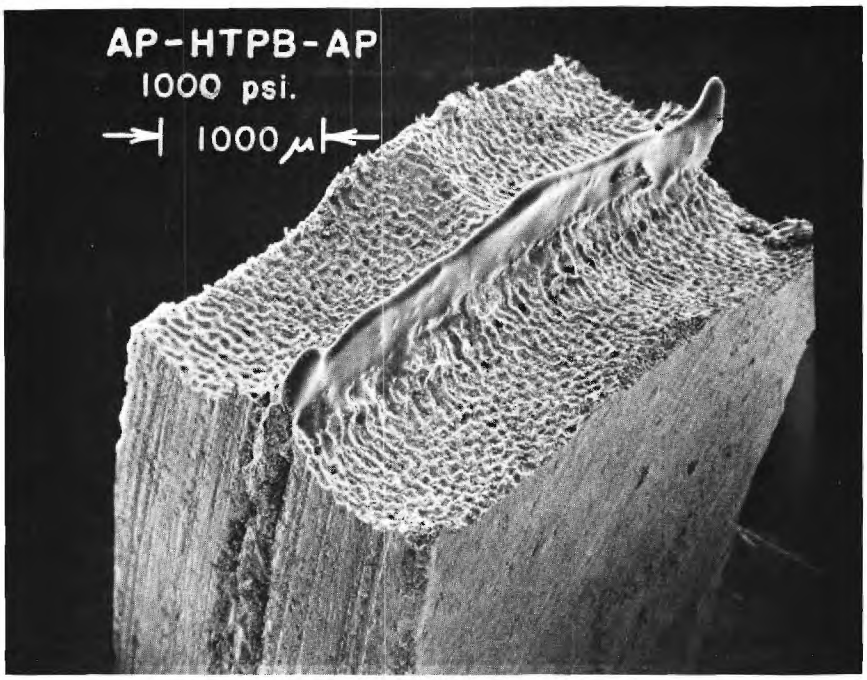

Figure III-3. AP-HTPB-AP 1000 psia (x21.2).

Figure III-4. AP-HTPB 1000 psia (x106).

Figure III-5. AP-HTPB 1000 psia (x110).

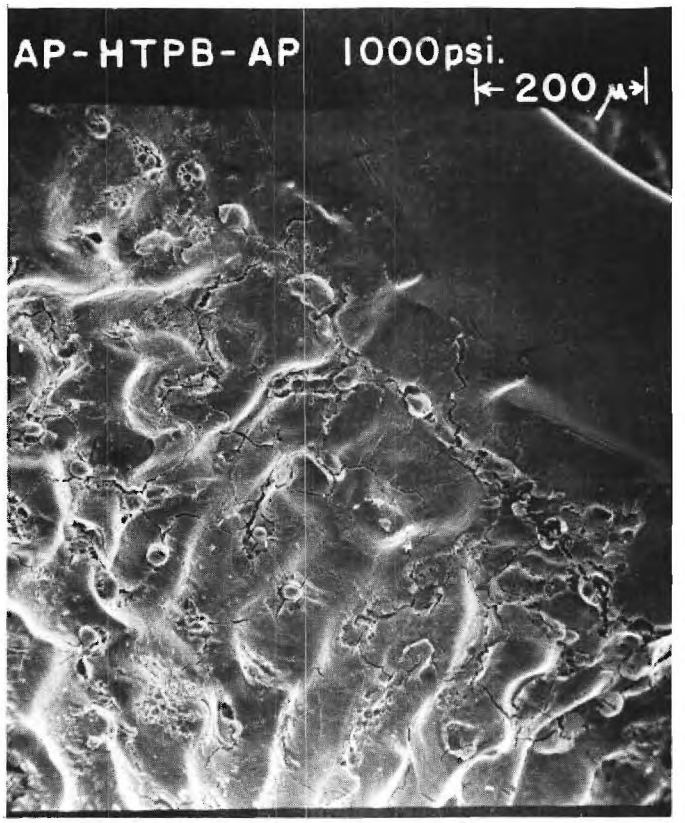

Figure III-6. AP-HTPB 1000 psia (x510).

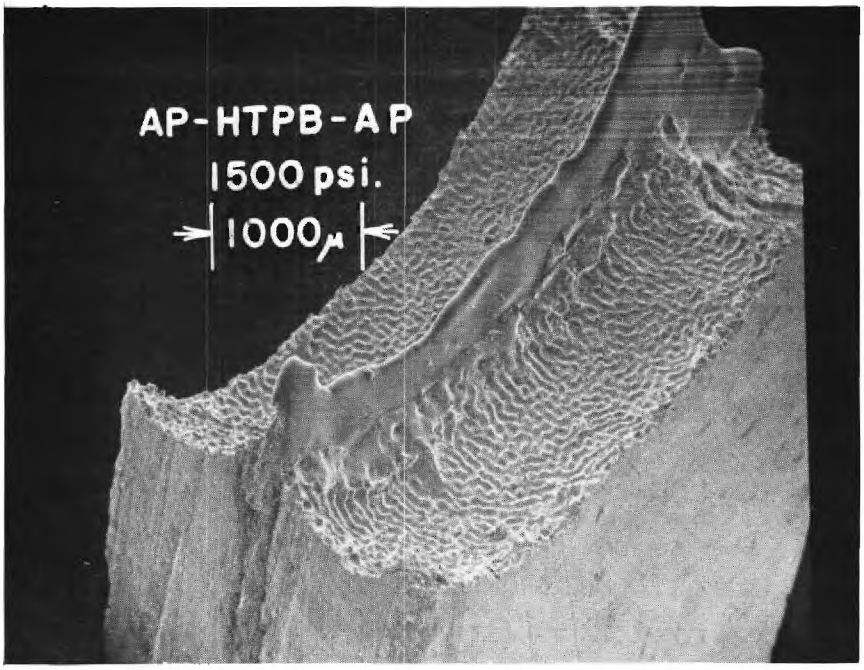

Figure III-7. AP-HTPB-AP 1500 psia (x20.8).

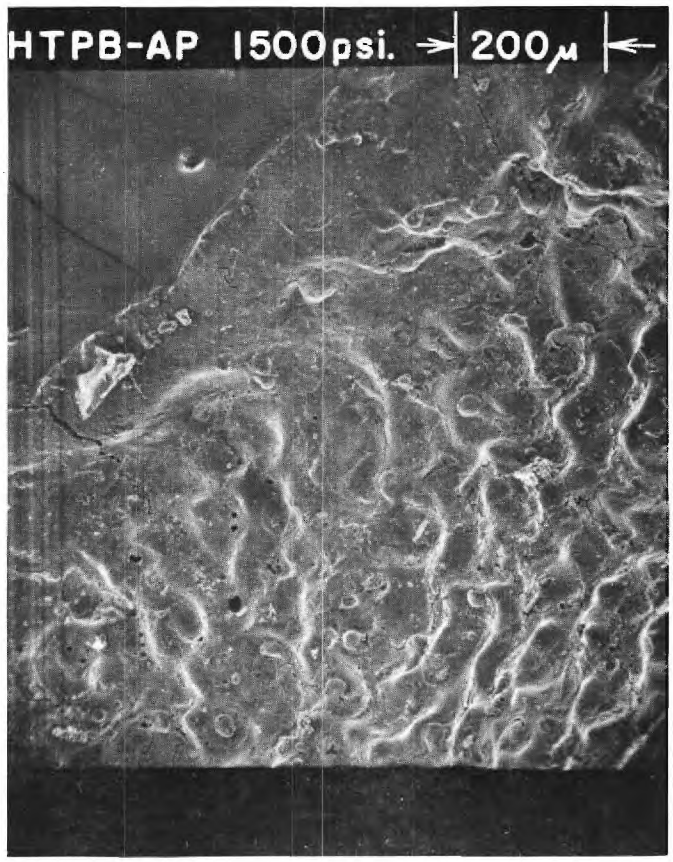

Figure III-8. HTPB-AP 1500 psia (x102).

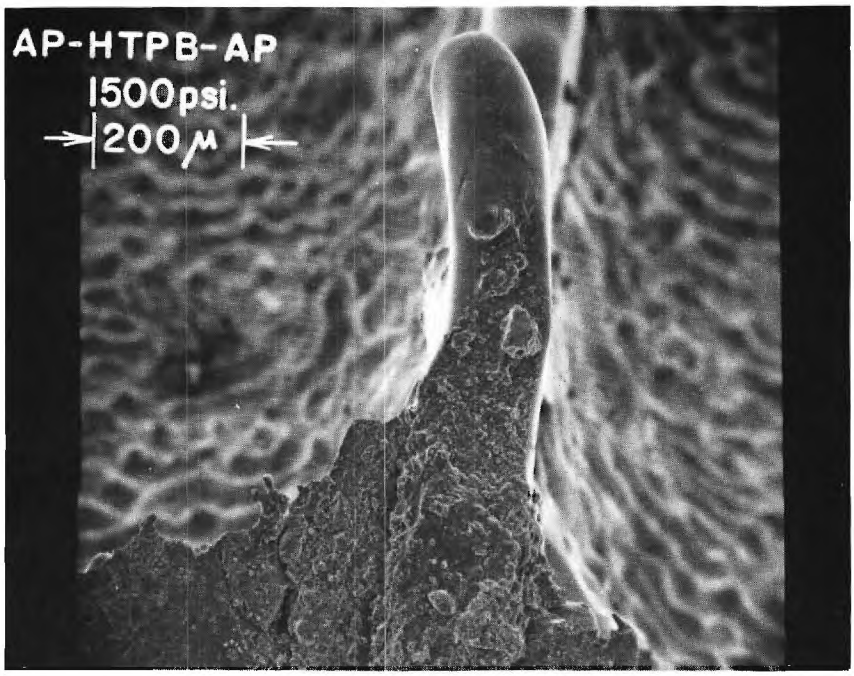

Figure III-9. AP-HTPB-AP 1500 psia (x102).

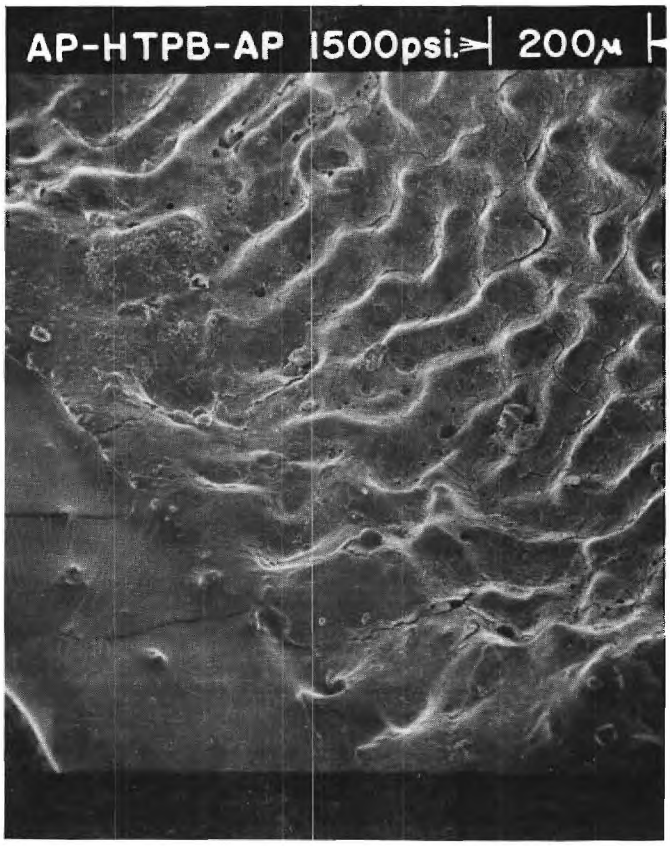

Figure III-10. HTPB-AP 1500 psia (x106).

uniform over the entire AP surface. The binder melt flow extends 200 μm over the oxidizer surface. The binder height is 400 μm. There is a continuous slope at the binder-oxidizer interface and the point of maximum regression has been displaced further from the interface than at lower pressures.

2000 psia. Figures III-11 through 13 -- The surface is still covered with ridges and valleys but in several areas a region of hemispherical protrusions with radii of 50 μm were observed. The binder melt flow is more irregular. It extends up to 350 μm onto the AP in some areas and is non-existent in other areas. The binder height is 500 μm. The location of the point of maximum regression varies with the binder melt flow. At one section it is located near the interface while at another section it has moved to the free edge of the oxidizer. There is also some indication of an edge cooling effect at one free edge, but it is not uniform and none was observed with the previous three samples. Therefore retardation of oxidizer burning rates near the free edges due to cooling effects has been considered unimportant.

In summary, for the pure AP-HTPB sandwiches, it can be said that as the pressure increases the mean surface irregularities increase, the binder height increases, the binder melt flow does exist and it's extent tends to increase. The point of maximum regression is always in the oxidizer and tends to move away from the binder as the pressure increases. There is no substantial cooling effect noted. These observations are in accord with the results of Boggs and Zurn.

Catalysts in the Oxidizer

The following section is devoted to a discussion of the electron

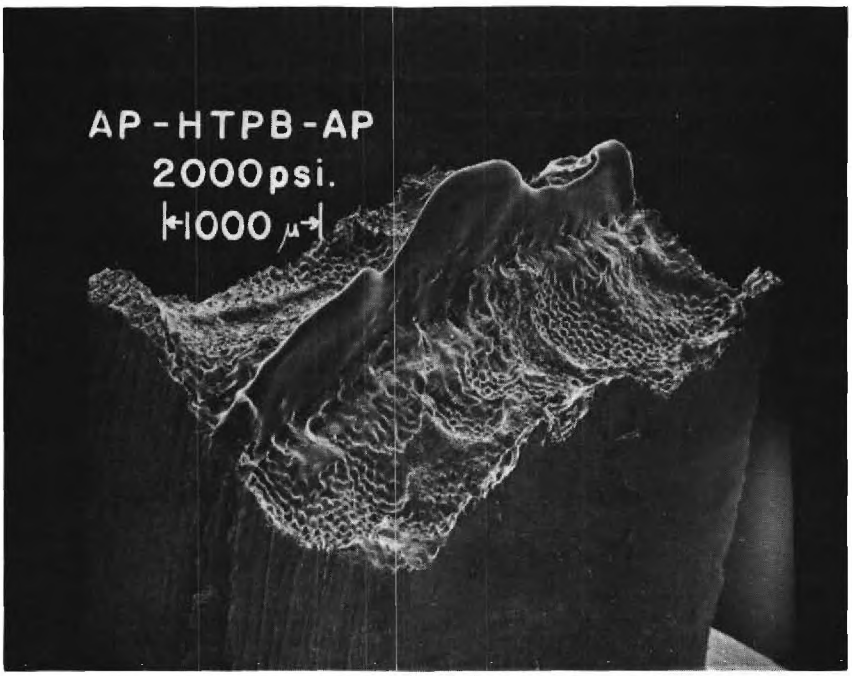

Figure III-11. AP-HTPB-AP 2000 psia (x20.4).

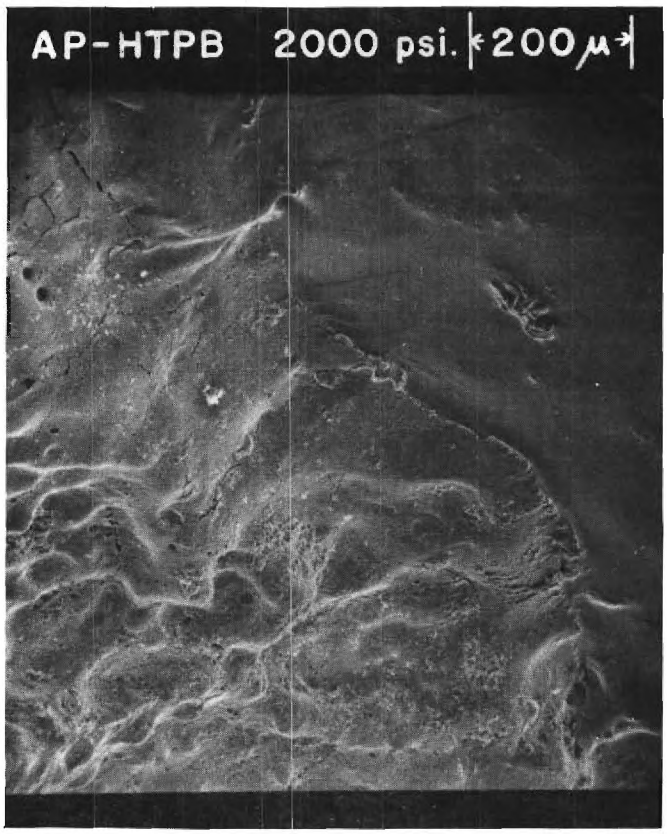

Figure III-12. A-HTPB 2000 psia (x106).

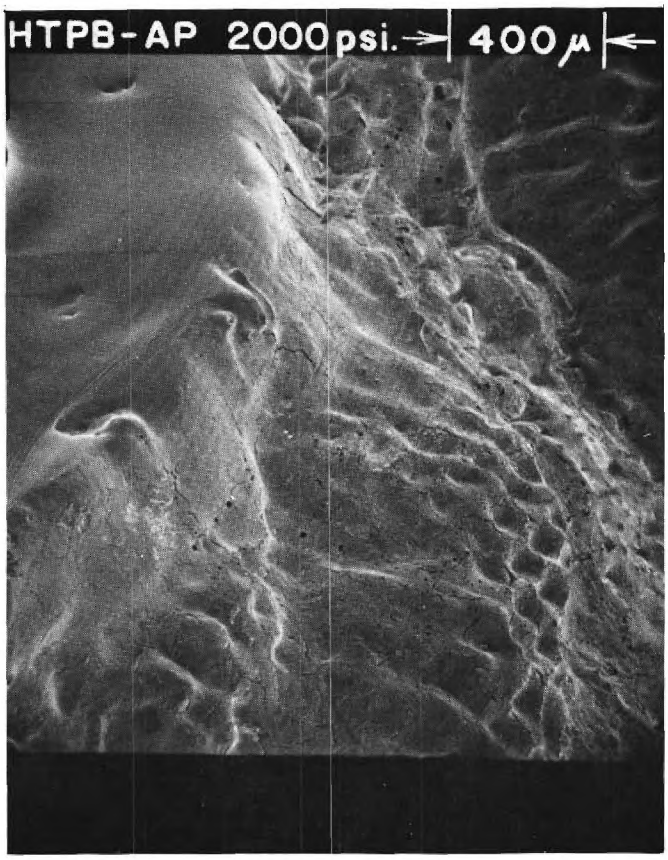

Figure III-13. HTPB-AP 2000 psia (x102).

micrographs from the samples containing the catalyst in the ammonium perchlorate. They were compared to each other and to the pure sandwiches just discussed. The micrographs are included in Figures III-14 through 52. These micrographs cover 13 samples and they are summarized in Table III-2.

Table III-2

Summary of Results from Scanning Electron Microscopy of Composite Solid Propellant Sandwiches with Catalyst in the Oxidizer

Catalyst	Location	Pressure psia	Figure No. III-	Binder Melt Flow μm	Binder-Oxidizer Interface Slope
CuO202(CC)	in AP	600	14,15	30	continuous
		1000	16,17,18	25-50	sections continuous
		1500	19,20	10-40	sections continuous
		2000	21,22	25	nearly discontinuous
Ferric Oxide (IO)	in AP	600	23,24,25	60-80	nearly discontinuous
		1000	26,27,28	none	discontinuous
		1500	29,30,31	<50	double dip
		2000	32,33,34	<25	double dip
Ferrocene (F)	in AP	600	35,36, 37,38	50	continuous
		1000	39,40	60	continuous
		1500	41,42,43	<50	continuous
		2000	44,45	<40	continuous
Iron Blue (IB)	in AP	600	35,46	<30	continuous
		1000	39,47,48	<10	continuous
		1500	41,49,50	30	continuous
		2000	51,52	none	slight undercutting or sag

AP and CC - HTPB.

600 psia. Figures III-14 and 15 -- The surface of the ammonium perchlorate with 2% by weight of CC is relatively smooth and uniform. There is a porous structure of holes of diameter less than 4 μm. The oxidizer surface with catalyst has a slope of between 40° and 48°. There is a slight binder melt flow over the oxidizer surface of 30 μm. The maximum regression is in the oxidizer. Some particles have been deposited on the binder, probably during the quench process.

1000 psia. Figures III-16 through 18 -- The surface of the oxidizer with catalyst resembles the 600 psia sample. The slope of this surface lies between 40° and 45°. It does not appear to be as steep as the previous case. The binder melt flow varies from 25 to 50 μm. There is a continuous slope at the interface at specific locations as shown in Figure III-18. The maximum regression point appears to be at the edge of the binder melt flow.

1500 psia. Figures 19 and 20 -- The surface of the oxidizer with catalyst continues to be relatively smooth. The slope of this surface is almost 49°. The binder melt flow has been reduced to between 10 μm and 40 μm. Again, the slope at the interface is continuous at specific locations where the binder melt flow is the most extensive.

2000 psia. Figures 21 and 22 -- The surface of the oxidizer with catalyst is relatively smooth and the slope of this surface has increased to 64°. The melt flow appears to extend approximately 25 μm. The maximum regression point occurs within 25 μ of the interface.

These four samples were very consistent; the AP with 2% by weight of CC exhibited a relatively smooth surface for the four pressures. The slope of

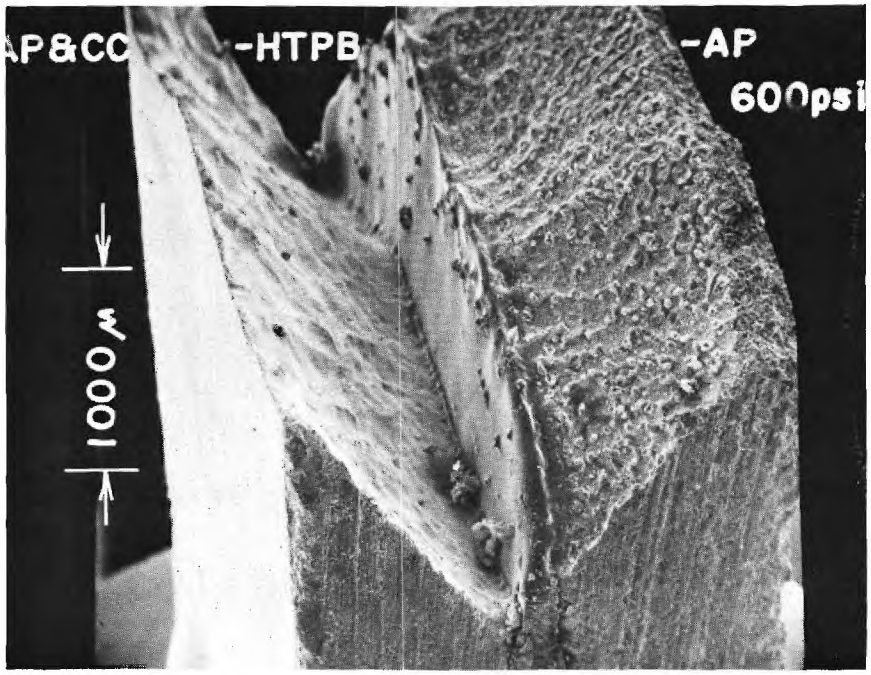

Figure III-14. AP and Cu0202(CC)-HTPB-AP 600 psia (x27).

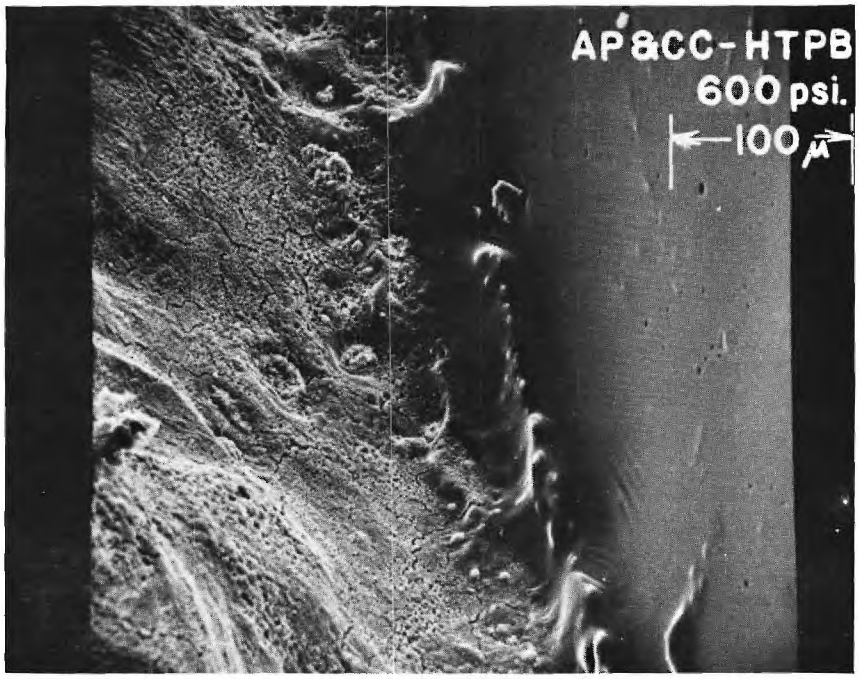

Figure III-15. AP and Cu0202(CCO-HTPB 600 psia (x240).

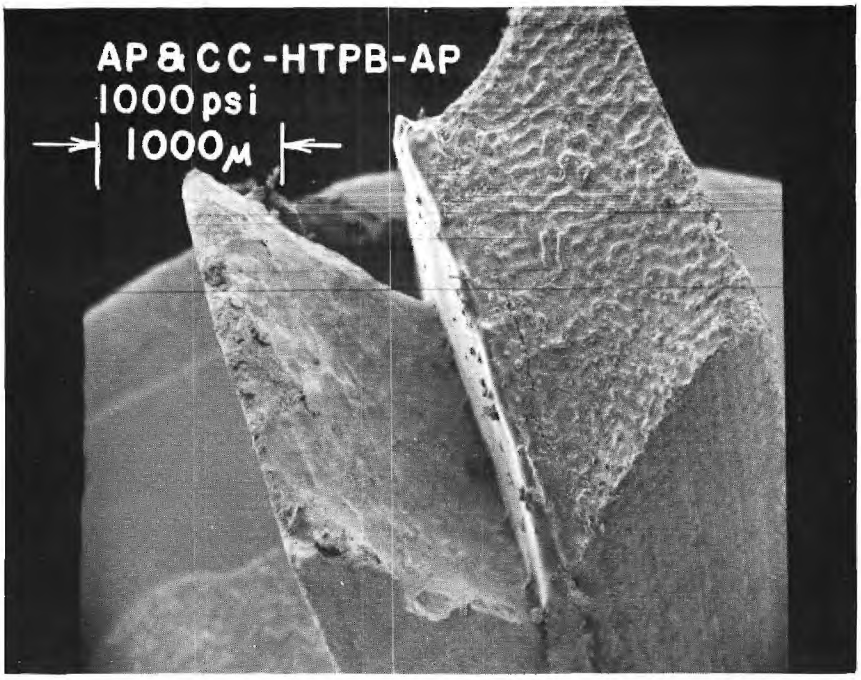

Figure III-16. AP and Cu0202(CC)-HTPB-AP 1000 psia (x24.6).

Figure III-17. HTPB-AP and Cu0202(CC) 1000 psia (x238).

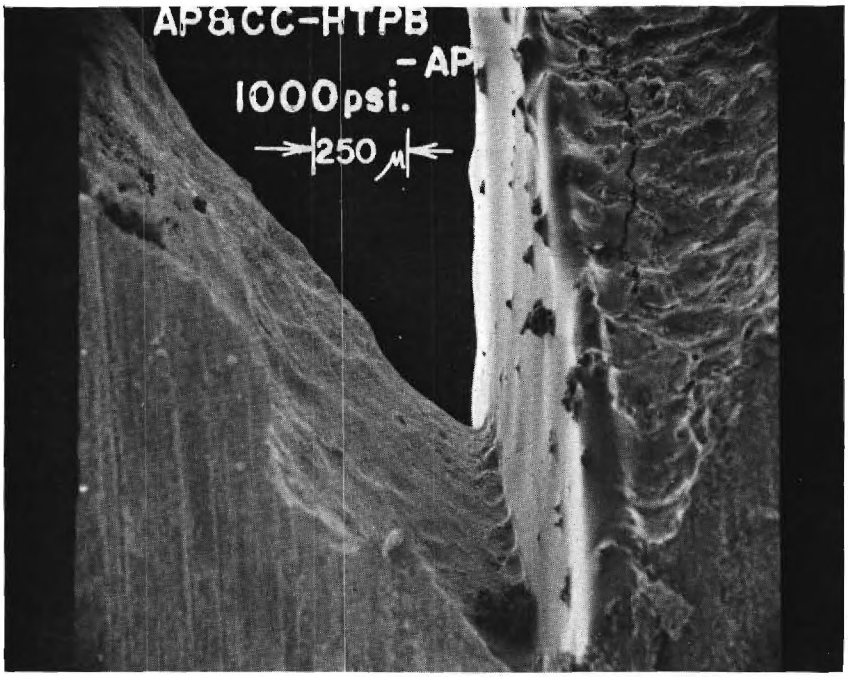

Figure III-18. AP and Cu0202 (CC)-HTPB-AP 1000 psia (x49.3).

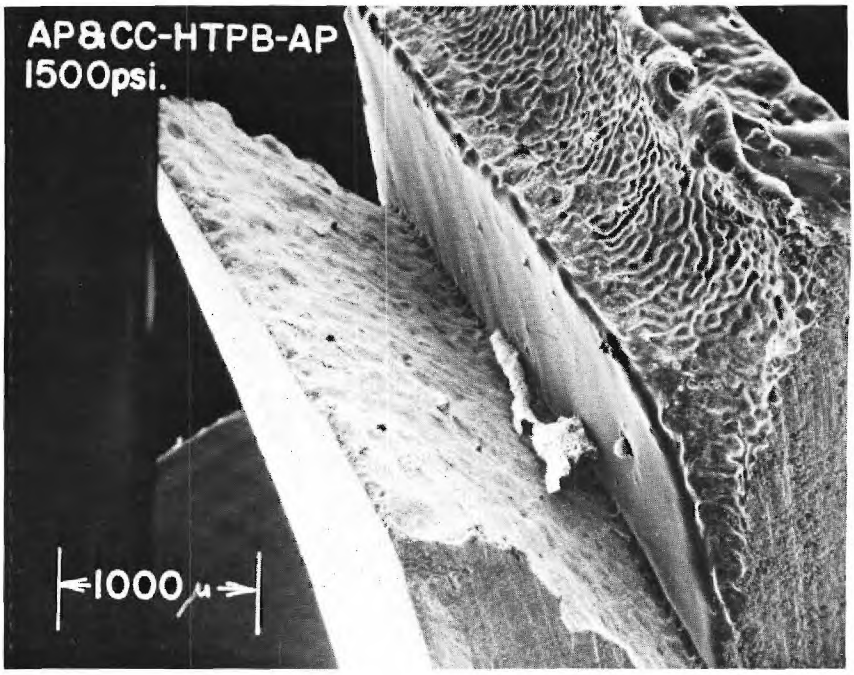

Figure III-19. AP and Cu0202 (CC)-HTPB-AP 1500 psia (x26.5).

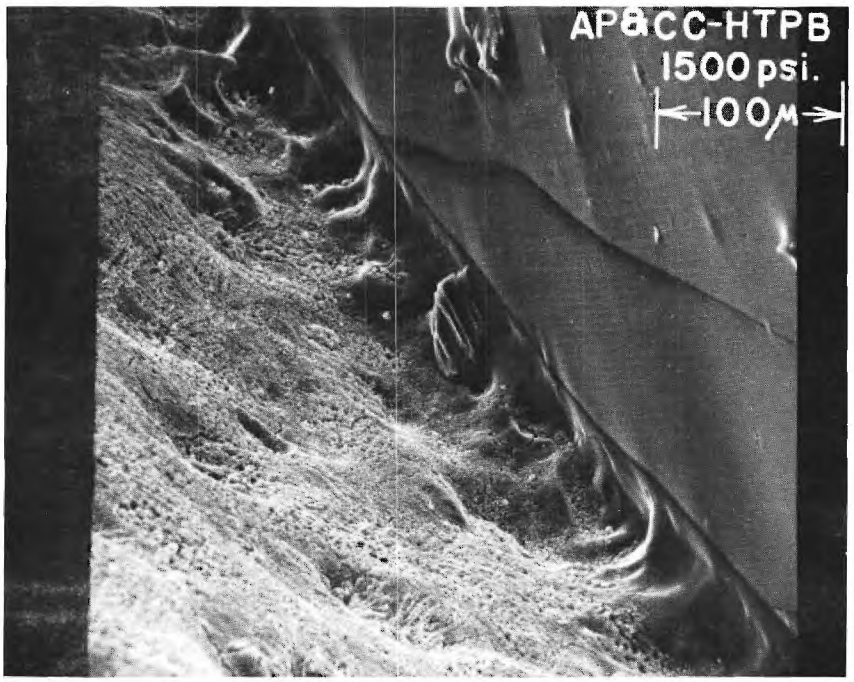

Figure III-20. AP and Cu0202 (CC)-HTPB 1500 psia (x250).

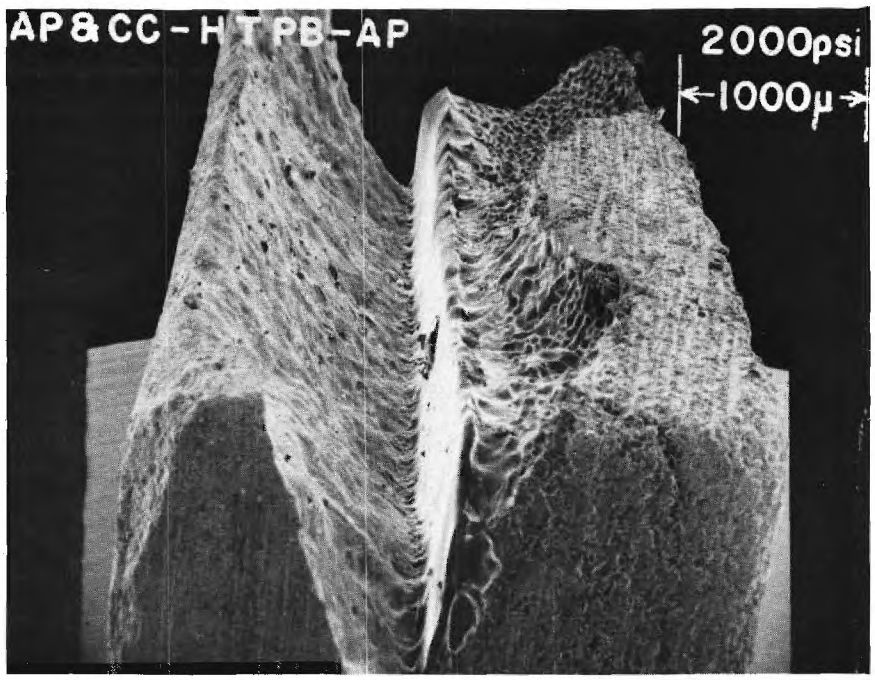

Figure III-21. AP and Cu0202 (CC)-HTPB-AP 2000 psia (x25).

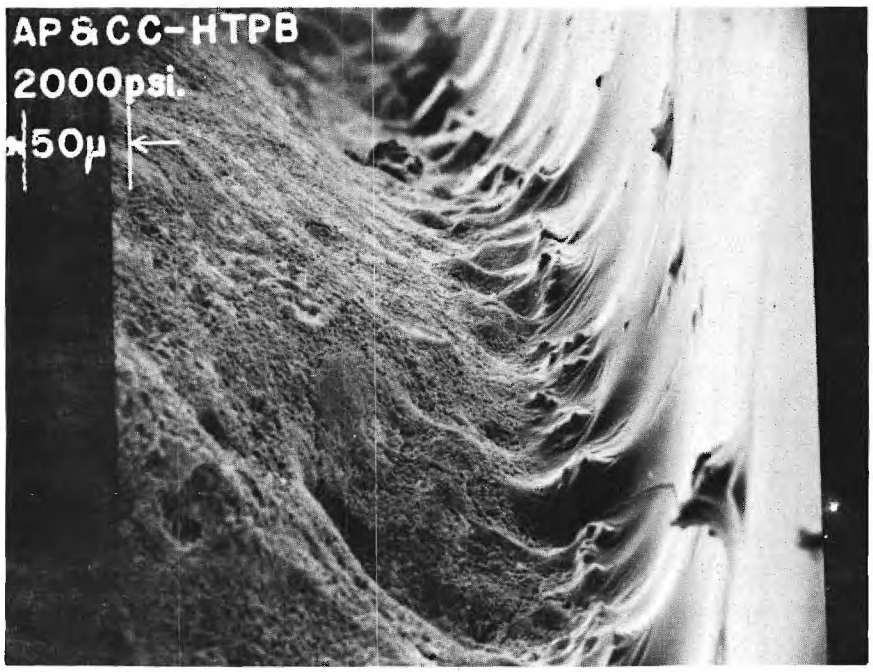

Figure III-22. AP and Cu0202 (CC)-HTPB 2000 psia (x280).

the oxidizer with catalyst surface appears to increase as the pressure increases. This was inconsistent with the results obtained from cinephotomacrography. The surface slope decreased as the pressure increased from 50° to 20°. There is a virtual discontinuity in slope at the interface, but the leading edge of regression, while appearing to be at the binder-oxidizer interface, is actually displaced outward by the slight melt flow.

AP and IO - HTPB.

600 psia. Figures III-23 through 25 -- The surface of the oxidizer, AP with 2% by weight of IO, consists of a smooth background with flakes of approximately 50 μm in diameter scattered over the entire surface. This flake structure is also visible on the solidified binder. There is a mild slant at the binder-oxidizer interface with evidence of retardation of the oxidizer at this interface due to a binder melt flow of 60 to 80 μm. There is a slope discontinuity indicated at this interface in Figures III-24 and 25.

1000 psia. Figures III-26 through 38 -- The flake structure is observed on the oxidizer surface. The size of individual particles has increased slightly to 60-100 μm. The structure of these flakes seems to be small petaloid structures of 10 μm diameter. The background oxidizer is still relatively smooth. There was no obvious binder melt flow. The maximum regression appears to be at the binder oxidizer interface where there is a definite discontinuity in slope.

1500 psia. Figures III-29 through 31 -- The entire oxidizer surface has been covered with a layer of particles probably related to a further coalescing of the flake structure observed at lower pressures. There are large cracks in this coating and sections missing, probably

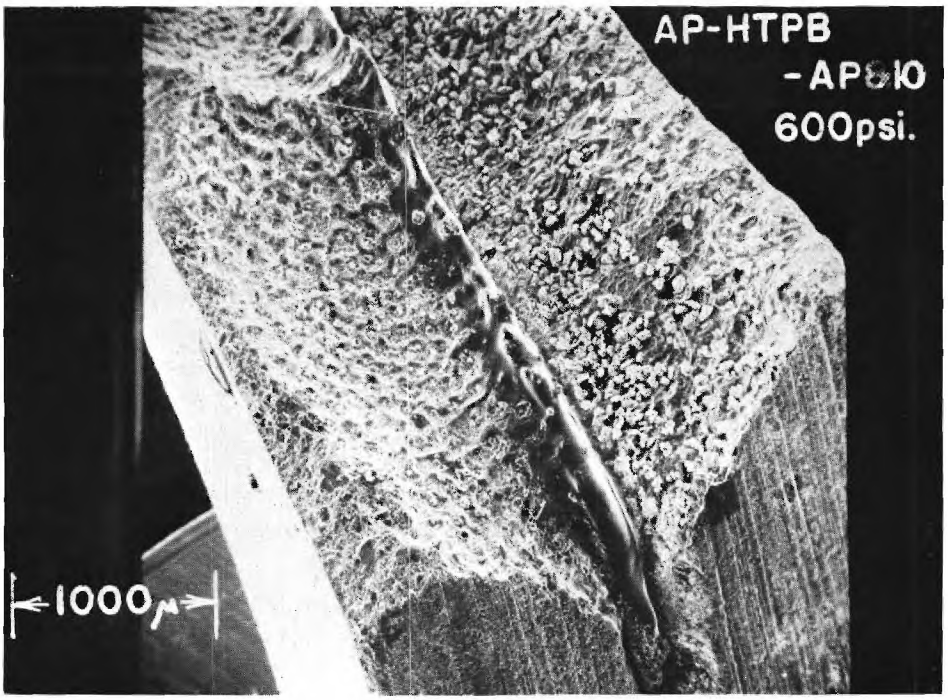

Figure III-23. AP-HTPB-AP and Ferric Oxide (IO) 600 psia (x27).

Figure III-24. HTPB-AP and Ferric Oxide (IO) 600 psia (x260).

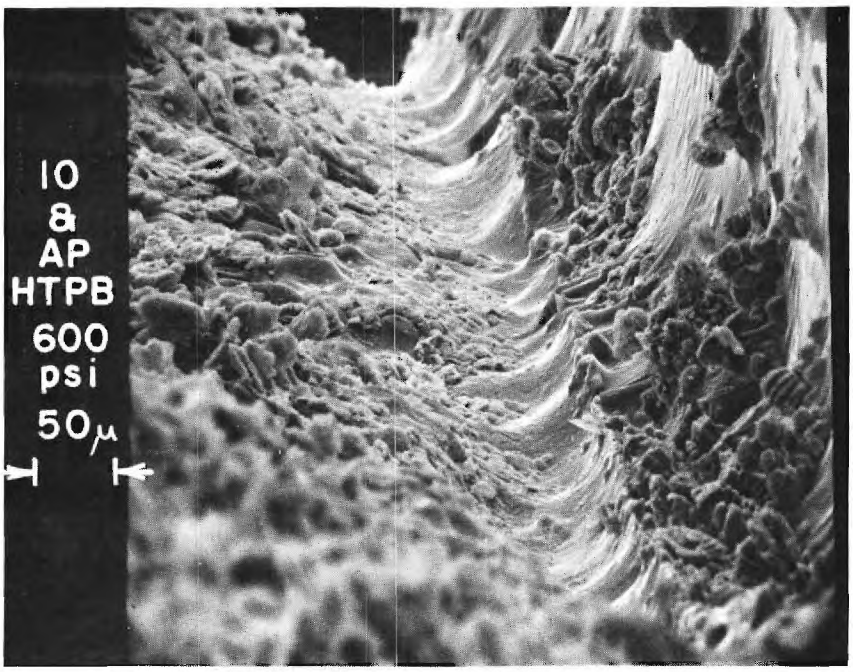

Figure III-25. AP and Ferric Oxide (IO)-HTPB 600 psia (x220).

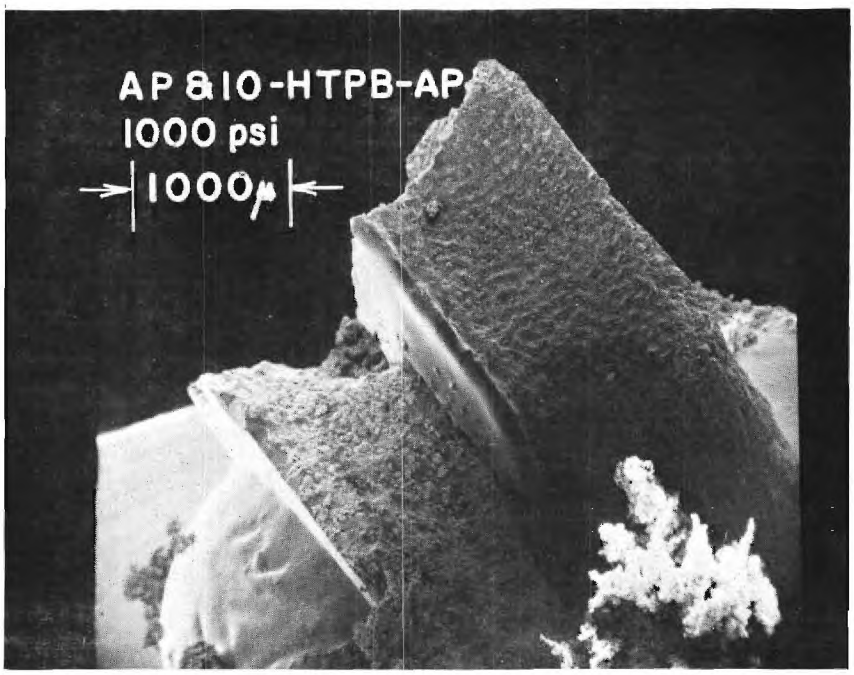

Figure III-26. AP and Ferric Oxide (IO)-HTPB-AP 1000 psia (x21.2).

Figure III-27. AP and Ferric Oxide (IO)-HTPB 1000 psia (x204).

Figure III-28. HTPB-AP and Ferric Oxide (IO) 1000 psia (x204).

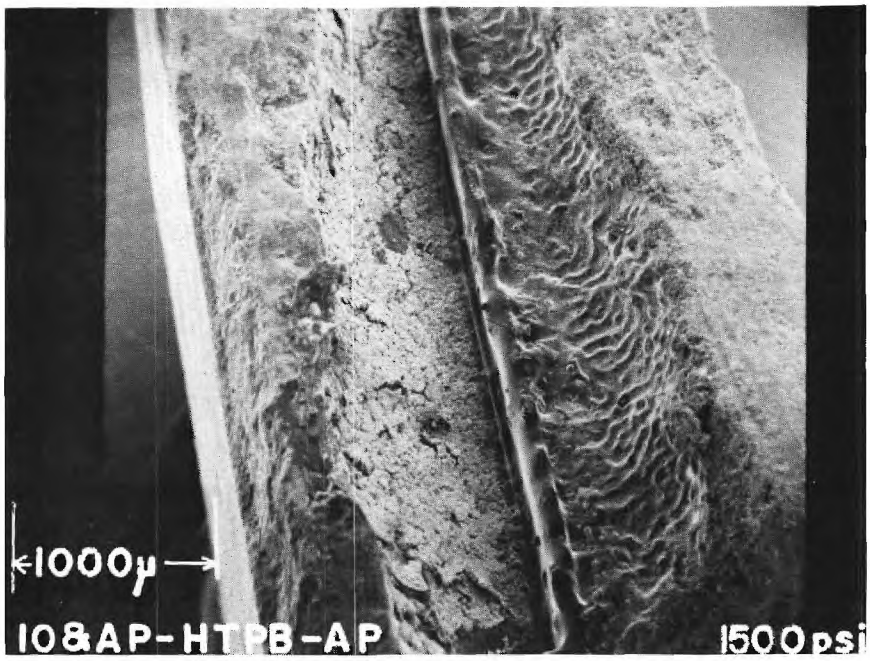

Figure III-29. AP and Ferric Oxide (IO)-HTPB-AP 1500 psia (x27).

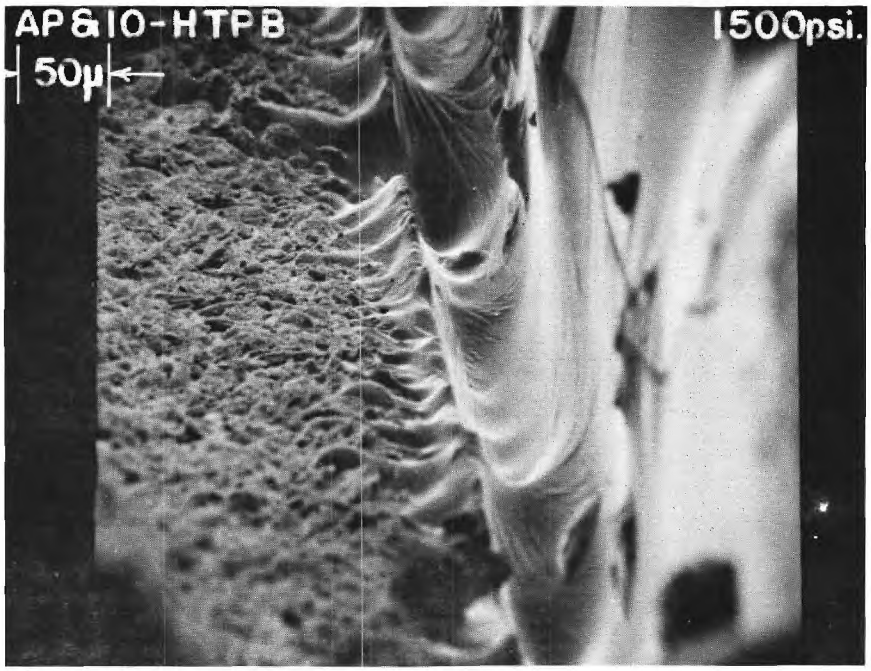

Figure III-30. AP and Ferric Oxide (IO)-HTPB 1500 psia (x240).

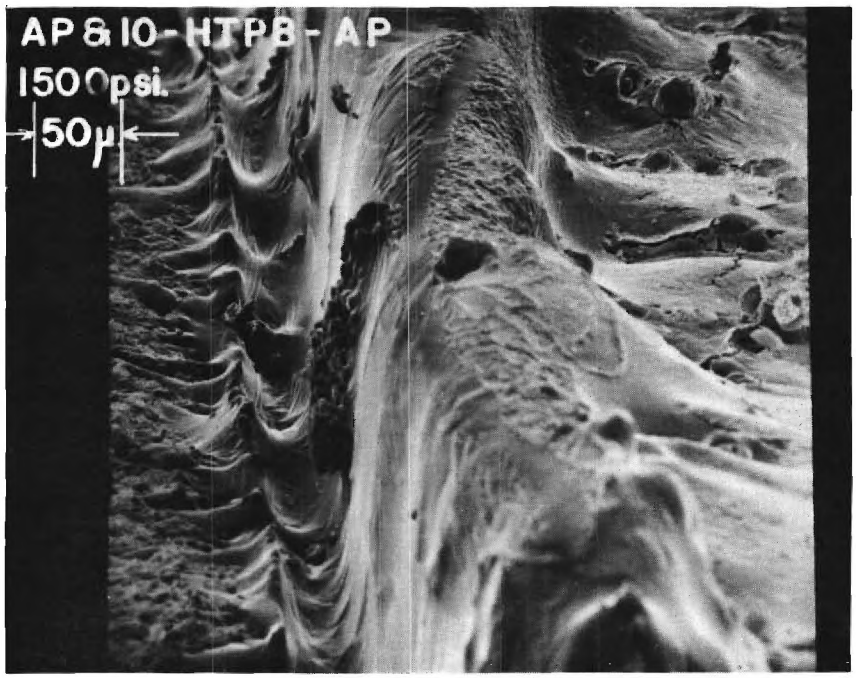

Figure III-31. AP and Ferric Oxide (IO)-HTPB-AP 1500 psia (x230).

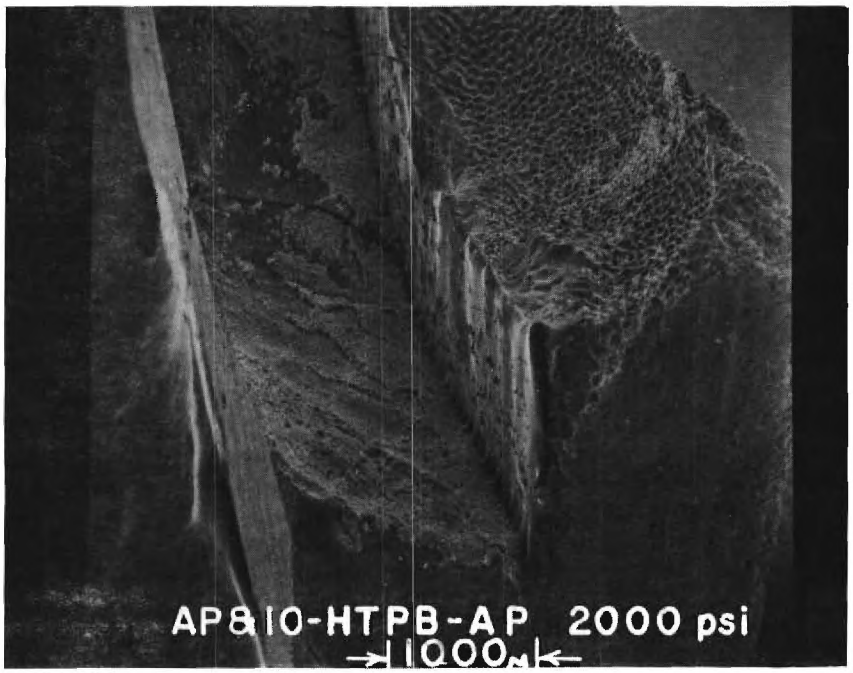

Figure III-32. AP and Ferric Oxide (IO)-HTPB-AP 2000 psia (x19.6).

removed by the rapid depressurization. There is an indication of a binder melt flow of less than 50 μm with a definite cusp or double dip of the binder surface visible in Figures III-30 and 31. Molten binder could be ejected during the quench process to form this double dip.

2000 psia. Figures III-32 through 34 -- Again the entire oxidizer surface has been covered with a definite crust-like structure. This has no resemblance to the flakes observed at lower pressures. The difference is easily seen in Figure III-34. The surface where the crust has been removed is similar to the background surface observed at lower pressures in Figures III-24 and 28. Large sections of this crust have been removed, probably in the quench process. The binder melt flow is intermittent and less than 25 μm in extent when it occurs. Again there is a relative maximum of the binder height giving the appearance of a cusp at the binder oxidizer interface. The leading edge of regression appears to be located at the binder-oxidizer interface or slightly into the binder; however, the latter possibility is doubtful.

There is a definite similarity of the background surface of the AP and IO for all pressures. From the cinephotomacrography for this series of experiments, the formation of a large scale frothy structure was indicated. The formation of this froth increased as the pressure increased. Sections of this structure can be observed to break off as the sample continues to burn. The flakes and the crust of the quenched samples are the only remnants of this frothy structure. The binder-oxidizer interface slope is not continuous and the slope of the oxidizer surface is similar for all pressures. This was not consistent with the cinephotomacrography results. The sample slopes varied from 55° to 60° at 600 psia to 20° at 2000 psia in the movies.

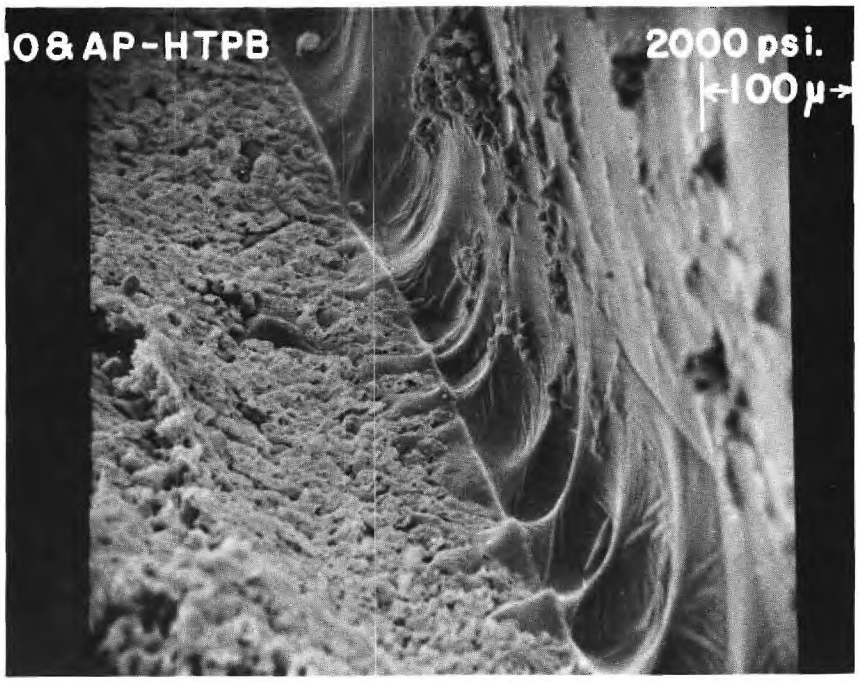

Figure III-33. AP and Ferric Oxide (IO)-HTPB 2000 psia (x195).

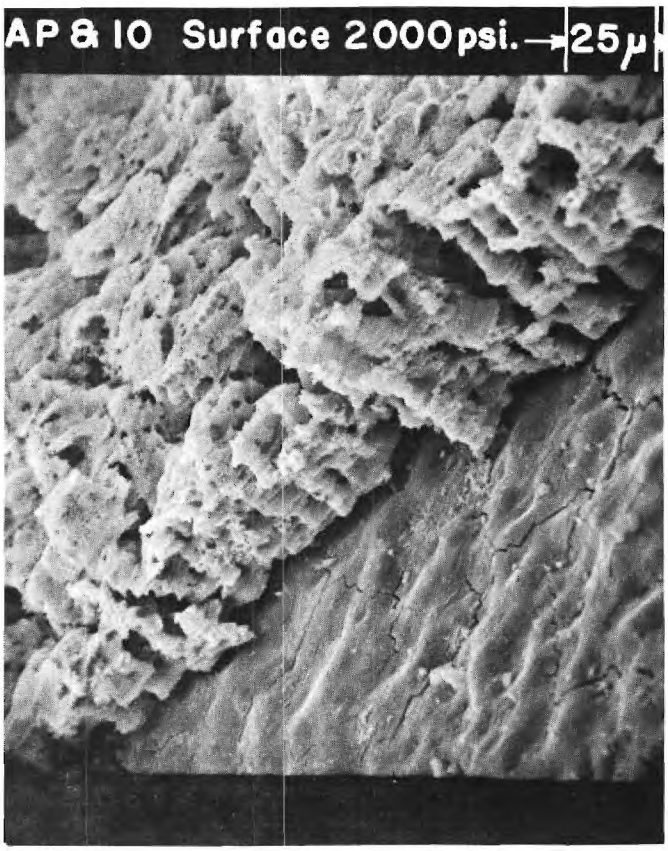

Figure III-34. AP and Ferric Oxide (IO) 2000 psia (x484).

AP and F - HTPB.

600 psia. Figures III-35 through 38 -- The surface of the oxidizer, AP with 2% by weight of F, is uneven and frothy. There is a resemblance to that of the pure AP. There appears to be a scattering of additional particles resting on the surface of the oxidizer. These particles do not appear to be in the binder melt flow. There is a definite binder flow of at least 50 μm in extent. The binder appears to sag more than in previous samples. This sag leads to the dark lines of Figures III-37 and 38.

1000 psia. Figures III-39 and 40 -- The surface continues to resemble that of pure AP with additional particles observed on the uneven surface. An optical microscopic investigation showed that these particles were red and black. The binder melt flow was 60 μm. The maximum regression is occurring at the edge of the binder melt flow. The slope is continuous at the interface.

1500 psia. Figures III-41 through 43 -- The appearance of the entire surface is slightly smoother than for the pure AP above. The ridges and valleys structure is apparent but the density of roughness is greater than with pure AP. Red and black particles again are obvious on the surface. The binder melt flow is less than 50 μm in extent; this is retarding the AP regression at the interface and displacing the point of maximum regression slightly to the oxidizer.

2000 psia. Figures III-44 and 45 -- The binder melt flow has been reduced to less than 40 μm. The oxidizer surface has lost any similarity with the pure AP case. The surface is irregular and frothy in appearance. Particles are still visible on the surface but their diameters have decreased.

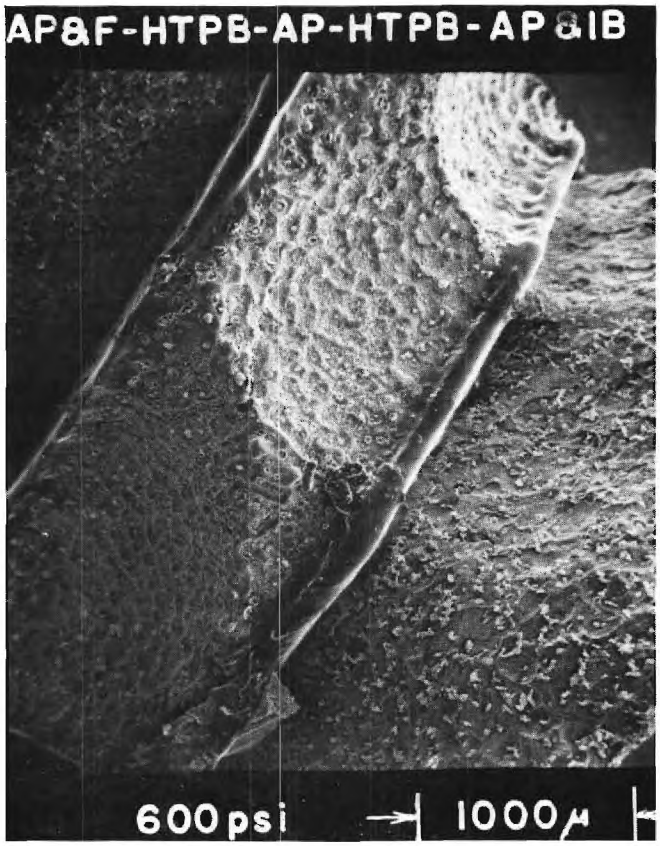

Figure III-35. AP and Ferrocene (F)-HTPB-AP-HTPB-AP and Iron Blue (IB) 600 psia (x28).

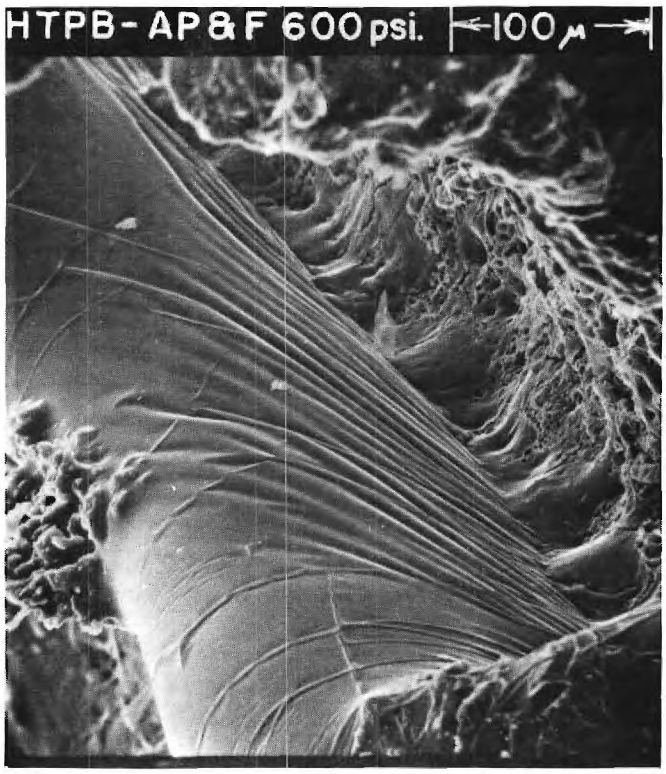

Figure III-36. HTPB-AP and Ferrocene (F) 600 psia (x262).

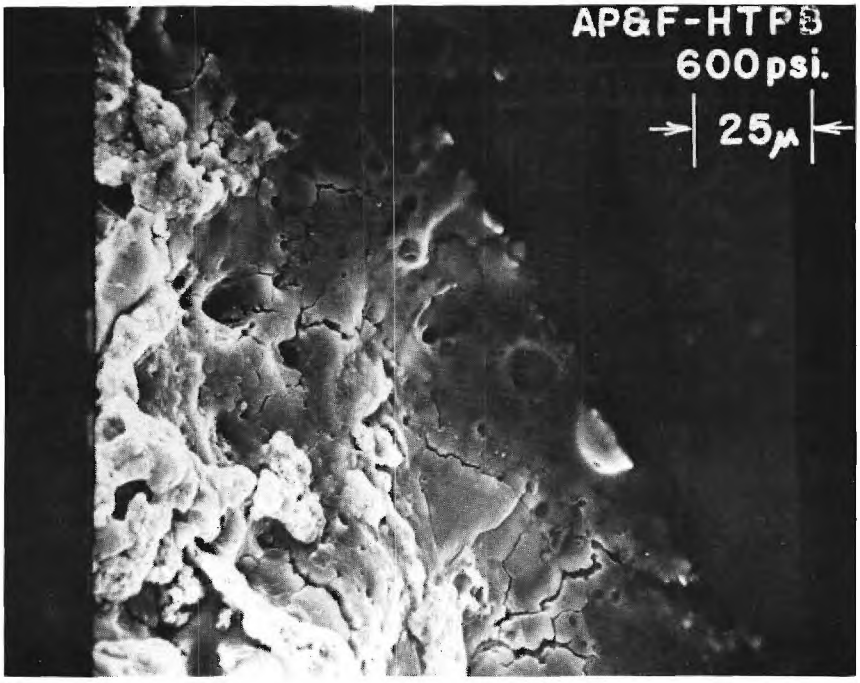

Figure III-37. AP and Ferrocene (F)-HTPB 600 psia (x650).

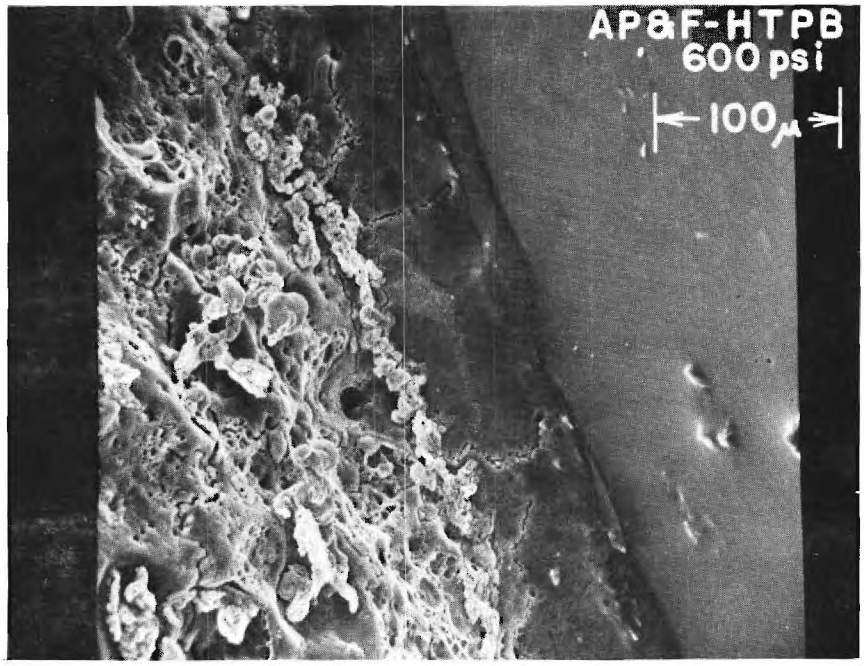

Figure III-38. AP and Ferrocene (F)-HTPB 600 psia (x250).

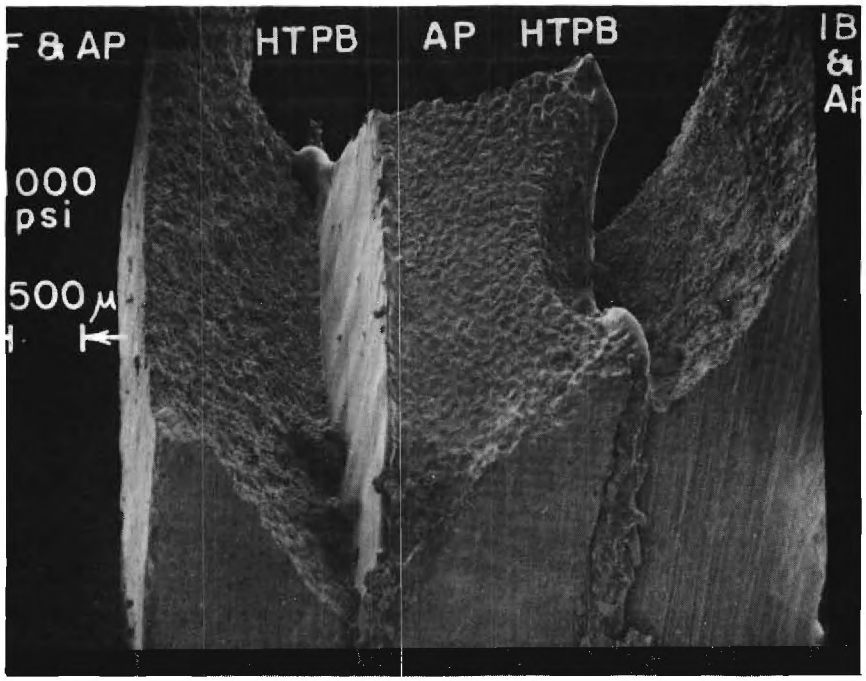

Figure III-39. AP and Ferrocene (F)-HTPB-AP-HTPB-AP and Iron Blue (IB) 1000 psia (x18.7).

Figure III-40. HTPB-AP and Ferrocene (F) 1000 psia (x221).

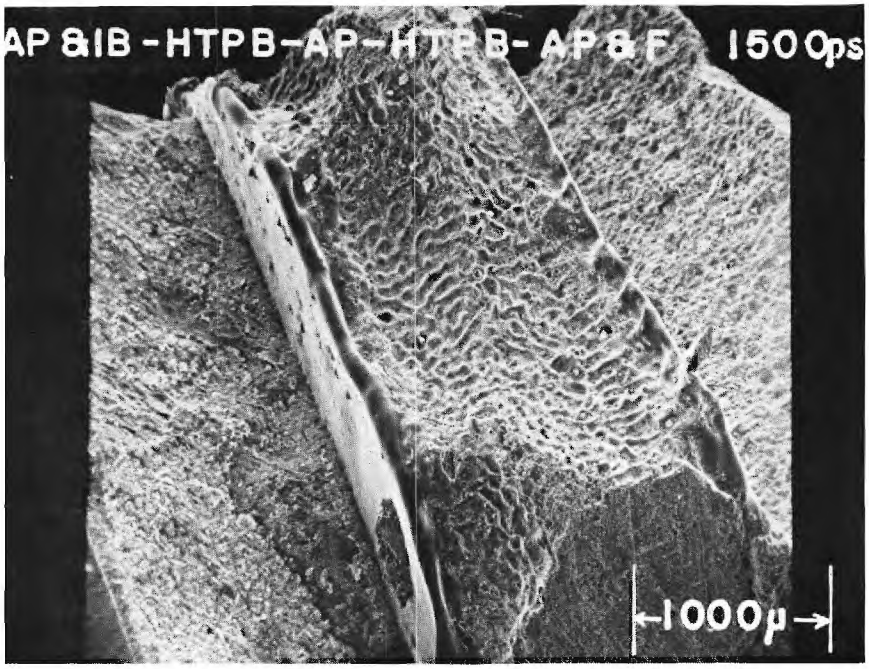

Figure III-41. AP and Iron Blue (IB)-HTPB-AP-HTPB-AP and Ferrocene (F) 1500 psia (x28.7).

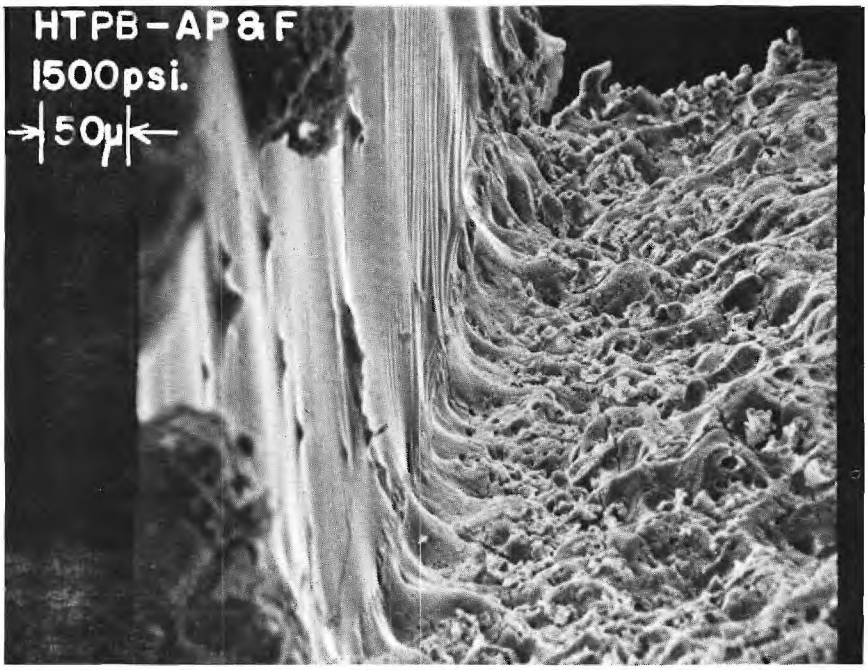

Figure III-42. HTPB-AP and Ferrocene (F) 1500 psia (x240).

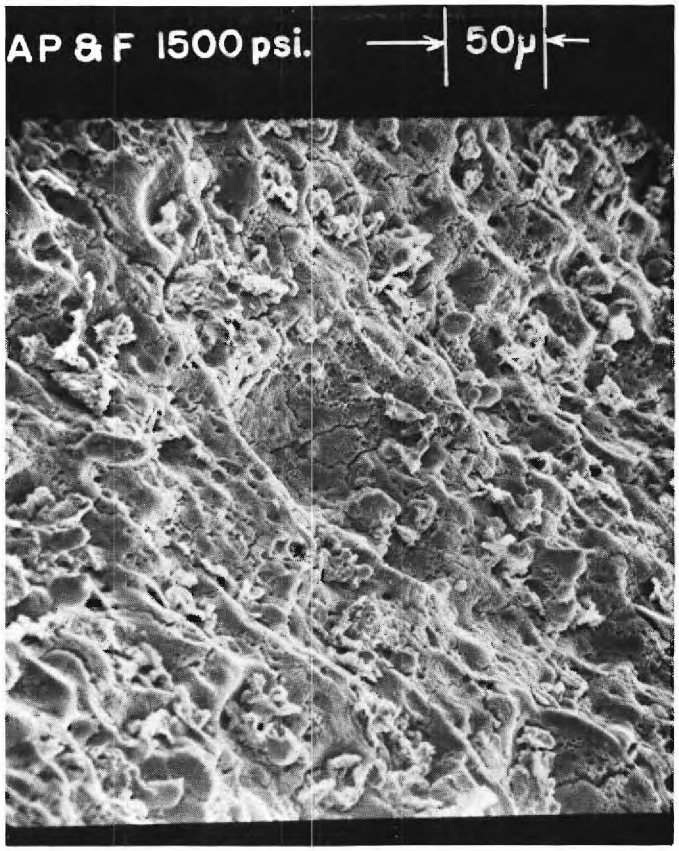

Figure III-43. AP and Ferrocene (F) 1500 psia (x260).

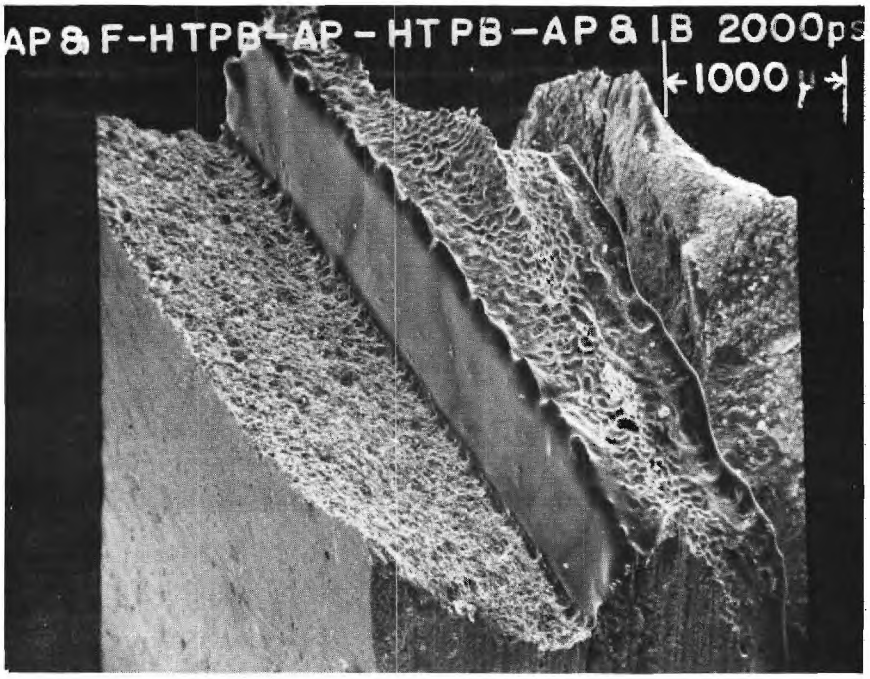

Figure III-44. AP and Ferrocene (F)-HTPB-AP-HTPB-AP and Iron Blue (IB) 2000 psia (x24.3).

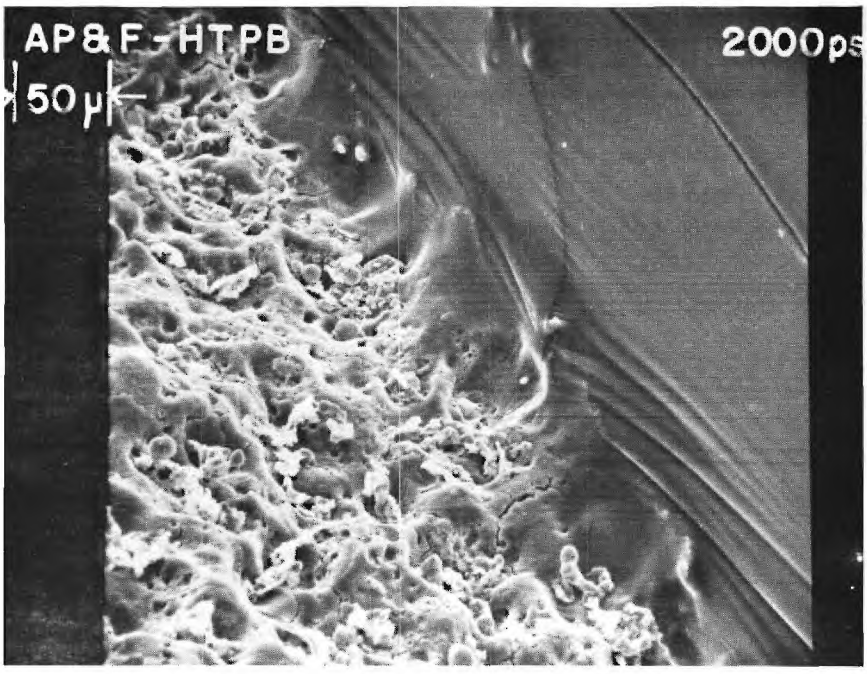

Figure III-45. AP and Ferrocene (F)-HTPB 2000 psia (x255).

There is a definite change in the surface composition for these cases as the pressure increases. Initially there seems to be little effect, while at the highest pressure the surface is completely different. The surface slope has remained essentially constant. This is in agreement with the cinephotomacrography results. The binder melt flow decreased as the pressure increased. This has allowed the point of maximum regression to be located very close to the binder-oxidizer interface at higher pressures.

AP and IB - HTPB.

600 psia. Figures III-35 and 46 -- Due to the use of triple sandwiches these micrographs are not in the proper order. The surface of the oxidizer appears to be very porous for this case. Again, particles of 20 μm diameter are visible on the surface. These appear red when viewed with the optical microscope. The binder melt flow is less than 30 μm. The slope at the binder oxidizer interface is continuous. There is indication of binder sag upon cooling.

1000 psia. Figures III-39, 47 and 48 -- The surface in this case closely resembles that of AP and F; the particles appear to be about the same size. There was a definite red residue on this sample, visible to the eye. The binder melt flow is less than 10 μm in extent. The slope is continuous at the interface and the radius of curvature of the surface is small.

1500 psia. Figures III-41, 49 and 56 -- The surface has a very porous appearance, again covered with a red residue. The binder melt flow extends up to 30 μm in sections, but is non-existent in others. The slope of the oxidizer surface has decreased as the pressure increased. There is no indication of cooling sags.

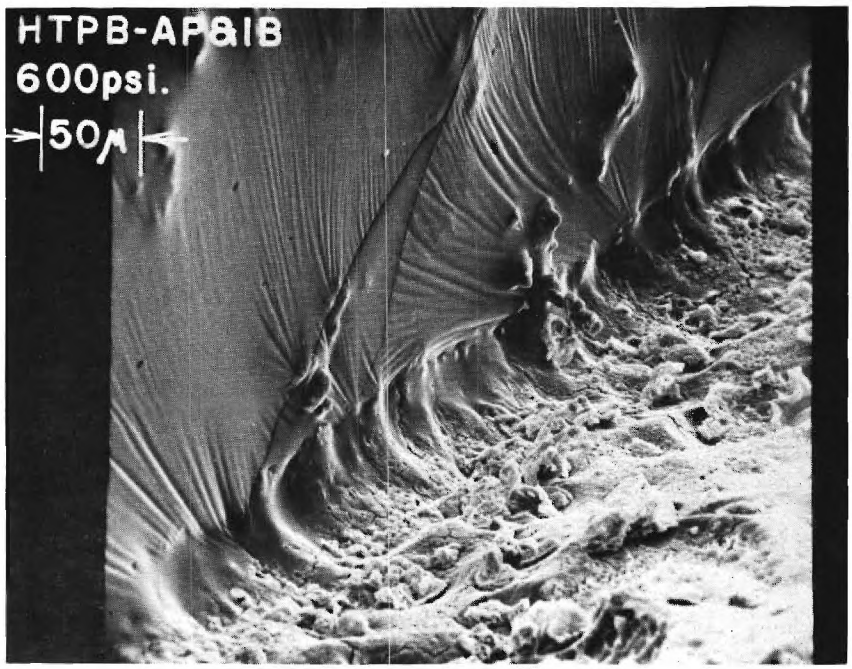

Figure III-46. HTPB-AP and Iron Blue (IB) 600 psia (x260).

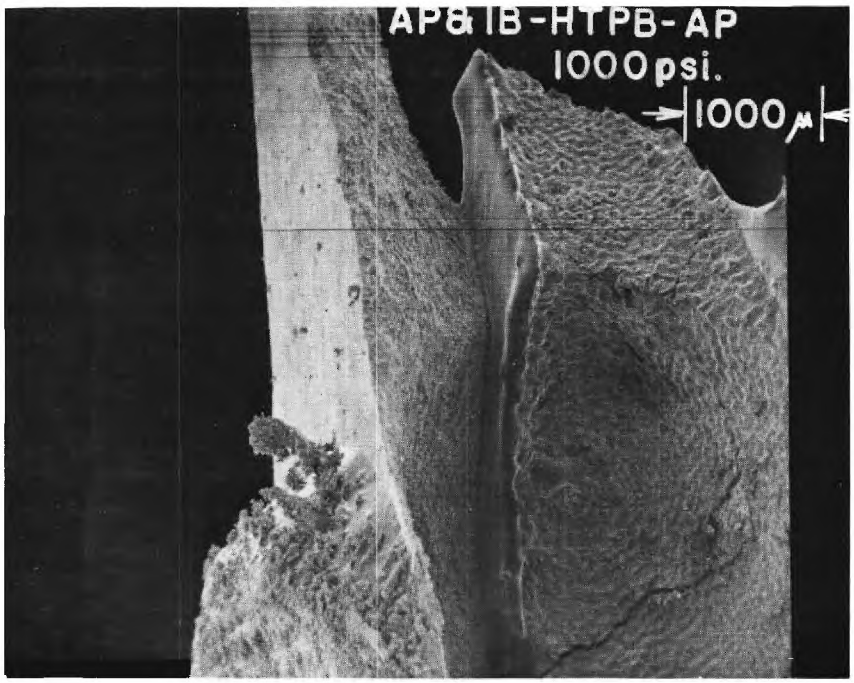

Figure III-47. AP and Iron Blue (IB)-HTPB-AP 1000 psia (x18.7).

Figure III-48. AP and Iron Blue (IB)-HTPB 1000 psia (x196).

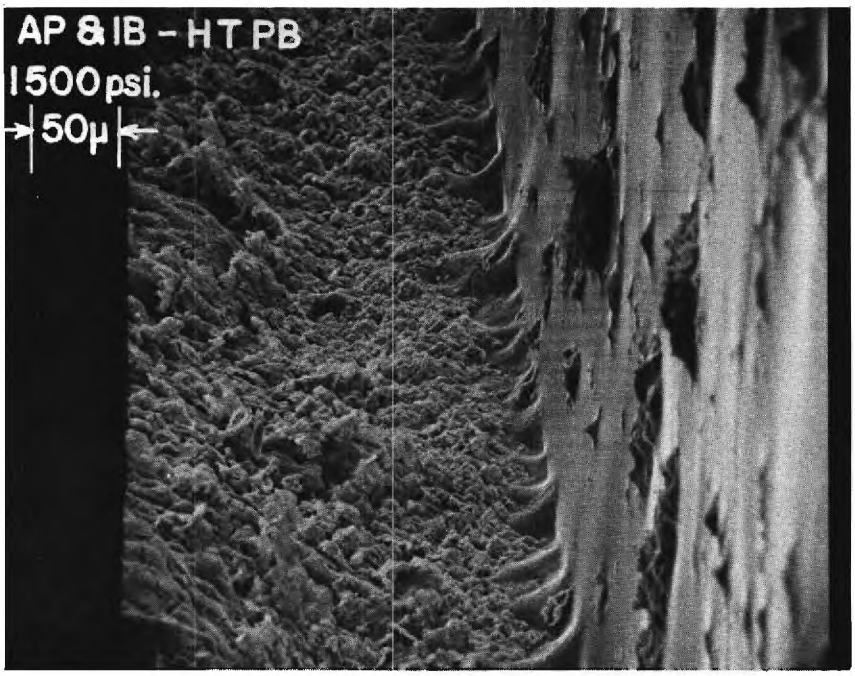

Figure III-49. AP and Iron Blue (IB)-HTPB 1500 psia (x230).

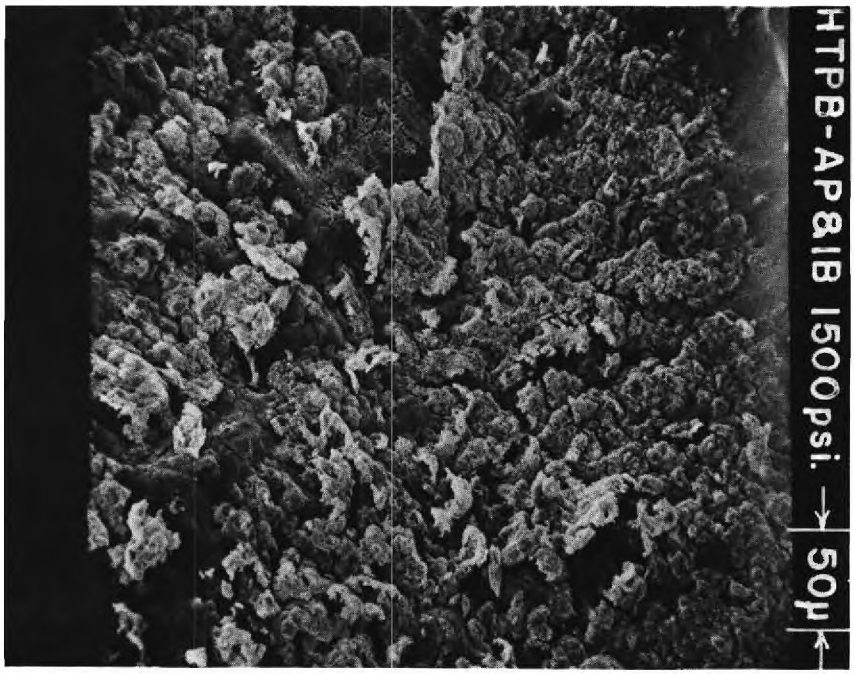

Figure III-50. AP and Iron Blue (IB-HTPB) 1500 psia (x270).

2000 psia. Figures III-51 and 52 -- The surface appears very porous with the indication of a crust coating which has been removed due to the depressurization process. There is no binder melt flow. There is considerable binder sag upon cooling with a possible indication of maximum regression in the binder. The surface slope has decreased for this case.

The surface of the AP and IB becomes smoother as the pressure increases. A surface coating of particles also increases. The slope of the surface decreases as the pressure increases and this was contrary to the cinephotomacrography results. A maximum slope of 64° was reached at 1500 psia for the movies.

Catalysts in the Binder

The following micrographs (Figures 53 through 79) show the details of the samples containing catalyst in the binder. All samples in this section were triple sandwiches allowing the comparison of two catalysts per run. A summary of these tests is given in Table III-3.

Several statements can be made which cover all four catalysts used in this phase of the investigation. There was no obvious change of the AP surface structure of these samples as compared to the pure AP-HTPB-AP sandwiches, which are used as standards of comparison. The binder melt flows are reduced or eliminated completely. The binder heights are reduced. In some cases it was impossible to determine a binder height due to the extensive sagging of the binder. The sagging and wrinkles in the solidified binder were much more noticeable in these samples. These binders seem to have higher viscosities. The binder melt flow decreased as the pressure increases. The binder-oxidizer interface slope is continuous for most

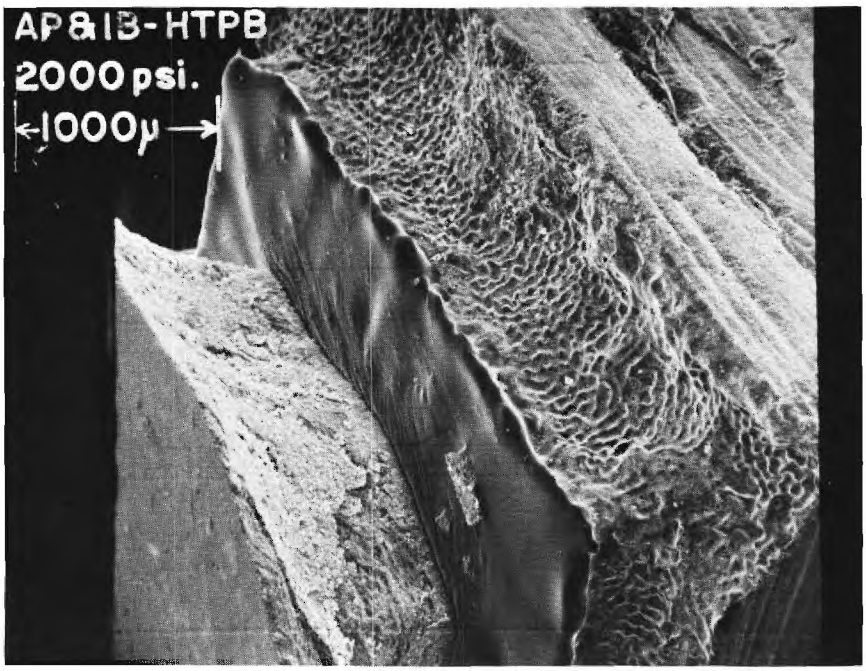

Figure III-51. AP and Iron Blue (IB)-HTPB 2000 psia (x26.5).

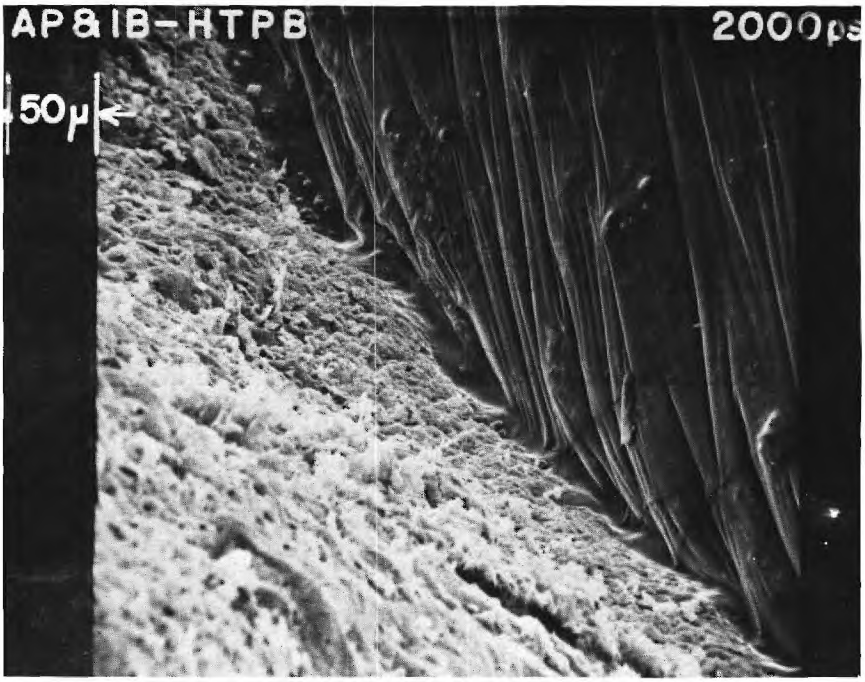

Figure III-52. AP and Iron Blue (IB-HTPB) 2000 psia (x240).

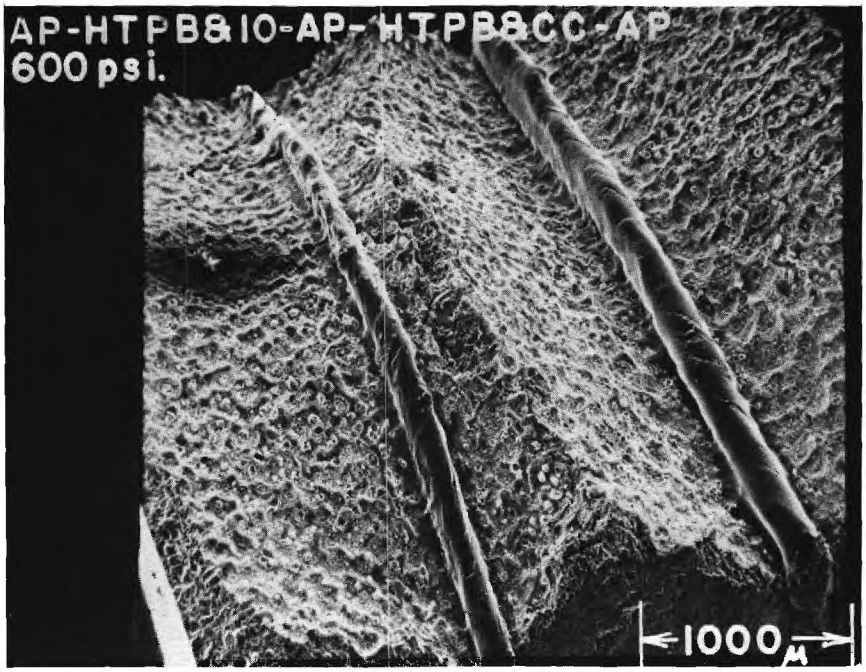

Figure III-53. AP-HTPB and Ferric Oxide (IO)-AP-HTPB and Cu0202 (CC)-AP 600 psia (x28).

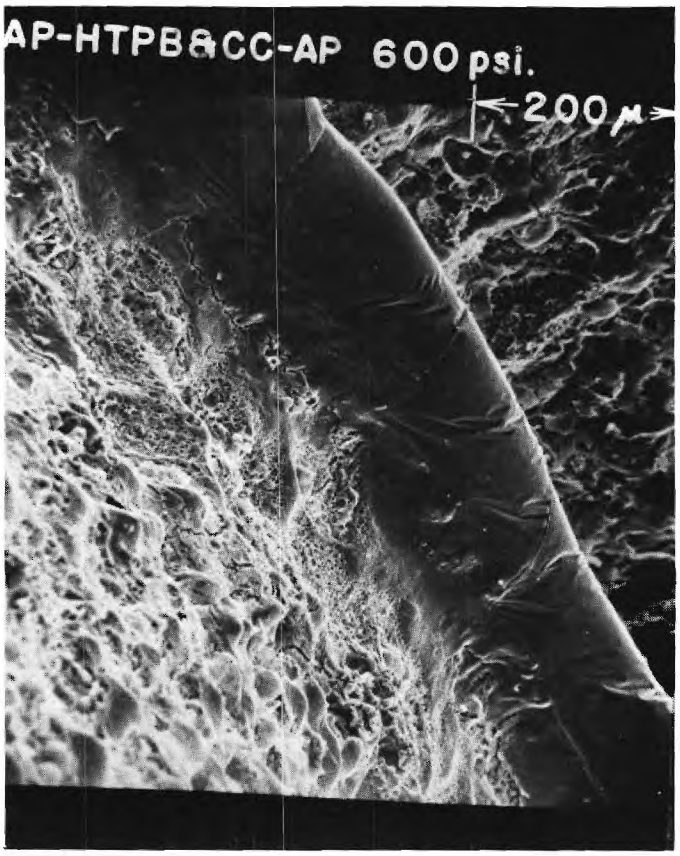

Figure III-54. AP-HTPB and Cu0202 (CC)-AP 600 psia (x136).

Figure III-55. AP-HTPB and Ferric Oxide (IO)-AP 600 psia (x139).

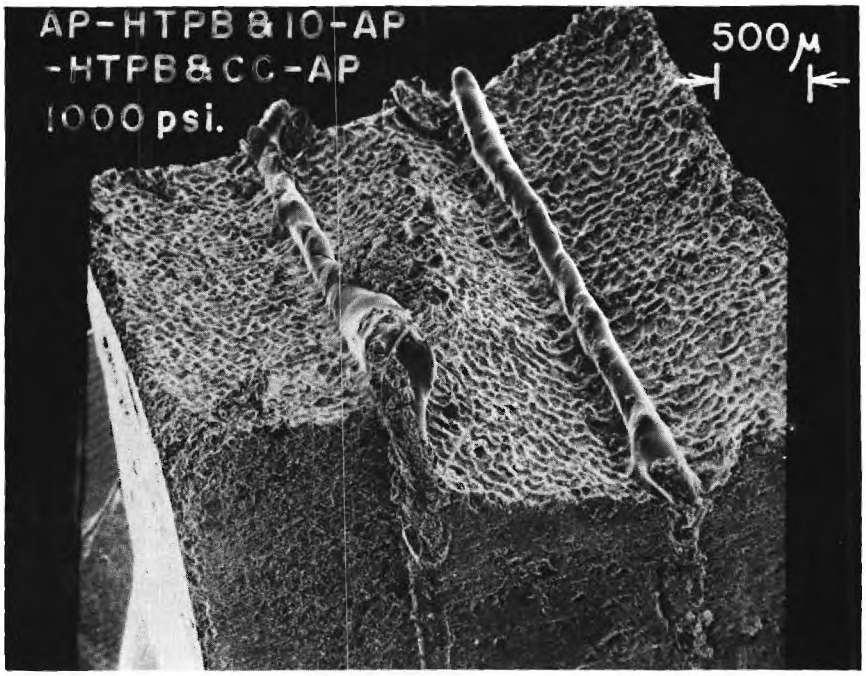

Figure III-56. AP-HTPB and Ferric Oxide (IO)-AP-HTPB and Cu0202 (CC) 1000 psia (x214).

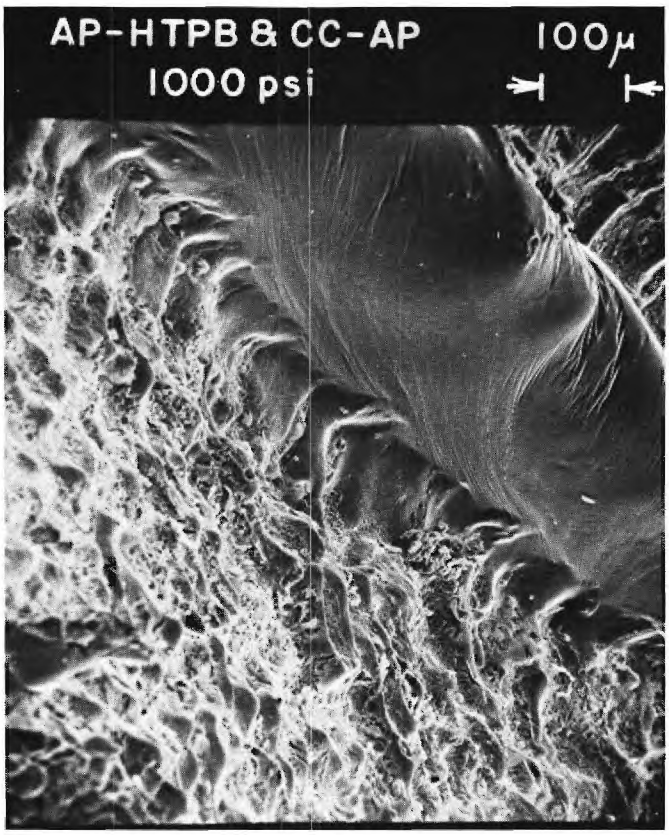

Figure III-57. AP-HTPB and Cu0202 (CC)-AP 1000 psia (x116).

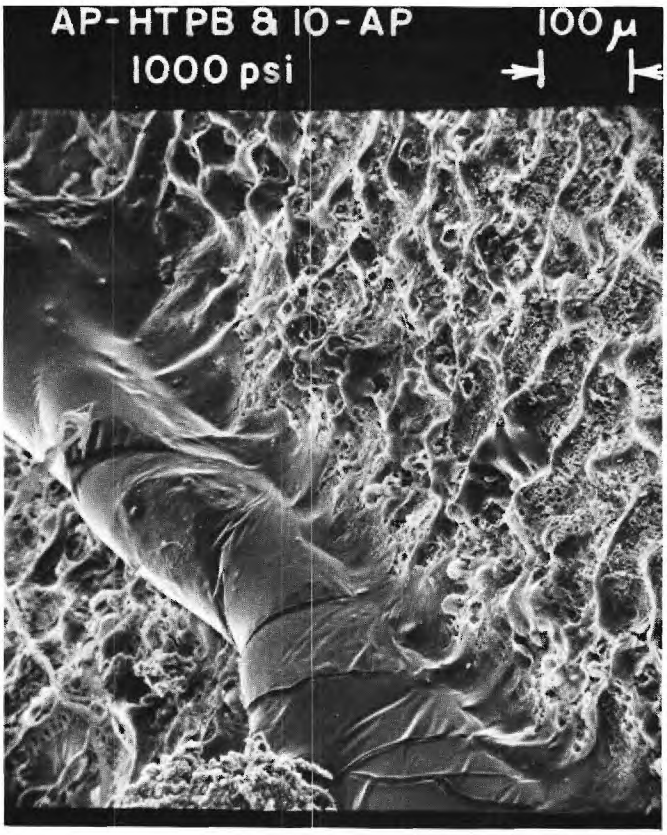

Figure III-58. AP and HTPB and Ferric Oxide (IO)-AP 1000 psia (x116).

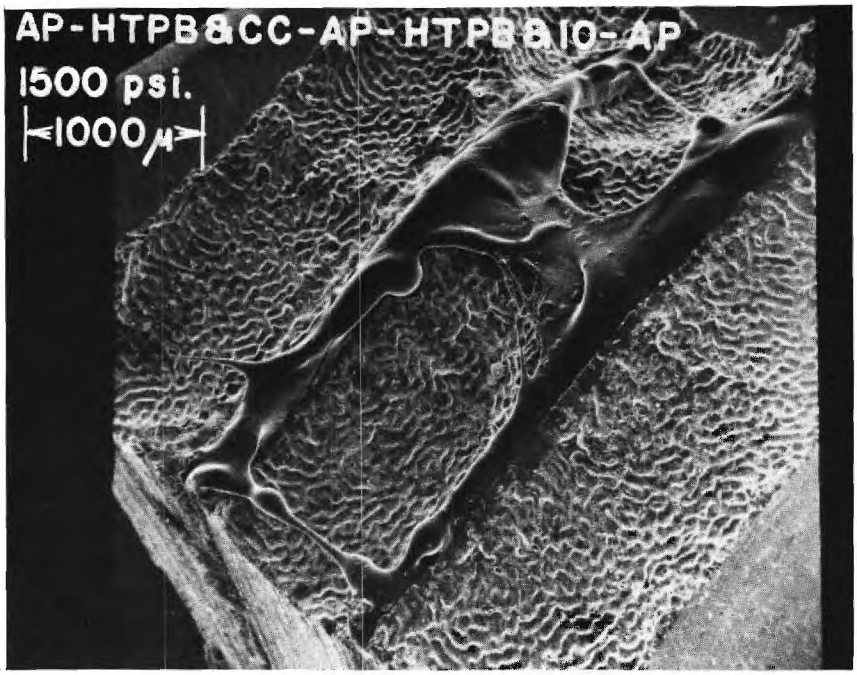

Figure III-59. AP-HTPB and Cu0202 (CC)-AP-HTPB and Ferric Oxide (IO)-AP 1500 psia (x24).

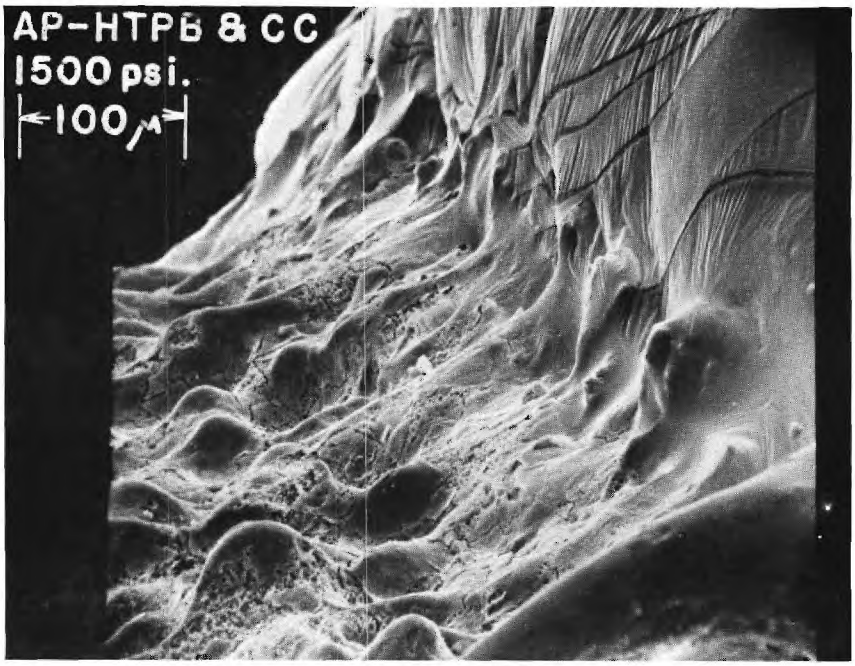

Figure III-60. AP-HTPB and Cu0202 (CC) 1500 psia (x223).

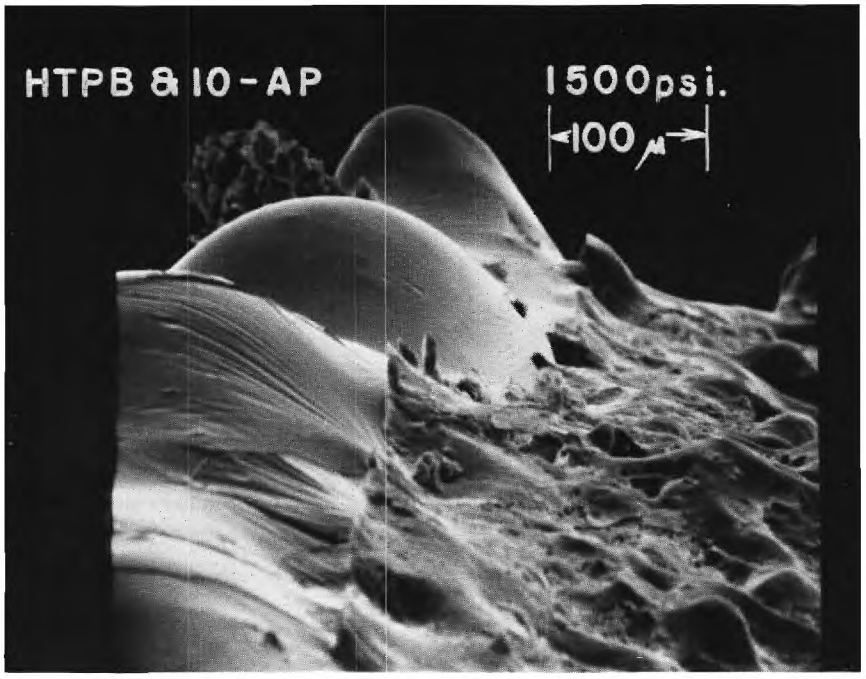

Figure III-61. HTPB and Ferric Oxide (IO)-AP 1500 psia (x210).

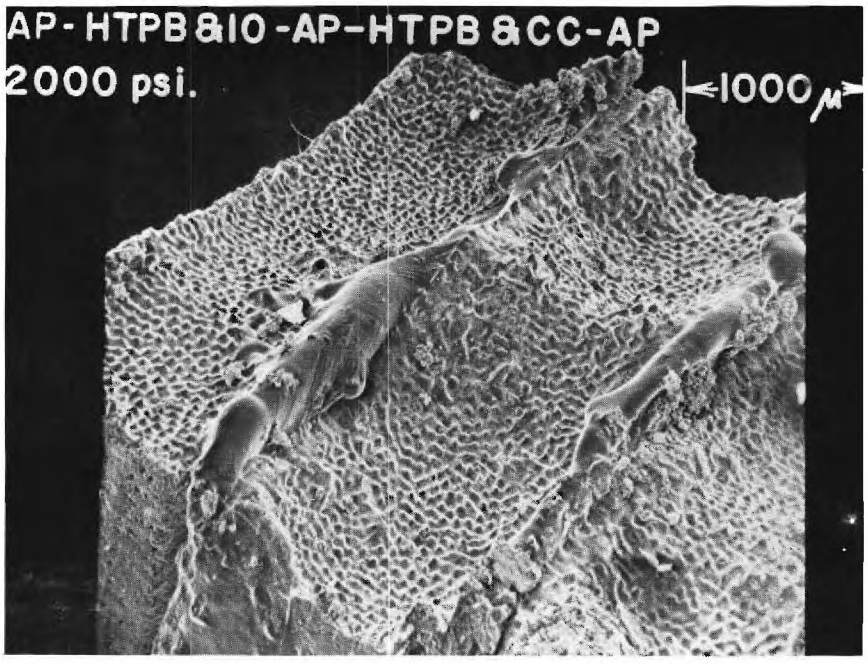

Figure III-62. AP-HTPB and Ferric Oxide (IO)-AP-HTPB and CuO202 (CC) 2000 psia (x24).

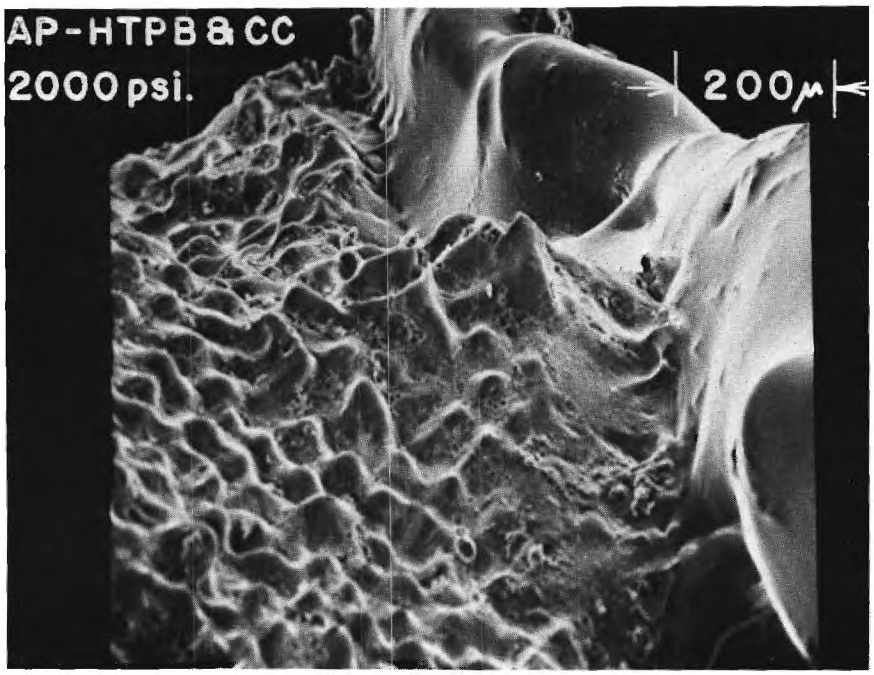

Figure III-63. AP-HTPB and Cu0202 (CC) 2000 psia (x106).

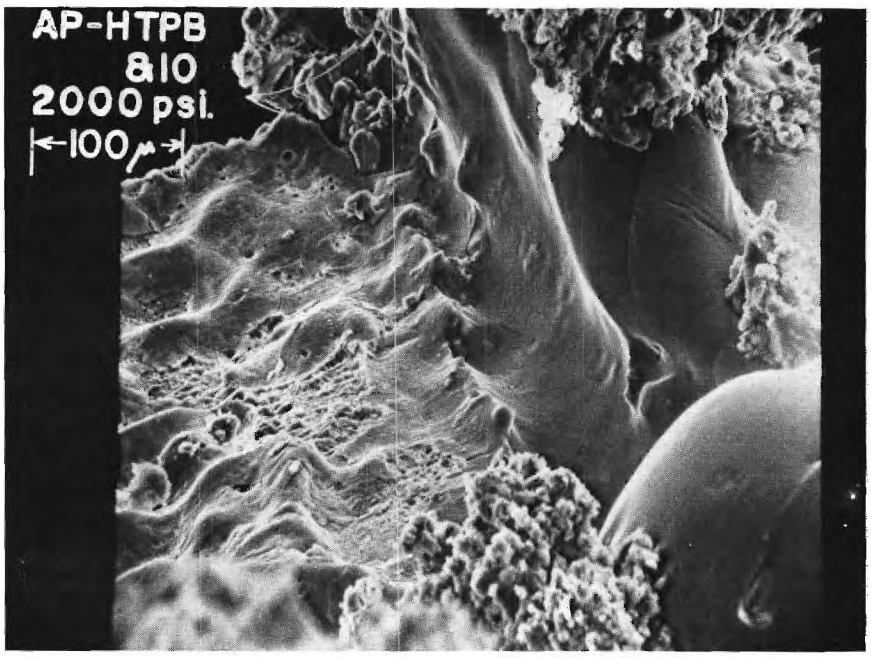

Figure III-64. AP-HTPB and Ferric Oxide (IO) 2000 psia (x200).

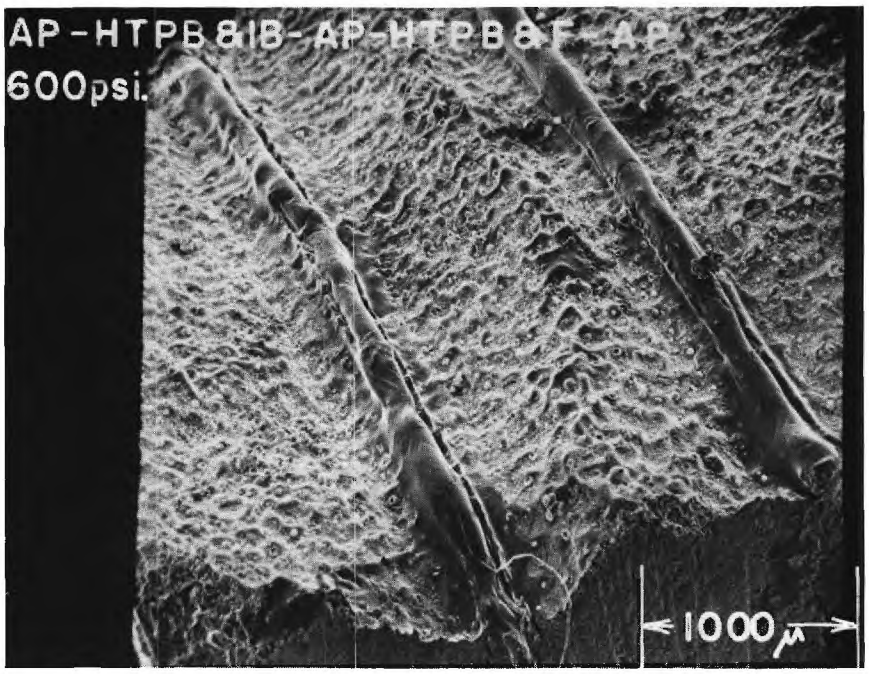

Figure III-65. AP-HTPB and Iron Blue (IB)-AP-HTPB and Ferrocene (F)-AP 1600 psia (x29).

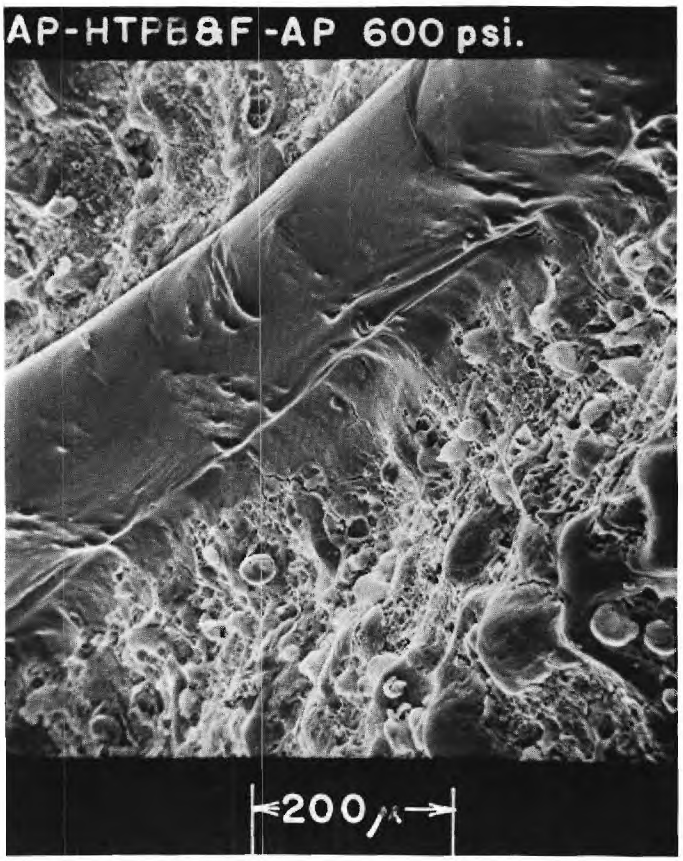

Figure III-66. AP-HTPB and Ferrocene (F)-AP 600 psia (x135).

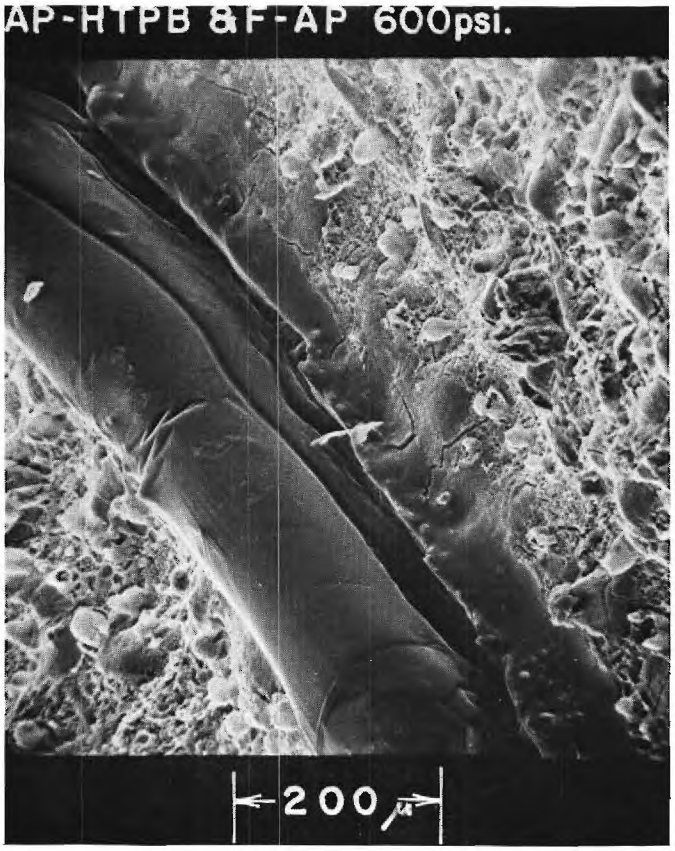

Figure III-67. AP-HTPB and Ferrocene (F)-AP 600 psia (x136).

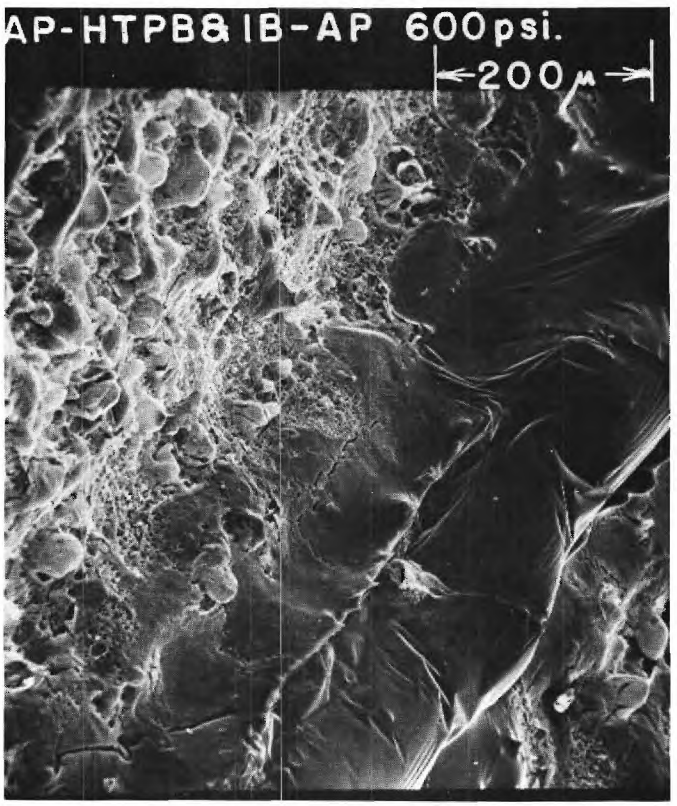

Figure III-68. AP-HTPB and Iron Blue (IB)-AP 600 psia (x143).

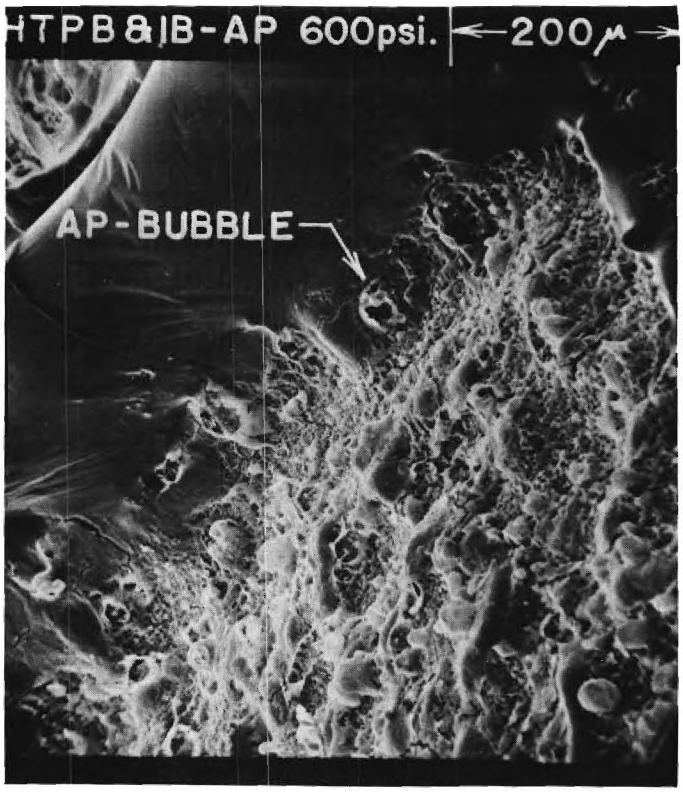

Figure III-69. AP-HTPB and Iron Blue (IB) 600 psia (x155).

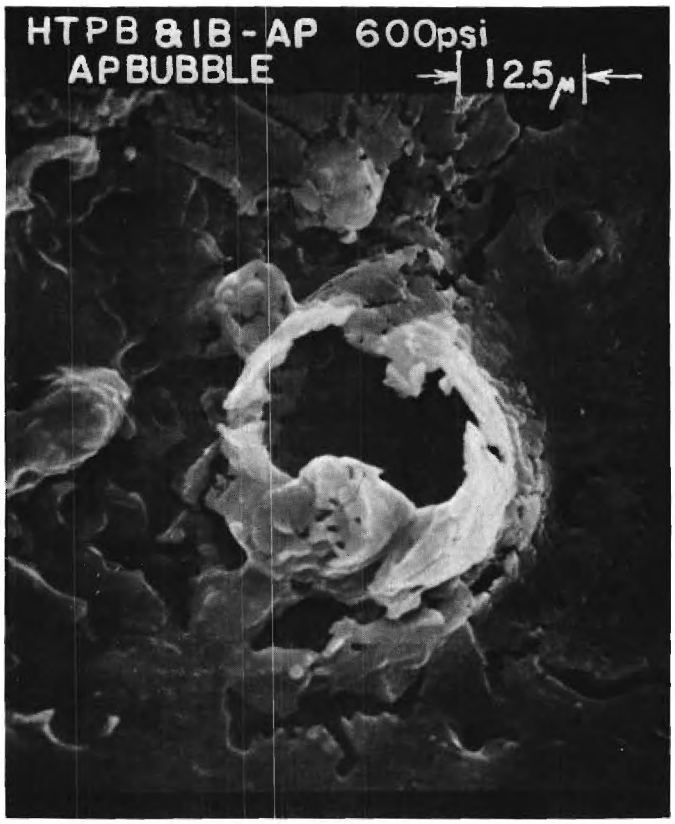

Figure III-70. AP Bubble 600 psia (x1300).

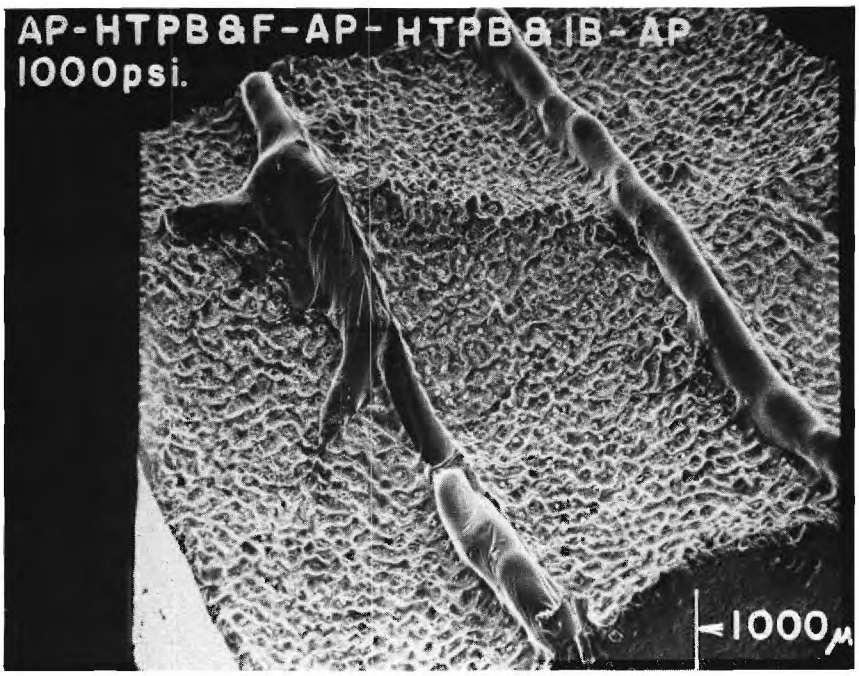

Figure III-71. AP-HTPB and Ferrocene (F)-AP-HTPB and Iron Blue (IB) 1000 psia (x27).

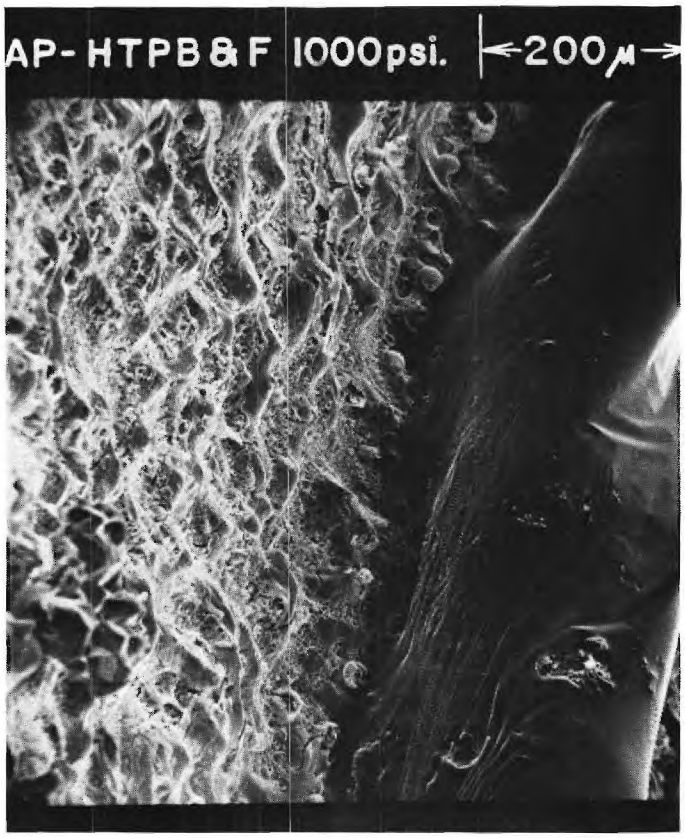

Figure III-72. AP-HTPB and Ferrocene (F) 1000 psia (x140).

Figure III-73. HTPB and Iron Blue (IB)-AP 1000 psia (x130).

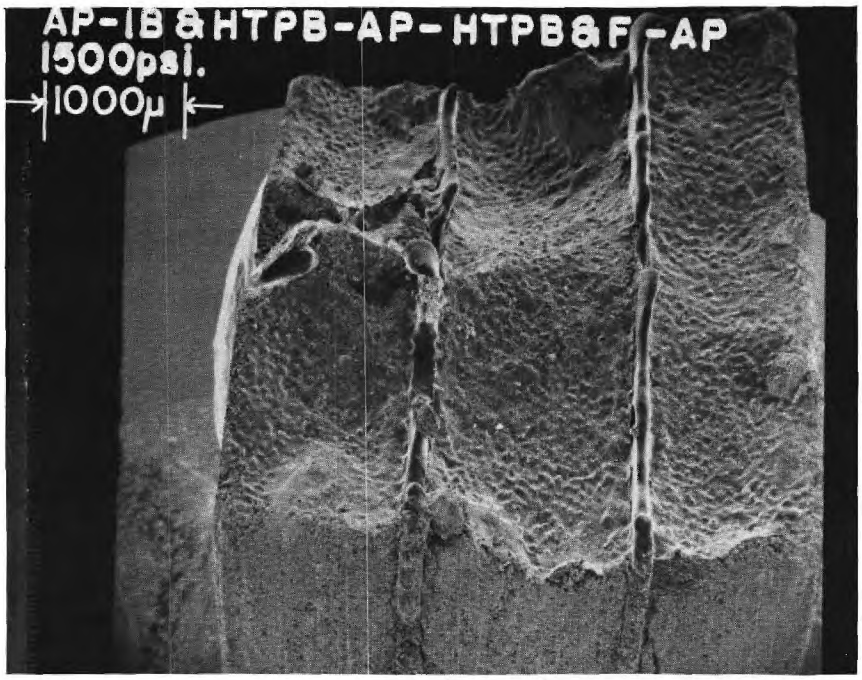

Figure III-74. AP-HTPB and Iron Blue (IB)-AP-HTPB and Ferrocene (F) 1500 psia (x18.7).

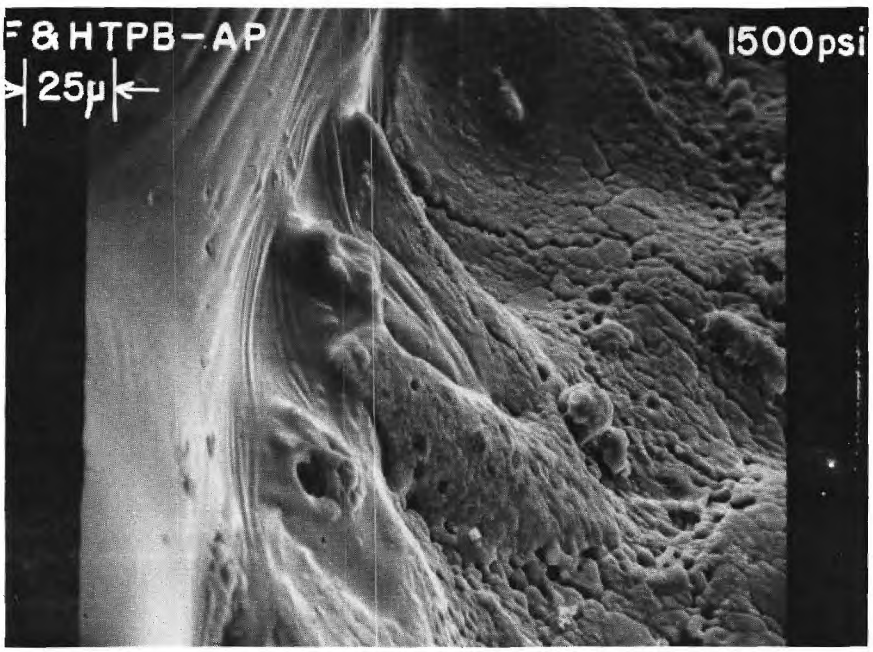

Figure III-75. HTPB and Ferrocene (F)-AP 1500 psia (x476).

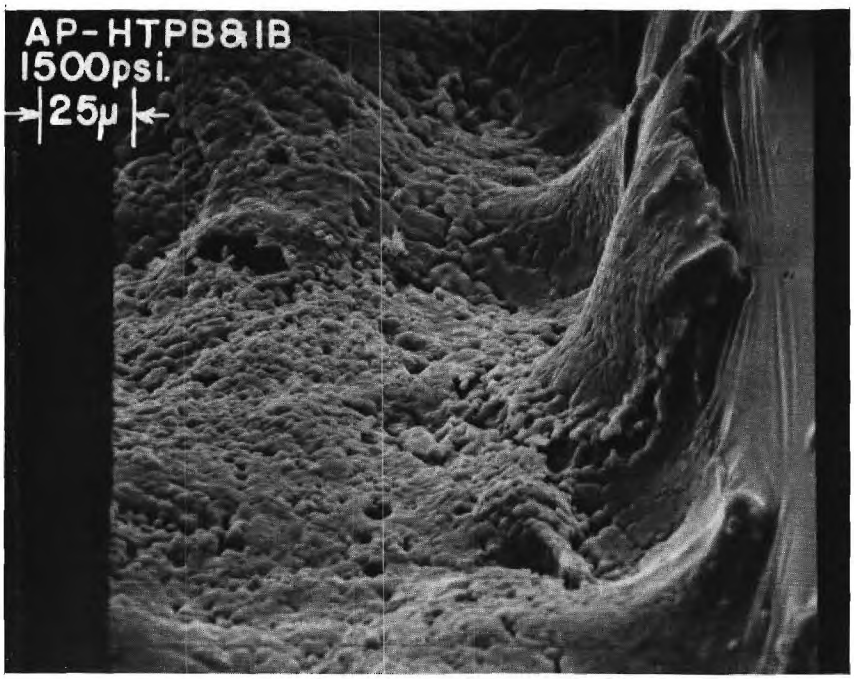

Figure III-76. AP-HTPB and Iron Blue (IB) 1500 psia (x476).

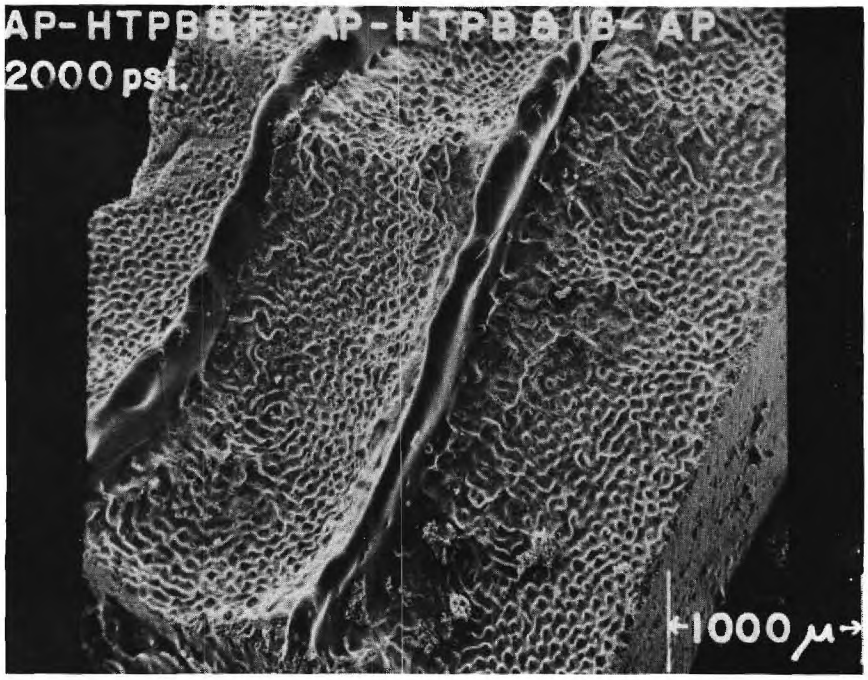

Figure III-77. AP-HTPB and Ferrocene (F)-AP-HTPB and Iron Blue (IB)-AP 2000 psia (x26).

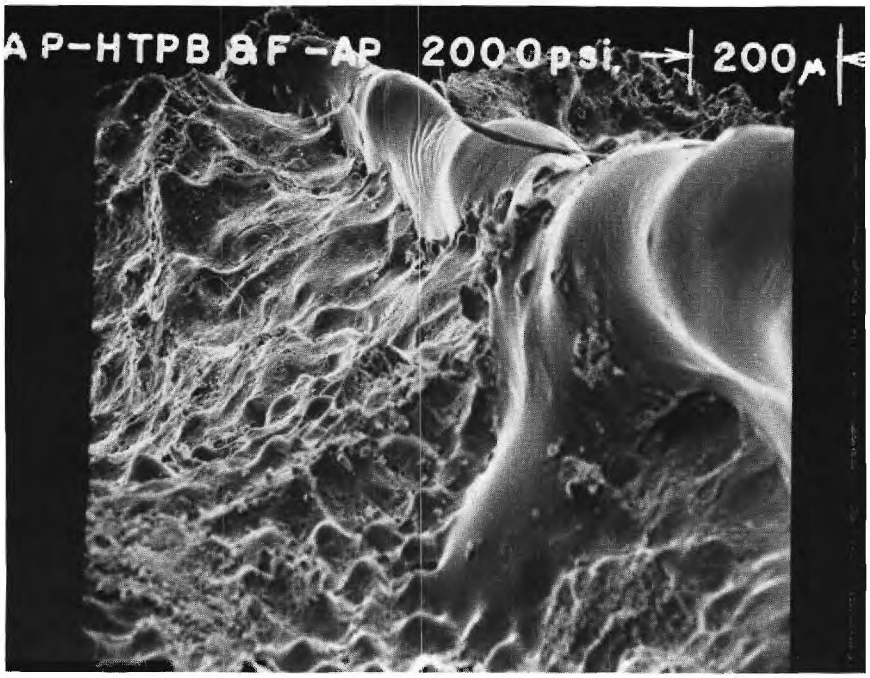

Figure III-78. AP-HTPB and Ferrocene 2000 psia (x98).

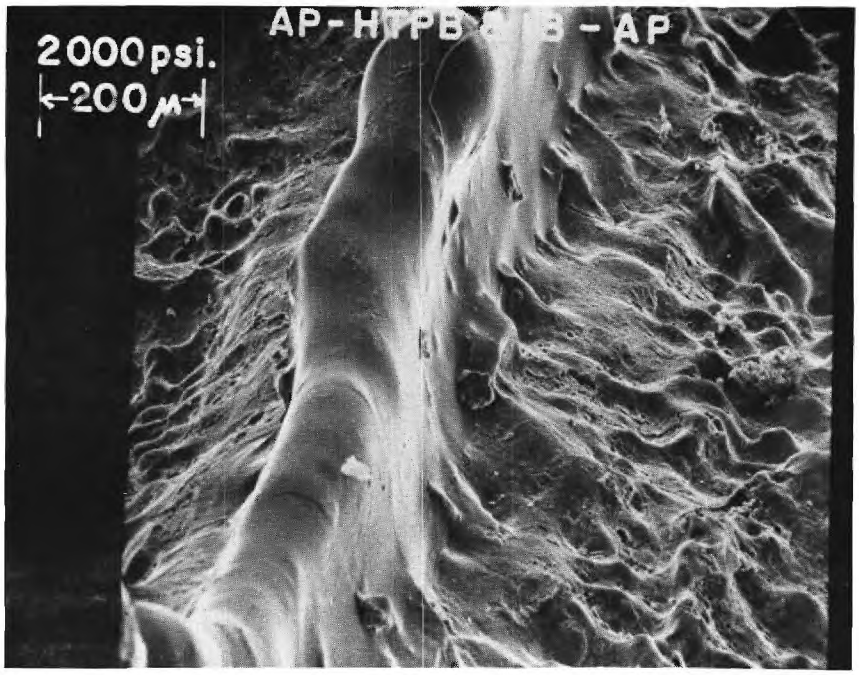

Figure III-79. AP-HTPB and Iron Blue (IB)-AP 2000 psia (x110).

Table III-3

Summary of Results from Scanning Electron Microscopy of Composite Solid Propellant Sandwiches with Catalyst in the Binder

Catalyst	Location	Pressure psia	Figure No. III-	Binder Melt Flow μm	Binder Height μm
Cu0202 (CC)	in HTPB	600	53,54	100	130
		1000	56,57	120	350
		1500	59,60	50	undetermined
		2000	62,63	none	250
Ferric Oxide (IO)	in HTPB	600	53,55	70	170
		1000	56,58	60	190
		1500	59,61	none	120
		2000	62,64	none	undetermined
Ferrocene (F)	in HTPB	600	65,66,67	45	165
		1000	71,72	20	270
		1500	74,75	20	undetermined
		2000	77,78	none	200
Iron Blue (IB)	in HTPB	600	65,68, 69,70	100	200
		1000	71,73	50	280
		1500	74,76	none	undetermined
		2000	77,79	50	250

cases but tends to be discontinuous as the pressure increases.

Summary and Interpretation

The scanning electron microscope observations have both agreed and disagreed with the cinephotomacrography results. The quenched samples have indicated higher oxidizer surface slopes as the pressure increases when Cu0202 catalyst was added to the AP. This was not indicated by the

high speed movies. This indicates that CuO202 may be the most effective catalyst for addition in real propellants. The AP and IO quenched samples did not exhibit any variation in surface slope with pressure. This conflicted with a distinct decrease observed in the high speed movies.

The delay times obtained from the sample burn rate curves of Chapter II were used to obtain partially burned samples. There was no disagreement for the cases of catalyst in the binder or oxidizer. Discrepancies were encountered when the catalyst was located at the interface. The micrographs obtained for these samples are included in Appendix A.

The point of maximum regression of the oxidizer surface was always located at the edge of the binder melt flow. The slope of the binder oxidizer interface slope is only discontinuous for the case of no binder melt flow.

A primary observation is that all catalysts at all pressures reduce the binder melt flow extent when either loaded into the AP or into the binder. This is most probably some form of catalytic effect because it occurs at low pressures when the overall sandwich rates are not augmented over the pure HTPB-AP burn rates. Since the binder melt flows retard the pure AP rate, this could be an important mechanism for propellant catalysis.

Although there is some disagreement between surface slopes in catalyzed cases when viewed through cinephotomacrography and scanning electron microscopy, the former results are accepted for determination of catalytic effectiveness in Section V. The reasons for this acceptance are that a) no knowledge of post-quench surface alterations is at hand and b) direct observation of the complete burn during the cinephotomacrography runs has assured that a steady profile was developed.

IV. ELECTRON MICROPROBE EXPLORATORY STUDIES

An electron probe x-ray microanalysis has been performed on two pairs of samples. Both burned and unburned samples of pure AP and AP with 2% Iron Blue were examined. The analysis was performed in the Physical Science Division of the Engineering Experiment Station of the Georgia Institute of Technology using an Acton Laboratories Electron Probe x-ray Microanalyzer, Model MS-64. This analyzer is equipped with a light element detection system. It is possible to detect elements from boron, atomic number 5, to uranium, atomic number 92. This system cannot detect the four lightest elements, hydrogen, helium, lithium and beryllium.

The electron probe x-ray microanalyzer is an instrument used for x-ray spectrochemical analysis of surfaces between 0.5 to 200 μm diameter on the surface of a solid specimen. The instrument consists of three basic components, an electron beam similar to the SEM, an x-ray optical system with a suitable detector, and an optical microscope to select the area to be analyzed. The x-ray optical system is arranged to accept x-rays with an effective emergent angle of 18° from the specimen surface for all wavelengths. The optical microscope has a resolution of better than one μm with a magnification of 400x.

An electron beam size of 100 μm was used to investigate the oxidizer samples. This beam size was chosen to minimize damage to the surface by the electron beam. This would not have been as serious of a problem, if the sample were an electrical conductor. The electrons remain near the irradiation site for a nonconductor and create a negative charge which causes the beam to jump back and forth at random on the surface. This is accompanied by sparking

which rapidly deteriorates the sample surface. This type of damage was noted for all samples.

The electron micrographs of Chapter III were obtained by observing the secondary or backscattered electrons emitted by the sample as the electron beam of .01 μm diameter scanned the sample. These electrons are prevented from reaching the x-ray detector by an electron trap consisting of a permanent magnet with a special pole piece designed to deflect any electrons out of the x-ray path before they can enter the spectrometer chamber. These electrons cause a high background noise level if they reach the x-ray detector.

The analyzing electronics of the electron probe result in a strip chart record of the x-ray spectrum of the sample. These are shown in Figures IV-1 and 2. The ordinate of the spectrum is the variation in intensity of the x-rays, as obtained from a linear ratemeter which displays a signal that has been processed by a pulse-height analyzer system. The abscissa of the trace is the distance from the mica crystal to the sample. The known identification spectra for this microprobe are tabulated in this dimension, which can be converted directly to wavelength by the equation

$$\lambda(\text{Å}) = 0.3978\ L(\text{mm})$$

The pure AP sample spectra are shown in Figure IV-1. The unburned sample exhibited more damage due to the electron beam than the other three samples. No dominant chlorine peak was detected by the strip chart record, but a direct reading of the pulse height analyzer output before beam damage could be appreciable showed equal counts for chlorine for both the burned and unburned samples. A small amount of carbon was indicated in the burned sample. The amount was just above the limit of detectability. A slightly higher indication of oxygen was obtained.

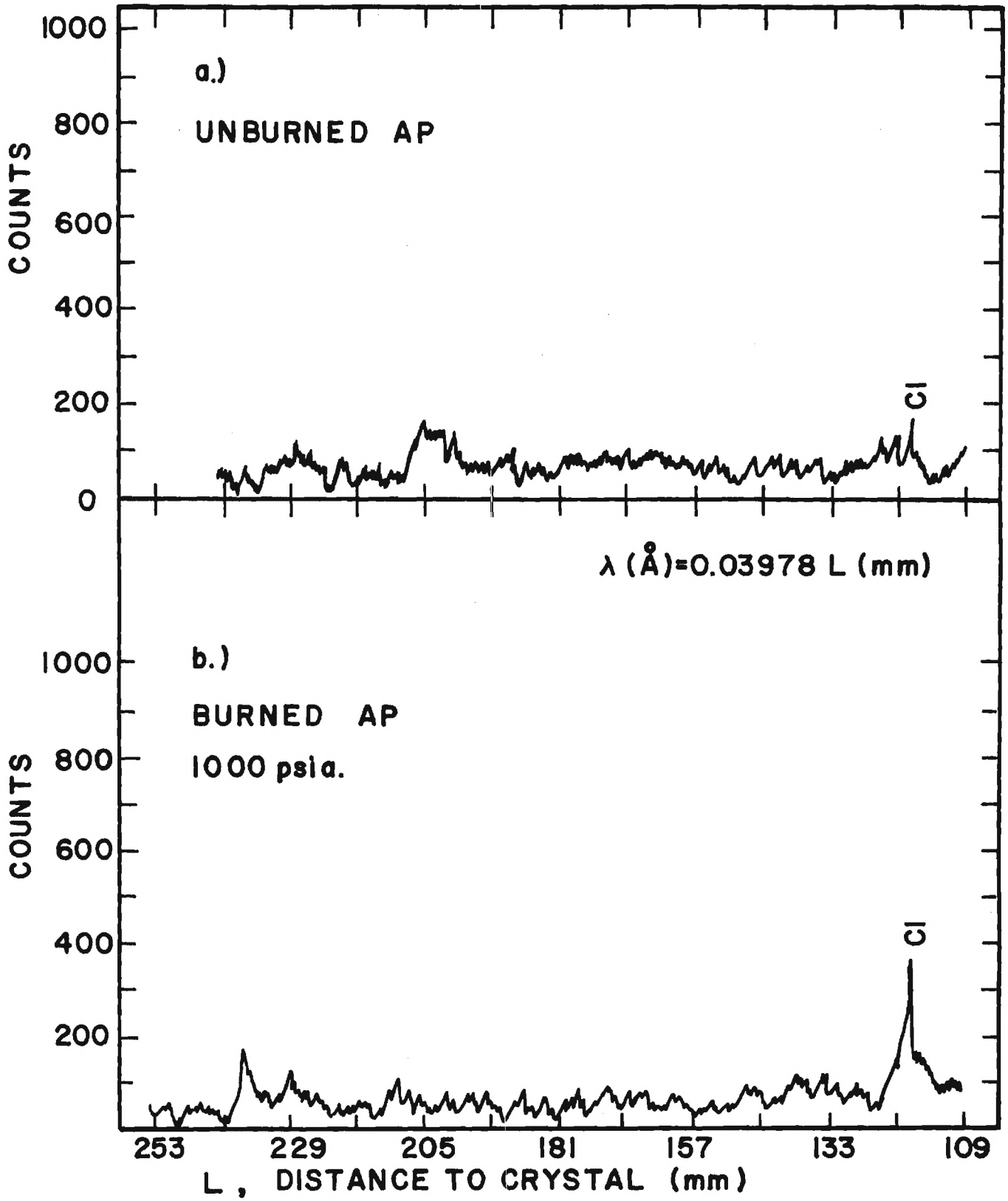

Figure IV-1. Characteristic X-Ray Spectra from Ammonium Perchlorate Samples.

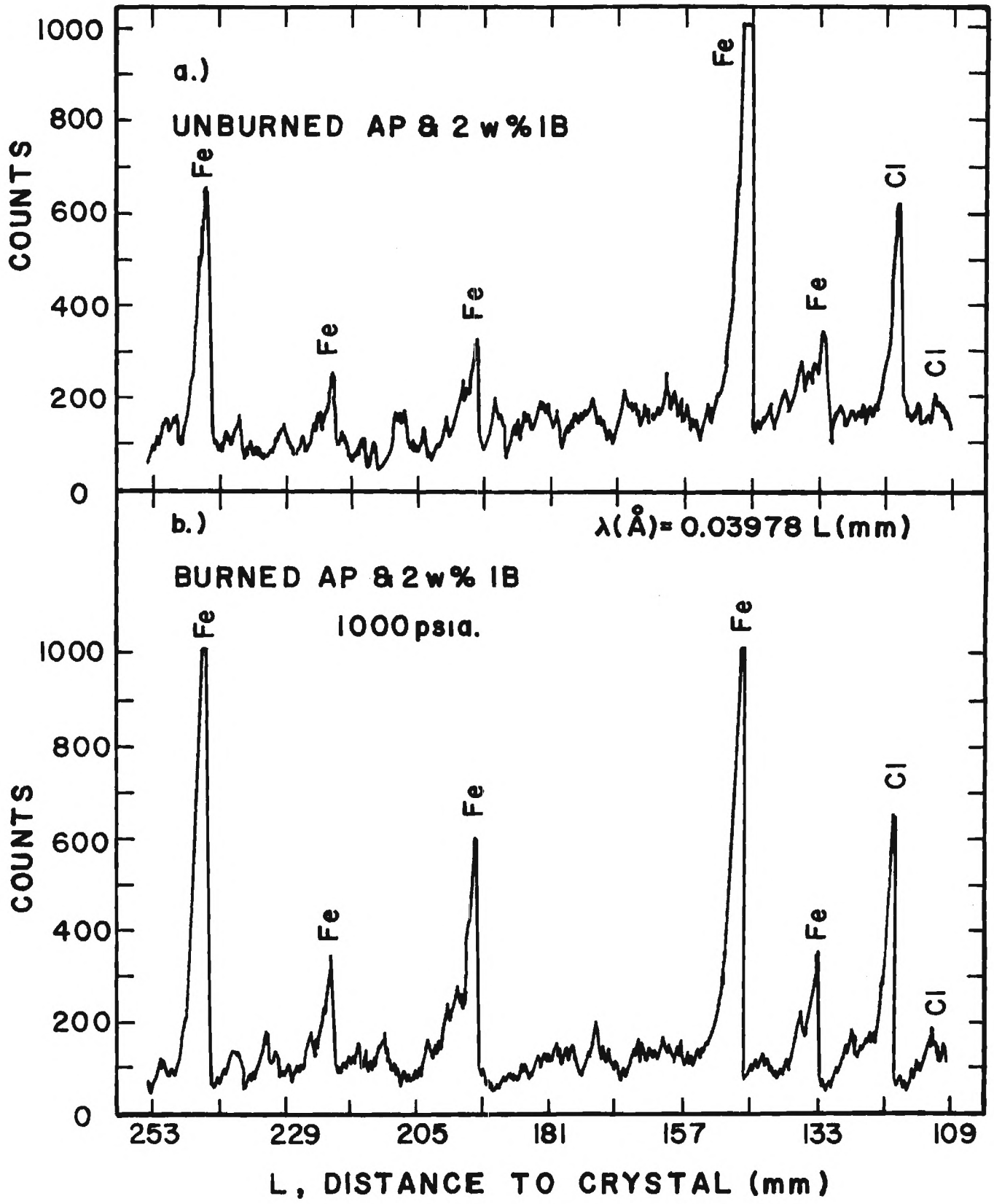

Figure IV-2. Characteristic X-Ray Spectra from Ammonium Perchlorate with 2% by Weight Iron Blue Samples.

The AP with 2% Iron Blue sample spectra are shown in Figure IV-2. The beam damaged these samples also. Quick counts were again taken to obtain a quantitative measure of the iron present in the samples. The unburned sample indicated a count equivalent to 3.06 weight % of a pure iron sample, while the burned sample showed a decrease to 2.60 weight %. This would be assuming the iron standard and the iron in the sample are in the same chemical state. This is not necessarily true here. There was an indication of sulfur present on the unburned sample but it was not present on the burned sample. The difference between the quick counts and the intensity of iron x-rays can be attributed to beam damage of the sample.

The results of the microprobe analysis were disappointing. A long delay was encountered in the analysis time due to equipment changes which had to be made with the light element detection system. It was felt that this time delay would result in quantitative measurements of relative concentrations of carbon, iron, nitrogen and oxygen. It is necessary to use special vacuum path with a 500 Å collodion window to isolate the detector from the sample for elements below an atomic number of 11. Since the only source of carbon and iron would be the iron blue with the chemical formula $Fe(NH_4)Fe(CN)_6$ and the only source of oxygen and chlorine would be the ammonium perchlorate, NH_4ClO_4, it was expected that a detailed quantitative chemical analysis of the surface layer of a burned and unburned sample would yield sufficient information to postulate the suitable chemical reactions which had taken place near the oxidizer surface. In some cases concentrations of one part in 10^5 have been reported by this type of microprobe analysis. If the reactions were known for the pure AP sample surface, then the significance of the catalyst, iron blue, could also be determined. As can

be seen from Figures IV-1 and 2 along with the discussion this was not possible. Because of the extremely long delay in analysis of these samples, it was not possible to formulate a new series of tests. It may have been possible to obtain suitable results without sample damage, if the electrically nonconducting samples had been coated as for the scanning electron microscope observations. No sample damage was detected during those observations with a much smaller, more intense beam, .01 as compared to 100 μm in diameter. The quick counts obtained at fixed detector locations would yield more accuracy than the entire spectrum scans. The fixed detector locations would be at known crystal distances for detection of x-ray radiation from specific elements. Further measurements would not be useful unless the light elements (below atomic number 12) could be detected with more accuracy.

V. RELEVANCE OF SANDWICH RESULTS TO COMPOSITE PROPELLANT BEHAVIOR

This section attempts to illustrate the use of mechanistic results inferred from sandwich tests to predict behavior in an actual composite propellant. The catalytic results mentioned in previous sections may be summarized by a) with the exception of IB and F below 800 psia addition of catalyst to the binder has no appreciable catalytic effect, b) with the exceptions of (i) CC above 1000 psia and (ii) IO above 1600 psia the primary catalytic mechanism appears to be augmentation of the binder-oxidizer gas phase kinetics and c) for the exceptions noted in b) the primary catalytic mechanism appears to be augmentation of the AP deflagration rate. In all cases it appears that through an unknown mechanism catalysts reduce the extent of binder melts and this may also be a rate-augmenting process. However, the primary differences between catalysts appear to lie in their ability to augment either the AP deflagration or the binder-oxidizer reaction kinetics. Furthermore, to make the binder-oxidizer reactions faster it appears desirable to introduce the catalyst from the AP side of the sandwich.

An indication for real propellants, which usually introduce the catalysts through a binder mix, is that the available surface area of AP should be made as large as possible (small particle size) to increase the probability of catalyst particles of reaching the hot gases of the AP decomposition and deflagration. This hypothesis will be tested below.

Since the catalyst is not usually loaded into the AP in a real propellant, the most likely mechanism for propellant catalysis would appear to be the enhancement of the binder-oxidizer reaction kinetics. Consequently, the sandwich indications along this line (separation of dashed and solid curves

in Figure II-2) should be directly applicable to propellant results. Summarizing the sandwich results and interpreting them insofar as propellant behavior is concerned, Table V-1 is constructed. The results of Table V-1 are only uncertain with regard to the strong AP enhancement of CC. If this mechanism does come into play in a real propellant the effects of CC could be underestimated at high pressure. Furthermore, IO behavior above 1200 psia could be underestimated.

Table V-1

Comparison of Catalyst Predictions in a Propellant Environment

Pressure	600-1000 psia	1000-1600 psia	1600-2000 psia
Observation	CC, IB, F, IO all equivalent in enhancing rate	IO, IB, F equivalent in enhancing rate. CC should be somewhat inferior	IB slightly superior to F which is slightly superior to IO which is superior to CC in rate augmentation

In order to test these predictions an unpublished Thiokol correlation formula for burn rate has been used[8]. Only IO and F catalysts were common to the Thiokol correlation and the current sandwich tests. The formula for HTPB binder reads

$$r(\text{in/sec}) = ap^n$$

$$a = \frac{1}{10}\left\{\text{antilog}_{10}\left[-.497 + .91\bar{D}_1^2 + A_o\omega + A_1\omega^2 - .28b\right]\right\}$$

$$n = .239 + .744\bar{D}_1 - .707\bar{D}_1^2 + .00085q + B_o\omega + B_1\omega^2$$

b = %binder
q = % AP
ω = % catalyst

} by weight

$$\bar{D}_1 = (q_1 + q_2 + \ldots + q_n)/(q_1 D_1^{\cdot 3} + \ldots + q_n D_n^{\cdot 3})$$

D_n = weight mean diameter of a given mode

	A_o	A_1	B_o	B_1
IO	-.301	.091	.191	-.049
F	.258	0	0	0

Sample results for a unimodal particle size distribution are shown in Figures V-1 and 2. The remaining ingredient percentage not indicated on the figures pertains to aluminum loading. Defining the catalyst effectiveness as the difference in burn rate between the catalyzed and no-catalysis cases, it is seen that the sandwich prediction of greater effectiveness as the AP size decreases is upheld.

With regard to pressure level the prediction of Table V-1 is correct in the 1000-1600 psia range; there is virtually no propellant difference between IO and F. F is somewhat better than IO at 600 psia, as seen in Figures V-1 and 2. This may be accounted for by the low pressure result with F that it becomes effective when located in the binder (see Figure II-3), in which case Table V-1 should be modified for IB also. In the pressure range 1600-2000 psia the propellant results show virtually no difference between F and IO whereas the sandwich results would predict a slight superiority of F. Again, this may be due to the action of IO on the AP deflagration, which was neglected in the construction of Table V-1. If this is the case, then the prediction for CC should be modified. By and large, however, the sandwich results predict that IO and F should be roughly equivalent and this is borne out experimentally for real propellants.

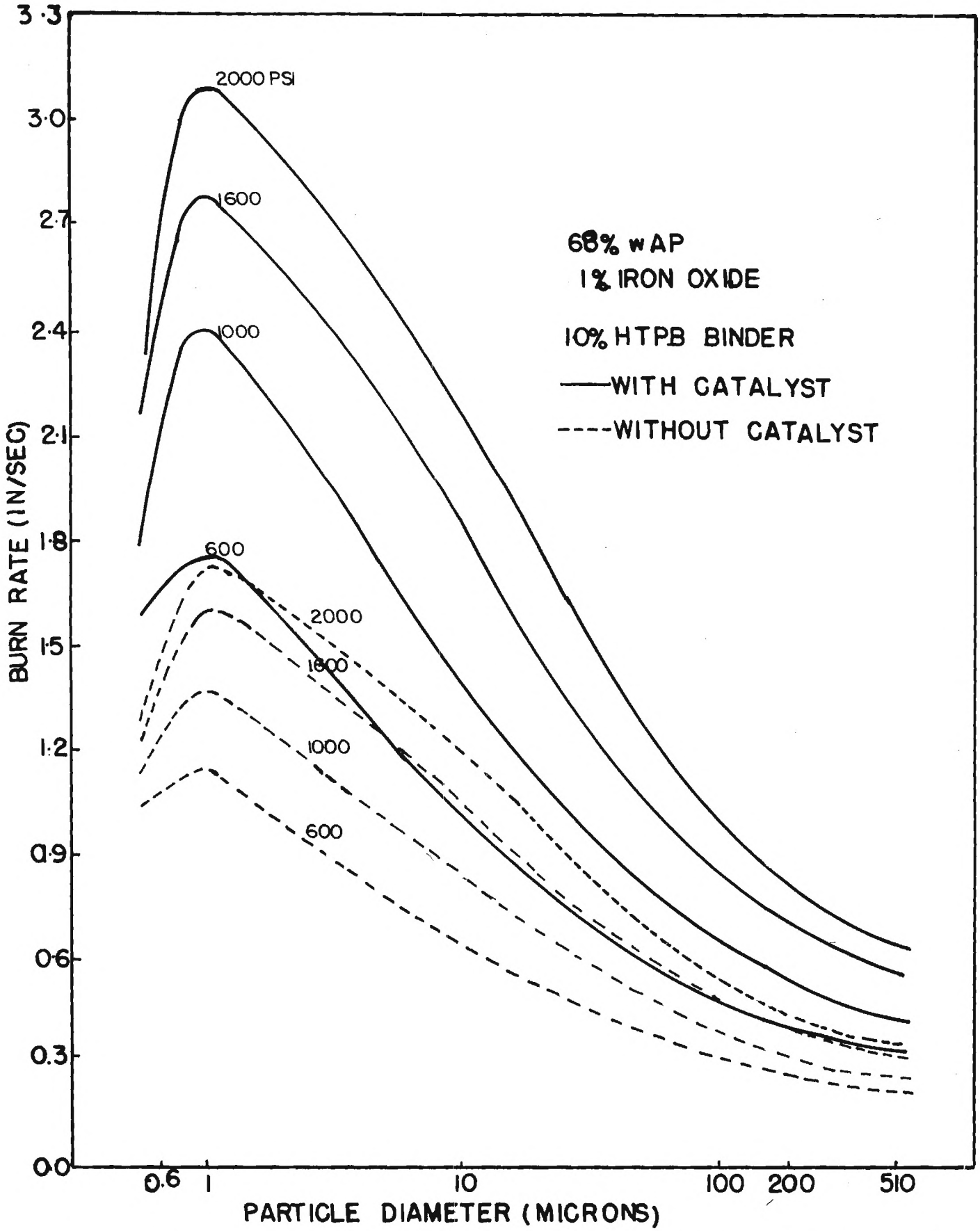

Figure V-1. The Effect of Iron Oxide Catalyst on HTPB-AP-Al Propellant.

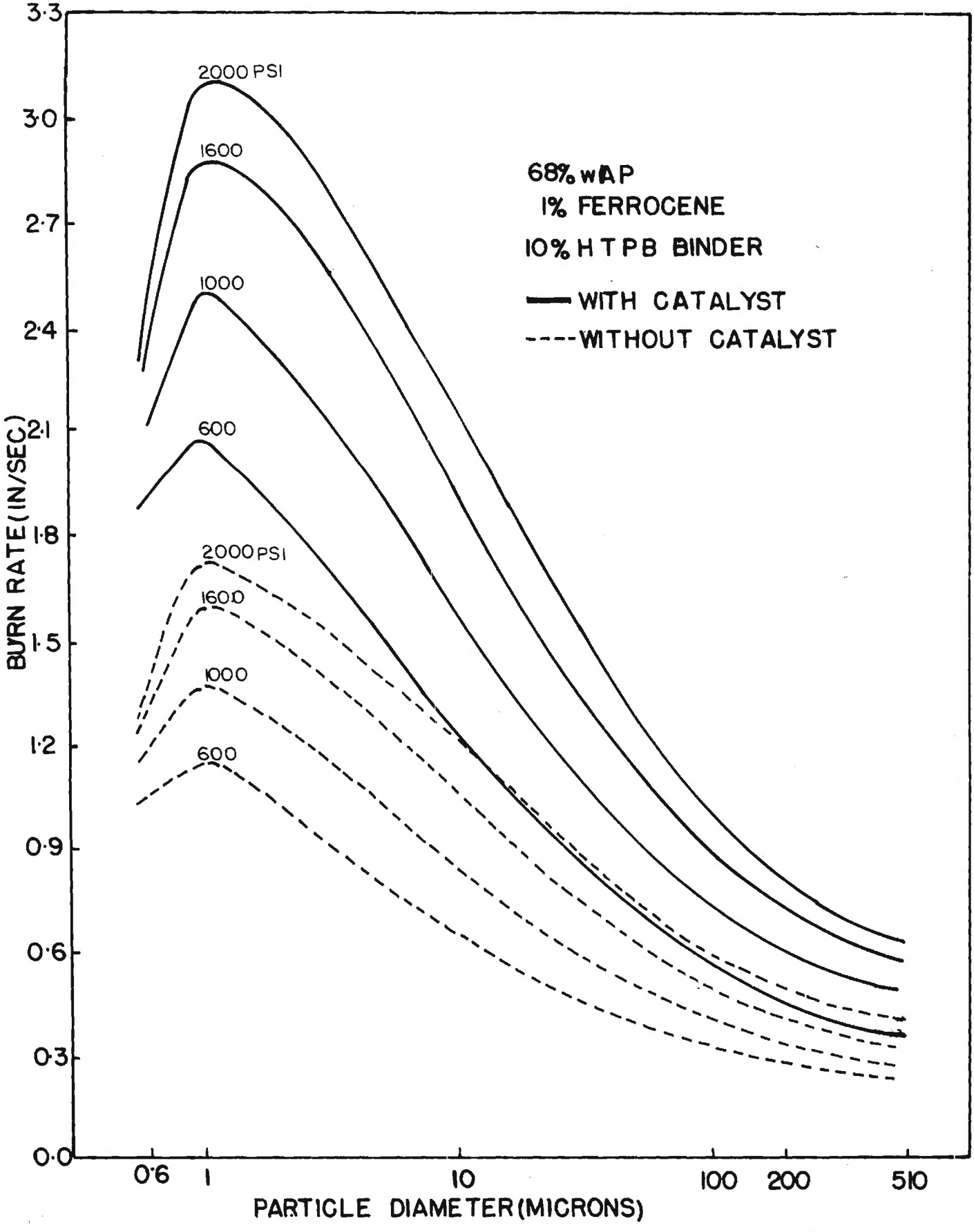

Figure V-2. The Effect of Ferrocene Catalyst on HTPB-AP-Al Propellants.

VI. SANDWICH ANALYSIS

Model Construction and Assumptions

As an aid in interpretation of experimental results it is desirable to have an analytical model of sandwich deflagration. Even in the two-dimensional case, however, the problem is highly complex due to a) an unknown surface shape, b) nonlinearities in the governing equations due to chemical reaction and the unknown surface shape, c) two phase heat transfer, d) multiple chemical reactions and e) a mathematically elliptic problem which reverts to a parabolic problem sufficiently far from the oxidizer surface (as will become apparent later). Accordingly, the maximum use of experimental information is sought which still does not restrict the usefulness of the model in understanding experimental results. The initial model therefore uses the following observations:

a) Far from the binder-oxidizer interface the AP regresses as pure AP. Furthermore, for binder thicknesses of the order used in the experimental studies ($\approx$ 150 μm) there is little effect of one side of a sandwich upon the other side even when dissimilar materials are used. Therefore, the initial model development is concerned with a semi-infinite slab of AP against a semi-infinite slab of binder.

b) A steady state is achieved experimentally with AP oxidizer. Consequently, time dependence is assumed absent.

c) For uncatalyzed sandwiches the experimental results show very little effect of the binder-oxidizer reactions upon the surface profile. The initial model is therefore constructed assuming binder-oxidizer reactions to have negligible rate. Furthermore, the effect of catalysis is not treated.

The initial model therefore asks the question of the surface shape attained by a semi-infinite slab of AP which pyrolyzes a semi-infinite slab of binder. Posed in this manner it is immediately recognized that the problem has neither a unique solution nor a steady solution because a) the final shape would depend upon the geometry of ignition and b) it would take an infinite time to establish a steady profile in a semi-infinite slab of inert binder. The ignition problem is seen by imagining two cases - one in which ignition is achieved by a line heat source (say an ignition wire) and a second in which ignition is achieved uniformly over the entire AP surface. In the first case the AP would take on the shape of ever-increasing circular radii from the ignition point. In the second case the AP would deflagrate in a planar fashion except in the vicinity of the binder. For the current analytical model the second case will be assumed. The question of attainment of a steady binder profile can be answered by imposing a "local" steadiness in the vicinity of the binder-oxidizer interface. While it is true that far from the AP surface the binder will continually change shape, as it is eaten away by the hot AP deflagration gases, it is reasonable that for a certain distance (to be suggested by analysis) above the binder-oxidizer interface the binder shape will be time-invariant, after a certain ignition transient.

For this initial model the absence of binder melts will be assumed. The limits of validity will then be determined by comparison of the model and experimental results. For the AP deflagration process the Guirao-Williams model[9] is accepted with an equilibrium assumption for the gas-solid interface. Some minor modifications are introduced into the model of

Reference (9) for computational convenience; these will be described below. Use of this model will restrict the sandwich theory validity to the pressure range 20-100 atm, because there is no AP theory capable of an explanation of observed phenomena above 100 atm.

Other usual assumptions are made to simplify the analysis which, while they lead to numerical errors of order unity, do not alter significantly the scaling rules developed with respect to other variables. These assumptions are: a) the thermal and transport processes of the solid AP and binder are identical, b) the thermal and transport properties of all gas phase species are identical, c) the Lewis number is everywhere unity in the gas phase, d) the deflagration process takes place at constant pressure, e) heat conduction and mass transfer take place by temperature and concentration gradients, only, respectively, and the transport coefficients are independent of temperature in both the solid and gas phases. A final major assumption is that on any vertical line parallel to the binder-oxidizer interface the ρv product (density times velocity) is that as determined in the solid phase and all lateral velocities are zero (strictly true in the solid phase). This is in the spirit of the Burke-Schumann approximation as expounded in Reference (10). This does yield error in convection effects upon heat transfer, but exact treatment of the problem is too complex.

The configuration is shown in Figure VI-1, in which the coordinate system is rendered stationary by a translation of the interface in the y direction at the rate r. Under the stated assumptions the equations for solution and the boundary conditions are:

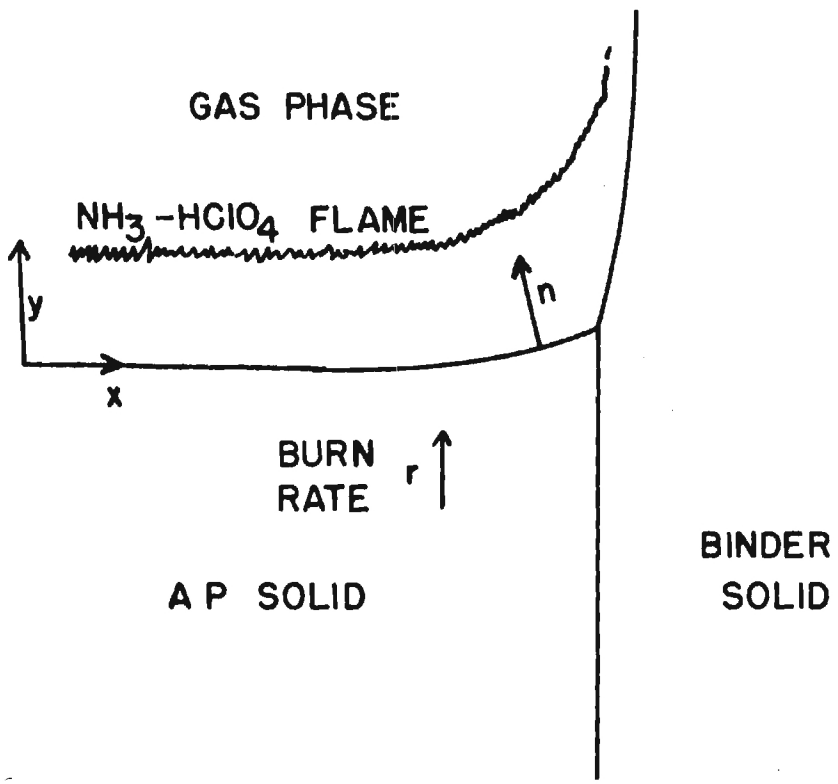

Figure VI-1. Sandwich Schematic and the Coordinate System.

Gas Phase Species Continuity

$$\frac{\lambda_g}{c_p}\left(\frac{\partial^2 Y_F}{\partial x^2} + \frac{\partial^2 Y_F}{\partial y^2}\right) = \rho v \frac{\partial Y_F}{\partial y} - w_F \qquad \text{(VI-1)}$$

Rate Law

$$w_F = -k\, Y_F^2\, e^{-E_g/RT} \qquad \text{(VI-2)}$$

Gas Phase Heat Transfer

$$\lambda_g\left(\frac{\partial^2 T}{\partial x^2} + \frac{\partial^2 T}{\partial y^2}\right) = \rho v c_p \frac{\partial T}{\partial y} + 2q_R w_F \qquad \text{(VI-3)}$$

Solid Phase Heat Transfer

$$\lambda_g\left(\frac{\partial^2 T}{\partial x^2} + \frac{\partial^2 T}{\partial y^2}\right) = \rho v c_s \frac{\partial T}{\partial y} \qquad \text{(VI-4)}$$

Boundary Conditions

$$Y_F(x,\infty) = 0 \qquad Y_F(-\infty,y) = \bar{Y}_F(y)$$

$$T(x,-\infty) = T_o \qquad T(-\infty,y) = \bar{T}(y) \qquad \text{(VI-5)}$$

$$T(\infty,y) = T_o \qquad T(x,\infty) = T_o$$

$$r_{n_B} = \vec{r}\cdot\vec{n}\Big|_B = b_B e^{-E_{s_B}/RT_s} \qquad \text{(VI-6)}$$

$$\lambda_g \frac{\partial T}{\partial n}\Big|_{s+} = \rho_s r_n q_s + \lambda_g \frac{\partial T}{\partial n}\Big|_{s-} \qquad \text{(VI-7)}$$

$$\rho D \frac{\partial Y_F}{\partial n}\Big|_{s+,AP} = -\rho_s r_n\left(\tfrac{1}{2} - Y_{F_s}\right) \qquad \text{(VI-8)}$$

$$p_{F_s} = b_F e^{-E_{s_F}/RT_s} \qquad \text{(VI-9)}$$

T continuous, ∇T continuous within a phase (VI-10)

$$dy_s/dx\,(-\infty) = 0 \qquad \text{(VI-11)}$$

The products of AP gasification are assumed NH_3 and $HClO_4$ which are assumed identical molecules for mass transfer computation. k is a rate coefficient for the assumed second order reaction; $k \propto p^2$. The factor 2 in front of $q_R w_F$ in Equation (VI-3) occurs because q_R is quoted per unit mass of AP rather than per unit mass NH_3. The equilibrium interface on AP is specified through Equation (VI-9). This formulation, as far as the AP deflagration process is concerned, differs from that of Reference (9) in the following respects: a) no dilution of the NH_3 and $HClO_4$ is assumed at the solid-gas interface, although it is tacitly accounted for by the choice of a number for q_S; b) calculations are simplified by taking the molecular weight of all species to be the same. The constants k and b_F will be so chosen to recover the same burn rate and surface temperature results as in Reference (9).

Equation (VI-6) is the pyrolysis law for the binder, Equation (VI-7) is the energy conservation law at the solid gas-interface, and Equation (VI-8) is the interface diffusion law. Note in Equation (VI-7) that q undergoes a discontinuity at the binder-oxidizer interface and Equation (VI-8) is only valid on the AP side of the interface. Shown in Table VI-1 are typical values used in this work for the various parameters.

Mathematical Character of the Problem

In this problem r will be specified from known AP results since the assumption is, as verified by experiment, that far from the binder the AP

undergoes a pure AP planar regression. The quantities k and b_F will be picked to make the analysis consistent, given r. Equations (VI-1 - 4) define an elliptic problem in the sense that what happens at one point in the field affects every other point. Yet, if the binder is hard to decompose and it assumes a nearly vertical surface, it appears obvious that the picture becomes one of a (nearly) flat plate of binder over which hot AP gases are flowing. If the Reynolds number based on distance along the binder were large enough this would revert to a parabolic problem because $\partial/\partial x \gg \partial/\partial y$ would result. However, exactly at the binder-oxidizer interface, the Reynolds number is zero. Since it is precisely this region that is of interest, the full elliptic problem must be solved. In order to gain an idea of magnitudes involved here the equations are nondimensionalized with respect to a distance scale α_s/r and temperature T_o. Heats of gasification are made dimensionless by $c_p T_o$ and activation energies by RT_o. The result is the following set of equations and boundary conditions:

$$Y_{F_{xx}} + Y_{F_{yy}} = \xi Y_{F_y} - \tilde{k} Y_F^2 e^{-\epsilon_g/g}$$

(Gas)
$$g_{xx} + g_{yy} = \xi g_y + 2q_R \tilde{k} Y_F^2 e^{-\epsilon_g/g}$$

(Solid)
$$g_{xx} + g_{yy} = g_y$$

$$Y_F(x,\infty) = 0 \qquad Y_F(-\infty,y) = \bar{Y}_F(y)$$

$$g(x,-\infty) = 1 \qquad g(-\infty,y) = \bar{g}(y)$$

$$g(\infty,y) = 1 \qquad g(x,\infty) = 1$$

$$1/z_B = \tilde{b}_B e^{-\epsilon_{S_B}/g_s}$$

$$\partial g/\partial n\big|_{s+} = \xi\left[q_s/z + \tilde{\eta}\,\partial g/\partial n\big|_{s-}\right]$$

$$\partial Y_F/\partial n\big|_{s+}^{AP} = -\xi\left(\tfrac{1}{2} - Y_{F_s}\right) \qquad \text{(VI-12)}$$

$$Y_{F_s} = \tilde{b}_F e^{-\epsilon_{s_F}/g_s}$$

g continuous, ∇g continuous within a phase

$$y_s'(-\infty) = 0$$

Table VI-1

Numerical Values for Various Parameters

Quantity	Value	Reference
T_o	300°K	Assumed
ρ_s	1.95 gm/cm^3	9
c_p	.3 cal/gm°K	9
c_s	.3 cal/gm°K	9
q_R	172 cal/gm	[to yield flame temperature of 1205°K of Ref. (9)]
$q_{S_{AP}}$	-100 cal/gm	9
λ_g	10^{-4} cal/cm sec°K	9
λ_s	9×10^{-4} cal/cm sec°K	9
E_g	15 kcal/mole	9
E_s	30 kcal/mole	9
E_{s_B}	8.7 - 17 kcal/mole	11
b_B	1 - 150 cm/sec	11
q_{s_B}	260 - 1004 cal/gm	11

The dimension α_s/r is known to be the "thickness" of the thermal wave which would occur in a planar regression. It is the reference dimension here. The parameter ξ in Equations (VI-12) is nothing more than the ratio of a characteristic solid phase dimension (α_s/r) to the characteristic gas phase dimension (α_g/v). If there were no modification due to the reaction rate term, the gas phase distance over which significant heat transfer would occur would be of the order of α_g/v. Using the parameters of Table VI-1, $\xi = 9.0$, showing that the gas and solid phase characteristic scales are quite different. Furthermore, constructing the Reynolds number based upon y, it is found that $Re_y = \xi y$, so that when y is of the order of $1/\xi$ a transition is taking place between "low" and "high" Reynolds numbers. If important field quantity variations are taking place only over a gas phase distance of the order of $1/\xi$, the problem must be treated as elliptic with no simplifications possible through a boundary layer assumption.

One characteristic of the problem does aid in simplifying the problem, however. The expectation is that fixing x and moving vertically above the surface the temperature would increase, reach a maximum near the point of reaction completion and then slowly decay due to heat transfer to the binder. This suggests the approximation that the temperature maximizes for fixed x at a point y where the reaction is complete. This will be adopted as an assumption and its use will be illustrated below. It is this assumption which allows a rather simple solution to be constructed.

That the problem is nonlinear can be easily seen in the chemical reaction times. A more subtle nonlinearity, arising from an unknown surface shape, can be best seen by changing the coordinate system from x, y to x, $\eta = y - y_s(x)$. Now all boundary conditions may be applied at the point

$\eta = 0$. Equations VI-12 become

$$Y_{F_{xx}} + z^2 Y_{F_{\eta\eta}} - 2y_s' Y_{F_{\eta x}} - y_s'' Y_{F_\eta} = \xi Y_{F_\eta} - \tilde{k} Y_F^2 e^{-\epsilon_g/g}$$

$$\text{(Gas)} \qquad g_{xx} + z^2 g_{\eta\eta} - 2y_s' g_{\eta x} - y_s'' g_\eta = \xi g_\eta + 2q_R \tilde{k} Y_F^2 e^{-\epsilon_g/g} \qquad \text{(VI-13)}$$

$$\text{(Solid)} \qquad g_{xx} + z^2 g_{\eta\eta} - 2y_s' g_{\eta x} - y_s'' g_\eta = g_\eta$$

Since y_s' is an unknown, the nonlinear appearance of Equations (VI-13) is apparent.

Solution by an Integral Technique

Pure AP Deflagration. Far from the binder the AP must undergo a planar deflagration. In this case Equations (VI-13) become

$$\bar{Y}_{F_{\eta\eta}} = \xi \bar{Y}_{F_\eta} - \tilde{k} \bar{Y}_F^2 e^{-\epsilon_g/g}$$

$$\text{Gas} \qquad \bar{g}_{\eta\eta} = \xi \bar{g}_\eta + 2q_R \tilde{k} \bar{Y}_F^2 e^{-\epsilon_g/g} \qquad \text{(VI-14)}$$

$$\text{Solid} \qquad \bar{g}_{\eta\eta} = \bar{g}_\eta$$

with the boundary conditions from Equations (VI-12) as

$$\bar{g}(-\infty) = 1 \qquad \bar{g}(\infty) = \bar{g}_f$$

$$\bar{T}_{\eta_g}(0) = \xi \left[q_s + \tilde{\eta} \bar{T}_{\eta_s}(0) \right]$$

$$\bar{Y}_F(\infty) = 0 \qquad \text{(VI-15)}$$

$$\bar{Y}_{F_\eta}(0) = -\xi \left(\tfrac{1}{2} - \bar{Y}_{F_s} \right)$$

$$\bar{Y}_{F_s} = \tilde{b}_F e^{-\epsilon_{s_F}/\bar{g}_s}$$

where the only independent variable is now η. A first integral of Equations (VI-14) subject to Equations (VI-15) is

$$\bar{g}(\eta) + 2q_R\bar{Y}_F(\eta) = \bar{g}_s + 2q_R\bar{Y}_{F_s} = \bar{g}_f \qquad \text{(VI-16)}$$

To gain an approximate solution to Equations (VI-14) let

$$\bar{Y}_F = \bar{Y}_{F_s}\left[1 - f(\eta/c)\right] \quad ; \quad \bar{g} - \bar{g}_s = (\bar{g}_f - \bar{g}_s)f(\eta/c)$$

where $f(0) = 0$, $f(1) = 1$ and c is the flame standoff distance. For simplicity, let $f = \eta/c$ and place this approximate form into the reaction rate expression of Equations (VI-14). Integrating the gas phase equations once and the solid phase equations twice yields

$$\begin{aligned}
&\text{(Solid)} \quad (\bar{g} - 1) = (\bar{g}_s - 1)e^{\eta} \\
&\text{(Gas)} \quad Y_{F_\eta} - \bar{Y}_{F_\eta}(0) = (\bar{Y}_F - \bar{Y}_{F_s})\xi - Q(\eta) \\
&\qquad \bar{g}_\eta - \bar{g}_\eta(0) = \xi(\bar{g} - \bar{g}_s) + 2q_R Q(\eta) \\
&\qquad\qquad Q(\eta) = \tilde{k}\bar{Y}_{F_s}^2 \int_0^\eta (1 - \eta/c)^2 \, e^{-\epsilon_g/\left[\bar{g}_s + (\bar{g}_f - \bar{g}_s)\,\eta/c\right]} d\eta
\end{aligned} \qquad \text{(VI-17)}$$

Furthermore, an overall energy balance yields

$$\bar{g}_f - \bar{g}_s = q_R - q_s - \tilde{\eta}(\bar{g}_s - 1) \qquad \text{(VI-18)}$$

which is the equation for the adiabatic flame temperature. Evaluation of Equations (VI-17) at $\eta = c$ and applying Equations (VI-15) there results

$$c = \bar{Y}_{F_s} / \xi (1/c - \bar{Y}_{F_s})$$

$$Q(c) = \bar{Y}_{F_s} \left(\frac{1}{c} + \xi\right) \qquad \text{(VI-19)}$$

$$\bar{Y}_{F_s} = \tilde{b}_F e^{-\epsilon_{s_F}/\bar{g}_s}$$

The procedure to complete the solution is the following: a) $\bar{g}_s$ as a function of pressure is taken from Reference (9); b) Equation (VI-18) yields $\bar{g}_f$ (which is actually constant here because $\tilde{\eta} = 1$ and q_R and q_s are assumed independent of pressure); c) Equation (VI-16) determines $\bar{Y}_{F_s}$; d) Equations (VI-19) determine c, $\tilde{b}_F$ and $\tilde{k}$.

From the nondimensionalization procedure it may be checked that $\tilde{k} \propto p^2/\bar{r}^2$. Therefore, if the rate, $\bar{r}$, is known at one pressure, it is known as a function of pressure. Shown in Table VI-2 are complete calculations for two sample pressures.

Table VI-2

One Dimensional AP Deflagration Results

p (atm)	$\bar{r}$ (cm/sec)	α_s/r (μm)	$\bar{T}_s$ (°K)	$\bar{g}_s$	$\bar{Y}_{F_s}$	$\bar{g}_f$	c	b_F (atm)	$\tilde{k}$
54.4	.735	20.9	880	2.93	.285	4.022	.1471	4.38×10^8	2.62×10^6
100.0	1.000	15.3	911	3.04	.258	4.022	.1183	4.06×10^8	3.39×10^6

In Table VI-2 it will be noted that b_F is not quite constant. This is due to the use of a slightly higher E_{s_F} than in Reference (9). Furthermore, $\tilde{k}$ is not quite proportional to $(p/\bar{r})^2$. This is due to the fact that $\bar{r}$ in Table VI-2 is the experimental value and it is known that between the two

values of pressure of Table VI-2 the theory of Reference (9) slightly overestimates the pressure sensitivity of the deflagration rate. These details are not considered important for the current theory because a precise model for AP deflagration is not sought; only the deviations from a planar regression, due to the binder essence , are required and the above theory appears adequate to serve as a baseline for perturbations due to the binder.

Perturbed Solution. Upon extensive investigation of the partial differential equations for small deviations from the one-dimensional regression it was determined that a) the deviations from the planar case in the gas phase could be expected to be simple deviations from the planar solution, but b) the solid phase deviations may be complex. By "simple" it is meant that the deviation is not oscillatory. Thus, if $g(x,y) = \bar{g}(x) + G(x,y)$ where $G(x,y)$ is the deviation from the pure AP case, $G(x,y)$ may be expected to have monatonic behavior in y between the two end values $G[x,y_s(x)]$ and $G[x,y_f(x)]$. Therefore, it was decided to attempt an integral solution where

$$Y_F = Y_{F_s}(x)\left[1 - \frac{\eta}{c(x)}\right]$$
$$g - g_s(x) = \left[g_1(x) - g_s(x)\right]\frac{\eta}{c} \qquad \text{(VI-20)}$$

are guessed forms of the solution. Equations (VI-20) are placed in Equations (VI-13) after an integration over η from $\eta = 0$ to $\eta = c$. The resulting nonlinear ordinary differential equations for the gas phase are

$$\left(Y_{F_s}\,\frac{c}{2}\right)'' = Q(c) - Y_{F_s}\left(\xi + \frac{z^2}{c}\right) - 2y_s' Y_{F_s}' - y_s'' Y_{F_s}$$

$$\left[(g_1 + g_s)\,\frac{c}{2}\right]'' = -2q_R Q + \xi(g_1 - g_s) + c'' g_1 \qquad \text{(VI-21)}$$

$$+ y_s''(g_1 - g_s) + 2y_s'(g_1' - g_s') + 2c' g_1'$$

The unknowns here are Y_{F_s}, c, y_s', g_1 and g_s. The boundary conditions from Equations (VI-12) become, using the assumed functional form of Equations (VI-20)

$$Y_{F_s}(-\infty) = \bar{Y}_{F_s} \qquad g_1(-\infty) = \bar{g}_f$$

$$g_s(-\infty) = \bar{g}_s \qquad c(-\infty) = \bar{c}$$

$$\bar{y}_s(-\infty) = 0$$

$$y_s' Y_{F_s}' = \xi\left(\tfrac{1}{2} - Y_{F_s}\right) - \frac{z^2 Y_{F_s}}{c}$$

$$\left(\frac{g_1 - g_s}{c}\right)_z + \left(\frac{y_s' g_s'}{z}\right) = \xi\left[\frac{q_s}{z} + \tilde{\eta}\left.\frac{\partial g}{\partial n}\right|_s\right] \qquad \text{(VI-22)}$$

$$Y_{F_s} = \tilde{b}_F e^{-\epsilon_{s_F}/g_s}$$

The first five of Equations (VI-22) are the left hand boundary conditions on the five unknowns of the ordinary differential equations, Equations (VI-21). The next two equations of Equations (VI-22) are the surface diffusion and heat transport relations, which form two more differential equations for the unknowns. The last of Equations (VI-22) is an algebraic relation between the unknowns. The system would be closed except for the

appearance of $\partial g/\partial n|_{s_-}$, so that the solid phase, of course, must be treated. A major difficulty in solution of the nonlinear problem may be seen in the terms $y_s' Y_{F_s}'$ and $y_s' g_s'$ of Equations (VI-22). At points of zero slope, $y_s' = 0$, a solution for g_s' and Y_{F_s}' is singular.

This singularity may be circumvented by first searching for asymptotic solutions to the problem which consists of the AP solution plus a small perturbation. The problem for the perturbation will be linear and the terms $y_s' g_s'$ and $y_s' Y_{F_s}'$ will be second order quantities (because $y_s'(-\infty)$ and $Y_{F_s}'(-\infty)$ are zero for the AP solution). Since this asymptotic solution would be required anyway because of the inability to carry out a machine integration to $x = -\infty$, this solution will be constructed. It will be seen below that this is all that is required for binder properties of usual interest.

Accordingly, the following forms are assumed:

$$Y_{F_s} = \bar{Y}_{F_s} + \mathcal{Y}_{F_s}(x) \qquad g_1 = \bar{g}_1 + G_1(x)$$

$$g_s = \bar{g}_s + G_s(x) \qquad c = \bar{c} + C(c)$$

$$y_s = Y(x)$$

Substituting into Equations (VI-21 and 22), making use of the AP solution properties, and neglecting products and squares of perturbation quantities, there results

$$\tfrac{1}{2}\left(\mathcal{Y}_{F_s}''\bar{c} + C''\bar{Y}_{F_s}\right) = G_1 Q_{g_1} + \mathcal{Y}_{F_s} Q_{y_{F_s}} + C Q_c - \bar{Y}'' Y_{F_s}$$

$$\tfrac{1}{2}\left[G_1''\bar{c} + G_s''\bar{c} + C''(\bar{g}_s - \bar{g}_1)\right] = -2q_R\left[G_1 Q_{q_1} + \mathcal{Y}_{F_s} Q_{y_{F_s}} + C Q_c\right]$$

$$+ Y''(\bar{g}_1 - \bar{g}_s) + (G_1 - G_s)\left(\xi + \frac{1}{\bar{c}}\right) - \frac{C(\bar{g}_1 - \bar{g}_s)}{\bar{c}^2}$$

$$Y_{F_s}\left(\xi + \frac{1}{\bar{c}}\right) = C\bar{Y}_{F_s}/\bar{c}^2 \qquad \text{(VI-23)}$$

$$\frac{G_1 - G_s}{\bar{c}} - \frac{(\bar{g}_1 - \bar{g}_s)\,C}{\bar{c}^2} = \bar{\eta}\left[\left.\frac{\partial g}{\partial n}\right|_{s-} - \left.\frac{\partial \bar{g}}{\partial n}\right|_{s-}\right]$$

$$Y_{F_s} = \frac{\bar{Y}_{F_s}\,\epsilon_{F_s}\,G_s}{\bar{g}_s^2}$$

$$Y_{F_s}(-\infty) = G_1(-\infty) = G_s(-\infty) = Y'(-\infty) = C(-\infty) = 0$$

Here Q_{g_1}, Q_c and $Q_{Y_{F_s}}$ are partial derivatives of the reaction rate integral which may be numerically evaluated.

Equations (VI-23) require a knowledge of the solid phase behavior through $\partial g/\partial n|_{s-}$. The linearized version of the solid phase equation of Equations (VI-13) is

$$g_{xx} + g_{\eta\eta} - g_\eta = Y'' g_\eta \qquad \text{(VI-24)}$$

In order to give sufficient freedom to the solid phase temperature profiles it is suggested from solutions to the homogeneous part of Equation (VI-24) to try

$$g = e^{m_{g_1}\eta}\left[G_o(x)\cos m_{g_2}\eta + G_1(x)\sin m_{g_2}\eta\right] + \bar{g}(\eta)$$

where m_{g_1} and m_{g_2} are constants to be determined. Inserting this assumed form into Equation (VI-24) and integrating over η from 0 to $-\infty$ there results

$$m_{g_2}G_1 + (m_{g_1} - 1)G_o + \frac{m_{g_1}}{m_{g_1}^2 + m_{g_2}^2}G_o'' + \frac{m_{g_2}}{m_{g_1}^2 + m_{g_2}^2}G_1'' = Y''(\bar{g}_s - 1) \qquad \text{(VI-25)}$$

Multiplying Equation (VI-24) by η, substituting in the expression for g and integrating from 0 to $-\infty$ there results a second differential equation for the unknowns G_1, G_o and Y':

$$G_o\left(\frac{m_{g_1}}{S} - 1\right) - G_1 \frac{m_{g_2}}{S} + \frac{m_{g_2}^2 - m_{g_1}^2}{S^2} G_o'' - \frac{2m_{g_1} m_{g_2}}{S^2} G_1'' = - Y''\left(g_s - 1\right) \qquad \text{(VI-26)}$$

$$S = m_{g_1}^2 + m_{g_2}^2$$

Note that at $\eta = 0$, $g_s = G_o + \bar{g}_s$, so that $G_s = G_o$ and G_o is not a new unknown. Calculating $\partial g/\partial n\big|_{s-}$ which is equal to $\partial g/\partial \eta\big|_{s-}$ to the linear approximation $\partial g/\partial n\big|_{s-} = \bar{g}_\eta(0) + G_1 m_{g_2} + G_o m_{g_1}$. Placing this result in the interface energy balance relation of Equations (VI-23) there results from Equations (VI-23, 25 and 26) four differential equations and three algebraic relations for the eight unknowns V_{F_s}, C, G_1, $G_s = G_o$, Y', G_1 and the two parameters m_{g_1} and m_{g_2}. The underspecification of the problem comes from the two arbitrary parameters m_{g_1} and m_{g_2} rather than specification of one of them. This difficulty will be resolved shortly. Consider for the moment that m_{g_1} and m_{g_2} have been specified; then there would be seven equations for the six field variables. By elimination of variables there could be chosen two independent sets of differential equations. But the equations are homogeneous and would posses solutions, for example, like $G_1 = A_{g_1} e^{mx}$. However, the root(s) m would have to be the same for the two independent sets of equations. This provides the condition for one of the parameters, say m_{g_1}. With two unknown parameters allowable roots would be obtained for a variety of $m_{g_1} = m_{g_1}(m_{g_2})$. This arbitrariness has been purposely introduced because this is a highly approximate technique and physical reasoning may have to be involved to choose the correct parameters.

In any event the procedure is the following: a) G_1'' is eliminated from Equations (VI-25 and 26), b) G_1 is solved for in this result and

placed into the interface energy conservation algebraic condition of Equations (VI-23), c) Y'' is solved for from the interface energy condition and placed in the differential equations of Equations (VI-23), d) the other two algebraic conditions are used in the differential equations of Equations (VI-23) to eliminate G_s and C in favor of V_{F_s}, and e) V_{F_s} is eliminated in favor of G_1 to yield a single fourth order, homogeneous differential equation of the form

$$a_1 G_1'''' + a_2 G_1'' + a_3 G_1 = 0$$

Now the a's are functions of the AP planar deflagration quantities and m_{g_1} and m_{g_2}. Setting $G_1 = A_{g_1} e^{mx}$ the four roots are

$$m = \pm \sqrt{\frac{-a_2 \pm \sqrt{a_2^2 - 4a_1 a_3}}{2a_1}} \qquad \text{(VI-27)}$$

A second independent differential equation is formed as follows: a) Y'' is eliminated between Equations (VI-26 and 26), yielding a differential equation in G_o and G_1, b) the energy conservation condition at the interface and one of the differential equations developed in step d) above is used to generate another differential equation in G_o and G_1, c) these differential equations are combined into a single fourth order differential equation of the form

$$b_1 G_o'''' + b_2 G_o'' + b_3 G_o = 0$$

where again the b's are functions of the quantities at $x = -\infty$ and m_{g_1} and

m_{g_2}. Letting $G_o = A_{G_o} e^{mx}$, an equation like Equation (VI-27) is developed with the b's replacing the a's. Since the roots m must be the same for a physically realistic result $m_{g_1} = m_{g_1}(m_{g_2})$, <u>if a solution exists</u>. There is no guarantee, however, that a solution satisfying these conditions may be found. Note that the quantity under the inner square root sign must be positive for m to be real. Although m could be allowed to be complex (not pure imaginary because the solution would not decay to the pure AP solution), a non-unique solution would arise. That is, the conditions developed below for attachment to a binder would be underspecified. It is imperative, therefore, that m be real for a realistic solution to be developed.

A numerical search for m_{g_1} and m_{g_2} to satisfy the requirements yields the surprising but satisfying results that a) m is real and b) solutions exist for only a very narrow range of m_{g_1} and m_{g_2} as seen in Figure VI-2. If $m_{g_1} = 1$, this would correspond to choosing the thermal wave "depth" the same as in the unperturbed case. Note also that $m_{g_1} = 1$ corresponds very nearly to the case when the allowable m_{g_2} becomes single-valued. Having confirmed an expectation that $m_{g_1} = 1$ is a reasonable choice, all further calculations assumed this value for m_{g_1}.

The perturbation solution is valid for A_{g_1} positive or negative; however, the only physically realistic solutions occur for negative A_{g_1} since the binder is a heat sink and will cool the gases of AP deflagration. In the perturbation solution (since the x and y origin is arbitrary) A_{g_1} is set equal to -0.01 at x = 0 and all other quantities may be computed from the linear differential equations, knowing m. The results for surface shape at two pressures are shown in Figure VI-3. Also shown are the temperature at the "edge" of the AP flame, the surface mass fraction of NH_3,

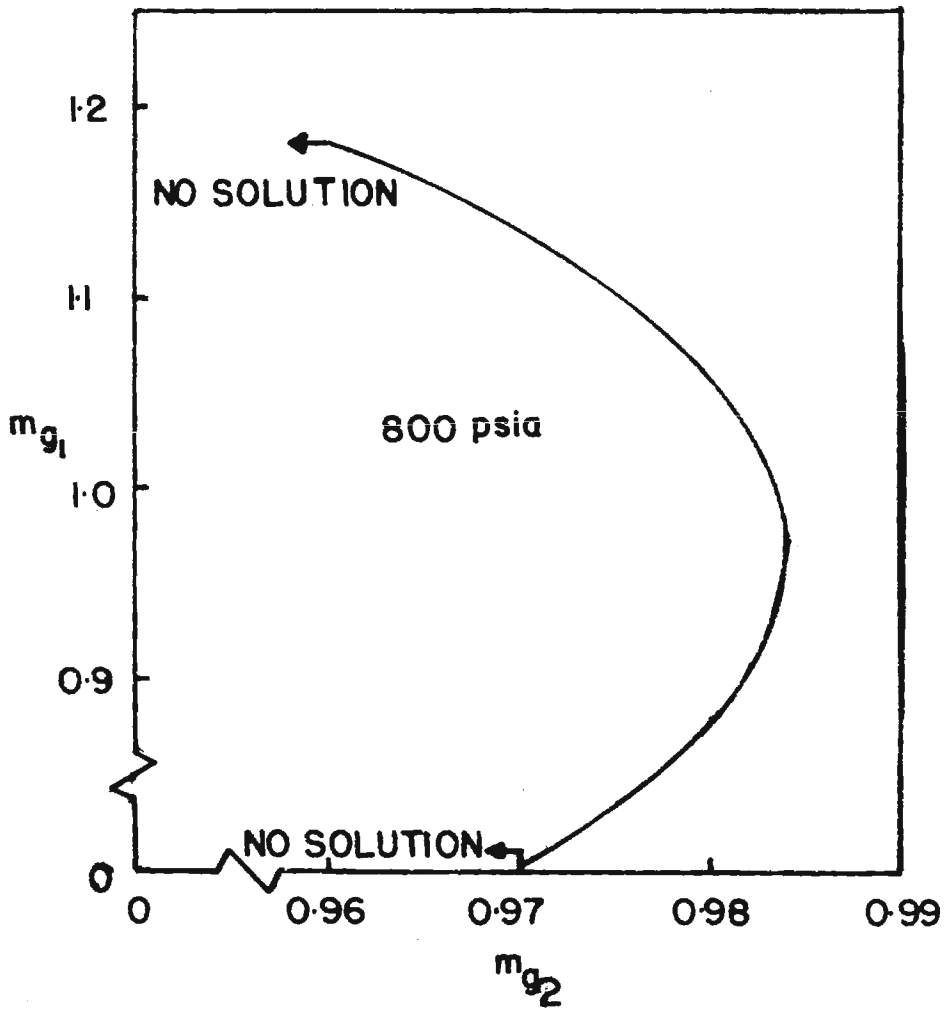

Figure VI-2. Allowable Values of the Solid Phase Temperature Profile Parameters.

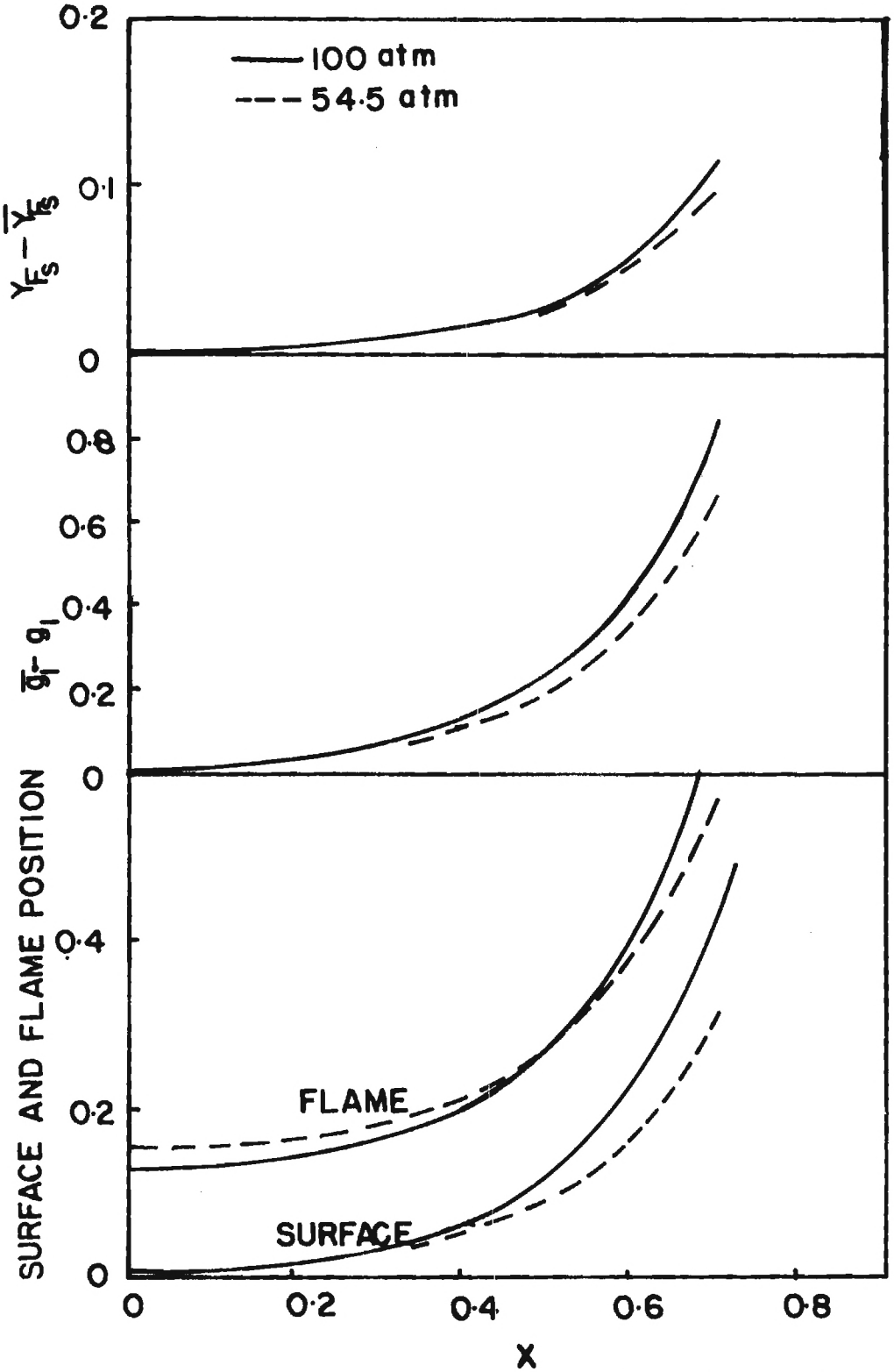

Figure VI-3. Surface, Flame Standoff, Surface NH_3 Mass Fraction and Flame Temperature Profiles.

and the flame height. It is seen that there is very little difference between the two cases when the results are in dimensionless form. The distance scales with which the variables y and x have been made dimensionless are 21 μm at 54.4 atm and 15.4 μm at 100 atm. Consequently, all surface profile changes are made in a somewhat shorter distance for the higher pressure case. It should also be noted that Y_{F_s} rises as the binder is approached; because of the equilibrium condition at the solid-gas interface this implies the surface temperature is rising as the binder is approached. Therefore, the heat transfer vector component parallel to the interface is toward the AP from the binder. This interesting result implies the maximum solid phase temperature will exist in the binder. It is physically due to the fact that the hot gases from the AP deflagration process sweep past the binder.

The foregoing is an "eigensolution" to the AP problem and is independent of the binder causing the perturbation from a planar regression. However, the location of the binder depends upon the properties of this eigensolution and the physical properties of the binder. A set of matching conditions to locate the binder on Figure VI-3 is now required.

Location of the Binder. At any x position in the eigensolution to the AP problem the heat transfer vector in the gas and solid phases is known. Since this must be a continuous quantity and the temperature is a continuous quantity, but q_s undergoes a discontinuity, there must be a surface slope discontinuity at the binder. In the interface energy conservation relation of Equations (VI-12) the solid and gas phase heat transfer vectors may be computed from the AP solution and this equation

becomes a relation for the binder heat of gasification as a function of its surface slope. The result is

$$q_{s_B} = y_B' G_o' \left(\tilde{\eta} - \frac{1}{\xi}\right) - \tilde{\eta}\left[m_{g_1} G_o + m_{g_2} G_1 + (\bar{g}_s - 1)\right] + \frac{(g_1 - g_s)(1 + y_B' y_F')}{c \qquad \xi} \tag{VI-28}$$

The pyrolysis condition of Equations (VI-12) gives an additional relation between the surface slope and the binder properties

$$\frac{1}{z_B} = \tilde{b}_B e^{-\epsilon_{s_B}/g_s} \tag{VI-29}$$

At any x position, then, Equations (VI-28 and 29) together with the AP eigensolution define an allowable binder attachment and a functional equation

$$b_B = b_B(\epsilon_{s_B}, q_{s_B}; x)$$

$$y_B' = y_B(\epsilon_{s_B}, q_{s_B}; x)$$

For the case of p = 54.4 atm these results are shown in Figures VI-4 and 5 for two values of ϵ_{s_B} which correspond closely to HTPB and CTPB binders[11]. Also, knowing q_s and b_B for HTPB and CTPB[11] the actual point at which these two binders would attach is shown on Figures VI-4 and 5. There are several points worthy of note. First, for these binders, the x position of compatability with the AP solution occurs where very little change

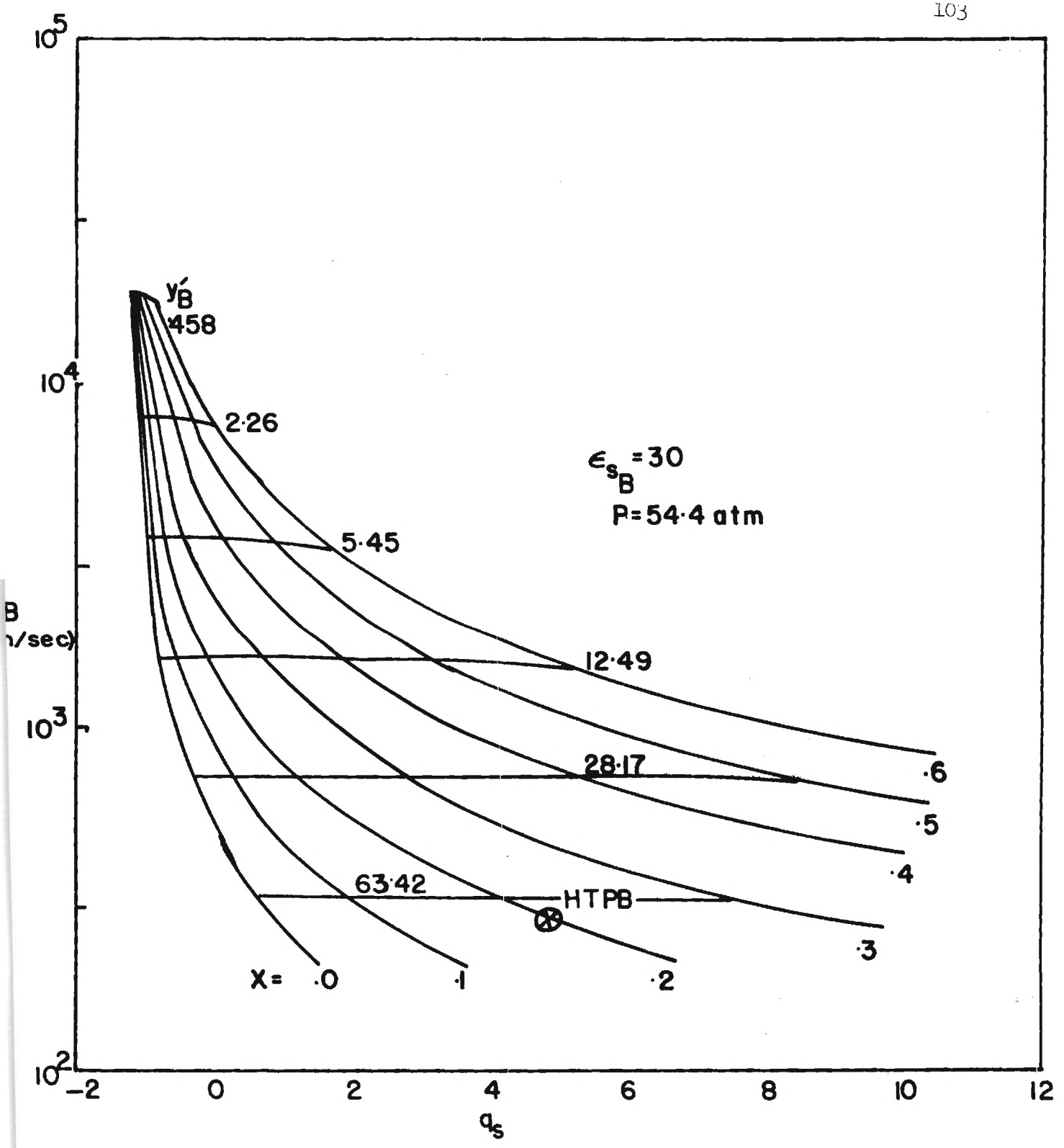

Figure VI-4. Binder Properties for Attachment to the AP Solution - p = 54.4 atm, ϵ_{s_B} = 15.

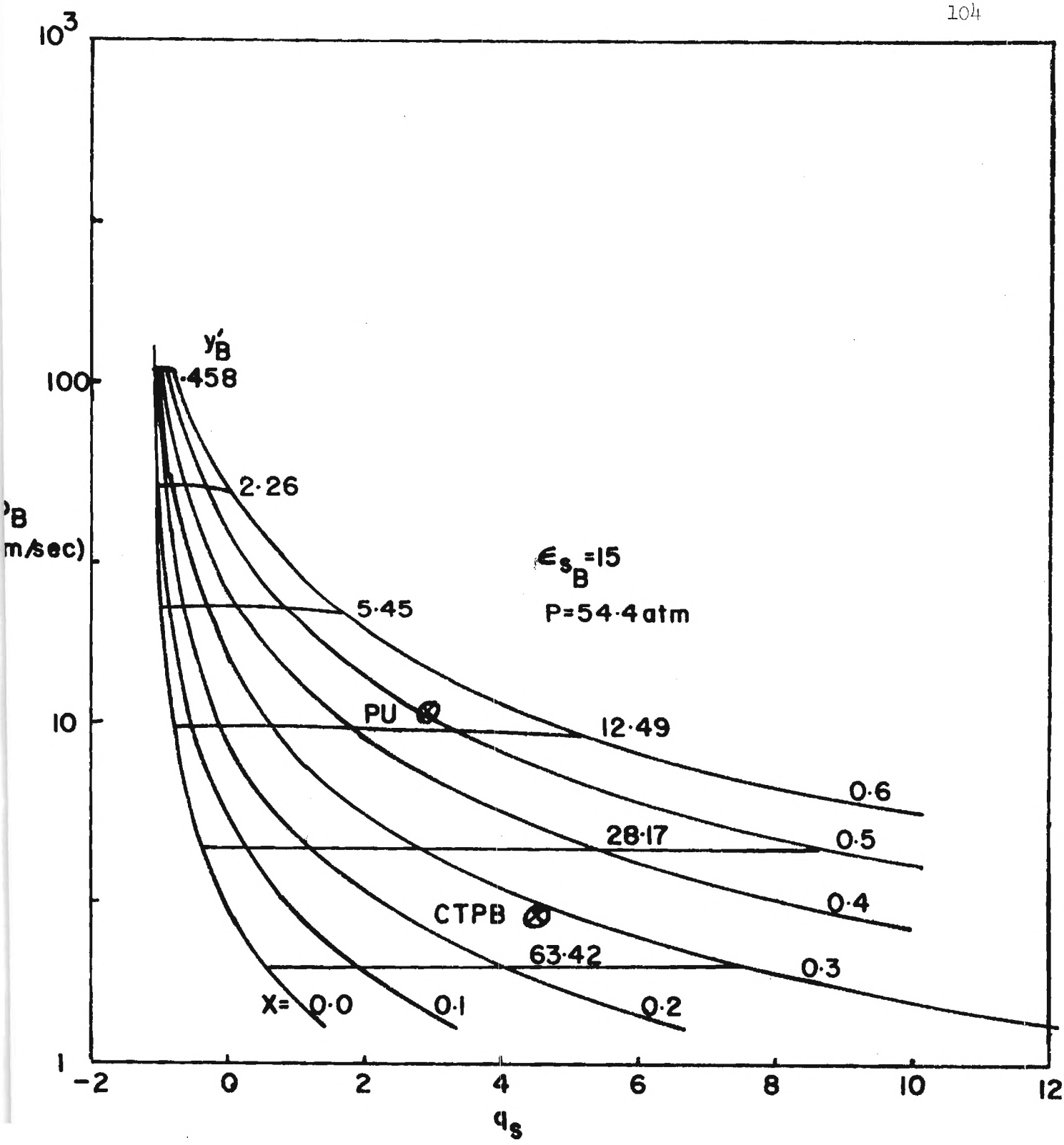

Figure VI-5. Binder Properties for Attachment to the AP Solution - p = 54.4 atm, ϵ_{s_B} = 30.

from a flat AP surface has taken place. Consequently, the linear AP eigensolution can be used with confidence as a good approximation to the solution of the nonlinear problem. Polyurethane, shown on Figure VI-4, would however attach in a region of reasonable surface slope and there is question concerning the adequacy of the solution. Fluorocarbon binder as used in Reference (11) would attach to the left of $x = 0$, or in a virtually flat region. The second point is that the values of y'_B are extremely high for all binders so that the slope would appear nearly vertical. This is the primary information desired, in addition to the AP surface profile, so no attempt is made to continue the solution to find the binder profile.

Shown on Figure VI-6 are the results for $p = 100$ atm for a surface activation energy $\epsilon_{s_B} = 30$. Noting the HTPB point, there would be virtually no visible distinction between the result at 100 atm and that at 54.4 atm.

Discussion of Results

A solution has been obtained for the shape of the deflagrating AP surface when it is adjacent to an inert binder. Except for selected binders there would be very little visible effect of the binder upon the surface shape and the result is virtually independent of pressure. The distance scale over which a visible transition would take place from planar AP to the binder is of the order of microns. The current theory assumes a dry binder; it is known, however, that binder melt flows exist for all binders tested heretofore in the sandwich configuration and that these melt flows run several hundred microns onto the AP surface. Consequently, none of the predicted phenomena are capable of being observed. A theory including the effects of melt flows is necessary.

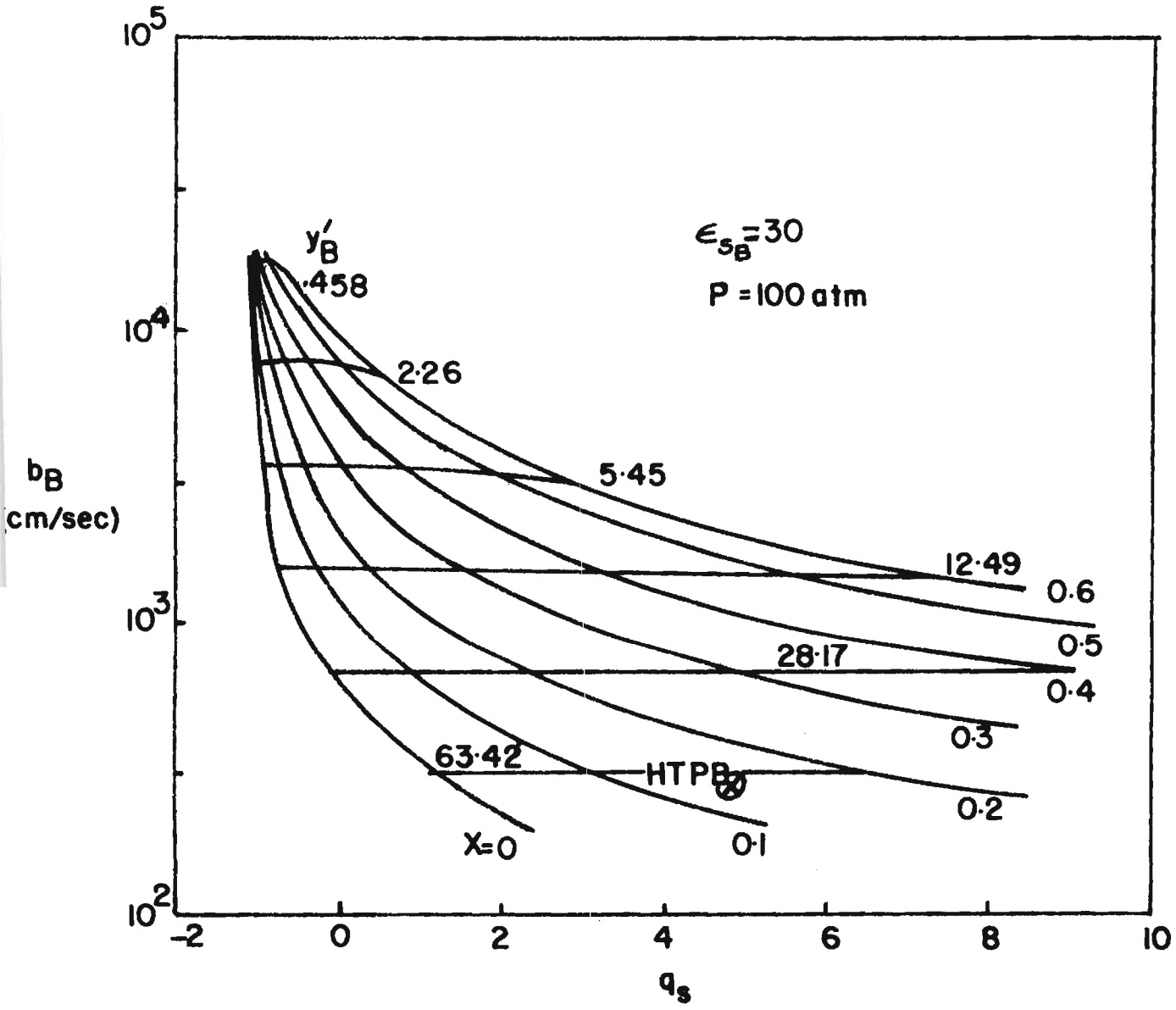

Figure VI-6. Binder Properties for Attachment to the AP Solution - p = 100 atm, ϵ_{s_B} = 30.

The theory predicts, however, that if the melts do not occur there should be a sharp discontinuity in slope at the binder-oxidizer interface. This has recently been seen for catalyzed sandwiches (Section III) for which the melt extent is markedly reduced (for unknown reasons). Although the current theory is not directly applicable to catalyzed situations the interface conditions responsible for the slope discontinuity are applicable. It appears that melt flows dominate the development of the surface shape if melts occur.

The current theory points to the fact that the surface temperature should increase as the binder is approached and the maximum solid phase temperature should occur in the binder. This might account for the appearance of "notches" in the binder, sometimes seen on quenched samples (e.g., see Figure III-30). The violence of the quenching process may eject the part of the binder above a surface of a prescribed strength level, which should be temperature sensitive. A rough sketch of isotherms near the interface should convince the reader that a weak binder may exist locally near the binder-AP interface.

The current analysis shows a very weak dependence of surface shape upon pressure. This independence has been observed experimentally, but the comparison between theory and experiment cannot be made precisely because binder melts have occurred in all the experiments.

The present theory contains no eigenvalue because the deflagration rate is determined by the AP deflagration process. If the binder were reactive, however, as occurs in catalyzed sandwiches, the burn rate must become an eigenvalue of the problem. It is not clear at this point how

this will enter the solution to the problem. Current analysis centers about this problem and the incorporation of binder melts into the solution.

SYMBOLS FOR SECTION VI

b	pyrolysis law constant or vapor pressure constant
$\tilde{b}$	dimensionless pyrolysis law constant or vapor pressure constant
c_s	solid phase specific heat
c_p	specific heat at constant pressure for gas phase
c	flame standoff distance
C	deviation of c from planar AP case
E	activation energy
g	T/T_o
G	deviation of temperature from planar AP case
G_o, G_1	solid phase temperature perturbation functions
k	preexponential factor in reaction rate law
$\tilde{k}$	dimensionless preexponential factor in reaction rate law
m_{g_1}, m_{g_2}, m	constants in eigensolution
n	coordinate normal to the solid-gas interface directed toward the gas phase
p	pressure
Q	reaction integral defined by Equations (VI-17)
q	exothermic reaction heat
R	universal gas constant
Re	Reynolds number
r, r_n	burn rate and regression rate normal to surface, respectively
T	temperature
v	gas velocity in y direction
w_F	production rate of NH_3

x,y	coordinates
Y	perturbed y position of solid surface
Y_k	mass fraction of species k
y	deviation of mass fraction from planar AP case
z	$\sqrt{1 + (dy_s/dx)^2}$
α	thermal diffusivity, $\lambda/\rho c$
ϵ	dimensionless activation energy, E/RT
η	c_s/c_p
λ	thermal conductivity
ξ	$c_p\lambda_s/c_s\lambda_g$
ρ	density

Subscripts

B	binder
f	flame temperature
F	NH_3
g	gas phase
o	cold solid
s	solid phase or surface
1	quantity evaluated at flame standoff position

Subscript by independent variable denotes partial differentiation with respect to that variable

Superscripts

$-$	quantity evaluated for the one-dimensional AP deflagration
$'$	ordinary derivative with respect to x

VII. CONCLUSIONS

1. Depending upon the catalyst type there are different degrees of catalysis or inhibition upon the AP deflagration rate and the reactions between the oxidizer and binder. Generally the copper compounds in CuO202 have a greater catalytic effect upon the AP deflagration rate than do the iron compounds, which often inhibit the AP rate, but the iron compounds appear to have a stronger catalytic effect upon the binder-oxidizer reactions.

2. A significant discovery of this program is the apparent removal or inhibition of the binder melt flow when catalysts are present. While the mechanism of removal is not certain, the melt removal alone may be an important "catalytic" mechanism in the augmentation of deflagration rate.

3. In an uncatalyzed state the binder is effectively an inert substance which inhibits the AP deflagration rate by acting as a heat sink and a source of a melt flow; when the catalysts are present, however, the reactions between the binder and oxidizer become sufficiently fast that heat feedback from these reactions augment the deflagration rate. The most effective placement of the catalyst, to produce this effect, is in the oxidizer, suggesting that the catalytic reactions take place away from the binder surface, whether the actual catalytic reactions are heterogeneous or not, and that the catalytic reactions prefer high temperatures.

4. In the pressure range 600-2000 psia there is very little change in catalytic mechanisms or overall sandwich deflagration behavior with a pressure variation. There is, of course, a general increase in rate of various rate processes with pressure and iron oxide changes from an inhibitor to an augmentor of the AP deflagration rate at about 1200 psia.

5. The surface structure of AP during deflagration changes markedly when catalysts are present, suggesting that alteration of condensed phase reactions may take place in the AP. Electron microprobe studies with iron blue in AP were inconclusive but suggested that iron is removed from the catalyst in the vicinity of the condensed phase surface at a faster rate than other elements.

6. At low pressures (<800 psia) iron blue and ferrocene appear to have a catalytic effect when placed into the binder, which is an effect not seen at higher pressures and with other catalysts. Consequently, the low pressure region should be explored in detail.

7. While it is possible to draw certain conclusions concerning real propellant results from the sandwich experiments with catalysts, especially with regard to pressure and AP particle size effects, there is uncertainty concerning the relative importance of AP catalysis and binder-oxidizer reaction catalysis in a real propellant. The results of this program are able to predict the near-equivalence of ferrocene and iron oxide in propellants, but there is uncertainty as to a comparison of the iron and copper compounds.

8. Regardless of the catalyst it should be most effective in a real propellant if it is a) loaded into the oxidizer, b) operated at high pressure and c) present in a propellant with small AP particle size (high specific area of the AP).

9. Analysis of the sandwich configuration for the case of no binder melt flows and negligible rate of the binder oxidizer kinetics has yielded an explanation for the following observed experimental facts: a) the sandwich shape for uncatalyzed cases should be pressure independent over the

range 20-100 atm; b) there should be very little distinction between the surface shapes for CTPB and HTPB binders, and c) in the case where melts are removed there should be a discontinuity in slope at the binder-oxidizer interface. Furthermore, the maximum condensed phase temperature should exist in the binder which may explain some interesting binder shapes, experimentally observed, caused by binder ejection during the quench process.

REFERENCES

1. Strahle, W. C., Handley, J. C. and Milkie, T. T., "Catalytic Effects in the Combustion of AP-HTPB Sandwiches to 3200 psia," AIAA Paper No. 72-1120 (1972).

2. Jones, H. E. and Strahle, W. C., "The Effects of Copper Chromite and Iron Oxide Catalysts on AP/CTPB Sandwiches," Fourteenth (International) Symposium on Combustion, The Combustion Institute, Pittsburgh (1973).

3. Hightower, J. D. and Price, E. W., "Experimental Studies Relating to the Combustion Mechanism of Composite Propellants," Astronautica Acta, 14, 11-21 (1968).

4. Varney, A. M. and Strahle, W. C., "Experimental Combustion Studies of Two-Dimensional Ammonium Perchlorate-Binder Sandwiches," Combustion Science and Technology, 4, 197-208 (1972).

5. Boggs, T. L. and Zurn, T. E., "The Deflagration of Ammonium Perchlorate-Polymeric Binder Sandwich Models," Combustion Science and Technology, 4, 279-292 (1972).

6. Boggs, T. L., "The Deflagration of Pure Single Crystals of Ammonium Perchlorate," AIAA Paper No. 69-142 (1969).

7. Friedman, R., Nugent, R. G., Rumbel, K. E. and Scurlock, A. C., "Deflagration of Ammonium Perchlorate," Sixth Symposium (International) on Combustion, Reinhold, New York (1957), pp. 612-618.

8. Lyles, B. J., Letter to W. C. Strahle dated 22 September 1972, Thiokol Chemical Corporation, Bristol, Pennsylvania.

9. Guirao, C. and Williams, F. A., "A Model for Ammonium Perchlorate Deflagration Between 20 and 100 atm," AIAA Journal 9, 1345-1356 (1971).

10. Williams, F. A., Combustion Theory, Addison-Wesley, Reading (1965), p. 39.

11. Cohen, N. S., Fleming, R. W. and Derr, R. L., "Role of Binder in Solid Propellant Combustion," AIAA Paper No. 72-1121 (1972).

APPENDIX A

CATALYSTS LOCATED AT THE BINDER-OXIDIZER INTERFACE

The samples for this phase of the investigation were prepared by adding a mixture of 2% AP and 2% catalyst (by weight) to the surface of a lightly pressed AP disk. This composite disk of catalyst and AP was then subjected to the normal disk and sample preparation procedure[1]. This narrow-band "interface" catalyst layer adhered well to both the binder and oxidizer. A series of 7 triple sandwiches, each containing two interface disks, is shown in Figures A-1 through 27. The results are summarized in Table A-1. The samples with CC, IB and F at the interface did not consistently exhibit continuous surface slopes at the binder-catalyst-oxidizer interface.

Table A-1

Summary of Results from Scanning Electron Microscopy of Catalyst Located at Binder-Oxidizer Interface

Catalyst	Pressure psia	Figure No. A-	Binder Melt μm	Binder-Catalyst-Oxidizer Interface
Cu0202	600	1,2,3	none	additional porous material at point of max regression, AP surface smooth.
	1000	5,6	none	uneven burn, porous material at interface, AP surface smooth for 300 μm from interface.
	1500	8,9,10	none	uneven burn, small amount of material at interface, AP surface smooth for 100 μm from interface.
	2000	13,14		same as above.

Table A-1 (Continued)

Catalyst	Pressure psia	Figure No. A-	Binder Melt μm	Binder-Catalyst-Oxidizer Interface
IO	600	1,4	<50	porous structure visible, continuous interface slope.
	1000	5,7	75	porous structure visible, continuous interface slope.
	1500	8,11,12	20	porous structure visible, continuous interface slope.
	2000	13,15	none	porous structure visible, discontinuous interface slope.
F	600	16,17	200	continuous interface.
	1000	19,20,21	175	continuous interface, bubble.
	2000	24,25,26	50	porous structure at interface, uneven burn.
IB	600	16,18	none	porous material at interface.
	1000	19,22,23	none	porous material at interface, uneven burn.
	2000	24,27	30	porous material at interface, uneven burn.

In most cases this was due to the additional porous or frothy material extending above the leading edge of regression and separated from the solidified HTPB. Some samples exhibited pockets of localized combustion. These were usually noted when several attempts were made to obtain a quenched sample. The delay times for the depressurization were not consistent with the results from the cinephotomacrography. The non-uniformity of the burns was also not expected after viewing the high speed movies.

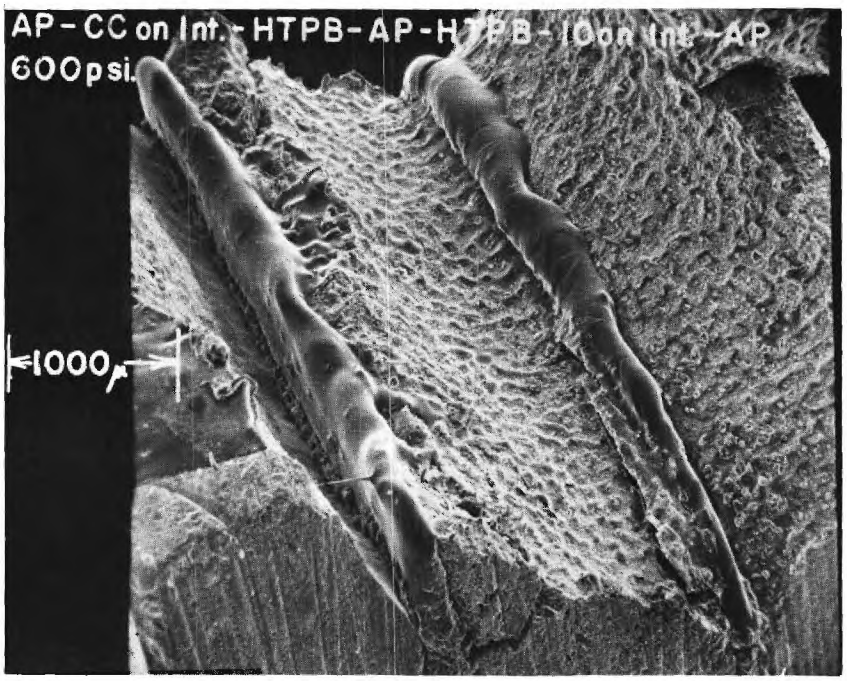

Figure A-1. AP-CC on Int.-HTPB-AP-HTPB-IO on Int.-AP 600 psia (x23).

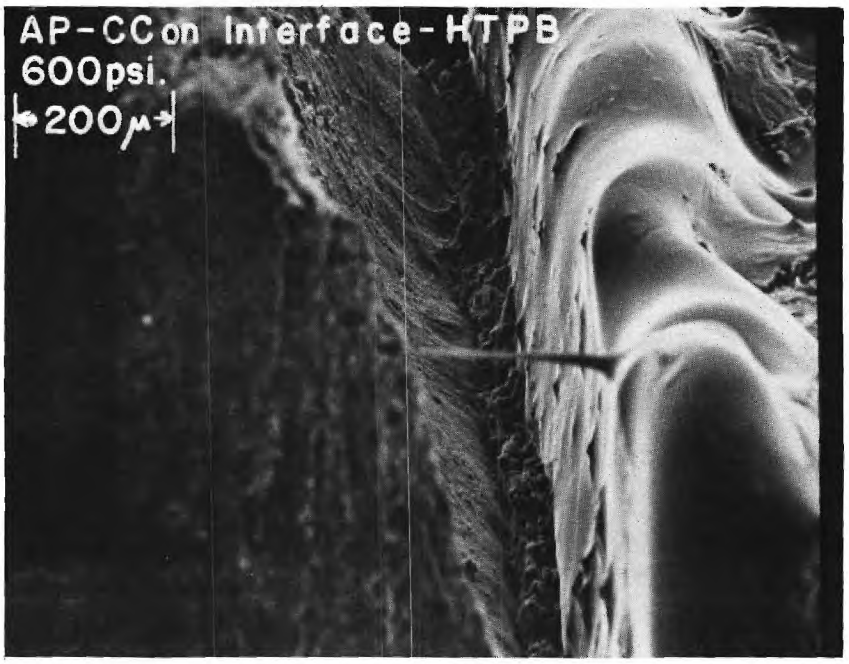

Figure A-2. AP-CC on Int.-HTPB 600 psia (x105).

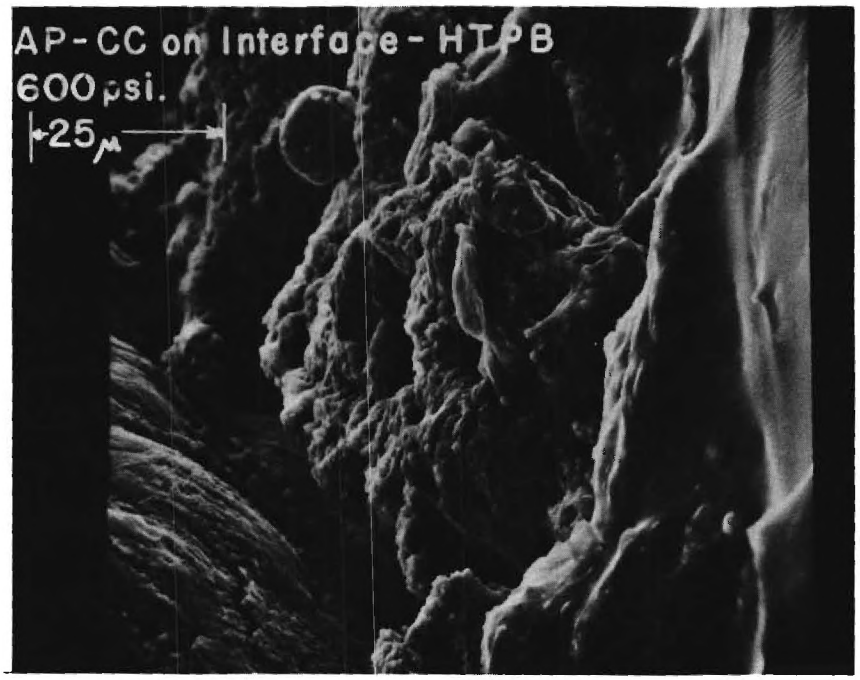

Figure A-3. AP-CC on Int.-HTPB 600 psia (x1050).

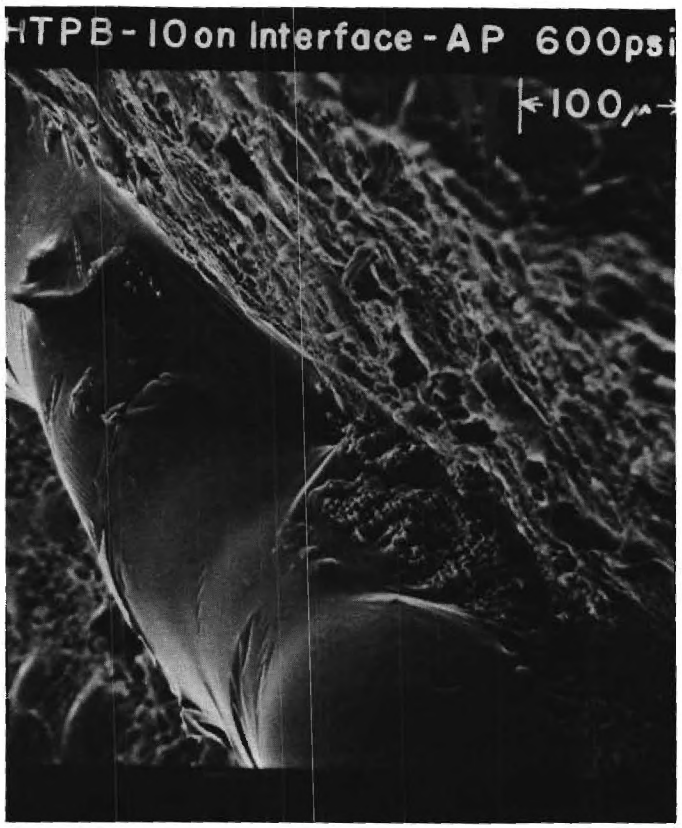

Figure A-4. AP-HTPB-10 on Int.-AP 600 psia (x225).

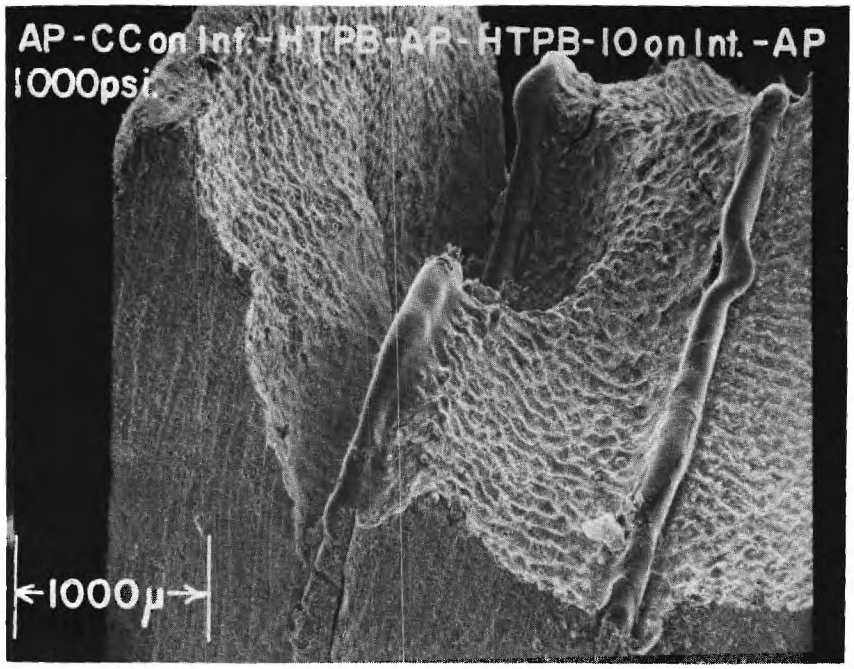

Figure A-5. AP-CC on Int.-HTPB-AP-HTPB-IO on Int.-AP 1000 psia (x26).

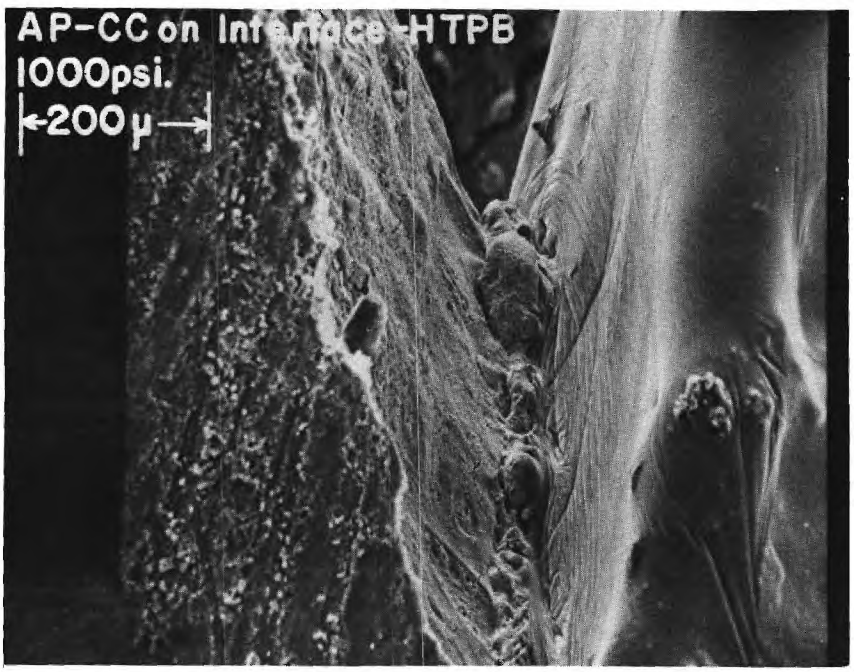

Figure A-6. AP-CC on Int.-HTPB 1000 psia (x125).

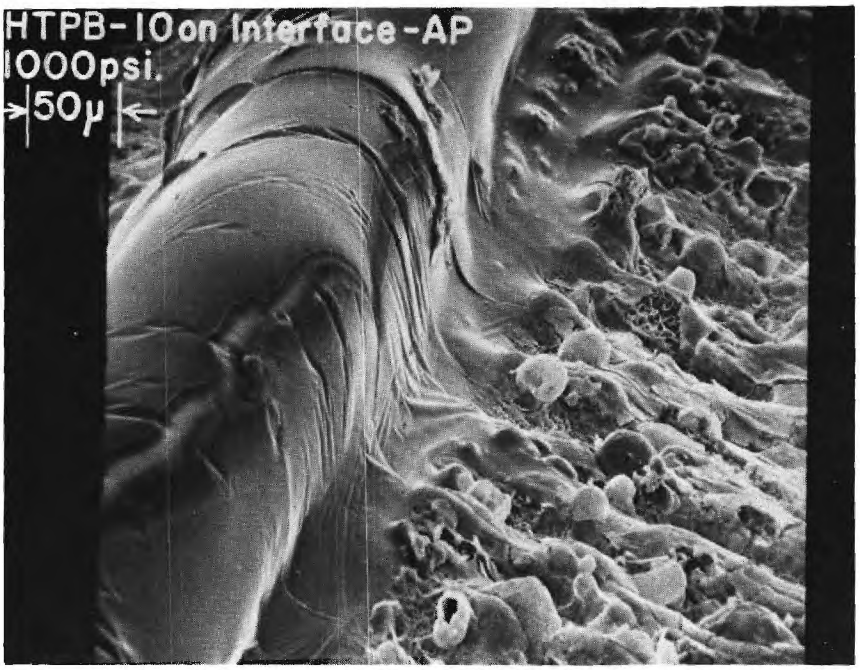

Figure A-7. HTPB-IO on Int.-AP 1000 psia (x250).

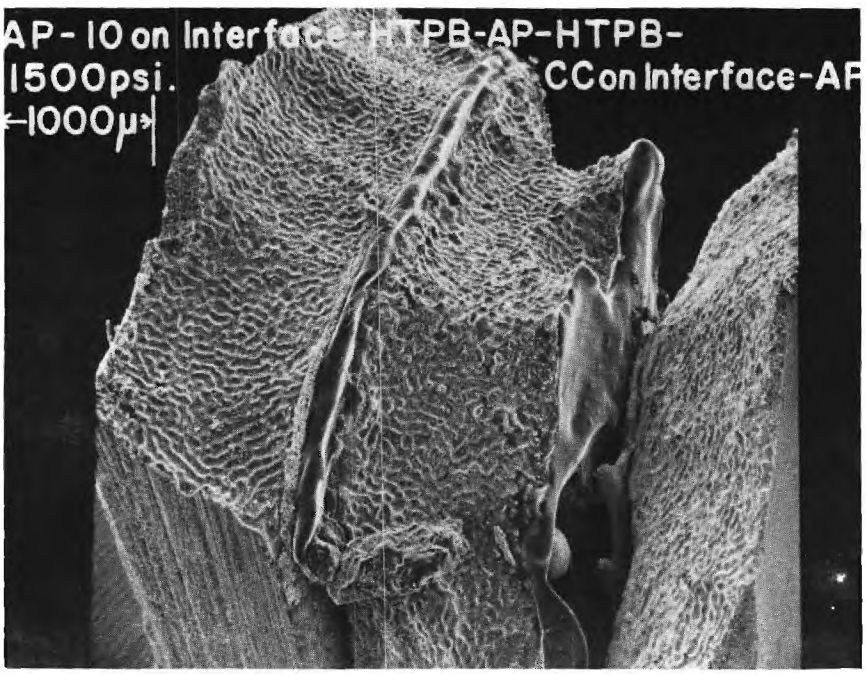

Figure A-8. AP-IO on Int.-HTPB-AP-HTPB-CC on Int.-AP 1500 psia (x20.4).

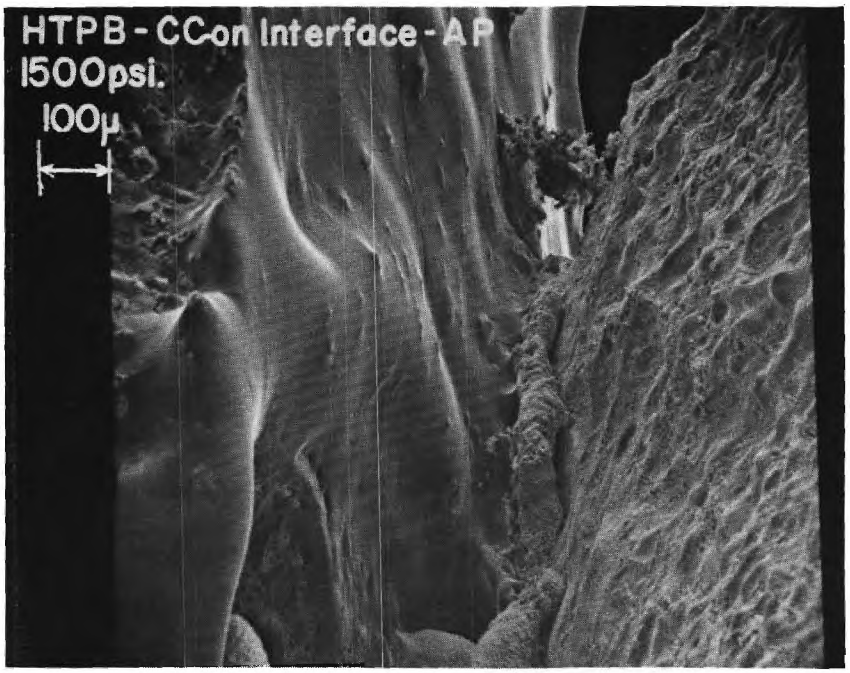

Figure A-9. HTPB-CC on Int.-AP 1500 psia (x90).

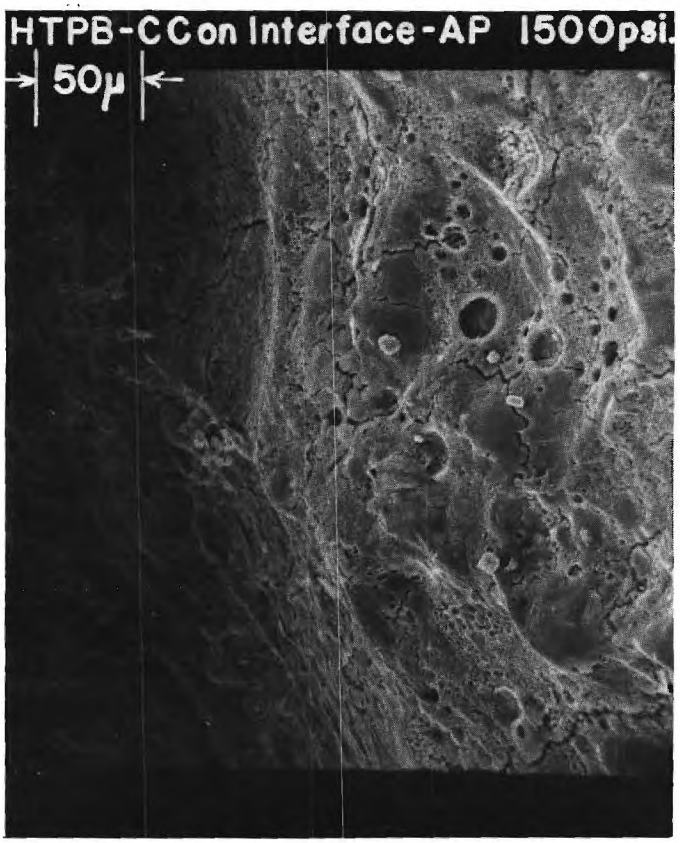

Figure A-10. HTPB-CC on Int.-AP 1500 psia (x273).

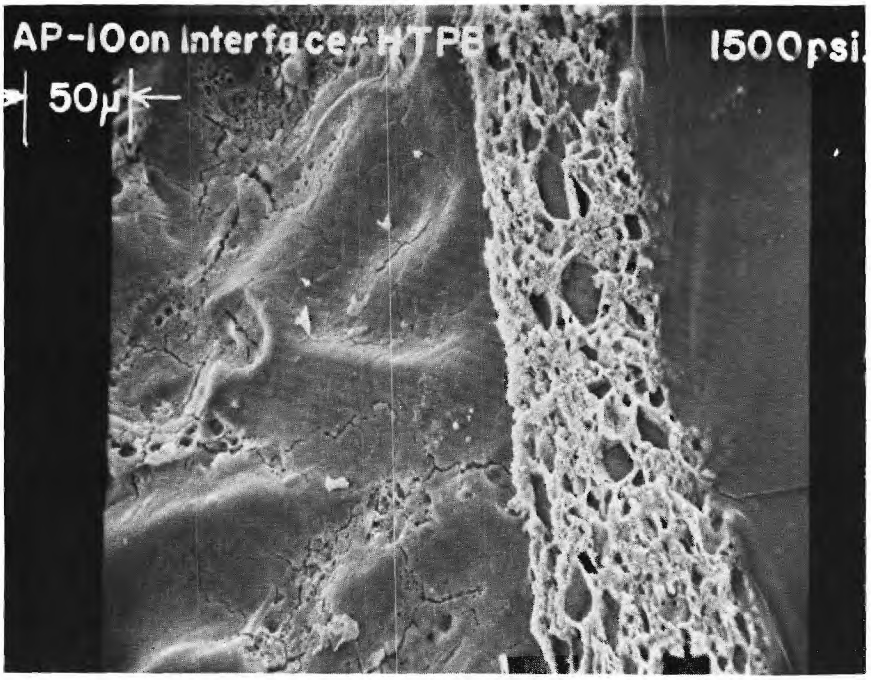

Figure A-11. AP-IO on Int.-HTPB 1500 psia (x280).

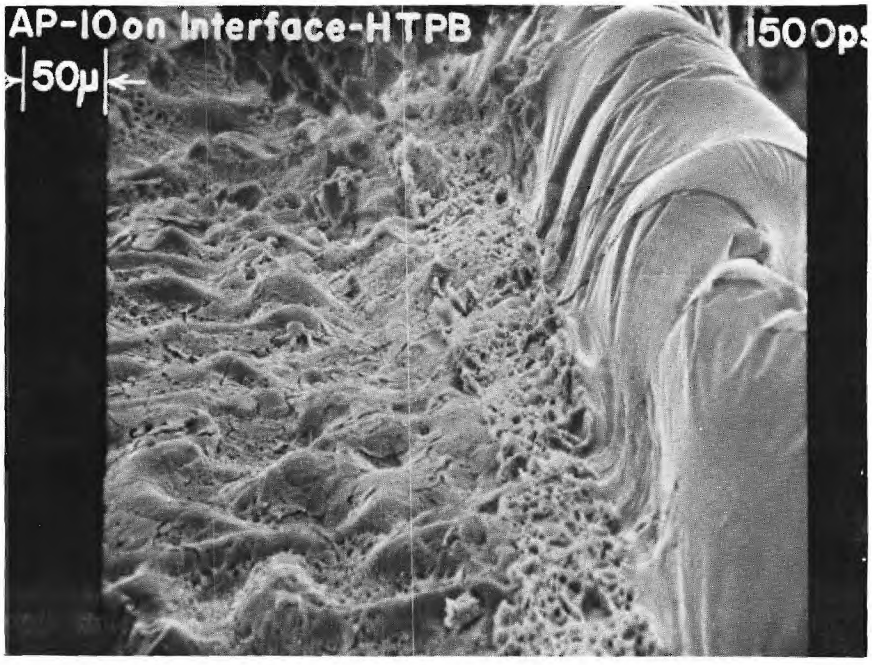

Figure A-12. AP-IO on Int.-HTPB 1500 psia (x228).

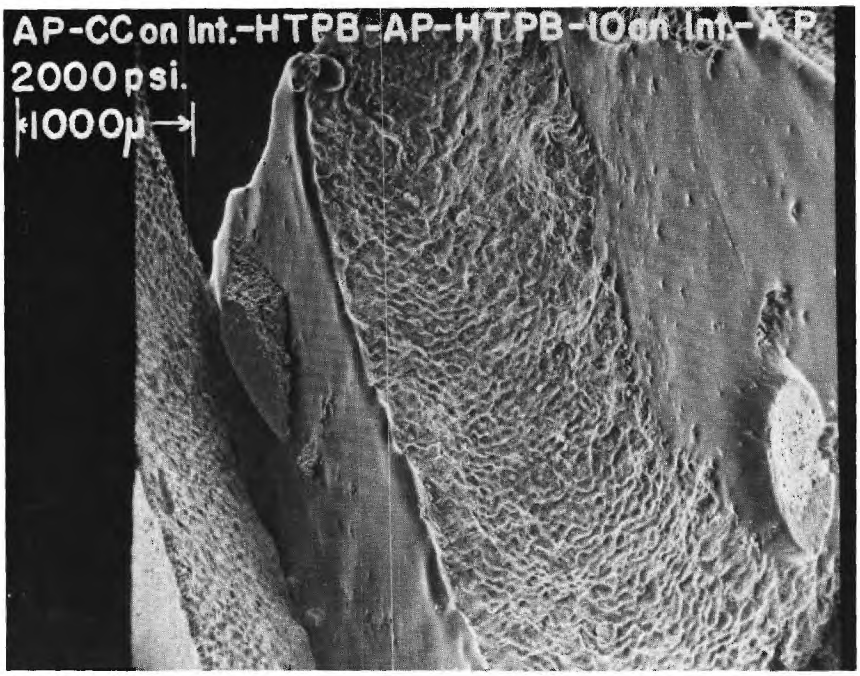

Figure A-13. AP-CC on Int.-HTPB-IO on Int.-AP 2000 psia (x23.5).

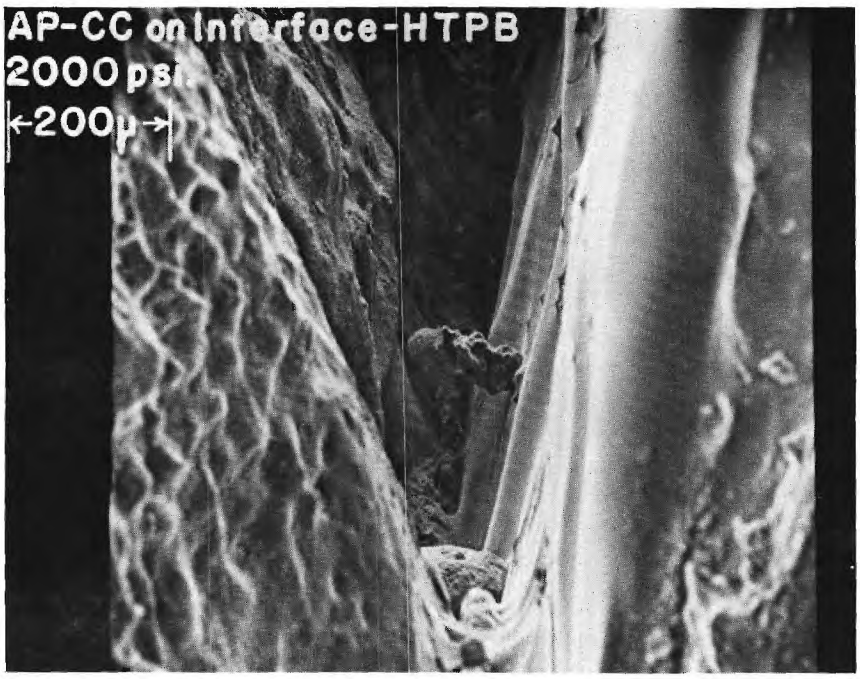

Figure A-14. AP-CC on Int.-HTPB 2000 psia (x108).

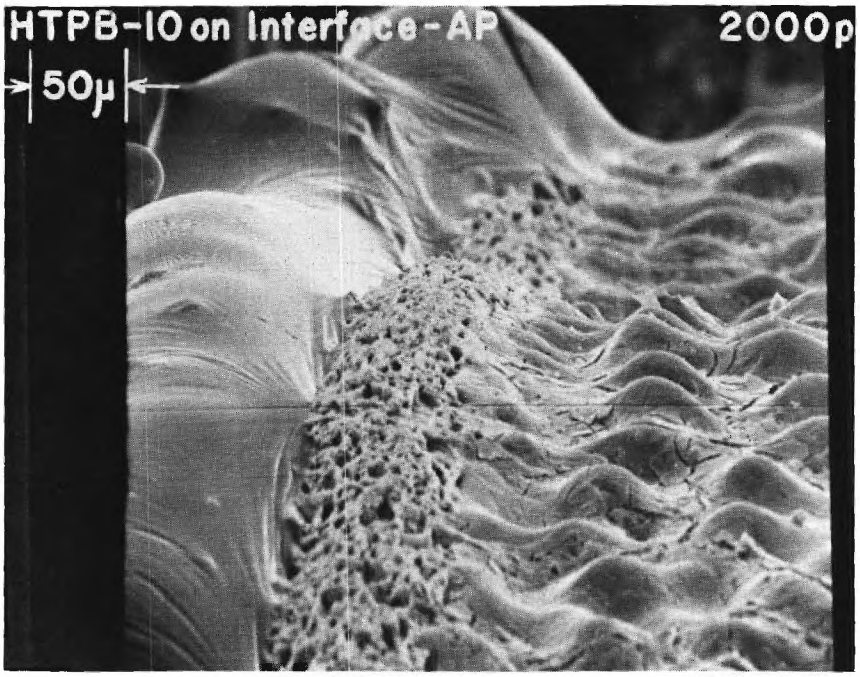

Figure A-15. HTPB-10 on Int.-AP 2000 psia (x260).

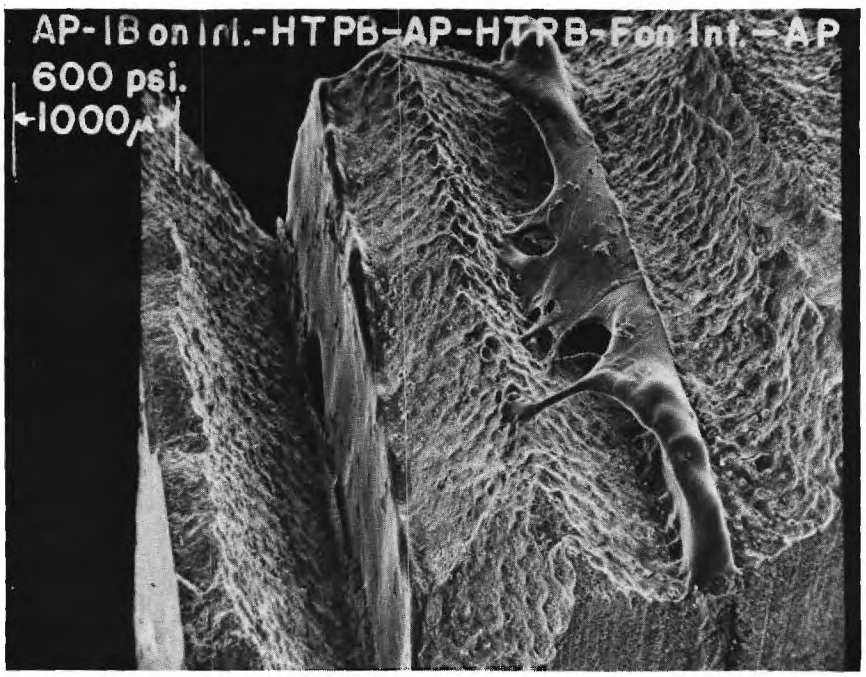

Figure A-16. AP-IB on Int.-HTPB-AP-HTPB-F on Int.-AP 600 psia (x22).

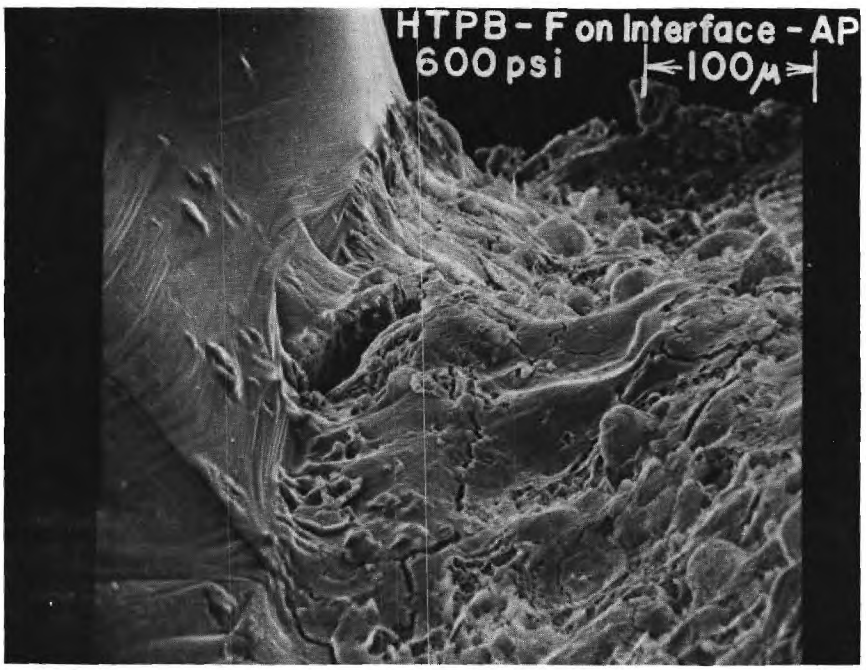

Figure A-17. HTPB-F on Int.-AP 600 psia (x225).

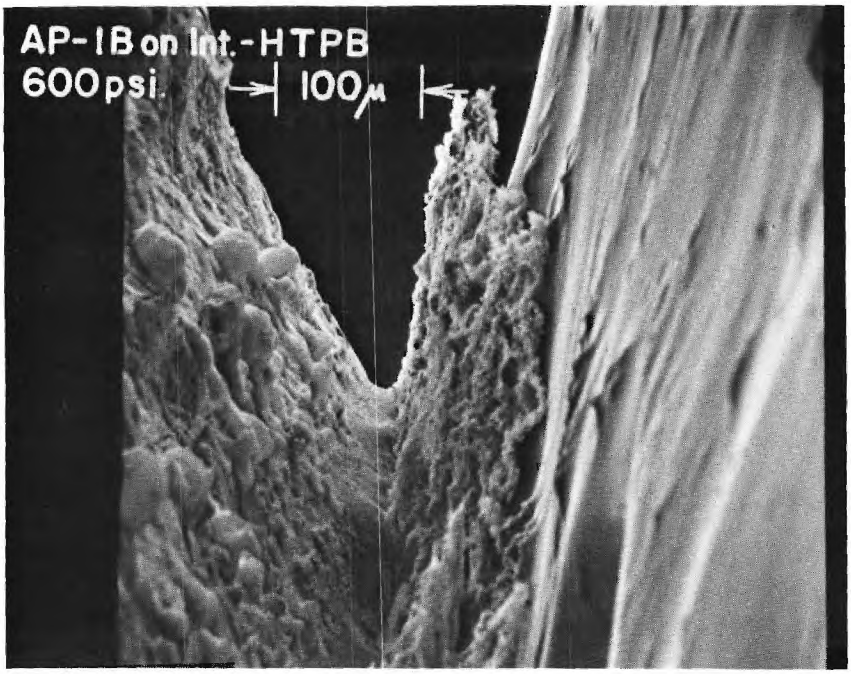

Figure A-18. AP-IB on Int.-HTPB 600 psia (x195).

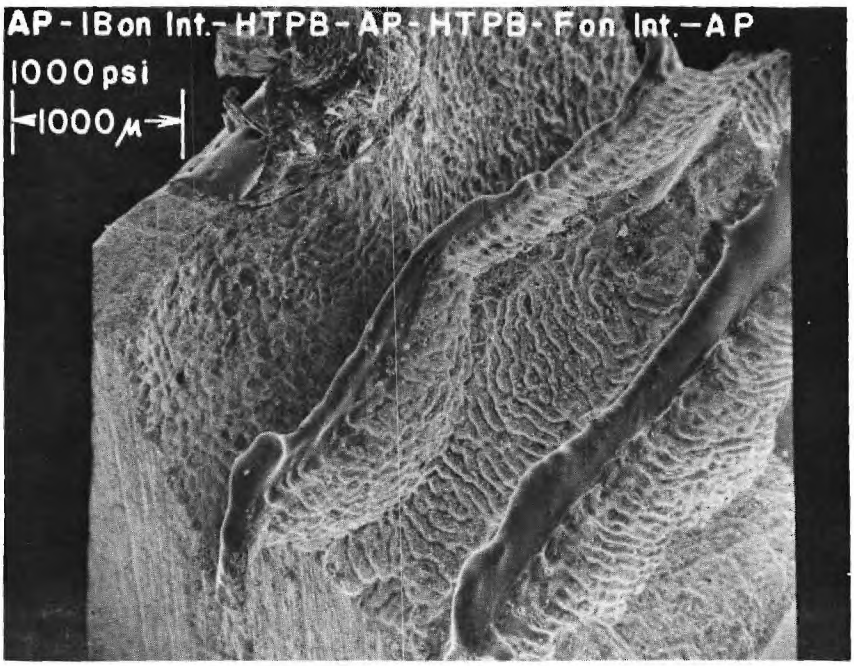

Figure A-19. AP-IB on Int.-HTPB-AP-HTPB-F on Int.-AP 1000 psia (x23).

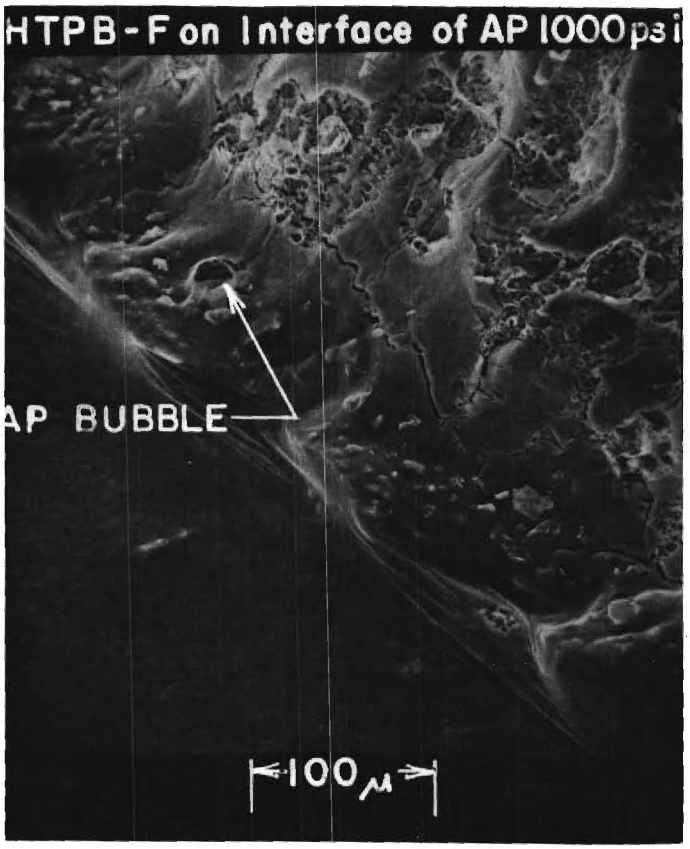

Figure A-20. HTPB-F on Int.-AP 1000 psia (x240).

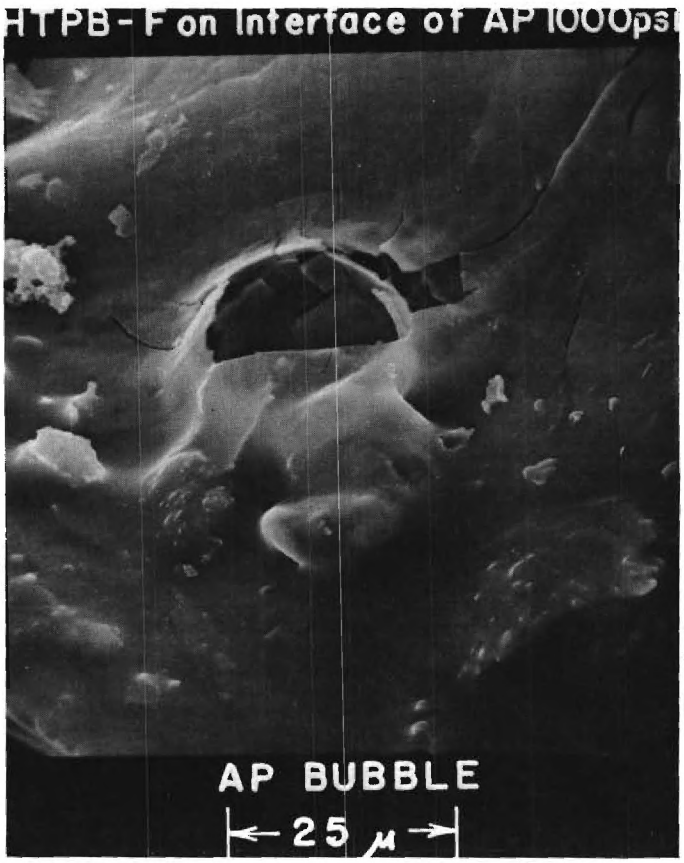

Figure A-21. HTPB-F on Int.-AP 1000 psia (x1200).

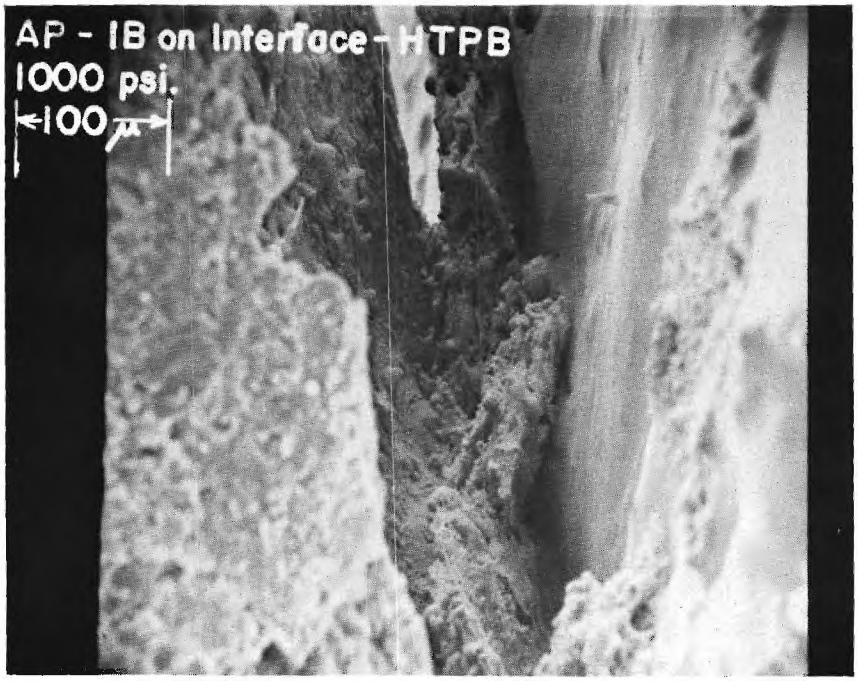

Figure A-22. AP-IB on Int.-HTPB 1000 psia (x208).

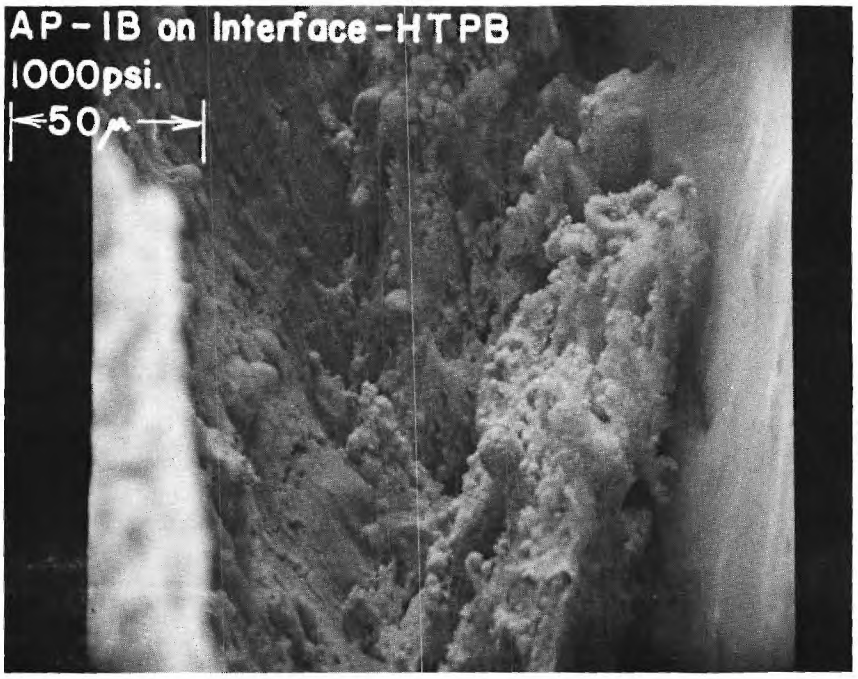

Figure A-23. AP-IB on Int.-HTPB 1000 psia (x520).

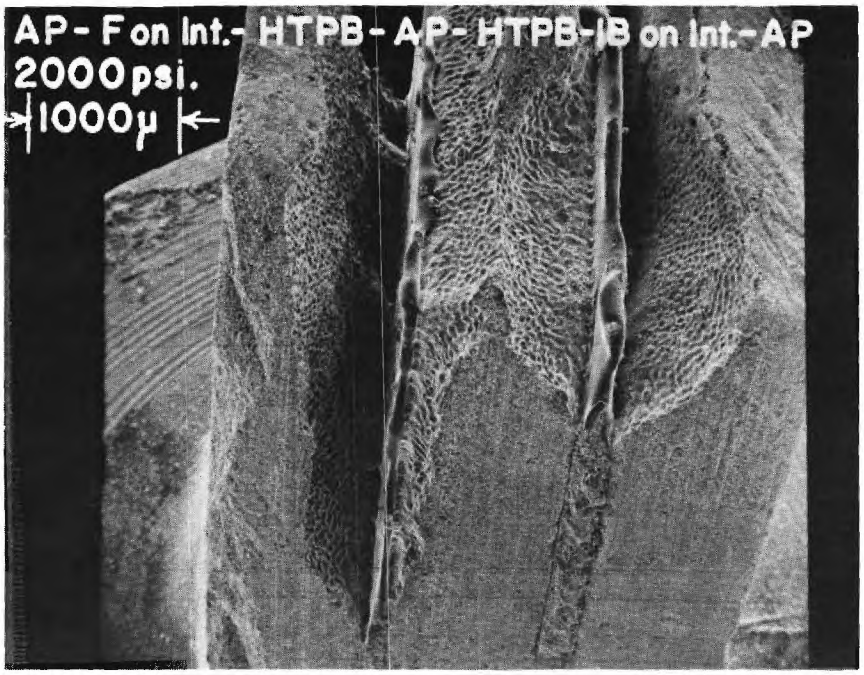

Figure A-24. AP-F on Int.-HTPB-AP-HTPB-IB on Int.-AP 2000 psia (x20.4).

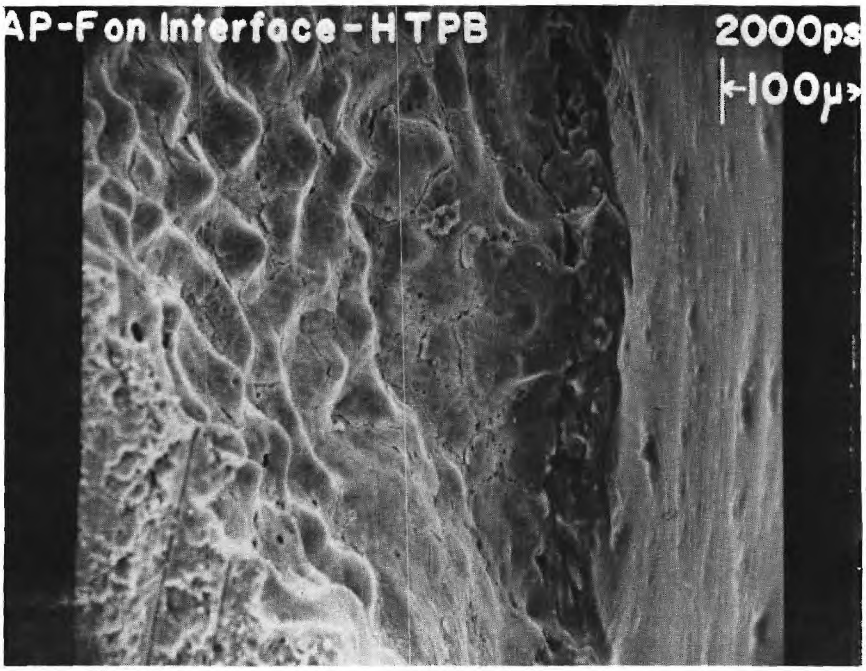

Figure A-25. AP-F on Int.-HTPB 2000 psia (x187).

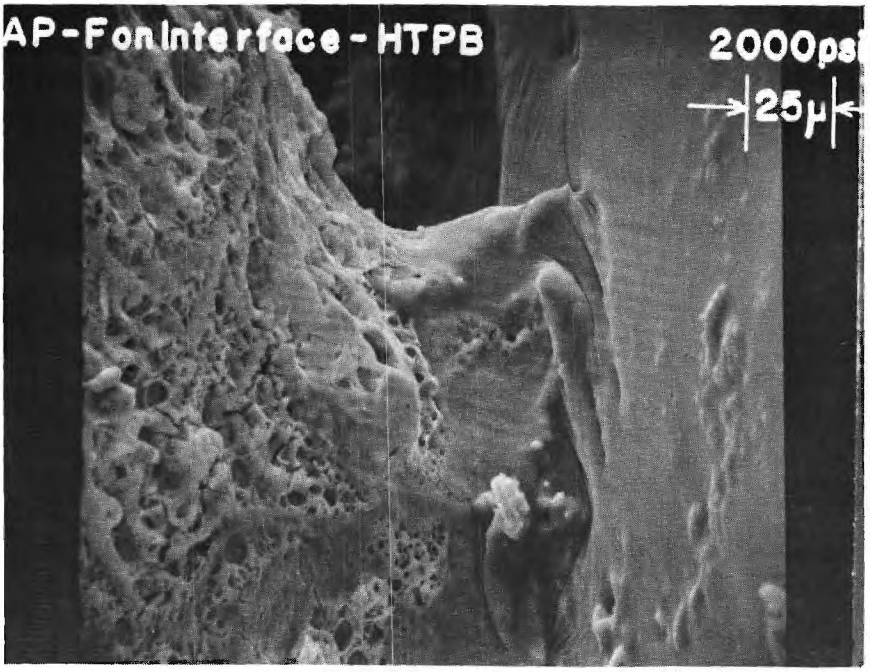

Figure A-26. AP-F on Int.-HTPB 2000 psia (x450).

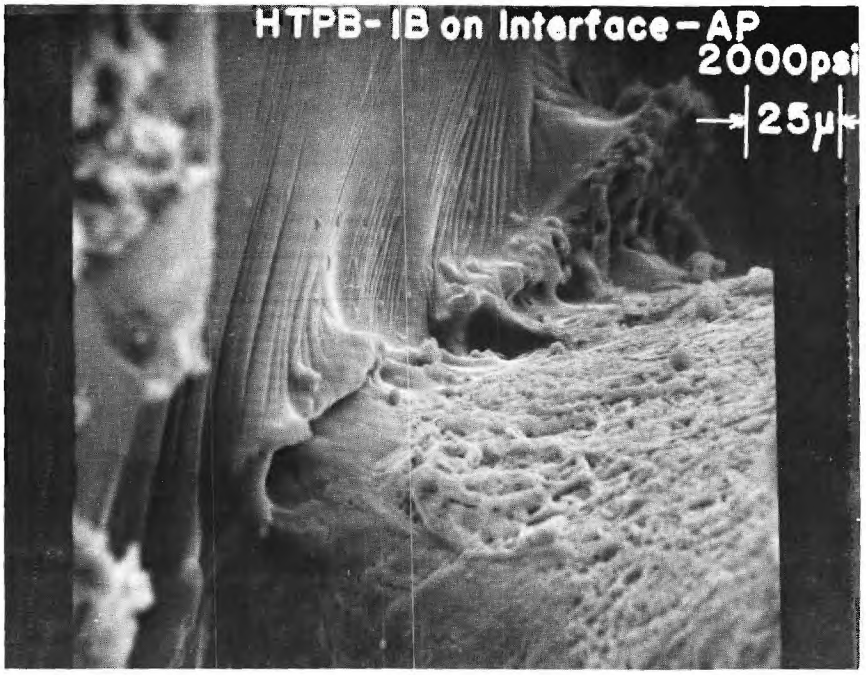

Figure A-27. HTPB-IB on Int.-AP 2000 psia (x484).

DISTRIBUTION LIST

Advanced Ballistic Missile
Defense Agency
Huntsville Office
Attn: M. L. Whitfield, CRDABH
P. O. Box 1500
Huntsville, Alabama 35807

Aerojet Solid Propulsion Company
Attn: Wilfred G. Schmidt
(Bldg. 0525, Dept. 4410)
P. O. Box 13400
Sacramento, California 95813

Aerospace Corporation
Attn: Ellis M. Landsbaum
2350 E. El Segundo Blvd.
El Segundo, California 90245

Air Force Armament Laboratory
Guns and Rockets Division
Attn: O. L. Heiney, DLDL
Eglin AFB, Florida 32542

Air Force Foreign Technology
Division (TDETT)
Attn: H. E. Wright
Wright Patterson AFB
Dayton, Ohio 45433

Air Force Office of Scientific
Research
Attn: Captain L. R. Lawrence
1400 Wilson Blvd.
Arlington, Virginia 22209

AFRPL (LK)
Attn: Dr. R. R. Weiss
Edwards, California 93523

Commanding Officer
Army Aberdeen Research and
Development Center
Attn: Mr. L. A. Watermeier, Code
AMXRD-BIL
Aberdeen Proving Ground, Maryland
21005

Commander
Army Missile Command
Attn: Dr. R. Rhodes
Redstone Arsenal, Alabama 35809

Brigham Young University
Chemical Engineering Department
Attn: Dr. R. L. Coates
Widstol Bldg.
Provo, Utah 84601

British Embassy
Attn: John Bell
3100 Mass. Avenue, N. W.
Washington, D. C. 20008

California Institute of Technology
Attn: Professor F. E. C. Culick
204 Karman Lab., (301-46)
1201 E. California Street
Pasadena, California 91109

California Institute of Technology
Jet Propulsion Laboratory
Attn: W. Dowler
4800 Oak Grove Drive
Pasadena, California 91103

Defense Research and Engineering
Attn: Mr. G. R. Makepeace
Asst. Director, Engineering
Technology
The Pentagon, Room 3D1089
Washington, D. C. 20301

Commanding Officer
Frankford Arsenal
Attn: M. Visnov, J8100, Bldg. 64-2
Bridge and Tacony Streets
Philadelphia, Pennsylvania 19137

Georgia Institute of Technology
Georgia Tech Res. Inst.
Attn: Res. Security Coordinator
Professor B. T. Zinn
Atlanta, Georgia 30332

Hercules, Inc.
Allegany Ballistics Laboratory
Attn: Dr. R. R. Miller
P. O. Box 210
Cumberland, Maryland 21502

Hercules, Inc.
Bacchus Works
Attn: Dr. M. W. Beckstead, 100K1-7
P. O. Box 98
Magna, Utah 84044

Institute for Defense Analyses
Attn: Dr. R. T. Oliver
400 Army-Navy Drive
Arlington, Virginia 22202

Johns Hopkins University/APL
Chemical Propulsion Information Agency
Attn: Thomas W. Christian
8621 Georgia Avenue
Silver Spring, Maryland 20910

Lockheed Propulsion Company
Attn: N. S. Cohen
P. O. Box 111
Redlands, California 92373

NASA Headquarters
Attn: Mr. William Cohen
Code RPT
600 Independence Avenue
Washington, D. C. 20546

NASA
Johnson Space Center
Attn: Joseph G. Thibodaux, EP
Houston, Texas 77058

NASA
George C. Marshall Space Flight Center
Attn: Mr. J. Q. Miller
Huntsville, Alabama 35812

Naval Air Systems Command
Attn: Dr. O. H. Johnson,
Code AIR 330
Jefferson Plaza, Bldg. 1
Washington, D. C. 20360

Naval Ordnance Station
Attn: Mr. A. T. Camp, Code FS
Indian Head, Maryland 20640

Naval Ordnance Systems Command
Attn: Mr. J. W. Murrin,
ORD 0331
National Center, Bldg. 2, Room 6S12
Washington, D. C. 20360

Naval Postgraduate School
Department of Aeronautics
Attn: Code 2124
Professor D. W. Netzer
Monterey, California 93940

Naval Research Office
Department of the Navy
Attn: Ralph Roberts (26 copies)
800 N. Quincy Street
Ballston Towers #1
Alexandria, Virginia 22217

Naval Weapons Center
Attn: Edward W. Price
Code 608
China Lake, California 93555

Pennsylvania State University
Attn: G. M. Faeth
University Park, Pennsylvania
16802

Commanding Officer
Picatinny Arsenal
Attn: SMUPA-TS-TS-Dr. Jean Picard
Dover, New Jersey 07801

Princeton University
Guggenheim Laboratories
Attn: M. Summerfield and
L. H. Caveny
Princeton, New Jersey 08540

Purdue University
School of Mechanical Engineering
Attn: Dr. J. R. Osborn
West Lafayette, Indiana 47907

Rockwell International
Rocketdyne Division
Attn: C. L. Oberg
6633 Canoga Avenue
Canoga Park, California 91304

Rockwell International
Rocketdyne Division
Attn: W. G. Haymes
P. O. Box 548
McGregor, Texas 76657

Shock Hydrodynamics, Inc.
Attn: W. H. Anderson
15010 Ventura Boulevard
Suite 201
Sherman Oaks, California 91403

Stanford Research Institute
Attn: H. Wise
333 Ravenswood Avenue
Menlo Park, California 94025

Stevens Institute of Technology
Mechanical Engineering Department
Attn: Richard B. Cole
Castle Point Station
Hoboken, New Jersey 07030

Susquehanna Corporation
Atlantic Research Group
Attn: Dr. Merrill K. King
Shirley Highway and Edsall Road
Alexandria, Virginia 22314

Rocket Research Corporation
Attn: P. L. Stang
Willow Road at N. E. 116th Street
Redmond, WA 98052

Bell Aerospace Company, Div.
Attn: Mr. Mort Shorr
P. O. Box One
Buffalo, New York 14240

Thiokol Chemical Corporation
Elkton Division
Attn: E. Sutton
Elkton, Maryland 21921

Thiokol Chemical Corporation
Huntsville Division
Attn: Dr. R. L. Glick
Huntsville, Alabama 35807

Thiokol Chemical Corporation
Wasatch Division
Attn: John A. Peterson
P. O. Box 524
Brigham City, Utah 94302

Ultrasystems
Dynamic Science Division
Attn: J. N. Levine
2400 Michelson Drive
Irvine, California 92664

United Technology Center
Attn: R. S. Brown
P. O. Box 358
Sunnyvale, California 94088

University of Illinois
Aeronautical and Astronautical
Engineering Department
101 Transportation Bldg.
Urbana, Illinois 61801

University of California, San Diego
Inst. Pure Applied Physical Sciences
Attn: F. A. Williams
P. O. Box 109
La Jolla, California 92037

University of Utah
Chemical Engineering Department
Attn: Alva D. Baer
Park Building, Room 307
Salt Lake City, Utah 84112

University of Waterloo
Department of Mechanical Engineering
Attn: Professor Clarke E. Hermance
Waterloo, Ontario, Canada

Whittaker Corporation
Tasker Industries
Bermite Division
Attn: William E. Robertson
22116 W. Soledad Canyon Road
Saugus, California 91350

Unclassified
Security Classification

DOCUMENT CONTROL DATA - R & D

(Security classification of title, body of abstract and indexing annotation must be entered when the overall report is classified)

1. ORIGINATING ACTIVITY *(Corporate author)*

Georgia Institute of Technology
Atlanta, Georgia 30332

2a. REPORT SECURITY CLASSIFICATION
Unclassified

2b. GROUP

3. REPORT TITLE

Catalytic Behavior in Composite Solid Propellant Combustion

4. DESCRIPTIVE NOTES *(Type of report and inclusive dates)*

Annual Summary September 1, 1972 - August 31, 1973

5. AUTHOR(S) *(First name, middle initial, last name)*

Warren C. Strahle, John C. Handley, Narendra Kumar

6. REPORT DATE	7a. TOTAL NO OF PAGES	7b. NO OF REFS
November 1, 1973	130	11

8a. CONTRACT OR GRANT NO.	9a. ORIGINATOR'S REPORT NUMBER(S)
N00014-67-A-0159-0016	
b. PROJECT NO.	
c.	9b. OTHER REPORT NO(S) *(Any other numbers that may be assigned this report)*
d.	

10. DISTRIBUTION STATEMENT

Approved for public release; distribution unlimited

11. SUPPLEMENTARY NOTES	12. SPONSORING MILITARY ACTIVITY
	Office of Naval Research Arlington, Virginia 22217

13. ABSTRACT

This report describes experiments and theoretical analysis concerned with sandwich combustion. The ingredients used in the experiment are compacted polycrystalline ammonium perchlorate as the oxidizer, hydroxyl terminated polybutadiene as the binder and four catalysts: Harshaw catalyst CU-0202, Fe_2O_3, ferrocene, and iron blue. The pressure range studied is 600-2000 psia. The experimental techniques used are cinephotomacrography for sample observation during burning and burn rate determination, scanning electron microscopy for observation of quenched samples, and electron microprobing for an exploratory study of surface composition. A theoretical solution to a simple sandwich deflagration problem is attained. The probable sites of catalytic activity are determined, results are compared with actual propellant experience, and the analysis is used to clarify experimental results.

DD FORM 1 NOV 65 1473

Unclassified
Security Classification

file: E-16-626

SYNERGISTIC AND NOVEL EFFECTS IN COMPOSITE SOLID PROPELLANT COMBUSTION

W. C. Strahle

J. C. Handley

October 1, 1974

Second Annual Summary Report – Research Sponsored
by
The Office of Naval Research

ONR Contract No. N0014-67-A-0159-0016
Requisition Purchase Request NR 092-543

Synergistic and Novel Effects in Composite Solid Propellant Combustion

W. C. Strahle
J. C. Handley

October 1, 1974

Second Annual Summary Report - Research Sponsored
by
The Office of Naval Research

ONR Contract No. N0014-67-A-0159-0016
Requisition Purchase Request NR 092-543

Approved for Public Release; Distribution Unlimited

Abstract

This report summarizes experiments and analysis concerned with sandwich and cast composite solid propellant combustion. The ingredients used in the experiments are ammonium pershlorate as the oxidizer, hydroxyl terminated polybutadiene as the binder and four catalysts: Harshaw catalyst CU-0202, Fe_2O_3, ferrocene and iron blue. Cinephotomacrography and the fuze wire technique are used for combustion visualization and burn rate determination. Scanning electron microscopy is used for quenched sample visualization. Areas investigated are a) analytical and experimental determination of synergistic catalytic effects in sandwich and propellant combustion, b) the loading of ferrocene into the binder at the molecular level and its effect on sandwich combustion, c) differential scanning calorimetry of catalyst laden binder and d) analysis of sandwich deflagration.

Table of Contents

	Page
Abstract	i
Chapters	
I. Introduction	1
II. Determination of Possible Synergistic Effects	2
a. Two-dimensional Sandwiches	2
b. Cast Composite Propellant	9
III. Indian Head Ferrocene	14
IV. Differential Scanning Calorimetry	18
V. Analytical Efforts	21
VI. Conclusions	27
References	29
Appendix	30
Solid Propellant Sandwich Deflagration Analysis	31
Distribution List	64

I. Introduction

This report summarizes efforts of the second year on contract ONR No. N0014-67-0159-0016. Prior results were concerned with the sandwich configuration and the individual effects of the catalysts Harshaw catalyst CU0202, Fe_2O_3, ferrocene and iron blue. This year's effort consisted of both sandwich and cast propellant investigations to determine a) possible synergistic catalytic effects whereby for the same total loading of catalyst the effect of two catalysts would be greater than either one alone and b) the behavior of a unique type of ferrocene loading at the molecular level into R-45 prepolymer. Differential scanning calorimeter studies were also performed on catalyst laden hydroxyl terminated polybutadriene (HTPB) binder. Analysis was conducted to explain synergistic catalytic effects and to improve on a previous model of sandwich deflagration.

The reason for investigating synergistic effects is that they were accidentally discovered on the prior year's program. Incorporation of this effect would allow the propellant chemist more flexibility in propellant formulation. The investigation of loading of ferrocene at the molecular level was motivated by prior conclusions that physical loading of catalyst into the binder is a poor way to obtain catalysis. The differential scanning calorimeter work was motivated by prior results that catalysts did not appear to change the pyrolysis mechanism of the binder; a confirmation was desired in other than a deflagration situation. The analysis was required as an aid in reasoning the significance of the experimental results and to see to what degree a sandwich analysis may be used for a cast composite propellant deflagration analysis.

II. Determination of Possible Synergistic Effects

a. Two-Dimensional Composite Solid Propellants

Two-dimensional composite solid propellant sandwiches were used to investigate the optimum location and the extent of the catalytic action of four possible burn rate modifiers.[1] Both the location and the compounds were varied independently. During that investigation it was determined that if one catalyst was added to the oxidizer prior to compaction of the disk and another effective catalyst was added to the binder, there was a net increase of the burn rate over that of the sum of the independent actions of the catalysts. This combined effect is denoted as a synergistic effect on the burn rate. The current study has systematically investigated this positive synergism for all combinations of the same four compounds.

The two-dimensional composite solid propellant sandwiches were prepared by the method outlined in Reference 2 from disks of polycrystalline oxidizer and layers of binder. The disks were pressed from crystalline ammonium perchlorate (AP) in a mold at 30,000 psi. The disks were assembled into multi-layered sandwiches by binding them together with layers of hydroxyl terminated polybutadiene (HTPB). The thickness of the binder layer was maintained at 150 μm during the curing process by using Teflon spacers and spring loaded sample clamps.

The four compounds investigated were Harshaw catalyst Cu0202, (CC), ferric oxide, (IO), iron blue, (IB), and ferrocene, (F). Harshaw catalyst Cu0202 is a commercially avaliable catalyst. It is a mixture of approximately 82% cupric oxide, CuO, and 17% chromic oxide, Cr_2O_3. It is used in accelerating both oxidation and reduction processes. It is commonly referred to as copper chromite. Ferric oxide, Fe_2O_3, exhibits, as do most

transition element compounds, a high degree of catalytic activity. It is used primarily for oxidation processes. Iron blue is commerically used as a pigment. It is a complex ammonium iron hexacyanoferrate with the chemical formula, $Fe(NH_4)Fe(CN)_6$. It has a cubic crystalline structure. The iron is present as both ferric and ferrous ions in the lattice. Ferrocene is an organometallic compound with the chemical name, biscydopentadienyl iron, $(C_2H_5)_2Fe$. It is a yellow crystalline solid with relatively high thermal stability for an organometallic compound.

The samples were prepared with constant volumetric loading of the compounds based on an addition of 2w% to the oxidizer. This amount of catalyst was added to the AP prior to grinding and pressing and 4.37w% of catalyst was added to the HTPB.

The cured oxidizer-fuel sandwiches were cut into 8 mm by 4 mm samples. These prepared samples were mounted in the pressurized combustion apparatus of Jones.[3] Motion pictures of the burning sample were obtained at a rate of 1600 frames per second at a latentimage magnification of 1:1 and 2:1. These motion pictures were used to obtain an accurate value of the sample burning rate. The sandwich vertical burn rate and the burn rate normal to the oxidizer surface, as defined in Reference (1), were obtained for all combinations of the four catalysts along with suitable base line cases at the same volumetric loading in the binder and oxidizer at a combustion pressure of 600 psia.

The tabulated results for the determination of possible synergistic effects are shown in Table 1. The base line comparison cases for a single catalyst present were for 2w% of catalyst added to the AP and 4.37w% of catalyst added to the HTPB. This gave a uniform volumetric loading of

TABLE I. BURN RATES FOR DETERMINATION OF SYNERGISTIC EFFECTS FOR SANDWICHES AT 600 PSIA.

CATALYST	r	r Cos θ
NONE	.22 in/sec	.21 in/sec
HARSHAW CATALST Cu0202 (CC)	.51	.33
FERRIC OXIDE (IO)	.33	.23
IRON BLUE (IB)	.37	.20
FERROCENE (F)	.30	.15
CC & IO	.54	.36
CC & IB	.50	.47
CC & F	.43	.29
IO & IB	.51	.25
IO & F	.44	.36
IB & F	.40	.31

catalyst across the binder-oxidizer interface of the two-dimensional sandwiches. The total weight of the catalyst was maintained constant for the combinations of catalysts. One weight percent of one catalyst along with 1w% of another catalyst was added to the AP and 2.2w% of each catalyst was added to the HTPB. The results obtained for the base line cases of single catalysts added to the sandwiches are in agreement with previous data.[1] It must be noted that the comparison cannot be exact since in the previous investigation[1] the catalyst loading was discontinuous across the binder-oxidizer interface, but in previous experiments catalyst in the binder was shown to be ineffective.

Ferric oxide, iron blue and ferrocene, when used alone, were burn rate inhibitors for AP at 600 psia.[1] The burn rate normal to the oxidizer surface was less than that of the uncatalyzed AP. This is also true in Table 1. When these proven inhibitors of the AP deflagration process were used in combinations with the same total mass of catalyst present, the burn rate normal to the oxidizer surface was increased over that of the uncatalyzed AP. This was noted for the IO-IB, IO-F and IB-F systems. Harshaw catalyst Cu0202 increased the AP deflagration rate when used alone at 600 psia. All combinations of Harshaw catalyst Cu0202 with the other three compounds exhibited a synergistic effect on the AP deflagration rate even though three of them acted as inhibitors when used alone.

The maximum sandwich burn rate (.54 inches/sec) has been obtained with the combination of Harshaw catalyst Cu0202 and ferric oxide. The largest synergistic effect (burn rate change as compared with either single catalyst alone) has been seen for a ferric oxide and iron blue mixture with a burn rate of .51 inches/sec. All combinations of catalysts did give some

degree of positive synergism of the sandwich vertical burn rate. For the combinations with Harshaw catalyst Cu0202 only ferric oxide was able to clearly increase the burn rate above that of Harshaw catalyst Cu0202 alone. All combinations of ferrocene in this configuration yielded relatively lower sandwich vertical burn rates.

Considering these results, the most promising two combinations of catalysts, Harshaw catalyst Cu0202 - ferric oxide and iron blue - ferric oxide were chosen for testing over the pressure range of 300 to 2000 psia.

The results for the Harshaw catalyst Cu0202-ferric oxide system tests are shown in Figure 1. The maximum effect is at 1500 psia. Both catalysts were equally effective in catalyzing the burn rate when used alone. When half of one catalyst was replaced by the same amount of the second catalyst the burn rate doubled. The sandwich vertical burn rate and the burn rate normal to the oxidizer surface both exhibited positive synergism over the entire pressure range.

For the iron blue - ferric oxide samples the results were not as clear. They are shown in Figure 2. The maximum positive effect occurs at 600 psia . It is not conclusive at 1000 and 1500 psia that a positive synergistic effect has been obtained, since the combined catalysts produce a burn rate that lies between the burn rates obtained for a single catalyst present. A negative effect has not been produced, i.e. the burn rates have not been inhibited. Within the experimental accuracy of the test the burn rate normal to the oxidizer surface for the combined catalysts loading has followed the burn rate for ferric oxide.

As in previous tests the separation between the dashed and solid curves is representative of the amount of catalytic activity taking place in the

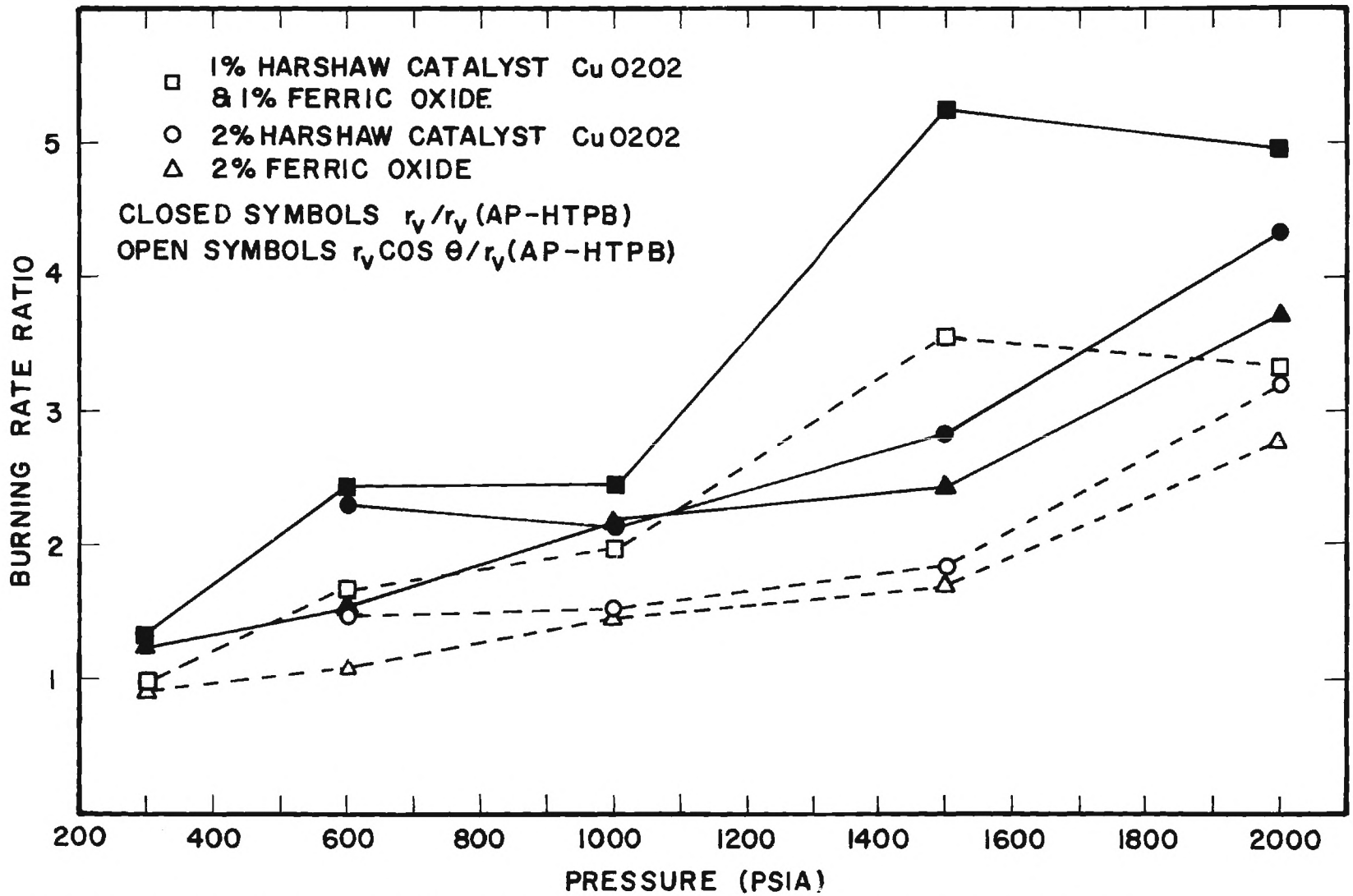

FIGURE I. BURN RATE RATIO FOR HARSHAW CATALYST Cu 0202 AND FERRIC OXIDE.

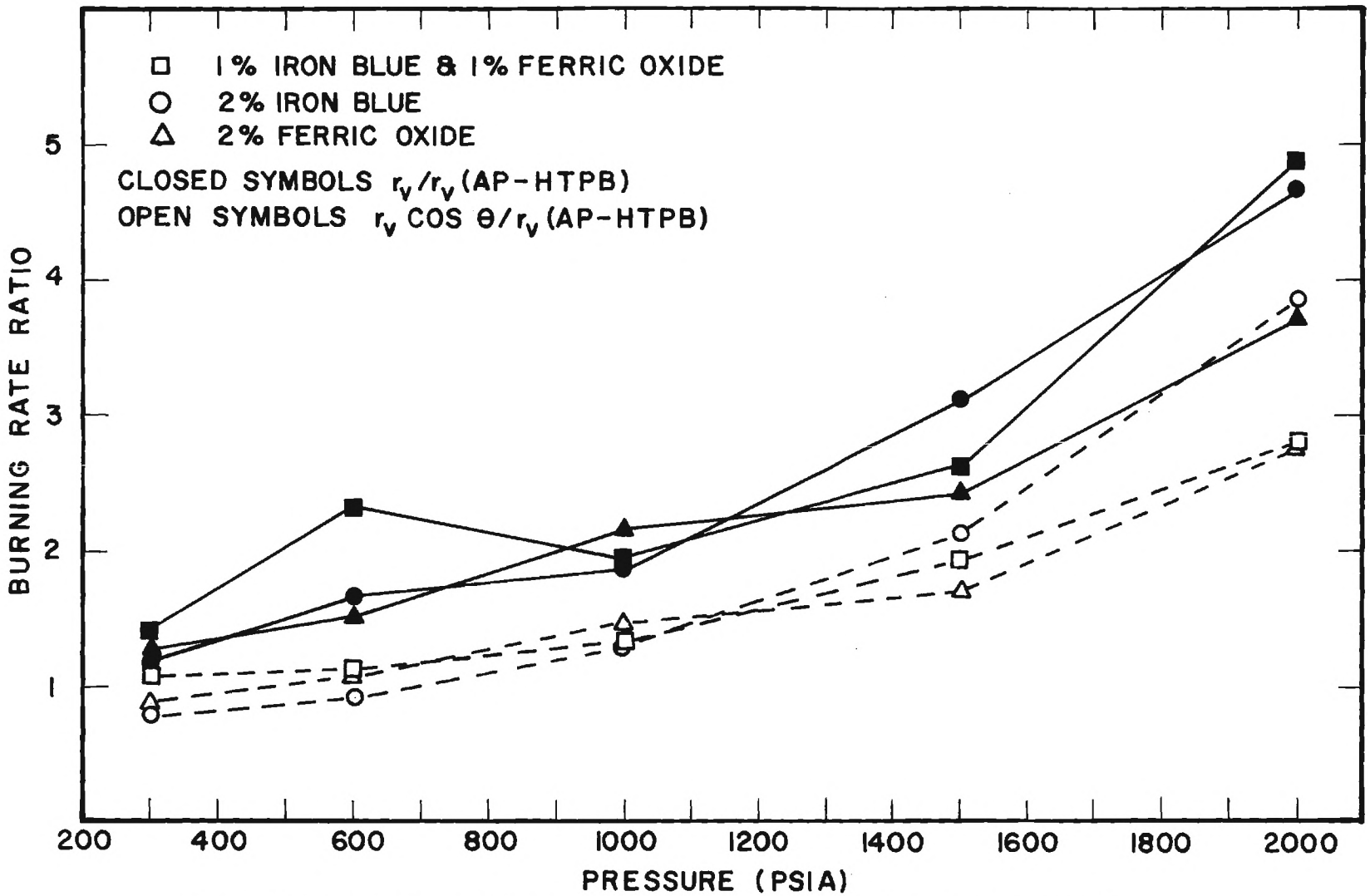

FIGURE 2. BURN RATE RATIO FOR IRON BLUE AND FERRIC OXIDE.

binder-oxidizer reactions. The tests that showed large positive synergistic effects, Harshaw catalyst Cu0202 and ferric oxide at 1500 and 2000 psia, and iron blue and ferric oxide at 600 and 2000 psia, also showed substantial increases in this separation of the two burn rates.

b. Cast Composite Propellants

Maintaining the same volumetric loading of catalysts as for the two-dimensional sandwiches, three-dimensional cast composite solid propellant strands were prepared to see if this synergistic effect would be carried over to the real cast propellant. These strands were prepared from a common lot of uncured composite propellant with an 83%/17% solids to binder loading. The oxidizer was chosen to have a bimodal ammonium perchlorate particle distribution of 30% 40 μm and 70%, 180 μm. The binder was hydroxyl terminated polybutadiene. Burning rate data are available for this uncatalyzed propellant.[4] It was similar to propellant #78 in the Princeton University test series. The catalyst was added to the uncured propellant at a weight percent of 2.41. This would give the same equivalent volumetric loading as in the sandwiches.

The strands were cast in teflon molds and all samples were cured for the same length of time. The strand size was .25 inch by .25 inch by 1.7 inches long. The burn rates were obtained by a fuse wire technique[4] using seven, $\frac{1}{2}$ ampere ($\sim$ .010 inch diameter), wires inserted in predrilled holes which were spaced .2 inches apart. Each fuse wire was connected in series to a 10 KΩ resistor. These seven resistors were connected in parallel with a 57 KΩ resistor across an 18 volt battery power supply. As each fuse wire burns through the equivalent resistence increases and the

voltage is recorded on an oscillograph.

The strand with fuse wires is shown in Figure 3. It is mounted on the bas of the combustion bomb. A sufficient nitrogen flow is passed over the sample to prevent recirculation of the hot gases that can cause premature melting of the fuse wires. This nitrogen flow has varied from .7 to 1.4 ft/sec. The most stable results were obtained at the higher flow rates. Sample oscillograph traces are shown in Figure 4 for an uncatalyzed strand and one with ferric oxide added to the strand.

The burn rates for the addition of the two most promising combinations of catalysts as determined from the two-dimensional composite solid propellant test are tabulated in Table 2. These strands of propellant were burned at 600 psia. For the combination of ferric oxide and iron blue, the burn rate is between the burn rates of the samples with only one catalyst present. The ferric oxide - Harshaw catalyst Cu0202 system showed a reduction of burn rate below that of either of the two catalysts used alone.

The burn rates do not compare favorably with the results obtained in Table 1 for the two-dimensional sandwiches. The burn rate for the uncatalyzed strands agree with the Princeton data. The structural strength and elasticity of the samples containing both Harshaw catalyst Cu0202 and iron blue were considerably different from the ferric oxide and pure samples. The ferric oxide and pure samples were softer and more easily removed from the mold while the samples containing iron blue and Harshaw-catalyst Cu0202 were brittle and exhibited several tests with very rapid burning. These tests were not considered in the preparation of Table 2.

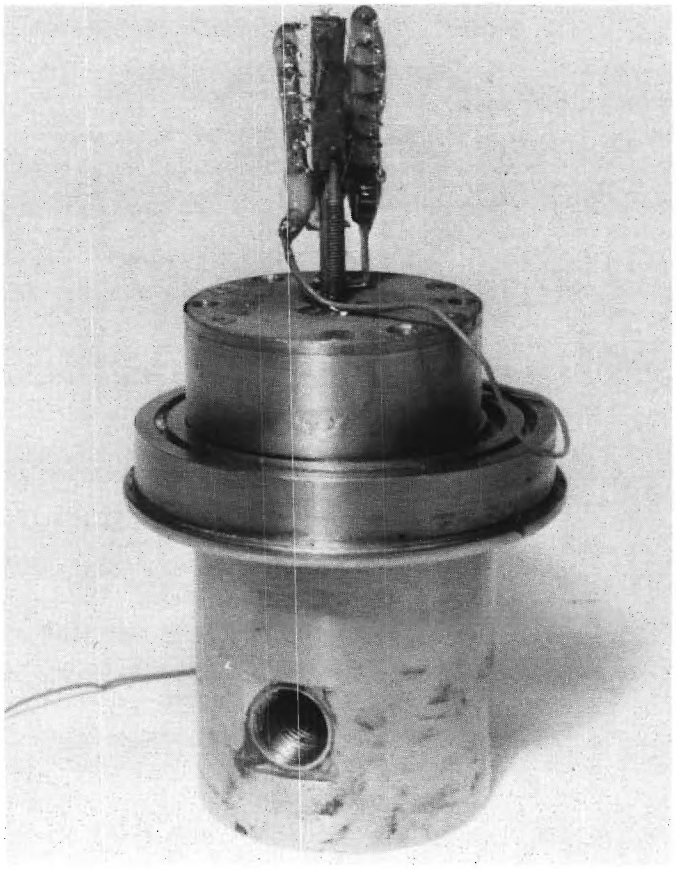

FIGURE 3. A STRAND WITH SEVEN FUSE WIRES MOUNTED ON THE COMBUSTION BOMB BASE.

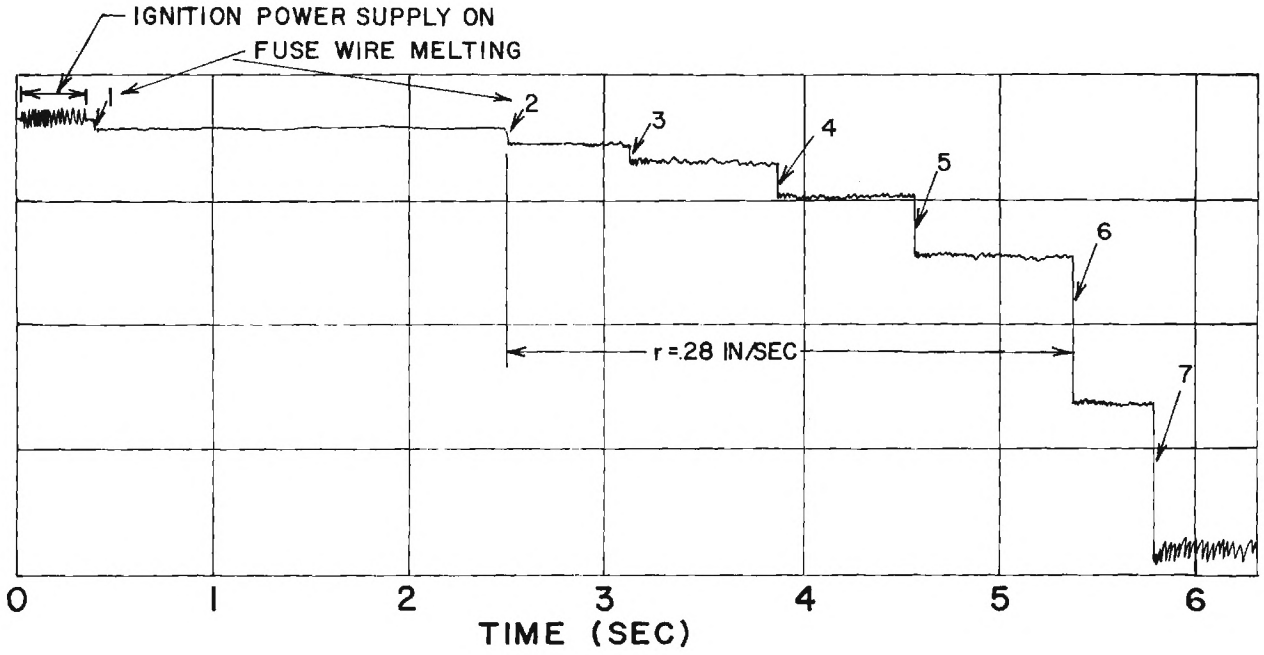

a) AP - HTPB NO CATALYST.

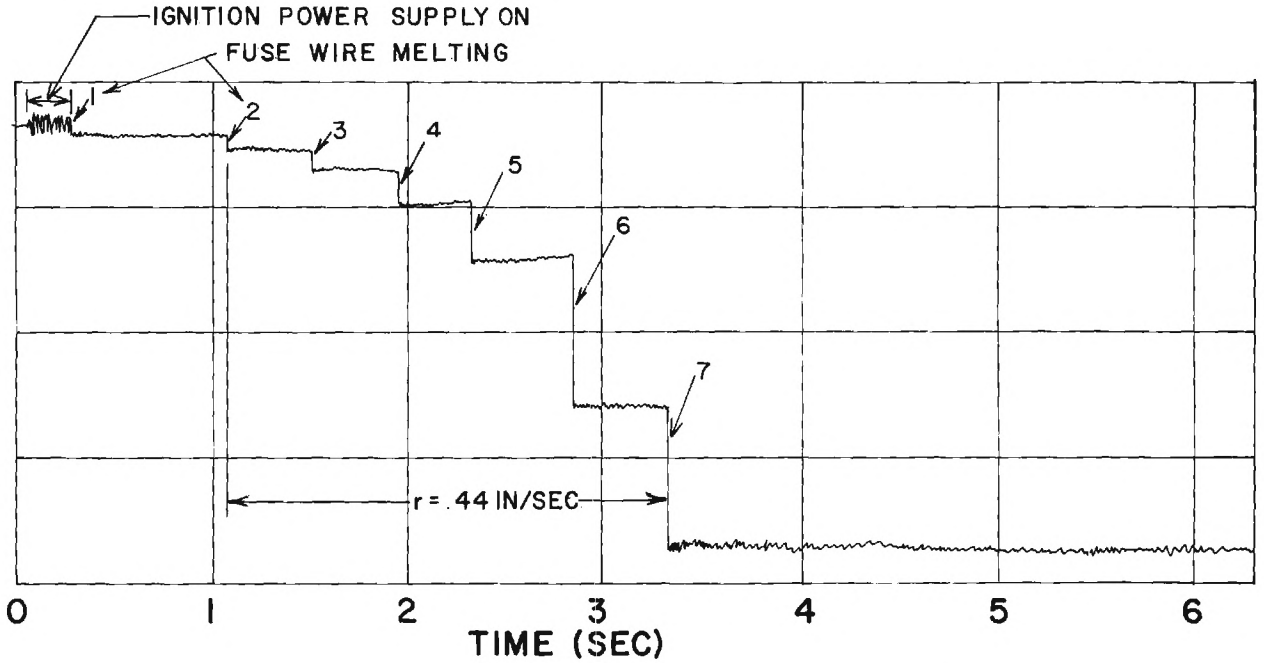

b) AP - HTPB 2.41 w % FERRIC OXIDE.

FIGURE 4. OSCILLOGRAPH RECORDS FOR TWO STRANDS.

TABLE II. BURN RATES FOR CAST COMPOSITE PROPELLANT STRANDS.

CATALYST	r
NONE	.28 in/sec
HARSHAW CATALYST Cu0202 (CC)	.50
FERRIC OXIDE (IO)	.44
IRON BLUE (IB)	.36
CC & IO	.41
IO & IB	.43

These cast propellant samples were initially prepared to contain on average the same volumetric loading of catalyst as the sandwiches. But for the cast propellants all of the catalyst is suspended in the binder matrix, which constitutes 17w% of the sample. Since 2.41w% of catalyst was added to the cast propellant samples, the binder matrix contains 14.2w% of the catalyst. The binder matrix for the sandwiches contained 4.4% of catalyst. This increase of catalyst in the binder effected the cure and the strength of the binder. This high catalyst loading in the binder may be above the amount required for maximum burn rate augmentation. It was determined earlier[1] that the addition of the catalyst directly into the polycrystalline structure was more effective than addition to the binder. If the catalyst could be distributed in the oxidizer crystalline structure to give the same volumetric loading as in the sandwiches a more realistic comparison could be made. This would require a development of a new ammonium perchlorate production technique. It may be possible to establish the existence of a synergistic effect in cast propellants if the total catalytic loading in the binder is reduced to a more comparable level with the two-dimensional sandwiches. This approach will be followed in future efforts.

III. Indian Head Ferrocene

It had been a prior conclusion[1], [2] that crystalline catalysts physically loaded into the binder were ineffective in augmenting sandwich deflagration rates. The apparent reason is that with the catalyst in the binder the diffusion of crystalline matter, once it is released into the gas phase, toward the hot AP is too slow to augment the binder-oxidizer

reactions fast enough to increase heat feedback to the sandwich surface. Furthermore, the dispersion of catalytic material must be greater for a substance dispersed at the molecular level rather than at a macroscopic crystalline level. Following this hypothesis, it would be desirable to introduce the catalyst in molecular rather than crystalline form, once the binder had pyrolysed to the gas phase. The diffusion of gas phase molecules should be faster than crystalline particles.

It was learned that the Naval Ordnance Station at Indian Head, Maryland was working in the area of chemically loading ferrocene into R-45 polymer.[5] Indian Head supplied some of the polymer with 5% Fe by weight in the polymer. Due to an advanced state of cure of the received material work with this substance was limited, but one sandwich was prepared with this material.

Figure 5 shows scanning electron microscope pictures of quenched samples burned at 1000 psia. One sample shown is from prior work with the crystalline ferrocene in the binder alone and the other sample is with the Indian Head ferrocene. The striking effect of the chemically loaded ferrocene is the depression of the AP in the vicinity of the oxidizer-binder interface. This is interpreted, as shown by many past results, as increased chemical rates between the binder and oxidizer for the Indian Head binder as compared with the binder with crystalline catalyst. Because the AP is not flat (horizontal) the vertical burn rate of the sandwich had to be greater with the Indian Head binder. This result is considered to confirm the hypothesis of molecular diffusion and greater dispersion as explained above.

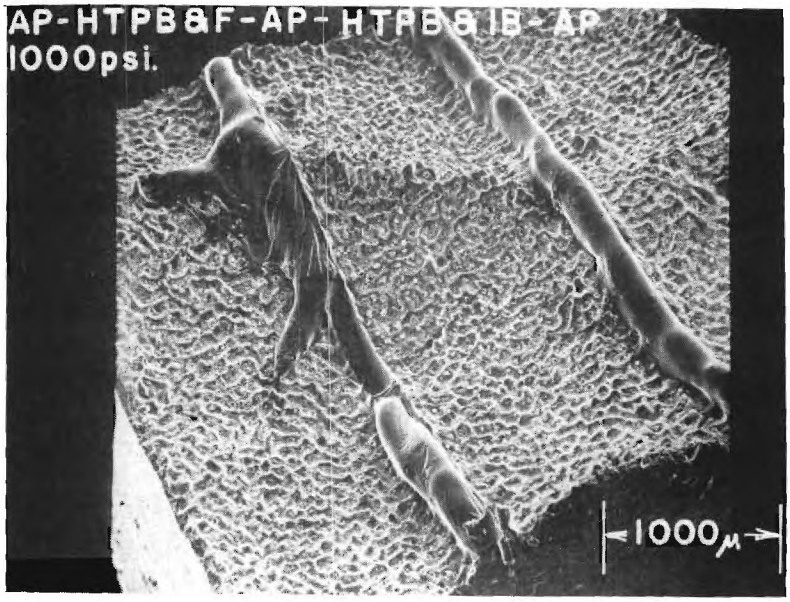

a) Ferrocene Mixed in HTPB x 27

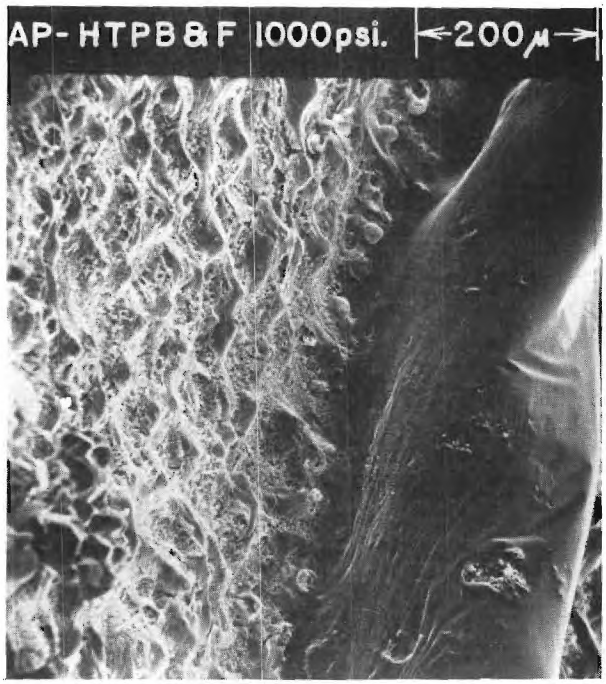

b) Ferrocene Mixed in HTPB x 140

FIGURE 5. ELECTRON MICROGRAPHS OF SAMPLES WITH FERROCENE IN THE BINDER.

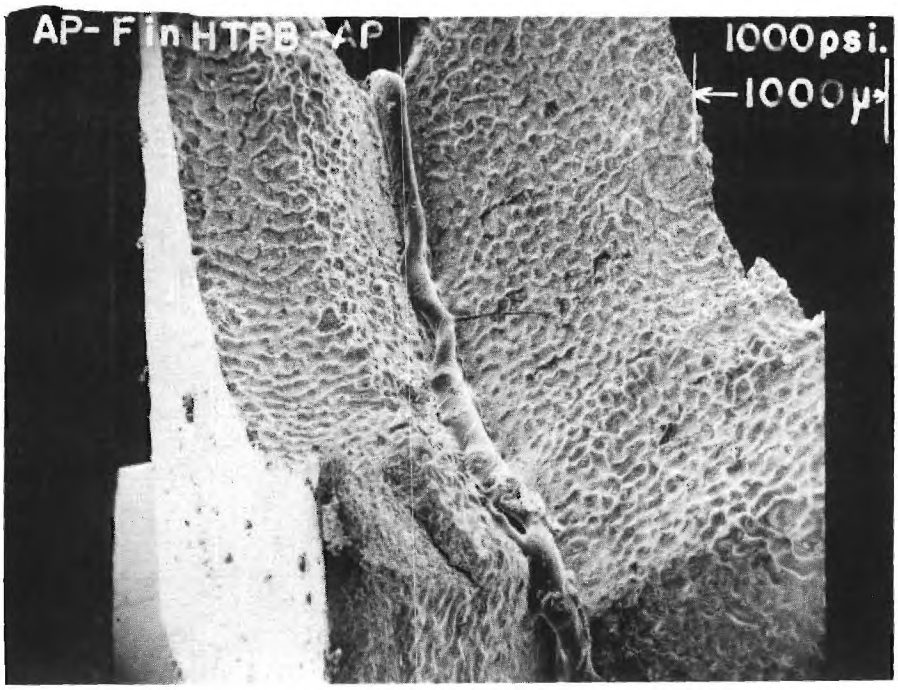

c) Ferrocene in R45 M Component of HTPB x 25

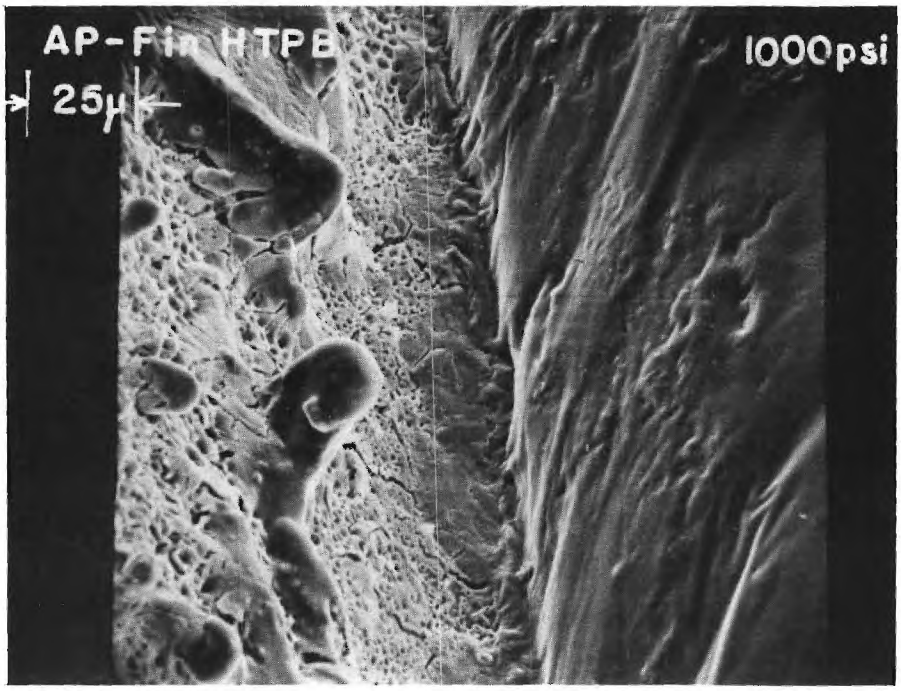

d) Ferrocene in R45 M Component of HTPB x 560

FIGURE 5. ELECTRON MICROGRAPHS OF SAMPLES WITH FERROCENE IN THE BINDER.

IV. Differential Scanning Calorimetry

Since prior sandwich results led to the conclusion that catalytic effectiveness is poor when the catalyst is loaded into the binder, and there has been no evidence that catalysts increase the binder pyrolysis rate, it was desired to check these conclusions by differential scanning colorimetry applied to catalyst-laden binder. The apparatus used was a Perkin-Elmer Differential Scanning Calorimeter, Model DSB-1B, and the procedures used were identical to those of Ref. 6. The binder used was HTPB and two catalysts, iron blue and ferrocene, were investigated. The nominal weight of each sample was 5 mg. and the amount of catalyst loading was consistent with that used in the sandwich deflagration tests, 4.4w%

The DSC unit measures the difference in power required to heat two samples, one inert and one containing the decomposing sample, through a programmed temperature rise. Sample graphs, shown on Figure 6 are two HTPB runs at a scan rate of 5 K/min. This figure shows the reproducibility attainable between runs. The heat of gasification is $q = \int_0^\infty \dot{Q}\, dt = \int_{T_o}^{T_f} \dot{Q}\,(1/dT/dt)\, dt$ where T_f is the temperature at which gasification for pure HTPB are shown in Table 3. In Table 3 there is a high degree of data scatter but an unmistakeable trend of heat of gasification with scan rate dependent. A plot of q v.s. 1/scan rate is given in Figure 7. A line through the most consistent set of data (HTPB-IB) shows an extrapolation to infinite scan rate of q = 265 cal/g. This should be compared with 433 cal/g obtained in Ref. 7, which was obtained at heating rates comparable to those found during propellant deflagration,

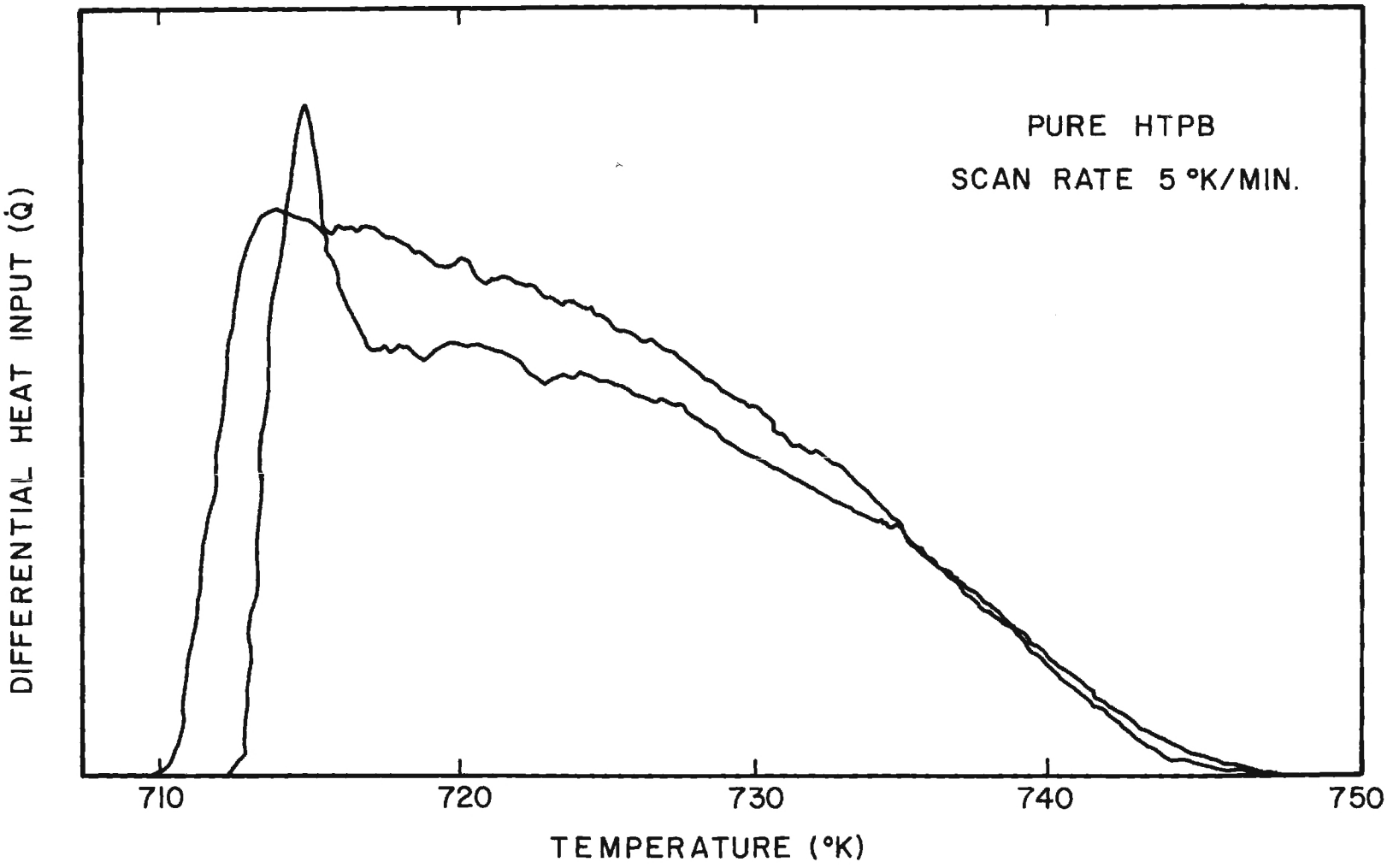

FIGURE 6. DIFFERENTIAL HEAT INPUT AS A FUNCTION OF TEMPERATURE.

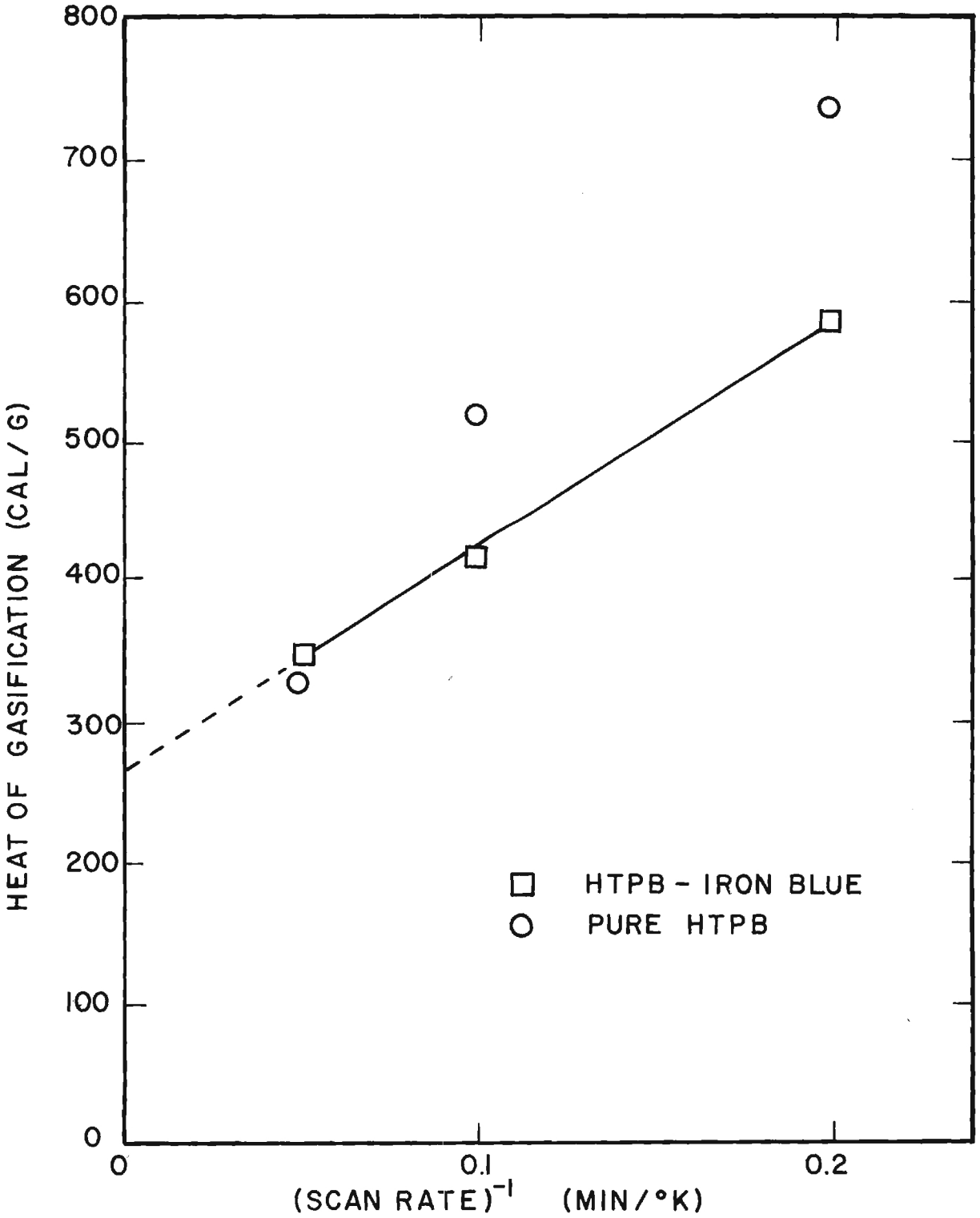

FIGURE 7. HEAT OF GASIFICATION AS A FUNCTION OF THE RECIPROCAL SCAN RATE.

Table 3

Heat of Gasification for HTPB and HTPB - catalyst

Scan Rate (K/min)	Binder	No. of Tests	q (cal/g)
20	HTPB	1	328
10	HTPB	3	$518 \begin{smallmatrix}+75\\-58\end{smallmatrix}$
5	HTPB	2	$735 \begin{smallmatrix}+129\\-129\end{smallmatrix}$
20	HTPB-IB	1	345
10	HTPB-IB	5	$415 \begin{smallmatrix}+94\\-129\end{smallmatrix}$
5	HTPB-IB	1	584
20	HTPB-F	1	285

which are orders of magnitude higher than may be found with the DSC unit. The primary conclusion, however, is that within the data scatter there appears no definite effect of IB or F on the heat of decomposition of HTPB.

Figures 8 and 9 show the actual traces for pure HTPB and HTPB-IB at scan rates of 10 K/min. The catalyst has very little effect upon the temperature at the onset of decomposition activity. There does appear, however, to be a minor effect of IB in smoothing out the roughness near the peak of the decomposition activity. Nevertheless, the overall temperature width of activity and the heat of gasification is affected in only a minor way. The same conclusion may be derived from the HTPB-F run.

V. Analytical Efforts

Two major analytical efforts have been conducted during the current year. One task concerned an explanation of synergistic effects and the other concerned an extension of a previous sandwich deflagration analysis.[8] During the course of extension of the sandwich analysis, two major items were discovered: a) the solution procedure used in the previous effort was

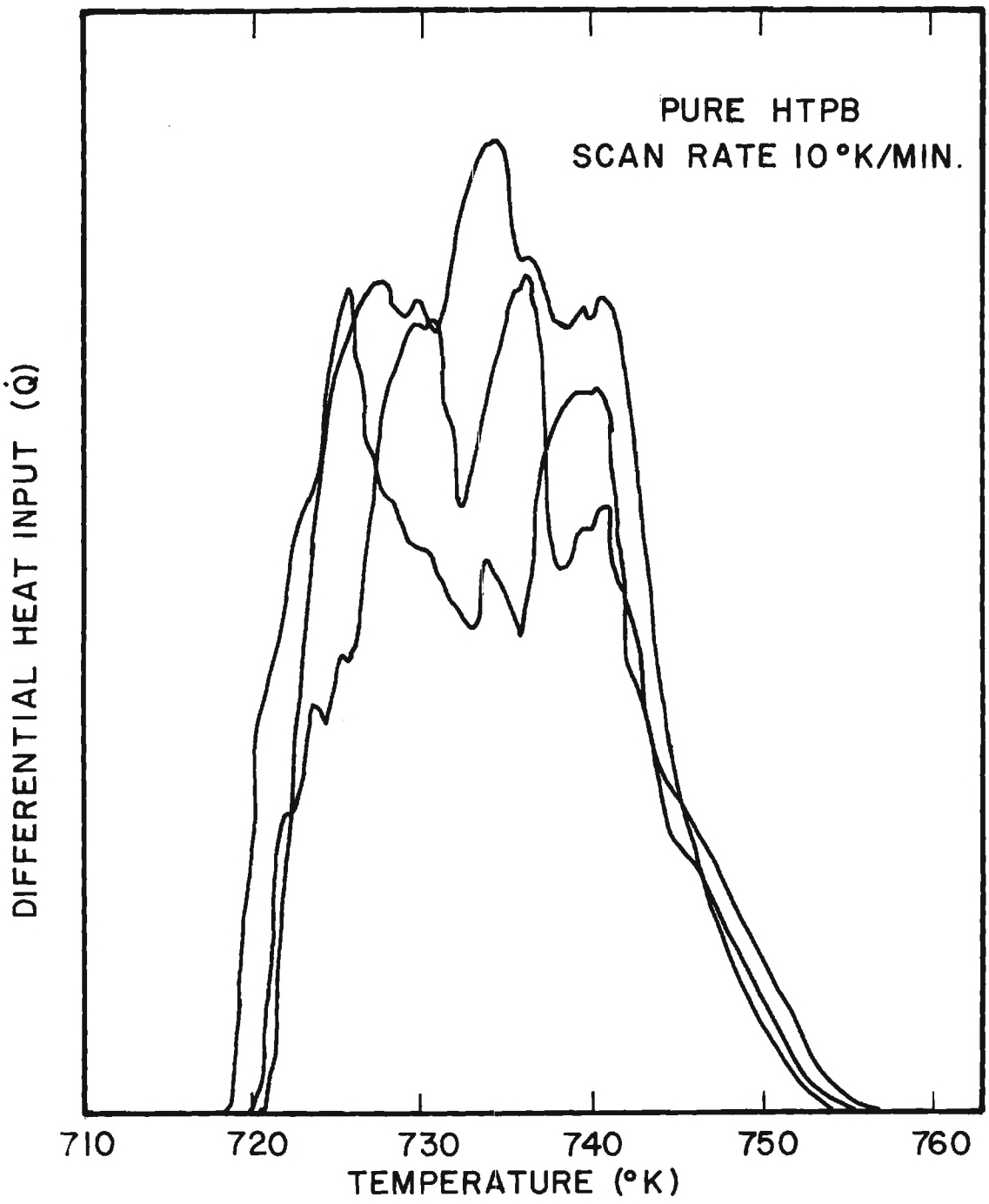

FIGURE 8. DIFFERENTIAL HEAT INPUT AS A FUNCTION OF TEMPERATURE.

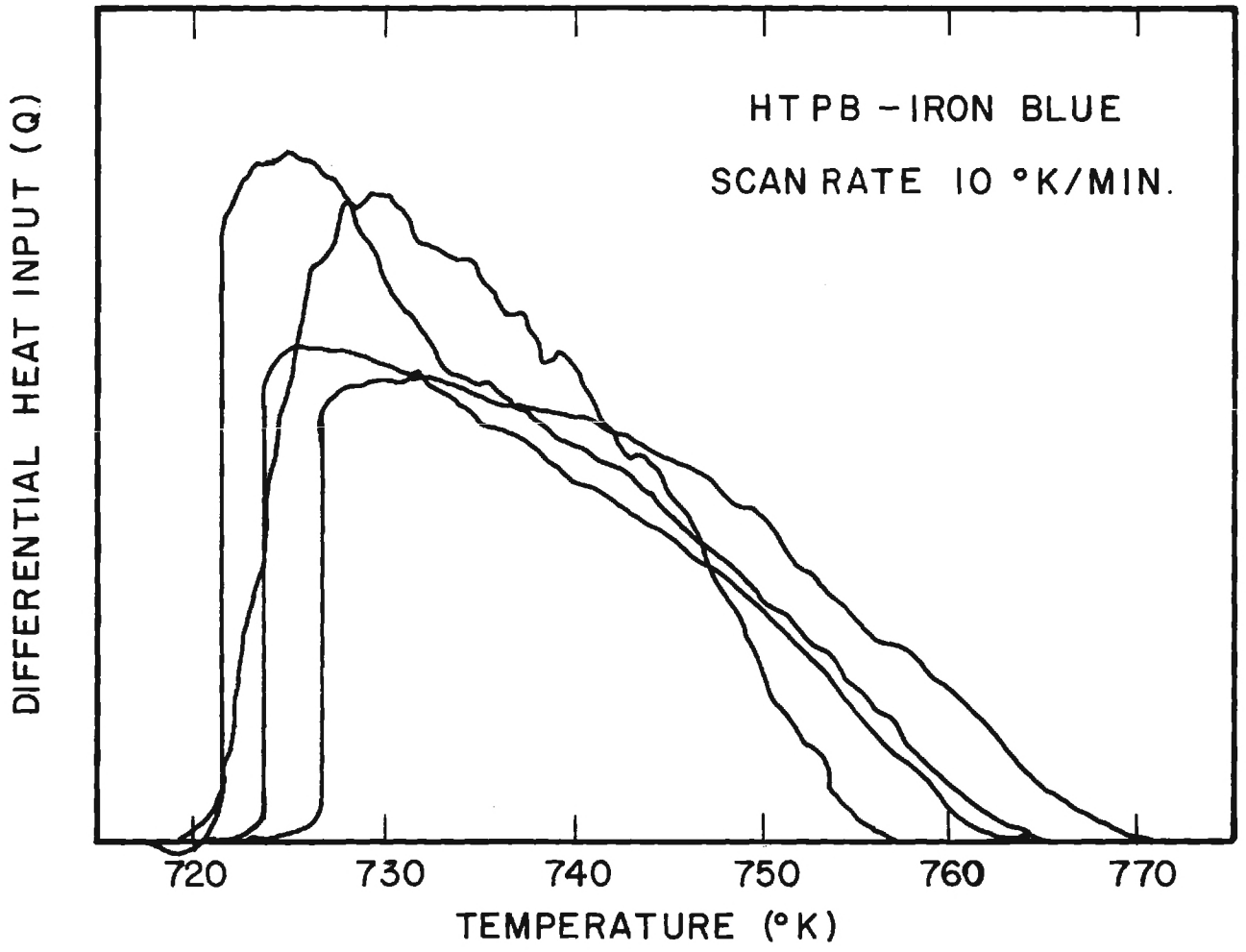

FIGURE 9. DIFFERENTIAL HEAT INPUT AS A FUNCTION OF TEMPERATURE.

in error and b) an improved solution could be found for the solid phase heat transfer problem. As a consequence it was found that the sandwich burn rate, which could not be found with the old procedure, appears as an eigenvalve to the problem. The restricted problem of an inert, dry binder adjacent to deflagration AP was therefore solved by the new procedure. The details are located in the Appendix.

Synergistic effects were first treated by insertion of two catalytic reactions in the chemical kinetics scheme of Ref. 9 for deflagrating AP. It is believed that the details should not be presented here because it may be construed that these catalytic reactions are being proposed as actual catalytic mechanisms; whereas, they were only introduced as a plausibility argument for synergistic effect. The plausibility argument which is presented here encompasses all of the results that were obtained from the AP deflagration model without confusing the issue with AP details.

To explain the results of the AP catalysis model on a simple basis the effect of two catalysts on the reaction rate, R, may be modeled as follows:

$$R_a = R_o \, f_1(Y_{c_1}) \, f_2(Y_{c_2}) \tag{1}$$

or

$$R_b = R_o + g_1(Y_{c_1}) + g_2(Y_{c_2}) \tag{2}$$

where the f's and g's as functions of the catalyst mass fraction, Y_c, are shown in Figure 10. Equations (1) and (2) merely represent two functional assumptions which yield expected behavior with respect to each catalyst. There is a general rise in rate with catalyst loading to a maximum, and a fall off in rate to zero must occur as the catalyst, which is in inert, saturates the propellant. Since the burn rate is roughly proportional to

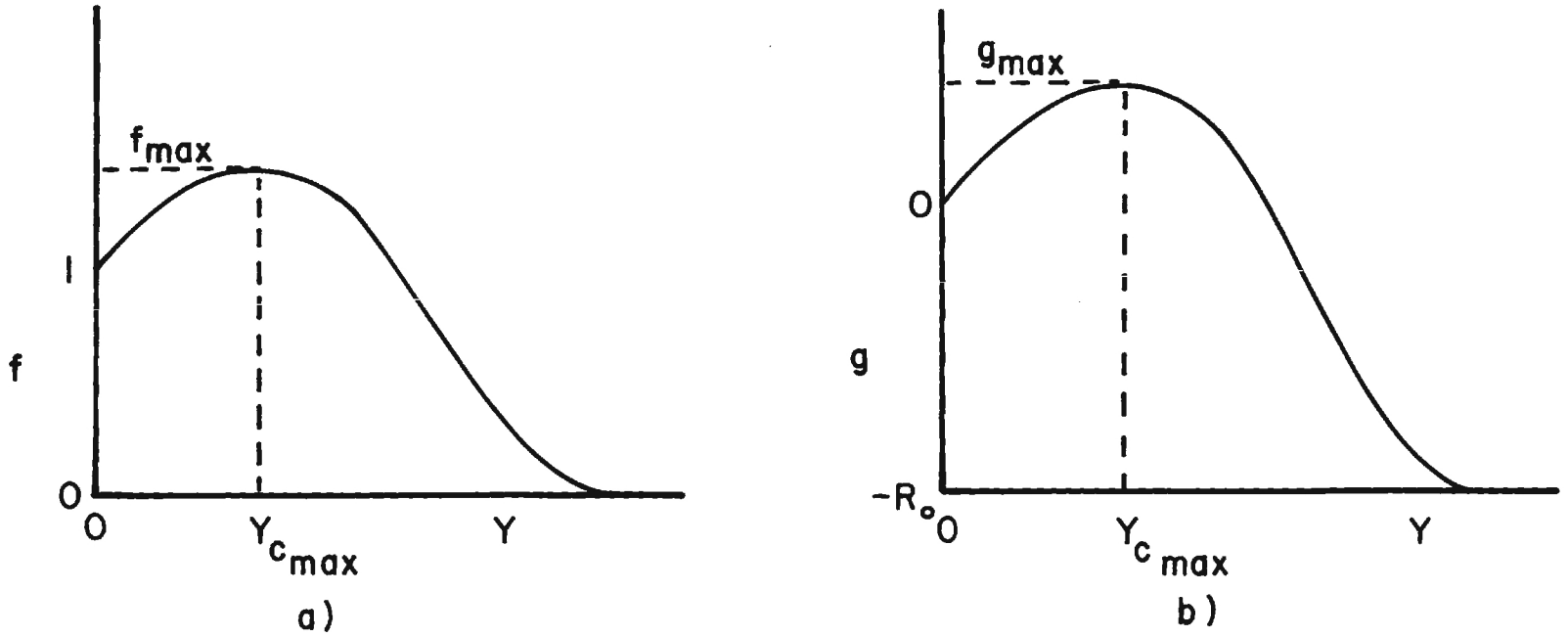

FIGURE 10. SAMPLE CATALYTIC RATE FUNCTIONS.

the square root of the reaction rate,[10] Eqs. (1) and (2) yield the two options for the burn rate:

$$r_a = KR_a^{\frac{1}{2}} \quad r_b = KR_b^{\frac{1}{2}} \tag{3}$$

where K is some constant. As long as the shape of the rate curves in Figures 10a and 10b is as shown, the following conclusions are valid:

a) $r(Y_{c_1}, Y_{c_2}) > r(Y_{c_1}, 0)$ or $r(0, Y_{c_2})$ for $Y_c \leq Y_{c_{max}}$

and b) $r_{max} = r(Y_{c_{1_{max}}}, Y_{c_{2_{max}}})$.

In this case the addition of a second catalyst will always augment the rate above what may be accomplished with a single catalyst. Moreover, for a fixed total mass of catalyst,

$$Y_{c_1} + Y_{c_2} = c,$$

and for equally effective catalysts so that

$$f_1 = f_2 \text{ or } g_1 = g_2$$

$$r(Y_{c_1}, c - Y_{c_1}) > r(c, 0) \text{ or } r(0, c) ,$$

as long as

$$c < Y_{c_{1_{max}}} = Y_{c_{2_{max}}} .$$

Therefore, with the appropriate restrictions, this simple demonstration shows that the presence of one catalyst augments the effect of the presence of another catalyst. This is a synergistic effect upon rate. Of course,

this is only a plausibility argument and no claim is being made that this is the actual mechanism or that Eqs. (1) and (2) are generally valid.

VI. Conclusions

1. All possible combinations of the four catalysts investigated exhibited a positive synergistic effect on the sandwich vertical burn rate when tested at 600 psia and a constant volumetric loading based on a total of 2w% addition of catalyst to the oxidizer.

2. The maximum sandwich burn rate at 600 psia was obtained for the combination of Harshaw catalyst Cu0202 and ferric oxide. When these samples were investigated over the pressure range of 300 to 2000 psia, the maximum synergistic effect occurs at 1500 psia. There was a positive synergistic effect over the entire pressure range.

3. The maximum synergistic effect with the two-dimensional sandwiches at 600 psia was obtained for the iron blue and ferric oxide combination. This combination was not as effective as the Harshaw catalyst Cu0202 and ferric oxide over the entire pressure range.

4. The cast composite propellant strands did not exhibit a positive synergistic effect when tested at 600 psia.

5. It is suspected that the heavy catalyst loading is responsible for the absence of synergistic effects in the cast propellants. A lower overall loading should be investigated.

6. From testing of ferrocene loaded into R-45 polymer at the molecular level it is concluded that molecular loading of a catalyst into a propellant is superior to physical loading of a crystalline material, as suspected from previous sandwich testing.

7. Differential scanning calorimetry of iron blue and ferrocene-loaded HTPB confirms earlier conclusions that these catalysts do not modify the pyrolysis mechanism of the binder to an appreciable extent.

8. For dry inert sandwiches analysis indicates that in the pressure range of 20 to 100 atm the sandwich should burn with a nearly flat surface and very close to the AP deflagration rate, as has always been observed for uncatalysed sandwiches with even wet binders.

9. A sharp slope discontinuity is predicted at the binder-oxidizer interface for dry binders, as has been seen experimentally for catalysed sandwiches.

10. For typical particle sizes of the order of 20 μm and larger the sandwich analysis can form the basis for a composite propellant deflagration theory, if the binder is dry.

References

1. Strahle, W. C., Handley, J. C., and Kumar, N., "Catalytic Behavior in Solid Propellant Combustion," Annual Summary Report for ONR Contract No. N0014-67-0159-0016. Georgia Institute of Technology, Atlanta, Georgia.

2. Strahle, W. C., Handley, J. C., and Milkie, T. T., "Catalytic Effects in the Combustion of AP-HTPB Sandwiches to 3200 psia," Combustion Science and Technology, Vol. 8, p. 297, (1974).

3. Jones, H. E., "An Experimental Investigation Relating to the Combustion Mechanism of Ammonium Perchlorate Composite Propellants," Ph.D. Dissertation, Georgia Institute of Technology, (1971).

4. Steinz, J. A., Stang, P. L., and Summerfield, M., "The Burning Mechanism of Ammonium Perchlorate-Based Composite Solid Propellants," AMS Report No. 830, ONR Contract Nonr 1858(32), February, 1969.

5. Gotzmer, C., Jr., "Modification of Propellant Binders: Quarterly Progress Report for 15 December 1971 through 15 March 1972," Indian Head Memorandum Report, 72-178, 18 March, (1972).

6. Varney, A. M., "An Experimental Investigation of the Burning Mechanisms of Ammonium Perchlorate Composite Solid Propellants," Ph.D. Dissertation, Georgia Institute of Technology, (1970).

7. Cohen, N. S., Fleming, R. W., and Derr, R. K., "Role of Binder in Solid Propellant Combustion," AIAA Paper No. 72-1121, (1972).

8. Strahle, W. C., "Solid Propellant Sandwich Deflagration Analysis," AIAA Paper No. 74-123, (1974).

9. Guirao, C. and Williams, F. A., "A Model for Ammonium Perchlorate Deflagration between 20 and 100 atm," AIAA Journal, 9, (1971), 1345-1356.

10. Culick, F. E. C. and Dehority, G. L., "An Elementary Calculation for the Burning Rate of Composite Solid Propellants," Combustion Science and Technology, 1, (1969), 193-204.

Appendix

Solid Propellant Sandwich Deflagration Analysis

SOLID PROPELLANT SANDWICH DEFLAGRATION ANALYSIS

Warren C. Strahle*
Georgia Institute of Technology, Atlanta, Ga.

ABSTRACT

A theoretical solution has been obtained for the shape of a deflagrating ammonium perchlorate surface when it is adjacent to an inert, pyrolysing, dry binder. The eigenvalue, the regression rate, is shown to be independent of binder type and very close to the burn rate of pure AP, as has been experimentally observed. A slope discontinuity of the surface should exist at the binder-oxidizer interface and typical binders should incline very near to 90° to the nearly horizontal AP surface, at the junction of the two. The transition from AP to binder should take place on a distance scale of the order of microns and all results are quite insensitive to pressure level.

This work was sponsored by the Office of Naval Research, Power Branch, under Contract No. N00014-67-0159-0016. Substantial aid in the calculations was given by Mr. Narendra Kumar.

Index categories: Combustion in Heterogeneous Media, Solid and Hybrid Rocket Engines.

*Professor, School of Aerospace Engineering, Member AIAA.

NOMENCLATURE

a	$g + 2q_R Y_F$
b	pyrolysis law constant of vapor pressure constant
$\tilde{b}$	dimensionless pyrolysis law constant or vapor pressure constant
c_s	solid phase specific heat
c_p	specific heat at constant pressure for gas phase
c	flame standoff distance
C	deviation of c from planar AP case
E	activation energy
g	T/T_o
G	deviation of temperature from planar AP case
G_o, G_1	solid phase temperature perturbation constants
k	preexponential factor in reaction rate law
$\tilde{k}$	dimensionless preexponential factor in reaction rate law
m, m_g	constants in eigensolution
n	coordinate normal to the solid-gas interface directed toward the gas phase
p	pressure
Q	reaction integral defined by Equations (18)
q	exothermic reaction heat in gas phase, endothermic in solid phase
R	universal gas constant
Re	Reynolds number
r, r_n	burn rate and regression rate normal to surface, respectively
T	temperature
v	gas velocity in y direction

w_F	production rate of NH_3
x,y	coordinates
Y	perturbed y position of solid surface
Y_k	mass fraction of species k
y	deviation of mass fraction from planar AP case
z	$1 + (dy_s/dx)^2$
α	thermal diffusivity, $\lambda/\rho c$
δ	inclination angle of binder
ϵ	dimensionless activation energy, E/RT
η	c_s/c_p
λ	thermal conductivity
ξ	$c_p\lambda_s/c_s\lambda_g$
ρ	density
θ	inclination angle of solid AP surface

Subscripts

B	binder
f	flame temperature
F	NH_3
g	gas phase
o	cold solid
s	solid phase or surface
1	quantity evaluated at flame standoff position

Superscripts

—	quantity evaluated for the one-dimensional AP deflagration

$'$	ordinary derivative with respect to x
$*$	dimensional quantity
$\wedge$	solid phase perturbation function

INTRODUCTION

A substantial number of experimental investigations of composite solid propellant ingredient behavior have dealt with the sandwich configuration (1-8). By a sandwich is meant a slab of oxidizer, usually ammonium perchlorate (AP) in the cited investigations, adjacent to a slab of polymeric fuel. This two-dimensional configuration is an important experimental configuration for the study of phenomena taking place near the binder-oxidizer interface during a deflagration process. By removing the difficulties of viewing the interface details in a real three-dimensional composite solid propellant, much information has been gathered concerning the behavior and existence of binder melts, catalytic additives, the relative importance of AP-binder reactions in driving the deflagration rate, fluid mechanical instabilities during deflagration, and the behavior of aluminum when placed into the sandwich.

In contrast to the many experimental studies there have appeared no analyses of the sandwich deflagration process with AP oxidizer which had as a goal the prediction of the actual shape of the gas-condensed phase interface Bakhman and Librovich[9] theoretically investigated a semi-infinite slab of oxidizer adjacent to a semi-infinite slab of fuel, but the oxidizer was not assumed to be capable of self-deflagration. Nachbar[10] investigated a periodic, two-dimensional array of oxidizer and fuel slabs as a model of an actual propellant. The goal was to predict a mean deflagration rate without predicting an actual achieved two-dimensional surface shape. Again, the oxidizer was assumed incapable of self-deflagration.

The need for an analytical model capable of prediction of the surface shape for an AP oxidized sandwich becomes apparent when trying to reason the behavior which is experimentally observed. Even in this two-dimensional configuration the problem is highly complex due to a) the appearance of binder

melts, b) three phase heat transfer and one phase (perhaps two phase) mass transfer, c) two-dimensional heat and mass transfer, d) non-linearities in the governing equations due to at least chemical reaction and an unknown surface shape, e) multiple chemical reactions and condensed phase reactions, f) a mathematically elliptic problem in an infinite region and g) the appearance of an eigenvalue - the deflagration rate. Under these difficulties an attempt to reason on a qualitative basis, given experimental information, is hampered by the lack of some computational framework and predictive capability.

A previous initial step toward providing a theory of the sandwich deflagration process[13] failed to yield the burn rate as an eigenvalue of the problem. Furthermore, an analytical error has been discovered in that treatment and the results are consequently in error. The current treatment corrects the error and recovers the burn rate as an eigenvalue of the problem by a more complex solution of the problem.

From a practical standpoint there are two major reasons for treating this problem. The first is to obtain an idea of the distance scales involved in the problem. That is, how far do the influence of the binder and oxidizer penetrate into each other? If these distance scales are small enough, this interface theory may be used in theory of an actual propellant. Secondly, the actual burn rate is desired. Is the influence of the binder on the self-deflagrating AP strong or weak? The current analysis addresses these issues.

ANALYSIS

Model Construction and Assumptions

Given the complicated nature of the problem, a model is first sought which uses available experimental information liberally but which still does not overly restrict the model in interpretation of experimental results. Accordingly, the initital model uses the following observations:

a) Far from the binder-oxidizer interface the AP regresses as pure AP. Furthermore, for binder thicknesses of the order used in some of the experimental studies (≈ 150 μm) there is little effect of one side of a sandwich upon the other side even when dissimilar materials are used. Therefore, the initial model development is concerned with a semi-infinite slab of AP against a semi-infinite slab of binder.

b) A steady state is achieved experimentally with AP oxidizer. Consequencly, time dependence is assumed absent.

c) For uncatalyzed sandwiches the experimental results show very little effect of the binder-oxidizer reactions upon the surface profile. That is, the heat feedback from the binder-oxidizer reactions does not drive the overall deflagration rate; the AP self-deflagration is responsible for the overall deflagration rate at pressures removed from the low pressure deflagration limit and below 2000 psia. The initial model is therefore constructed assuming binder-oxidizer reactions to have negligible rate. This does not mean that a diffusion flame between the binder and oxidizer is absent, but it means this flame is not close enough to the interface to play a role in the deflagration behavior. Furthermore, the effect of catalysis is not treated.

The initial model therefore asks the question of the surface shape

attained by a semi-infinite slab of AP which pyrolyzes a semi-infinite slab of binder. Posed in this manner it is immediately recognized that the problem has neither a unique solution nor a steady solution because a) the final shape would depend upon the geometry of ignition and b) it would take an infinite time to establish a steady profile in a semi-infinite slab of inert binder. The ignition problem is seen by imagining two cases - one in which ignition is achieved by a line heat source (say an ignition wire) and a second in which ignition is achieved uniformly over the entire AP surface. In the first case the AP would take on the shape of ever-increasing circular radii from the ignition point. In the second case the AP would deflagrate in a planar fashion except in the vicinity of the binder. However, these comments neglect the fact that the inert nature of the binder may affect the shape attained by the AP, even far away from the binder. Surely, at long enough time the profile in the interface vicinity will have become shape-invariant, but it is not obvious that the AP will be horizontal (assuming top-to-bottom deflagration). In fact, this is to be determined by the solution. Concerning the binder, it appears clear that after a sufficiently long time the processes in the interface vicinity will not depend upon processes taking place at a large vertical distance from the interface. Consequently, local steadiness may be presumed, as, in fact, experimentally occurs.

For this initial model the absence of binder melts will be assumed. The limits of validity will then be determined by comparison of the model and experimental results. For the AP deflagration process the Guirao-Williams model[11] is accepted with an equilibrium assumption for the gas-solid (or viscous liquid) AP interface. Some minor modifications are introduced into this model for computational convenience; these will be described below. Use of this model will restrict the sandwich theory validity to the pressure

range 20-100 atm, because there is no AP theory capable of an explanation of observed phenomena above 100 atm and the low pressure deflagration limit of AP occurs near 20 atm.

Other usual assumptions are made to simplify the analysis which, while they lead to numerical error of order unity, do not alter significantly the scaling rules developed with respect to other variables. These assumptions are: a) the thermal and transport processes of the solid AP and binder are identical, b) the thermal and transport properties of all gas phase species are identical, c) the Lewis number is everywhere unity in the gas phase, d) the deflagration process takes place at constant pressure, e) heat conduction and mass transfer take place by temperature and concentration gradients, only, respectively, and the transport coefficients are independent of temperature in both the solid and gas phases. A final major assumption is that on any vertical line parallel to the binder-oxidizer interface the ρv product (density times velocity) is that as determined in the solid phase and all lateral velocities are zero (strictly true in the solid phase). This is in the spirit of the Burke-Schumann approximation as expounded in Reference (2). This does yield error in convection effects upon heat transfer, but exact treatment of the problem appears too complex at the present time.

The configuration is shown in Figure 1, in which the coordinate system is rendered stationary by a translation of the interface in the y direction at the rate r. Under the stated assumptions the equations for solution and the boundary conditions are:

Gas Phase Species Continuity

$$\lambda_g^* \left(\frac{\partial^2 Y_F^*}{\partial x^{*2}} + \frac{\partial^2 Y_F^*}{\partial y^{*2}} \right) = \rho^* v^* \frac{\partial y_F}{\partial y^*} - w_F^* \qquad (1)$$

$$\frac{\lambda_g^*}{c_p^*}\left(\frac{\partial^2 Y_B}{\partial x^{*2}} + \frac{\partial^2 Y_B}{\partial y^{*2}}\right) = \rho^* v^* \frac{\partial Y_B}{\partial y} \tag{2}$$

Rate Law

$$w_F^* = -k^* Y_F^2 \, e^{-E_g^*/R^* T^*} \tag{3}$$

Gas Phase Heat Transfer

$$\lambda_g^*\left(\frac{\partial^2 T^*}{\partial x^{*2}} + \frac{\partial^2 T^*}{\partial y^{*2}}\right) = \rho^* v^* c_p^* \frac{\partial T^*}{\partial y^*} + 2 q_R^* w_F^* \tag{4}$$

Solid Phase Heat Transfer

$$\lambda_g^*\left(\frac{\partial^2 T^*}{\partial x^{*2}} + \frac{\partial^2 T^*}{\partial y^{*2}}\right) = \rho^* v^* c_s^* \frac{\partial T^*}{\partial y^*} \tag{5}$$

Boundary Conditions

$$\begin{aligned} Y_F(x,\infty) &= 0 & Y_F(-\infty,y) &= \bar{Y}_F(y) \\ T^*(x,-\infty) &= T_o^* & T^*(-\infty,y) &= \bar{T}^*(y) \\ T^*(\infty,y) &= T_o^* & T^*(x,\infty) &= T_o^* \end{aligned} \tag{6}$$

$$r_{n_B}^* = \vec{r}^* \cdot \vec{n}^*\Big|_B = b_B^* e^{-E_{s_B}^*/R^* T_s^*} \tag{7}$$

$$\lambda_g^* \frac{\partial T^*}{\partial n^*}\Big|_{s+} = \rho_S^* r_n^* q_S^* + \lambda_g^* \frac{\partial T^*}{\partial n^*}\Big|_{s-} \tag{8}$$

$$\rho^* D^* \frac{\partial Y_F}{\partial n^*}\Big|_{s+,\,AP} = -\rho_s^* r_n^* \left(\tfrac{1}{2} - Y_{F_s}\right) \tag{9}$$

$$\rho^* D^* \frac{\partial Y_B}{\partial n^*}\Big|_{s+,\,AP} = \rho_s^* r_n^* Y_{B_s} \tag{10}$$

$$p_{F_s}^* = b_F^* e^{-E_{s_F}^*/RT_s^*} \tag{11}$$

T^* continuous, ∇T^* continuous within a phase (12)

The products of AP gasification are assumed NH_3 and $HClO_4$ which are assumed identical molecules for mass transfer computation. k^* is a rate coefficient for the assumed second order reaction; as written in Equation (3) k^* is not a fundamental preexponential constant but already has molecular constants and a factor p^{*2} absorbed into it. The factor 2 in front of $q_R^* w_F^*$ in Equation (4) occurs because q_R^* will be quoted per unit mass of AP rather than per unit mass NH_3. The equilibrium interface on AP is specified through Equation (10). The formulation, as far as the AP deflagration process is concerned, differs from that of Reference (11) in the following respects: a) no dilution of the NH_3 and $HClO_4$ is assumed at tht solid-gas interface, although it is tacitly accounted for by the choice of a number for q_S^*; b) calculations are simplified by taking the molecular weight of all species to be the same. The constants k^* and b_F^* will be so chosen to recover the same burn rate and surface temperature results as in Reference (10).

Equation (7) is the pyrolysis law for the binder, Equation (8) is the energy conservation law at tht solid-gas interface, and Equations (9) and (10) are the interface diffusion laws. Note in Equation (8) that q_S^* undergoes a discontinuity at the binder-oxidizer interface and Equations (9) and (10) are only valid on the AP side of the interface. Shown in Table 1 are typical values used in this work for the various parameters.

Table 1

Numerical Values for Various Parameters

Quantity	Value	Reference
T_o^*	300 ^oK	Assumed
ρ_s^*	1.95 gm/cm^3	11
c_p^*	.3 cal/gm^oK	11
c_s^*	.3 cal/gm^oK	11
q_R^*	173 cal/gm	[to yield flame temperature of 1205^oK of Ref. (11)]
$q_{S_{AP}}^*$	-100 cal/gm	11
λ_g^*	10^{-4} $cal/cm\ sec^oK$	11
λ_s^*	9×10^{-4} $cal/cm\ sec^oK$	11
E_g^*	15 kcal/mole	11
E_s^*	30 kcal/mole	11
$E_{s_B}^*$	8.7 - 17 kcal/mole	14
b_B^*	1 - 150 cm/sec	14
$q_{s_B}^*$	160 - 1004 cal/gm	14

Mathematical Character of the Problem

Equations (1) - (5) define an elliptic problem in the sense that what happens at one point in the field affects every other point. Furthermore an eigenvalue appears, $\rho^* v^* = \rho_s^* r^*$.

If the binder is hard to decompose and it assumes a nearly vertical surface, it appears obvious that the picture becomes one of a (nearly) flat plate of binder over which hot AP gases are flowing. If the Reynolds number based on distance along the binder were large enough this would revert to a parabolic problem because $\partial/\partial x \gg \partial/\partial y$ would result. However,

exactly at the binder-oxidizer interface, the Reynolds number is zero. Since it is precisely this region that is of interest, the full elliptic problem must be solved. In order to gain an idea of magnitudes involved here the equations are nondimensionalized with respect to a distance scale α_s^*/r^* and temperature T_o^*. Heats of gasification are made dimensionless by $c_p^* T_o^*$ and activation energies by $R^* T_o^*$. In order to locate the condensed phase - gas phase interface at a constant position the y variable is replaced by $\eta = y - y_s(x)$. The resulting dimensionless equations and boundary conditions are

$$L\left[Y_F\right] = \tilde{k} Y_F^{\,2}\, e^{-\epsilon_g/g}$$

$$L\left[Y_B\right] = 0$$

$$\text{(Gas)} \quad L\left[g\right] = -2q_R \tilde{k}\, Y_F^{\,2}\, e^{-\epsilon_g/g}$$

$$\text{(Solid)} \quad L\left[g\right] = (1 - \xi)\, g.$$

$$L = \frac{\partial^2}{\partial x^2} + z^2 \frac{\partial^2}{\partial \eta^2} - 2y_s' \frac{\partial^2}{\partial \eta \partial x} - y_s'' \frac{\partial}{\partial \eta} - \xi \frac{\partial}{\partial \eta}$$

$$Y_F(x,\infty) = 0 \qquad Y_F(-\infty,y) = \bar{Y}_F(y)$$

$$g(x,-\infty) = 1 \qquad g(-\infty,y) = \bar{g}(y)$$

$$g(\infty,y) = 1 \qquad g(x,\infty) = 1$$

$$1/z_B = \tilde{b}_B e^{-\epsilon_{S_B}/g_s}$$

$$\partial g/\partial n\big|_{s+} = \xi\left[q_s/z + \eta \partial g/\partial n\big|_{s-}\right]$$

$$\partial Y_F/\partial n\big|_{s+_{AP}} = -\frac{\xi}{z}\left(\tfrac{1}{2} - Y_{F_s}\right)$$

$$\partial Y_B/\partial n\big|_{s+_{AP}} = \xi \frac{Y_{B_s}}{z}$$

$$Y_{F_s} = \tilde{b}_F e^{-\epsilon_{s_F}/g_s}$$

g continuous, ∇g continuous within a phase (13)

Since y' and y_s'' are unknowns, the nonlinear character in Equations (13) is apparent. Nonlinearities also arise from the chemical reaction terms. The dimension α_s^*/r^* is known to be the "thickness" of the thermal wave which would occur in a planar regression. It is the reference dimension here. The parameter ξ in Equations (12) is nothing more than the ratio of a characteristic solid phase dimension (α_s^*/r^*) to the characteristic gas phase dimension (α_g^*/v^*). If there were no modification due to the reaction rate term, the gas phase distance over which significant heat transfer would occur would be of the order of α_g^*/v^*. Using the parameters of Table 1, $\xi = 9.0$, showing that the gas and solid phase characteristic scales are quite different. Furthermore, constructing the Reynolds number based upon y, it is found that $Re_y = \xi y$, so that when y is of the order of $1/\xi$ a transition is taking place between "low" and "high" Reynolds numbers. If important field quantity variations are taking place only over a gas phase distance of the order of $1/\xi$, the problem must be treated as elliptic with no simplifications possible through a boundary layer assumption. However, a rather simple method of solution will emerge if at some point in the flow field the boundary layer approximation may be involved. The use of this approximation will be illustrated below.

Solution by an Integral Technique

Pure AP Deflagration

Far from the binder the AP must undergo a planar deflagration but the angle θ is unknown; it is the eigenvalue of the problem. All

x-derivatives must vanish and Equations (13) become nonlinear ordinary differential equations in η along with the appropriate boundary conditions. The equation for the solid phase heat transfer may be solved exactly. The solution is

$$\bar{g} - 1 = (\bar{g}_s - 1)\ e^{\eta/z^2} \tag{14}$$

An overall energy balance yields the adiabatic flame temperature

$$\bar{g}_f = \bar{g}_s + q_R - q_s - \tilde{\eta}(\bar{g}_s - 1) \tag{15}$$

A first integral of the gas phase heat and mass transfer equations, subject to the boundary conditions, is

$$\bar{a}(\eta) \equiv \bar{g}(\eta) + 2q_R\bar{y}_F(\eta) = \bar{g}_f = \bar{g}_s + 2q_R\bar{Y}_{F_s} \tag{16}$$

The solution is completed by assuming a functional form for $g(\eta)$ as

$$\bar{g}(\eta) - \bar{g}_s = (\bar{g}_f - \bar{g}_s)\ \frac{\eta}{\bar{c}} \qquad \eta < \bar{c}$$

$$\bar{g}(\eta) = \bar{g}_f \qquad \eta \geq \bar{c} \tag{17}$$

where $\bar{c}$ is the η position where $\bar{Y}_F(\eta)$ vanishes, i.e. reaction is complete. Now integrating the gas phase energy equation between $\eta = 0$ and $\eta = \bar{c}$ using the assumed form for $\bar{g}(\eta)$ from Equation (16), using the solid-gas interface boundary conditions and the equilibrium condition from Equations (12), the solution for the AP deflagration is completed as

$$\bar{c} = \frac{Y_{F_s} z^2}{\xi(\frac{1}{2} - \bar{Y}_{F_s})}$$

$$Q(\bar{c}) = \tilde{k}\bar{Y}_{F_s}^2\bar{c}\int_0^1 \left(1 - \frac{\eta}{\bar{c}}\right)^2 e^{-\epsilon_g/\left[\bar{g}_s + (\bar{g}_f - \bar{g}_s)\frac{\eta}{\bar{c}}\right]} d\left(\frac{\eta}{\bar{c}}\right)$$

$$= Y_{F_s}\left(\frac{z}{\bar{c}}^2 + \xi\right) = \xi/2$$

$$\bar{Y}_{F_s} = \tilde{b}_F e^{-\epsilon_{s_F}/\bar{g}_s} \tag{18}$$

An extremely important point to note from Eqs. (18) is that they imply that the regression rate normal to the gas-solid interface is independent of $\bar{\theta}$, the inclination to the horizontal. For note, $Q(\bar{c})$ is an invariant. For a fixed $\bar{g}_s$, $\bar{Y}_{F_s}$ is fixed and $\bar{c} \propto z^2$. Therefore, $Q \propto \tilde{k}\bar{Y}_{F_s}^2\bar{c} \propto \tilde{k}z^2$. But $\tilde{k} \propto 1/r^2$ so that $r \propto z$ and $r_n = r\cos\theta = r/z$ is an invariant. Consequently, for any sandwich vertical regression rate, r, which is the eigenvalue of the problem, the AP far from the binder will regress normal to its surface at a fixed, unique value. The pertinent values for AP combustion are consequently only presented for $\bar{\theta} = 0$. To numerically complete the solution the following procedure is used. a) $\bar{g}_s$ as a function of pressure is taken from Reference (11); b) Equation (14) yields $\bar{g}_f$ (which is actually constant here because $\tilde{\eta} = 1$ and q_R and q_s are assumed independent of pressure); c) Equation (16) determines $\bar{Y}_{F_s}$; d) Equations (17) determine $\bar{c}$, $\tilde{b}_F$ and $\tilde{k}$.

From the nondimensionalization procedure it may be recalled that $\tilde{k} \propto p^2/\bar{r}^2$. Therefore, if the rate, $\bar{r}$, is known at one pressure, it is known as a function of pressure. Shown in Table 2 are complete calculations for two sample pressures.

In Table 2 it will be noted that b_F is not quite constant. This is due to the use of a slightly higher E_{s_F} than in Reference (10). Furthermore,

$\tilde{k}$ is not quite proportional to $(p/\bar{r})^2$. This is due to the fact that $\bar{r}$ in Table 2 is the experimental value and it is known that between the two values of pressure of Table 2 the theory of Reference (11) slightly overestimates the pressure sensitivity of the deflagration rate. These details are not considered important for the current theory because a precise model for AP deflagration is not sought; only the deviations from a planar regression, due to the binder presence, are required and the above theory appears adequate to serve as a baseline for perturbations due to the binder.

Table 2

One Dimensional AP Deflagration Results

p (atm)	$\bar{r}$ (cm/sec)	α_s/r (μm)	$\bar{T}_s$ (^oK)	$\bar{g}_s$	$\bar{Y}_{F_s}$	$\bar{g}_f$	$\bar{c}$	b_F (atm)	$\tilde{k}$
54.4	.735	20.9	880	2.93	.285	4.022	.1471	4.38×10^8	2.62×10^6
100.0	1.000	15.3	911	3.04	.258	4.022	.1183	4.06×10^8	3.39×10^6

Perturbed Solution

It is noted that there is only a very weak variation of the dimensionless parameters with pressure in Table 2 (because $\bar{g}_s$ variations are weak with pressure) and therefore Eqs. (13) are nearly pressure invariant. Consequently, all further work will be carried out for the conditions that $\bar{g}_s = 2.93$ corresponding to $p = 54.4$ atm. = 800 psia.

Upon extensive investigation of the partial differential equations for small deviations from the one-dimensional regression it was determined that a) the deviations from the planar case in the gas phase could be expected to be simple deviations from the planar solution, but b) the solid phase deviations may be complex. By "simple" it is meant that the deviation is not oscillatory. Thus, if $g(x,y) = \bar{g}(x) + G(x,y)$ where $G(x,y)$ is the deviation from the pure AP case, $G(x,y)$ may be expected to have

monatonic behavior in y between the two end values $G[x,y_f(x)]$. Therefore it was decided to attempt an integral solution where

$$
\begin{aligned}
Y_F &= Y_{F_s}(x)\left[1 - \frac{\eta}{c(x)}\right] && \eta < c \\
Y_B &= Y_{B_s} + (Y_{B_c} - Y_{B_s})\ \frac{\eta}{c} && \eta < c \\
Y_F &= 0 && \eta > c \\
g - g_s(x) &= \left[g_1(x) - g_s(x)\right]\frac{\eta}{c(x)} && \eta < c
\end{aligned}
\tag{19}
$$

are guessed forms of the solution for the gas phase.

If the Eqs. (19) are placed in Eqs. (13) and integrated from $\eta = 0$ to $c(x)$ the result is three nonlinear ordinary differential equations in the unknowns Y_{F_s}, Y_{B_s}, Y_{B_c}, c, g_1, g_s, y_s' and the η derivatives of g and Y_B at $\eta = c$. These derivatives appear because no functional form is specified for $\eta > c$. It is anticipated that these derivatives will be very small beyond the reaction region and one possible assumption is that they are zero. An alternate assumption has been employed and is discussed below. The diffusion boundary conditions and the equilibrium interface boundary condition provide three more relations for the nine unknowns. At $\eta = c$ which is of the order of magnitude of $1/\xi$, the Reynolds number is making a transition from low to high values, and it appears at this point reasonable to assume that $\frac{\partial}{\partial x} \gg \partial/\partial y = \frac{\partial}{\partial \eta}$. Making this assumption in Eqs. (13) there results

$$
\begin{aligned}
\frac{\partial g}{\partial \eta}\Big)_{\eta = c} &= \frac{1}{\xi}\frac{\partial^2 g}{\partial x^2}\Big)_{\eta = c} = \frac{1}{\xi}\frac{d^2 g_1}{dx^2} \\
\frac{\partial Y_B}{\partial \eta}\Big)_{\eta = c} &= \frac{1}{\xi}\frac{\partial^2 Y_B}{\partial x^2}\Big)_{\eta = c} = \frac{1}{\xi}\frac{d^2 Y_{B_c}}{dx^2}
\end{aligned}
\tag{20}
$$

Eqs. (20) eliminate two of the above unknowns and one further relation is needed. For algebraic simplicity another differential equation is obtained by taking an η - moment of the equation

$$L[a] = 0 \qquad a = g + 2q_R Y_F,$$

deriveable from Eqs. (13), and integrating from o to c.

In order for a numerical integration to proceed smoothly to $x = -\infty$ an asymptotic solution is desirable. Consequently, a solution was first sought which is a small perturbation about the planar AP deflagration state. Letting

$$Y_{F_s} = \bar{Y}_{F_s} + \gamma_{F_s}(x) \qquad g_1 = \bar{g}_1 + G_1(x)$$

$$g_s = \bar{g}_s + G_s(x) \qquad c = \bar{c} + C(x)$$

$$y_s = Y(x), \qquad Y_{B_s} = \gamma_{B_s}(x)$$

$$Y_{B_c} = \gamma_{B_c}(x)$$

substituting these forms into the nonlinear ordinary differential equations and boundary conditions, making use of the AP solution properties, and neglecting products and squares of perturbation quantities, there results the following linearized set of equations and boundary conditions

$$\tfrac{1}{2}[\bar{Y}_{F_s} C'' + \bar{c}\gamma_{F_s}''] + Y''\bar{Y}_{F_s} + \bar{y}_s'\gamma_{F_s}' = Q_{g_1} G + Q_{Y_{F_s}} \gamma_{F_s} + Q_c C + Q_{g_s} G_s \qquad (21)$$

$$\tfrac{1}{2}[\bar{c}G_1'' + \bar{c}G_s'' + C''(\bar{g}_s - \bar{g}_1)] + \frac{z}{\xi}^2 G_1'' = (G_1 - G_s)(\frac{z^2}{\bar{c}} + \xi) + 2\bar{y}_s'(G_1' - G_s')$$

$$- (\frac{-2Y'\bar{\gamma}_s'}{\bar{c}} + \frac{\bar{z}^2 C}{\bar{c}^2})(\bar{g}_1 - \bar{g}_s) + Y''(\bar{g}_1 - \bar{g}_s) - 2q_R(Q_{Y_{F_s}} \gamma_{F_s} + Q_{g_1} G_1 + Q_c C$$

$$+ Q_{g_s} G_s \qquad (22)$$

$$\frac{1}{2}\bar{c}\left(\gamma_{B_c}'' + \gamma_{B_s}''\right) + \frac{\bar{z}^2\gamma_{B_c}''}{\xi} = \left(\xi + \frac{\bar{z}^2}{\bar{c}}\right)\left(\gamma_{B_c} - \gamma_{B_s}\right) + 2\bar{y}_s'\left(\gamma_{B_c}' - \gamma_{B_s}'\right) \tag{23}$$

$$\left(\gamma_{B_c} - \gamma_{B_s}\right)\frac{\bar{z}^2}{\bar{c}} - \bar{y}_s'\gamma_{B_s}' = \xi\gamma_{B_s} \tag{24}$$

$$\bar{y}_s'\,\gamma_{F_s}' = -\xi\gamma_{F_s} + \frac{\bar{z}^2 C\bar{Y}_{F_s}}{\bar{c}^2} - 2\bar{y}_s'\,\bar{Y}_{F_s}Y' - \frac{\bar{z}^2}{\bar{c}}\gamma_{F_s} \tag{25}$$

$$\gamma_{F_s} = \frac{\bar{Y}_{F_s}\,E_{s_F}}{\bar{g}_s^2}G_s \tag{26}$$

$$G_1(-\infty) = G_s(-\infty) = \gamma_{F_s}(-\infty) = \gamma_{B_c}(-\infty) = \gamma_{B_s}(-\infty) = Y'(-\infty) = C(-\infty) = 0 \tag{27}$$

Here Q_{g_1}, Q_c, Q_{g_s} and $Q_{Y_{F_s}}$ are partial derivatives of the reaction rate integral which may be numerically evaluated. Note that Eqs. (23) and (24) are decoupled from the rest of the system. Because Eqs. (21)-(27) are linear and homogeneous, they possess solutions like, say, $G_1 = A_{G_1} e^{mx}$. Since $2Y_F + Y_B + Y_p = 1$, the binder equations must also have solutions $\gamma_{B_c} = A_{\gamma_{B_c}} e^{mx}$ where the m is the same. So there are two sets of equations which may be investigated. Since the equations are homogeneous, the determinant of the coefficient matrix must equal zero for a solution to exist. From Eqs. (21), (22), and (25) $m = m_1(\bar{\theta})$ is therefore developed. From Eqs. (24) and (25) $m = m_2(\bar{\theta})$ is developed and the results are shown on Fig. 2. Only real values of m were numerically investigated because the only unique solutions which will properly attach to the binder are for real m, as will be seen later. It is seen that there is a unique $\bar{\theta}$ for

$$m = 6.4 \quad \bar{\theta} = 2^{\circ}$$

That is, an eigenvalue exists. The AP assumes a nearly horizontal surface far from the binder so that the burn rate is only slightly higher

and the physical properties of thebinder. A question now to be asked is whether or not this linear solution may be used instead of a full nonlinear solution for binders of practical interest. The usual physical expectation is that a linearized theory will be reasonable if the perturbation quantities remain within some prescribed fraction of the corresponding baseline quantity. Viewing Fig. 3 and focusing on g_1, for example, if an arbitrary limit of validity is set that $(g_1 - \bar{g}_1)/\bar{g}_1 < 10\%$, it appears that the solution might be expected to be valid for $x < 0.6$. Adopting this criterion, a procedure to match to the binder is required for the linearized solution.

Location of the Binder

It will be noticed that the above solution is independent of the solid phase solution. In fact the heat transfer condition of Eqs. (13) and the surface temperature of the gas phase solution form boundary conditions for the solid phase heat transfer. Since the attempt here is to work with the asymptotic solution to a linear set of equations, the consistent linearized solid phase equation from Eqs. (13) is for $g = \bar{g}(\eta) + G(x,\eta)$

$$\frac{\partial^2 G}{\partial x^2} + \frac{\partial^2 G}{\partial \eta^2} - \frac{\partial G}{\partial \eta} = Y'' \frac{\partial \bar{g}}{\partial \eta} \tag{28}$$

where the simplifying assumption of $\bar{y}_s' = 0$ has been made in accordance with the above gas phase solution. Letting $G = \hat{g} + Y \frac{\partial \bar{g}}{\partial \eta}$, Eq. (27) becomes

$$\frac{\partial^2 \hat{g}}{\partial \eta^2} + \frac{\partial^2 \hat{g}}{\partial x^2} - \frac{\partial \hat{g}}{\partial \eta} = 0$$

which has the solution

$$\hat{g} = e^{\eta/2} e^{mx} [G_o \cos m_g \eta + G_1 \sin m_g \eta] \tag{29}$$

$$m_g = (m^2 - \tfrac{1}{4})^{\frac{1}{2}}$$

This solution has a feature that

$$G_s = G_o e^{mx} + Y \frac{\partial \bar{g}}{\partial \eta} (0)$$

which determines G_o from the gas phase solution. A most important feature of the solution is the creation of an oscillatory ripple of very short wavelength (of order $1/m_g \approx 1/m$) superimposed on the monotonically varying temperature of the undisturbed solution. What happens, therefore, is that in both the solid phase and gas phase the distance scales over which rapid transitions are made are now of the same order of magnitude (of order $1/\xi$). In a sense, the short distance scale of the gas phase is imposed upon the solid phase.

To complete the solid phase solution Eq. (28) is substituted into the interface heat transfer condition of Eqs. (13) and G_1 is determined. Now at any x position in the eigensolution to the AP problem the heat transfer vector in the gas and solid phases is known. Since this must be a continuous quantity and the temperature is a continuous quantity, but q_s undergoes a discontinuity, there must be a surface slope discontinuity at the binder. In the interface energy conservation relation of Equations (13) the solid and gas phase heat transfer vectors may be computed from the AP solution and this equation becomes a relation for the binder heat of gasification as a function of its surface slope. The result is

$$q_{s_B} = mG_s\, y_B' \frac{(\xi - 1)}{\xi} + (1 + y_B' y_s') \left\{ \frac{g_1 - g_s}{\xi c} - (g_s - 1)\,(1 + Y) - \frac{G_o}{2} - m_g G_1 \right\} \qquad (30)$$

The pyrolysis condition of Equations (13) gives an additional relation between the surface slope and the binder properties

$$\frac{1}{z_B} = \tilde{b}_B e^{-\epsilon_{s_B}/g_s} \tag{31}$$

At any x position, then, Equations (29 and 30) together with the AP eigensolution define an allowable binder attachment and a functional equation

$$b_B = b_B\left(\epsilon_{s_B}, q_{s_B}; x\right)$$

$$y_B' = y_B\left(\epsilon_{s_B}, q_{s_B}; x\right)$$

For the case of p = 54.4 atm these results are shown in Figures 4 and 5 for two values of ϵ_{s_B} which correspond closely to HTPB and CTPB binders.[14] Also, knowing q_s and b_B for HTPB and CTPB[14] the actual point at which these two binders would attach is shown on Figures 4 and 5.* There are several points worthy of note. First, for these binders, the x position of compatability with the AP solution occurs where very little change from a flat AP surface has taken place. Consequently, the linear AP eigensolution can be used with confidence as a good approximation to the solution of the nonlinear problem. Polyurethane, shown on Fig. 4 would also attach to a nearly flat AP surface. A check of the fluorocarbon binder data of Ref. (14) also shows an attachment at negative x. The second important point is that the binder slope is very nearly vertical at the attachment point. This is the primary information desired, in addition to the AP surface profile, so no attempt is made to continue the solution to the right of the attachment point to find the binder profile. The third major point, refering back to Fig. 3, is that the solid phase heat

*The activation energies for HTPB and CTPB do not exactly fit the numbers of Figs. 4 and 5. What has been done is to compute a b_B to fit the known binder pyrolysis data at a temperature g_s, assuming the activation energies of the figures.

transfer vector points from the binder toward the AP. This indicates that at least for a short distance above the interface the binder temperature must be increasing, probably due to the fact that the highest temperature AP gases are at positive η.

DISCUSSION OF RESULTS

A solution has been obtained for the shape of the deflagrating AP surface when it is adjacent to an inert dry binder. The eigenvalue, the vertical regression rate, has been found to be independent of binder type and to deviate only very slightly from the pure AP burn rate, as has been experimentally observed. Except for selected binders there would be very little visible effect of the binder upon the surface shape and the result is virtually independent of pressure. The distance scale over which a visible transition would take place from planar AP to the binder is of the order of microns. The current theory assumes a dry binder; it is known, however, that binder melt flows exist for all binders tested heretofore in the sandwich configuration and that these melt flows run several hundred microns onto the AP surface. Furthermore, surface roughness demensions of the order of microns develops during deflagrations. Consequently, few of the predicted phenomena are capable of being observed. A theory including the effects of melt flows is necessary.

The theory predicts, however, that if the melts do not occur there should be a sharp discontinuity in slope at the binder-oxidizer interface. This has recently been seen for catalyzed sandwiches[15] for which the melt extent is markedly reduced (for unknown reasons). Although the current theory is not directly applicable to catalyzed situations the interface conditions responsible for the slope discontinuity are applicable. It appears that melt flows dominate the development of the

surface shape if melts occur.

The current theory shows that the heat flow vector near the gas-solid interface and AP-binder solid interface is from the binder toward the AP in the solid phase. Consequently, there must exist a weak (hot) portion of the binder slightly up from the four-corner interface and into the binder. This might account for the appearance of "notches" in the binder sometimes seen in quenched samples.[1,2,4,15] The violence of the quenching process may eject the part of the binder which is weaker than surrounding parts.

The current analysis shows a very weak dependence of surface shape upon pressure. This independence has been observed experimentally, but the comparison between theory and experiment cannot be made precisely because binder melts have occurred in all the experiments.

If the AP particle size is sufficiently large the current analysis may form the basis for a deflagration theory of a heterogeneous propellant, if the binder were dry. The largest natural dimension which occurs in this theory is the thermal wave depth which is of the order of 20 μm at 800 psia. Consequently, for AP particle sizes larger than this dimension there may be some merit in applying this technique to a real propellant. An extension to the case of a finite binder thickness would be required, however, unless AP particle sizes substantially in excess of the thermal wave depth were considered because the typical binder widths would be less than the typical thermal depth in the binder. Such an extension is not deemed difficult to attain.

REFERENCES

1. Hightower, J. D. and Price, E. W., "Experimental Studies Relating to the Combustion Mechanism of Composite Propellants," Astronautica Acta, 14, (1968), 11-21.

2. Varney, A. M., "Experimental Investigation of the Burning Mechanism of Ammonium Perchlorate Composite Propellants, Ph.D. Dissertation, Georgia Institute of Technology, (1971).

3. Jones, H. E., "An Experimental Investigation Relating to the Combustion Mechanism of Ammonium Perchlorate Composite Propellants," Ph.D. Dissertation, Georgia Institute of Technology, (1971).

4. Boggs, T. L. and Zurn, T. E., "The Deflagration of Ammonium Perchlorate-Polymeric Binder Sandwich Models," Combustion Science and Technology, 4, (1972), 279-292.

5. Boggs, T. L., Zurn, D. E., Strahle, W. C., Handley, J. C., and Milkie, T. T., "Mechanisms of Combustion," NWC TP 5514, July 1973.

6. Nadaud, L., "Models Used at ONERA to Interpret Combustion Phenomena in Heterogeneous Solid Propellants, "Combustion and Flame, 12, (1968), 177-195.

7. Austin, T. D., "Flame Temperature Profile of Ammonium Perchlorate Fuel Binder Sandwiches," 4th ICRPG Combustion Conference, CPIA Publication No. 162, Vol. 1, (1967).

8. Brown, W. E., Kennedy, J. R., and Netzer, D. W., "A Study of AP/PBAA Sandwich and AP Pellet Combustion," 9th JANNAF Combustion Meeting, CPIA Publication 231, Vol. II, (1972).

9. Bakhman, N. and Librovich, V. B., "Flame Propagation Along Solid Fuel-Solid Oxidizer Interface," Combustion and Flame, 15, (1970), 143-155.

10. Nachbar, W., "A Theoretical Study of the Burning of a Solid Propellant Sandwich," Solid Propellant Rocket Research, Academic Press, New York, 1960.

11. Guirao, C. and Williams, F. A., "A Model for Ammonium Perchlorate Deflagration between 20 and 100 atm," AIAA Journal, 9, (1971), 1345-1356.

12. Williams, F. A., Combustion Theory, Addison-Wesley, Reading (1965), p. 39.

13. Strahle, W. C., "Solid Propellant Sandwich Deflagration Analysis, AIAA Paper No. 74-123, 1974.

14. Cohen, N. S., Fleming, R. W., and Derr, R. L., "Role of Binder in Solid Propellant Combustion," AIAA Paper No. 72-1121, (1972).

15. Handley, J. C. and Strahle, W. C., "The Behavior of Several Catalysts in the Combustion of Solid Propellant Sandwiches," AIAA Paper No. 74-122, 1974.

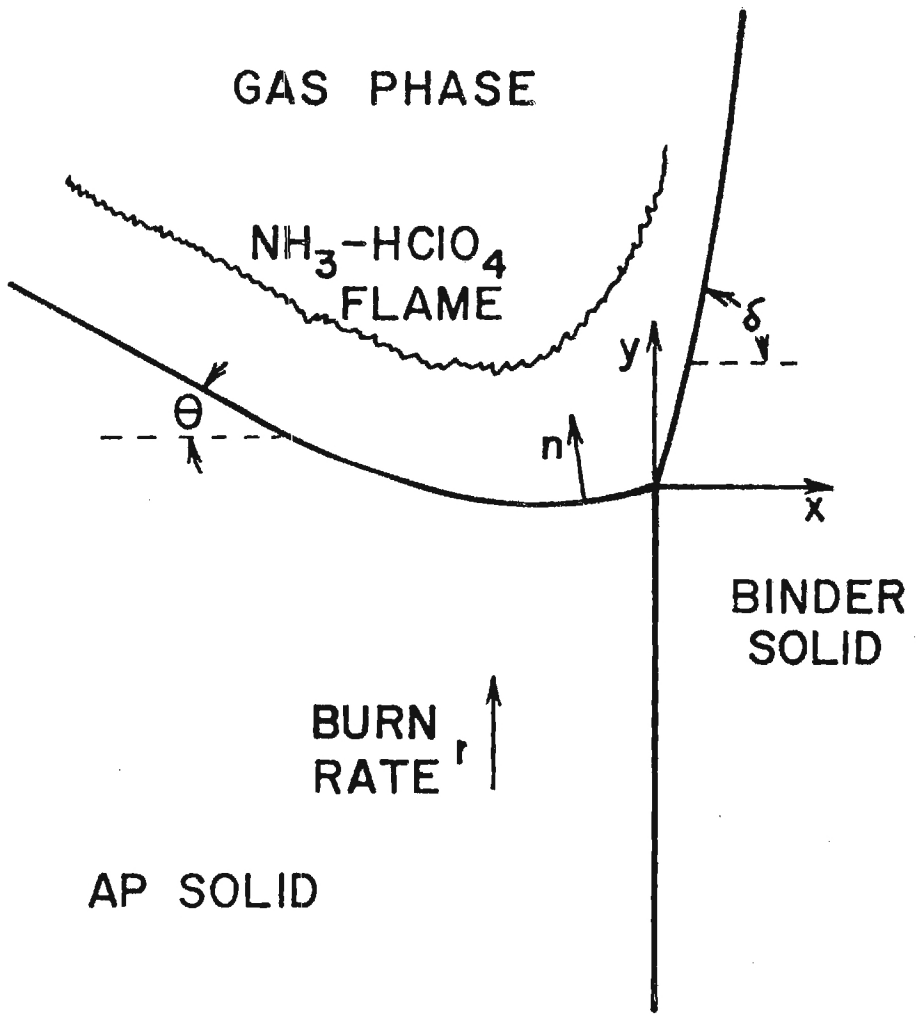

Figure 1. Sandwich Schematic and the Coordinate System

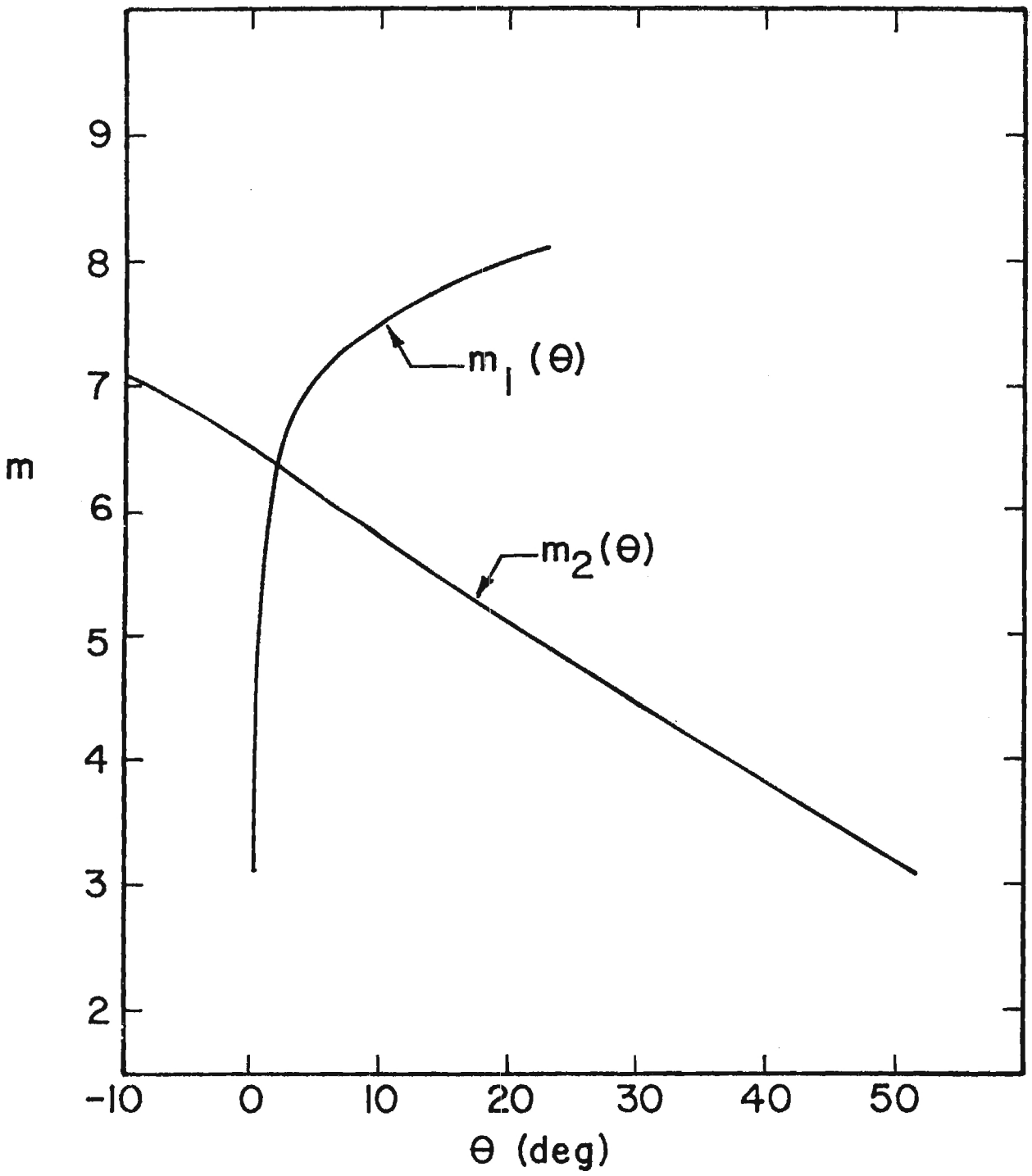

Figure 2. Roots of the Linearized Sets of Equations

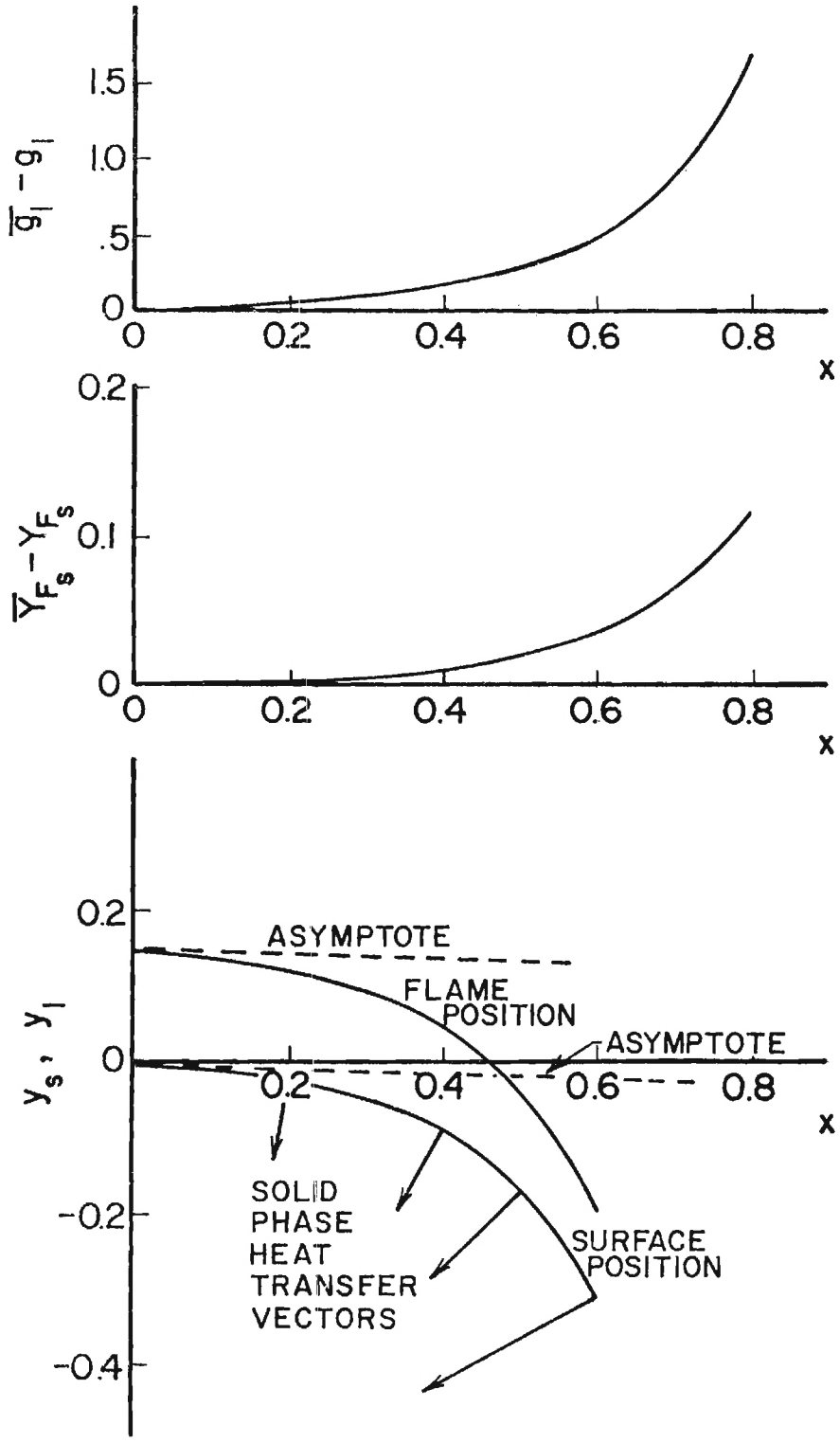

Figure 3. Surface, Flame Standoff, Surface NH_3 Mass Fraction, Flame Temperature and Solid Phase Heat Transfer Vector Profiles

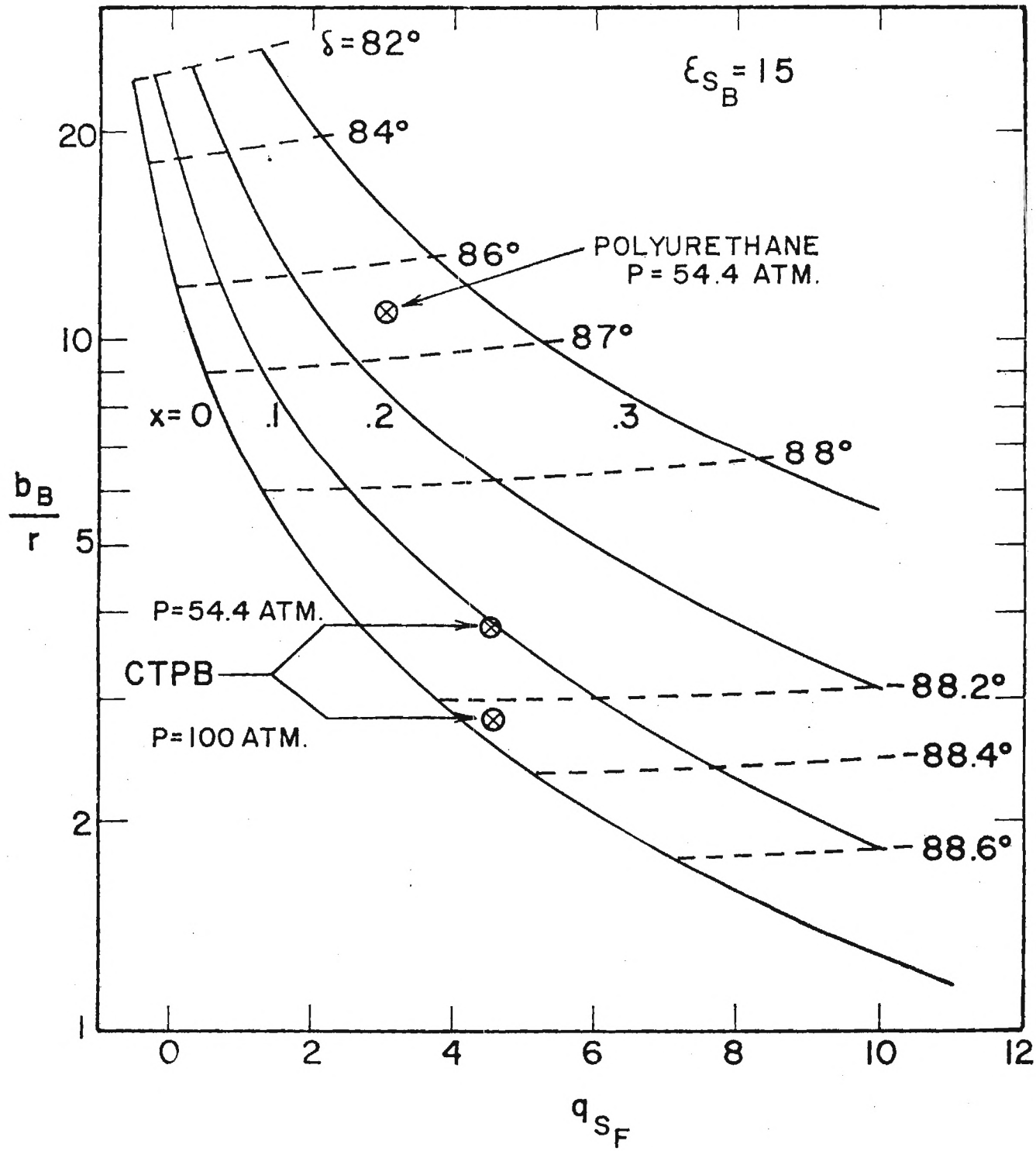

Figure 4. Binder Properties for Attachment to the AP Solution, ε_{s_B} = 15

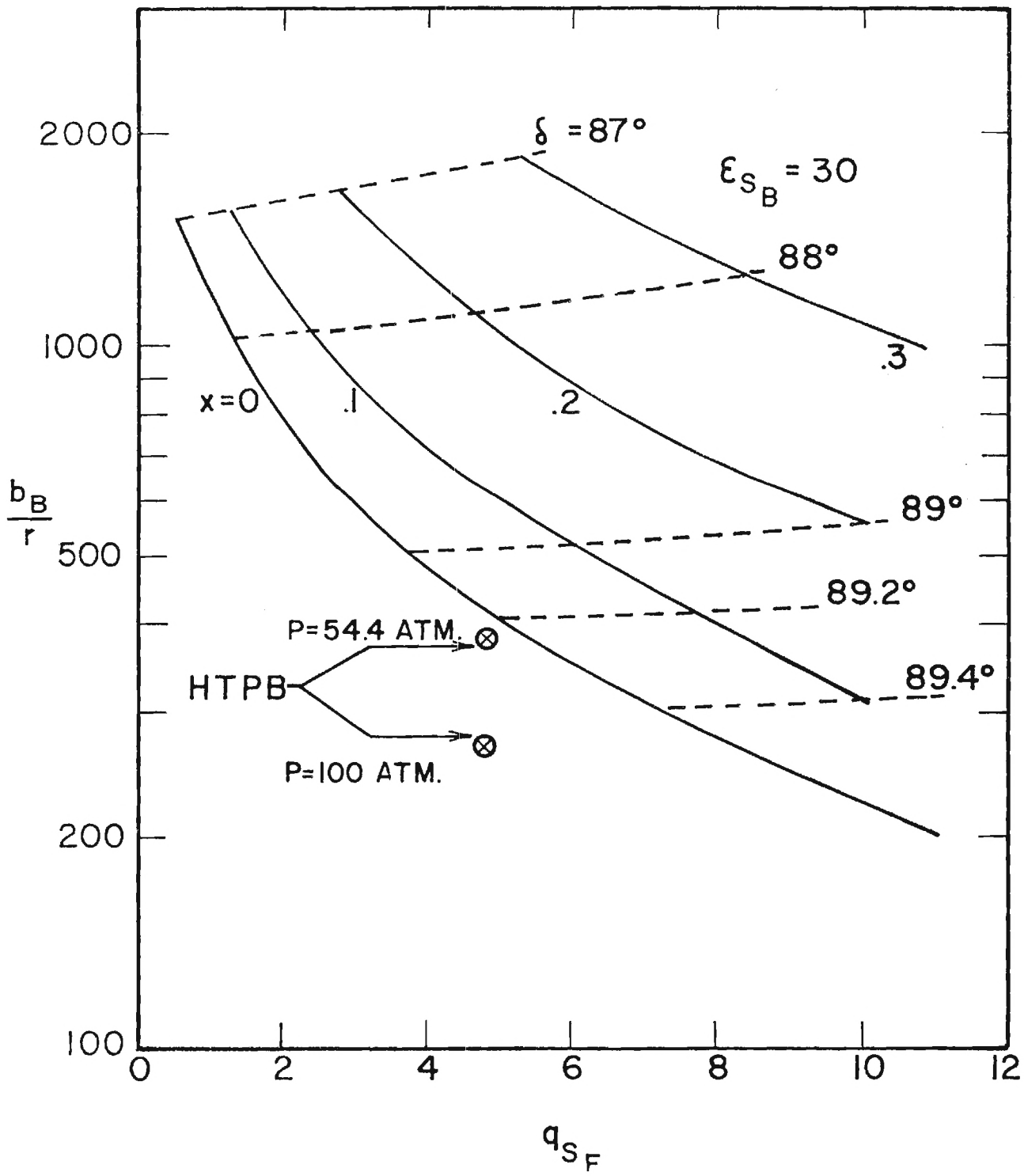

Figure 5. Binder Properties for Attachment to the AP Solution, $\varepsilon_{S_B} = 30$

Distribution List

Advanced Ballistic Missle
Defense Agency
Huntsville Office
Attn: M. L. Whitfield, CRDABH
P.O. Box 1500
Huntsville, Alabama 35807

Aerojet Solid Propulsion Company
Attn: Wilfred G. Schmidt
(Bldg. 0525, Dept. 4410)
P.O. Box 13400
Sacramento, Calif. 95813

Aerospace Corporation
Attn: Ellis M. Landsbaum
2350 E. El Segundo Blvd.
El Segundo, Calif. 90245

Air Force Armament Laboratory
Guns & Rockets Division
Attn: O. K. Heiney, DLDL
Eglin AFB, Fla. 32542

AF Foreign Technology Div. (TDETT)
Attn: H. E. Wright
Wright Patterson AFB
Dayton, Ohio 45433

AF Office of Scientific Research
1400 Wilson Blvd.
Arlington, Va. 22209

AFRPL (LK)
Attn: Dr. R. R. Weiss
Edwards, Calif. 93523

Commanding Officer
Army Aberdeen Research & Development Center
Attn: Mr. L. A. Watermier, Code AMXRD-BIL
Aberdeen Proving Ground, Md. 21005

Commander
Army Missle Command
Attn: Dr. R. Rhodes
Redstone Arsenal, Ala. 35809

Brigham Young University
Chemical Eng. Dept.
Attn: Dr. R. L. Coates
Widtsol Bldg.
Provo, Utah 84601

British Embassy
Attn: John Bell
3100 Mass. Ave., N. W.
Washington, D. C. 20008

California Institute of Technology
Attn: Prof. F. E. C. Culick
204 Karman Lab., (301-46)
1201 E. California St.
Pasadena, Calif. 91109

California Inst. of Technology
Jet Propulsion Laboratory
Attn: W. Dowler
4800 Oak Grove Drive
Pasadena, Calif. 91103

Defense Research & Engineering
Attn: Mr. G. R. Makepeace
Asst. Dir., Engineering Technology
The Pentagon, Rm. 3D1089
Washington, D. C. 20301

Commanding Officer
Frankford Arsenal
Attn: M. Visnov, J8100, Bldg. 64-2
Bridge & Tacony Streets
Philadelphia, Pa. 19137

Georgia Institute of Technology
Georgia Tech. Res. Inst.
Attn: Res. Security Coordinator
Prof. B. T. Zinn
Atlanta, Ga. 30332

Hercules, Inc.
Allegany Ballistics Laboratory
Attn: Dr. R. R. Miller
P. O. Box 210
Cumberland, Md. 21502

Hercules, Inc.
Bacchus Works
Attn: Dr. M. W. Beckstead, 100K1-7
P. O. Box 98
Magna, Utah 84044

Institute for Defense Analyses
Attn: Dr. R. T. Oliver
400 Army-Navy Drive
Arlington, Va. 22202

Johns Hopkins Univ./APL
Chemical Propulsion Information
Agency
Attn: Thomas W. Christian
8621 Georgia Avenue
Silver Spring, Md. 20910

Lockheed Propulsion Company
Attn: N. S. Cohen
P. O. Box 111
Redlands, Calif. 92373

NASA Headquarters
Attn: Mr. William Cohen
Code RPT
600 Independence Avenue
Washington, D. C. 20546

NASA
Johnson Space Center
Attn: Joseph G. Thibodaux, EP
Houston, Texas 77058

NASA
George C. Marshall Space Flt. Ctr.
Attn: Mr. J. O. Miller
Huntsville, Ala. 35812

Naval Air Systems Command
Attn: Dr. O. H. Johnson,
Code AIR 330
Jefferson Plaza, Bldg. 1
Washington, D. C. 20360

Naval Ordnance Station
Attn: Mr. A. T. Camp, Code FS
Indian Head, Md. 20640

Naval Ordnance Systems Command
Attn: Mr. J. W. Murrin,
ORD 0331
National Center, Bldg. 2,
Room 6S12
Washington, D. C. 20360

Naval Postgraduate School
Department of Aeronautics
Attn: Code 2124
Prof. D. W. Netzer
Monterey, Calif. 93940

Naval Research Office
Dept. of the Navy
Attn: Ralph Roberts (2)
800 N. Quincy St.,
Ballston Towers #1
Alexandria, Va. 22217

Naval Weapons Center
Attn: Dr. Ronald Derr
Code 608
China Lake, Calif. 93555
Pennsylvania State University
Attn: G. M. Faeth
University Park, Pa. 16802

Commanding Officer
Picatinny Arsenal
Attn: SMUPA-TS-TS-Dr. Jean Picard
Dover, N. J. 07801

Princeton University
Guggenheim Laboratories
Attn: M. Summerfield and
L. H. Caveny
Princeton, N. J. 08540

Purdue University
School of Mechanical Engineering
Attn: Dr. J. R. Osborn
West Lafayette, Indiana 47907

Rockwell International
Rocketdyne Division
Attn: C. L. Oberg
6633 Canoga Avenue
Canoga Park, Calif. 91304

Rockwell International
Rocketdyne Division
Attn: W. G. Haymes
P. O. Box 548
McGregor, Texas 76657

Shock Hydrodynamics, Inc.
Attn: W. H. Anderson
15010 Ventura Boulevard
Suite 201
Sherman Oaks, Calif. 91403

Stanford Research Inst.
Attn: H. Wise
333 Ravenswood Ave.
Menlo Park, Calif. 94025

Stevens Institute of Technology
Mech. Eng. Dept.
Attn: Richard B. Cole
Castle Point Station
Hoboken, N. J. 07030

Susquehanna Corporation
Atlantic Research Group
Attn: Dr. Merrill K. King
Shirley Highway & Edsall Road
Alexandria, Va. 22314

Rocket Research Corp.
Attn: P. L. Stang
Willow Rd. at N.E. 116th St.
Redmond, Va. 98052

Bell Aerospace Co., Div.
Attn: Mr. Mort Shorr
P. O. Box One
Buffalo, N. Y. 14240

Thiokol Chemical Corp.
Elkton Division
Attn: E. Sutton
Elkton, Md. 21921

Thiokol Chemical Corp.
Huntsville Division
Attn: Dr. R. L. Glick
Huntsville, Ala. 35807

Thiokol Chemical Corp.
Wasatch Division
Attn: John A. Peterson
P. O. Box 524
Brigham City, Utah 94302

Ultrasystems
Dynamic Science Div.
Attn: J. N. Levine
2400 Michelson Drive
Irvine, Calif. 92664

United Technology Ctr.
Attn: R. S. Brown
P. O. Box 358
Sunnyvale, Calif. 94088

University of Illinois
Aeronautical & Astro. Engr. Dept.
Attn: Prof. Herman Krier
101 Transportation Bldg.
Urbana, Ill. 61801

University of Calif., San Diego
Inst. Pure Applied Phys. Scis.
Attn: F. A. Williams
P. O. Box 109
La Jolla, Calif. 92037

University of Utah
Chemical Engr. Dept.
Attn: Alva D. Baer
Park Bldg., Room 307
Salt Lake City, Utah 84112

University of Waterloo
Dept. of Mech. Engr.
Attn: Prof. Clarke E. Hermance
Waterloo, Ontario, Canada

Whittaker Corp.
Tasker Industries
Bermite Division
Attn: William E. Robertson
22116 W. Soledad Canyon Road
Saugus, Calif. 91350

UNCLASSIFIED

SECURITY CLASSIFICATION OF THIS PAGE *(When Data Entered)*

REPORT DOCUMENTATION PAGE		READ INSTRUCTIONS BEFORE COMPLETING FORM
1. REPORT NUMBER	2. GOVT ACCESSION NO.	3. RECIPIENT'S CATALOG NUMBER
4. TITLE *(and Subtitle)* SYNERGISTIC AND NOVEL EFFECTS IN COMPOSITE SOLID PROPELLANT COMBUSTION		5. TYPE OF REPORT & PERIOD COVERED Annual Summary Report Sept. 1, 1973-August 31, 1974 6. PERFORMING ORG. REPORT NUMBER
7. AUTHOR(s) Warren C. Strahle John C. Handley		8. CONTRACT OR GRANT NUMBER(s) N0014-67-A-0159-0016
9. PERFORMING ORGANIZATION NAME AND ADDRESS Georgia Institute of Technology Atlanta, Georgia 30332		10. PROGRAM ELEMENT, PROJECT, TASK AREA & WORK UNIT NUMBERS
11. CONTROLLING OFFICE NAME AND ADDRESS Office of Naval Research Power Branch Arlington, Virginia		12. REPORT DATE October, 1974 13. NUMBER OF PAGES 65
14. MONITORING AGENCY NAME & ADDRESS*(if different from Controlling Office)*		15. SECURITY CLASS. *(of this report)* UNCLASSIFIED 15a. DECLASSIFICATION/DOWNGRADING SCHEDULE

16. DISTRIBUTION STATEMENT *(of this Report)*

Approved for public release; distribution unlimited

17. DISTRIBUTION STATEMENT *(of the abstract entered in Block 20, if different from Report)*

18. SUPPLEMENTARY NOTES

19. KEY WORDS *(Continue on reverse side if necessary and identify by block number)*

Combustion
Solid Propellants
Catalysts
Ammonium Perchlorate
Hydroxyl terminated Polybutadiene

20. ABSTRACT *(Continue on reverse side if necessary and identify by block number)*

This report summarizes experiments and analysis concerned with sandwich and cast composite solid propellant combustion. The ingredients used in the experiments are ammonium perchlorate as the oxidizer, hydroxyl terminated polybutadiene as the binder and four catalysts: Harshaw catalyst Cu-0202, Fe_2O_3, ferrocene and iron blue. Cinephotomacrography and the fuze wire technique are used for combustion visualization and burn rate determination. Scanning electron microscopy is used for quenched sample visualization.

DD FORM 1 JAN 73 1473 EDITION OF 1 NOV 65 IS OBSOLETE

UNCLASSIFIED

SECURITY CLASSIFICATION OF THIS PAGE *(When Data Entered)*

20. (continue abstract)
Areas investigated are a) analytical and experimental determination of synergistic catalytic effects in sandwich and propellant combustion, b) the loading of ferrocene into the binder at the molecular level and its effect on sandwich combustion, c) differential scanning calorimetry of catalyst laden binder and d) analysis of sandwich deflagration.